Universidade do Minho
Escola de Engenharia

Nuno Miguel Ferrete Ribeiro

Senior-oriented Robotic Devices and Algorithms for Personalised Fall Prediction and Prevention

July 2022

Senior-oriented Robotic Devices and Algorithms for Personalised Fall Prediction and Prevention

Nuno Miguel Ferrete Ribeiro

UMinho | 2022

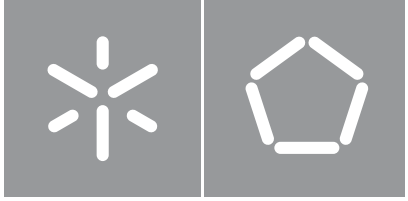

Universidade do Minho
Escola de Engenharia

Nuno Miguel Ferrete Ribeiro

Senior-oriented Robotic Devices and Algorithms for Personalised Fall Prediction and Prevention

Doctoral Thesis
Doctorate in Leaders for Technical Industries / Engineering Design and Advanced Manufacturing
LTI/EDAM - MIT Portugal

Work supervised by
Professor Dr. Cristina P. Santos

Juy 2022

STATEMENT OF INTEGRITY

I hereby declare having conducted this academic work with integrity. I confirm that I have not used plagiarism or any form of undue use of information or falsification of results along the process leading to its elaboration.

I further declare that I have fully acknowledged the Code of Ethical Conduct of the Universidade do Minho.

Acknowledgements

I want to thank Professor Cristina P. Santos, who was invaluable not only in terms of scientific supervision, but also in terms of support, advice, encouragement, and suggestions, and who was always present during these four years. Undoubtedly, Professor Cristina enabled the materialisation of the project's ideas through a methodical and planned approach. It has been a huge honour to be guided by you. You have always allowed and stimulated my professional and personal development as only you know. Thanks to you, your passion, and your commitment, I am better today. I therefore had to use this chance to express my gratitude and particular affection for you. For having always believed in me and in my potential, you will forever remain in my memory and my heart as someone who illuminated my path.

I also would like to thank Doctor Gorjão-Clara, Marta Sousa, Daniela Oliveira, Marta Simões, David Rodrigues, Eva Gonçalves and Áurea your clinical and field support, and so helpful collaboration. Thank all elderly subjects who kindly participated in the preliminary studies. Thank all the partner institutions for providing facilities, equipment and access to volunteers. I would also like to thank *Fundação para a Ciência e Tecnologia* for the scholarship PD/BD/141515/2018.

My best regards to my friends and colleagues of BiRD Lab, for their help in this achievement, patience in my stressful moments, and the good times we spent together. A special thanks to all who accepted to work within the scope of fall prediction and detection, specially Pedro Mouta, Ana Pereira, Rúben Durães, Henrique Pires, Luís Martins, Rafael Ferreira, Rodolfo Cerqueira, Ricardo Andrade, João Nunes and Raimundo Barros. You have no idea how proud I am of the job we have done as a team. I feel myself fortunate to have had your presence that pushed me to go further, which made me a better person and professional. You are exceptional people.

I would also like to express my gratitude to my friends Rita, Teresa, Mariana, Rute, César, Luís Serrador and Roberto, who have been unconditionally by my side during this phase as always. I thank Ana Silva for all the sensitivity, affection, patience, support and love she has shown over the last years, being always ready to help me and give me the strength to continue. I am very proud of you. By your presence, a huge thank you.

Finally, I want to thank my family for the unconditional and marvellous support they have shown throughout my life, for being always present in all important moments, for always believing in my abilities and for never letting me give up or discourage by the difficulties or obstacles that have crossed my path.

In particular, I should also thank my parents for providing me with the best conditions for my academic training, and for always indicating to me the best way forward. The solid base on which I stand and on which I am extremely proud of is my family. Additionally, I want to dedicate this PhD thesis to my grandparents who, while leading challenging lives, were always capable of overcoming the obstacles that came their way. Because they did not have the same opportunity to study as I did due to their inherent social constraints, they symbolise for me an example of triumph and inspiration that I will keep for the rest of my life. Just a word for my late grandfather Carlos Ribeiro. You have no idea how much I wish you were here to watch me achieving a dream that is also yours. I have always fought for what I wanted, and you have never left my thoughts. I owe you a lot.

To all of you, my most sincere and humble thank you!

Nuno Ferrete Ribeiro

«Success is not the key to happiness. Happiness is the key to success. If you love what you are doing, you will be successful.» - Albert Schweitzer

Abstract

Senior-oriented Robotic Devices and Algorithms for Personalised Fall Prediction and Prevention

The phenomenon of falls has become a global public health concern due to their prevalence in a projected constantly ageing population ($\geq$ 65 years), as well as its effects on mortality, lower Quality of Life (QoL) (annually: 684.000 deaths; 37,3 millions of accidents with injury) and higher costs. On the other hand, the lack of real-world fall data makes it difficult to develop and implement different technological solutions on a daily basis. This research solution aims, in a first phase, to collect data on falls and dynamic gait, both in institutions and in safe laboratory environments. Several protocols were developed and conducted to serve the development of algorithms and devices to further contribute to minimise or reduce the incidence of falls among the elderly. A conventional wood cane was instrumented to detect falls (>99%; *lead time* of 373ms) and 4 cane events (>85% per event). A cane-type robot prototype was designed, following a design and product development approach, to detect falls and act to prevent them. So far, the cane has a hardware and software architecture capable of recognising the user's motion intention and gait phases. A Multifactorial Fall Risk Assessment (FRA) Strategy with 3 modules was initiated during this thesis, starting with the recognition of 16 daily activities and 4 types of fall (96.53%) using a *waistband* equipped with an inertial sensor. Bio-inspired *Central Pattern Generator* (CPG) controllers are the basis of a fall prevention strategy for a knee orthosis, where the objective is to detect slips using the knee angle information (80%, mean detection time of 250 ms). Finally, a realistic virtual environment (VE) that closely resembles the typical home setting was created to apply fall-related visual disturbances while using a *Head-Mounted Display* (HMD), following the concepts of place illusion, plausibility and ecological validity, in order to collect data on compensatory postural reactions.

Keywords: Fall Prevention, Fall Prediction, Fall Risk Assessment, Artificial Intelligence, Robotic Devices, Quality of Life.

Resumo

Dispositivos Robóticos orientados ao Sénior para a Previsão e Prevenção Personalizada da Queda

O fenómeno das quedas tornou-se uma preocupação de saúde pública global devido à sua prevalência numa população projetada em constante envelhecimento (≥ 65 anos), bem como os seus efeitos na mortalidade, menor Qualidade de Vida (QoL) (anualmente: 684.000 mortes; 37,3 milhões de acidentes com lesão) e maiores custos. Por outro lado, o desenvolvimento e a aplicação diária de várias soluções tecnológicas são travados pela escassez de dados de quedas do mundo-real. Esta solução de investigação visa, numa primeira fase, recolher dados sobre quedas e marcha dinâmica, tanto em instituições como em ambientes laboratoriais seguros. Diversos protocolos foram desenvolvidos e conduzidos para servir o desenvolvimento de algoritmos e dispositivos para posteriormente contribuírem para minimizar ou reduzir a incidência de quedas entre os idosos. Uma bengala de madeira convencional foi instrumentada para detetar quedas (>99%; *lead time* de 373ms) e 4 eventos da bengala (>85% por evento). Um protótipo de uma bengala robot foi projetado, seguindo uma abordagem de *design* e desenvolvimento de produto, para detetar quedas e atuar para as evitar. Até ao momento, a bengala possui uma arquitetura de hardware e software capaz de reconhecer a intenção de movimento do utilizador e as fases da marcha. Uma Estratégia Multifactorial de Avaliação de Risco de Queda (FRA) com 3 módulos foi iniciada nesta tese, tendo começado pelo reconhecimento de 16 atividades diárias e 4 tipos de queda (96,53%) a partir de uma *waistband* equipada com um sensor inercial. Controladores *Central Pattern Generator* (CPG) bio-inspirados estão na base de uma estratégia de prevenção de queda para uma ortótese do joelho, onde o objetivo é detetar escorregões usando a informação do ângulo do joelho (80%, tempo médio de deteção de 250 ms). Finalmente, um ambiente virtual (VE) realista que se assemelha ao ambiente doméstico típico foi criado para aplicar perturbações visuais relacionadas a quedas ao usar um *Head-Mounted Display* (HMD), seguindo conceitos de ilusão de lugar, plausibilidade e validade ecológica, por forma a recolher dados de reações posturais compensatórias.

Palavras-chave: Prevenção de Queda, Previsão de Queda, Avaliação do Risco de Queda, Inteligência Artificial, Dispositivos Robóticos, Qualidade de Vida.

Contents

List of Figures

List of Tables

Acronyms

30SCS 30-second Chair Stand

3D Three-Dimensional

6MWT 6-Minute Walking Test

ACC Accuracy

ADC Analog-to-Digital Converter

ADL Activities of Daily Living

AFO Adaptive Frequency Oscillators

AI Artificial Intelligence

ANN Artificial Neural Networks

ANOVA Analysis of Variance

AP Anteroposterior

ASMA Activity Signal Magnitude Area

BBS Berg Balance Scale

BESTest Balance Evaluation Systems Test

BMI Body Mass Index

BNC Bayonet Neill–Concelman

BoS Base of Support

CCW Counter-Clockwise

CFS Correlation-based Feature Selection

CLSTM Convolutional Long Short-Term Memory

CMSW Cane Middle MidSwing

CNN Convolutional Neural Network

CNS Central Nervous System

COF Coefficient of Friction

CoM Centre of Mass

COP Centre of Pressure

CPG Central Pattern Generator

CV Cross-Validation

CW Clockwise

DA Discriminant Analysis

DoF Degrees of Freedom

DT Decision Tree

ECFS Extended CFS

ECG Electrocardiography

EEG Electroencephalography

EMA Exponential Moving Average

EMG Electromyography

FAC Functional Ambulation Categories

FCO Full Cane Off

FES-I Falls Efficacy Scale – International

FGC First Ground Contact

FNR False Negative Rate

FOG Freezing of Gait

FOS Factor of Safety

FPR False Positive Rate

FRA Fall Risk Assessment

FSM Finite State-Machine

FSR Force Sensitive Resistor

GDS Geriatric Depression Scale

GSR Galvanic Skin Response

HMD Head-Mounted Display

HMM Hidden Markov Model

HO Hold-Out

HS Heel-Strike

IDE Integrated Development Environment

ILFS Infinite Latent Feature Selection

IMU Inertial Measurement Unit

INFS Infinite Feature Selection

IPQ Igroup Presence Questionnaire

ISO International Organisation for Standardisation

KNN K-Nearest Neighbours

KPI Key Performance Indicator

LASSO Least Absolute Shrinkage and Selection Operator

LDR Light Dependent Resistor

LED Light Emitting Diode

LOB Loss of Balance

LOO Leave-One-Out

LRF Laser Range Finder

LSTM Long Short-Term Memory

MCC Mathew's Correlation Coefficient

MCFS Multi-Cluster Feature Selection

ML Mediolateral

MMSE Mini Mental State Examination

MMSt Middle Mid-Stance

MMSw Middle Mid-Swing

MoCap Motion Capture

mRMR Minimum-Redundancy Maximum-Relevancy

MSM Maximum Support Moment

MutInfFS Mutual Information Feature Selection

MVC Maximum Voluntary Contraction

PBT Perturbation-based Balance Training

PC Principal Components

PCA Principal Component Analysis

PCB Printed Circuit Board

PKO Powered Knee Orthosis

PLA Polylactic Acid

PPG Photoplethysmography

PPV Peak-to-Peak Values

PRISMA Preferred Reporting Items for Systematic Reviews and Meta-Analyses

PVC Premature Ventricular Contractions

PWM Pulse Width Modulation

QoL Quality of Life

RAA Resultant Angular Acceleration

RI Ratio Index

RMS Root Mean Square

RMSE Root Mean Square Error

RQ Research Question

SENS Sensitivity

SMA Signal Magnitude Area

SPEC Specificity

SSQ Simulation Sickness Questionnaire

SumVM Sum Vector Magnitude

SVM Support Vector Machine

TO Toe-Off

TRL Technology Readiness Level

TUG Timed Up and Go Test

V Vertical

VE Virtual Environment

VR Virtual Reality

WHO World Health Organisation

Chapter 1

Introduction

The research and development projects conducted over the last four years are detailed in this PhD thesis as part of the doctoral programme in Leaders for Technical Industries / Engineering Design and Advanced Manufacturing (LTI/EDAM) - MIT Portugal. Although the doctoral programme is connected to three national institutions, namely, the School of Engineering - University of Minho, the Faculty of Engineering - University of Porto and the Técnico - University of Lisbon, the research activities were performed in the Biomedical Robotic Devices Laboratory (BiRD Lab) included in the Center for MicroElectroMechanical Systems (CMEMS), a research center of the Department of Industrial Electronics from the University of Minho, and in LABBELS - Associate Laboratory (Braga/Guimarães).

The developed biomedical research seeks to assist elders, enhancing their Quality of Life (QoL), estimulating healthy and active ageing, and providing senior-oriented robotic assistive devices with fall prediction and cross prevention capabilities that interacts with caregivers or health professionals to provide timely support before and after a fall. This PhD thesis tackles the problem of falls from several perspectives through the development of: i) monitoring systems, i.e., an instrumented conventional cane and a cane-type robot to monitor human-robot interaction, validate the gait segmentation detection and detect or predict falls; ii) a strategy to assess the fall risk using activity recognition using a smart waistband; iii) a strategy to detect slips for a Powered Knee Orthosis (PKO); and iv) a Virtual Environment (VE) full of visual perturbations capable of inducing imbalance and accelerating the data collection process. These developments represent the first initiatives towards the project main goal.

1.1 Motivation

Among the most difficult healthy issues elderly persons deal with are falls and unsteady balance control. They are a significant factor in immobility [1] and early nursing home placement [2], as well as large rates of death and morbidity. Currently, the World Health Organisation (WHO) states that a fall is "an event which results in a person coming to rest inadvertently on the ground or floor or other lower level"[3]. Before a fall occurs an event that is more frequent and potentially predicts fall risk: the near-fall. According to Maidan et al. [4] a near-fall is considered "a stumble event or a Loss of Balance (LOB) that would result in a fall if sufficient recovery mechanisms were not activated". The problem of falls in the elderly population is a combination of a high incidence along with a high susceptibility to injury due to a high frequency of clinical disorders (e.g. osteoporosis, neurological diseases) [5, 6] and age-related physiological changes (e.g. slowed protective reflexes) [7] that make even a relatively minor fall particularly dangerous.

Around 28-42% of seniors (>65 years) fall at least once each year [3]. According to the WHO, falls are the second leading cause of unintentional injury death, after road traffic injuries, accounting an average of 684 000 fatal falls and an estimated 37.3 million non-fatal falls, which require medical attention, each year [3]. In the United States, almost three-fourths of all fall-related fatalities occur in the 13% of the population over the age of 65, indicating largely a geriatric syndrome. Approximately 40% of this age group living at home will fall at least once each year, and approximately 1 in 40 will be hospitalised. Only approximately half of individuals hospitalised following a fall will be alive a year later [8]. Instability and recurrent non-fatal falls are frequent warning signs of nursing home admissions [2]. According to the European Mortality Database [9], in 2019, Germany recorded 16 657 deaths being the European Union member with the higher number of deaths by accidental falls. In the same database, the last results from Portugal correspond to 2018, where 815 deaths were registered. Non-fatal falls that result in motor injuries decrease the QoL. Fallers develop fear of falling with consequent depression and restricted autonomy, social and physical activity [10]. This further contributes to deconditioning, weakness and abnormal gait and in the long run may actually increase risk of falls [11]. Additionally, recovery from fall injury is often delayed among the elderly.

The expenses associated with fall-related injuries are significant from a financial standpoint. It is expected that social and health costs may reach 4% of European health care expenditures, expecting to double in 2050 to €50 billion in the European Union [12]. Only in the United States of America, $19 billion were spent on the direct medical costs of fall-related injuries in 2000 [13]. In 2015, this has risen to more than $31 billion in the Medicare alone [14], and Cates et al. [15] expected a $43.8 billion costs in 2020. Other studies also demonstrated the average health system cost per fall injury. In the Republic of Finland and Australia these costs are US$3611 and US$1049, respectively. In Portugal, the value can rise to approximately €3000 if the injury is serious [16]. Pressure on the national health service has intensified as the ageing population is growing and, unfortunately, tends to get worse. According to the United Nations, the elderly population will be triple the existing number by 2085 [17].

The socioeconomic impact of falls highlight how crucial it is to implement strategies that mitigate or eliminate the risk of falling. According to evidences from Canada, a 20% reduction in the incidence of falls might result in a net savings of more than US$ 120 million per year [3]. To alleviate this social and economic burden, existing systems primarily focus on detecting a fall [18] with little emphasis on fall prediction [19]. Impact detection is the basis of **fall detection systems**, which notify the user and the healthcare provider when a fall has happened to hasten and enhance the medical care given. Since these systems cannot avoid falls, scientific literature also explores **fall prediction systems**, which are designed to alert users before a fall occurs, avoiding the emotional and physical effects of a fall. They should be able to recognise all potential fall situations and conditions and offer a framework for predicting them [19]. **Fall prediction systems or Fall Risk Assessment (FRA)** tools can also be divided into two different categories [19, 20]: i) **future fall prediction** - which can estimate the fall risk through some clinical assessment tests. Questionnaires or functional assessments of posture, gait, cognition, and other risk variables are frequently used in these exams. These clinical assessments are subjective and qualitative, with threshold evaluation scores commonly used to classify persons as fallers or non-fallers. To evaluate balance and lower limb strength, these tests are typically the Timed Up and Go Test (TUG), Berg Balance Scale (BBS), sit to stand, and one leg stand; and ii) **real-time fall prediction system** - it recognises abnormal gait patterns in order to calculate the probability of a real-time fall occurrence, continuously assessing the risk of fall using data from sensors while the user is doing his/her Activities of Daily Living (ADL) (e.g. walking, climb stairs, sit, stand, pick objects). When it detects abnormal situations, the user can be timely warned or an external help, such as a walker or a robot, can be used as a **fall prevention technique**. Robotised walking-aid devices provide security and stability by assisting in many stages of ADL, according to the user's level of mobility, which results in a higher QoL and autonomy for the elderly.

Falls do happen occasionally and come in many different forms. On average, nursing home residents incur 2.6 falls per person per year [8]. Their low frequency combined with the difficulty of instrumenting a subject and their unexpectedness lead to a lack of data to be used in several algorithms for **fall detection and prediction systems**. On the other hand, there are several types of falls that might happen as well as the number of reasons that lead to a fall. Thus, fall prediction is challenging. Collecting fall data can be laborious because it may require the person to actually undergo a real fall which may be harmful and unsafe. Alternatively, data on simulated falls can be gathered in controlled lab environments. However, that might not adequately depict actual falls [21, 22]. Thus, alternative methods must be used to generate imbalance and provoke falls while ensuring participant's safety.

1.2 Problem Statement and Scope

Although technology-based fall prevention systems have shown potential to reduce falls-rate and related injuries, more effective solutions are demanded to face the associated challenges. There is evidence that to reliably prevent a fall it is necessary to continuously assess multiple fall risks from multimodal (kinematic, physiologic, environmental data) sensors tracking human and context data, robustly detect falling onset, and timely activating mitigation strategies against falling [23]. Furthermore, the worldwide trend is toward assisted living solutions with multiple fall prevention measures adapted to the needs of the users for continuous usage during ADLs in natural settings [24]. No solution has been found that takes all these factors into account. Current clinical FRA tools present insufficient predictive validity, subject-dependent Accuracy (ACC), and do not provide continuous assessment throughout fallers' ADLs [10, 19, 25]. Additionally, they fall short of fully addressing the present user's motor requirements and fall risk in real-world settings for more effective prevention [10, 19, 24]. Artificial Intelligence (AI)-based assessment tools fed by objective measures on gait and balance are more accurate [25, 26] but do not estimate immediate fall risk in real-settings [19]. This PhD thesis pursues a multifactorial AI tool that continuously assesses future and imminent fall risk and risk factors in seniors' ADLs. Innovation is literature-driven by fusing instrument-based multimodal data with clinical assessments and easy to self-report behavioural and context factors [19].

A major need is to identify risky ADLs and inform seniors about them, raising their confidence and decreasing fear of falling. Accordingly, this PhD thesis will use ADLs-related risk factors and motor indicators [27, 28] to pursue the design of proactive strategies to aware seniors of fall risk and risky ADLs through senior-oriented digital solutions, empowering seniors' functional ability and QoL. These efficient apps would supplement clinicians on prompt and reliable assessments [19]. A key step is the data gathering from seniors at different institutional settings as an integrated, non-obtrusive part of their ADLs, recording contextual data by wearable sensors for longer periods [28]. This offers a unique insight to better assess fall risk in natural settings and identify risky-ADLs [24]. Further, during this PhD thesis, falls will be induced among healthy subjects through different types of perturbations during risky-ADLs, to identify adequate, human-inspired prevention strategies [29]. Sensory perturbation will be explored via Virtual Reality (VR) to induce audio-visual stimuli that alter the subject's balance [30] to achieve more realistic fall datasets [31–33].

Early predicting incipient falls is a key requirement of a fall prevention tool. Despite their high ACC, current AI tools only consider kinematic status under controlled settings or intentionally simulated falls [34, 35], with limited evidence in real ADLs [19]. This PhD thesis will give a step forward over these tools, by using current human context during ADLs, to predict, in real-time, the ADL, the fall onset, direction, and type with smaller detection times(<100ms) [34, 35], delving teamwork [36]. Additional progress ensures a minimal sensor setup by combining AI, human modelling, and biomechanical analysis [37], and a robust distinguishment of ADLs from falls [38, 39].

Few robotics devices have presented customised active prevention strategies able to close the loop from perception to action, in real life, during risky-ADLs [38]. Knee [37] and hip [40] exoskeletons drive joint motion for balance recovery, preventing slip-induced falls. Impedance-controlled smart walkers prevent multi-directional fall by applying supportive forces [41] or adjusting the human-robot distance to remain within the Base of Support (BoS) [42], as also exploited in cane robots [43]. Sensory augmentation devices with vibrotactile feedback synchronised to tilt angle have improved the elderly balance [44]. During this work, key technologies are incorporated to guarantee a more time-effective, senior-oriented fall mitigation strategy to minimise falls' risk and injuries. Enhanced or developed robotic devices, able to attend to different seniors' motor impairments, risks and needs, will be empowered with bioinspired control architectures that close the loop from estimated fall onset, user's needs, and context to generate suitable biomechanical countermeasures to manage diverse fall-types and perturbations [40, 45]. Assist-as-needed strategies extending the teamwork in impedance control [46], adaptive oscillator [47] and reflexes-based control [48], will be explored to guarantee a safe, compliant and symbiotic assistance by the real-time adjustment of the robot dynamics to the context, users' needs and state.

Finally, this PhD thesis will fill a gap by presenting solutions towards the deployment of the fall prevention solution in real-life settings among community-dwelling end-users. It covers high-quality, user-centred research, including seniors and caregivers, with technology validation in institutional settings in conformity with users' privacy. Scientific and societal challenges are joint to boost the development of more useful and safer products than existing solutions, potentially improving elderly QoL.

1.3 Goals and Research Questions

More effective and non-intrusive fall prevention technologies are needed to minimise fall-related risks in an ageing society. This PhD thesis proposes senior-oriented robotic assistive devices with reliable, safe fall prediction and cross prevention capabilities to customise balance recovery of senior fallers (> 65 years) during their ADLs and according to seniors' mobility impairment level. It focuses on bringing healthcare technology capable of preventing and mitigating fall incidence rates to the elderly population, with the ambition of making them more physically and socially active. It will contribute to long-term development in the health and social aspects by reducing the incidence of falls, empowering seniors' functional ability and QoL. Stimulating the usability and acceptability of cutting-edge technology while safely engaging seniors in physical activities aims to achieve a sustainable behaviour change according to risk factors, minimising fall occurrence. This work aims both fall prevention in real-time and assess the risk of falling, while fighting the scarcity of real-world fall data. To achieve these final goals, the present thesis focuses on pursuing the following first objectives towards the outlined solution. This work is aligned with the global action for Healthy Ageing and 3rd Sustainable Development Goal.

- **Objective 1: To identify systems' specifications and requirements** based on a technological survey, and user-centred design approach, with regulatory/ethical concerns,establishing an end-users and stakeholders panel. The survey reviews fall-related studies about: i) FRA using wearable sensors, distinguishing different types of performing this assessment through wearable technology and how researchers perform their validation; ii) robotic assistive devices, identifying the current work developed for robotic canes, smart walkers and powered orthoses. As a result, pertinent information on hardware architecture, device specifications, and fall prevention or detection mechanisms is provided; iii) real-world falls, revealing how data were collected and for what purpose is being used throughout the literature search; iv) mechanisms to provoke artificially slips and trips, describing them differing studies between overground walking and treadmill walking; and v) VR-based visual perturbations capable of triggering dynamic or static anticipatory and compensatory postural behaviours. The first review is helpful for Chapter 6, the second review for Chapters 5 and 7, the fourth review for Chapter 7 and the last for Chapter 8. Key Performance Indicators (KPIs): i) number of stakeholders (target: 10 elders, 3 caregivers from different institutions, 1 healthcare professional); ii) requirements, functional and technical specifications.

- **Objective 2: Enhance or develop monitoring robotic devices** through hardware and software optimisations, develop user-friendly digital solutions, and test in the laboratory their interoperability, safety, reliability, and intuitive use through benchmarks to specifications on latencies, autonomy, and usability. Chapter 3 addresses this goal by developing an instrumented conventional cane. In Chapter 5, a cane-type robot is created from scratch, while in Chapter 6, a team-owned waistband is enhanced. KPIs: i) synchronous data collection (latency<1ms); ii) targeted specifications of latencies and autonomy; iii) functional prototypes (Technology Readiness Level (TRL) 4); and iv) intuitive eHealth app (rated user experience>4).

- **Objective 3: Record comprehensive databases** of elderly natural falls during ADLs and healthy induced falls in laboratory, and develop an ecologically realistic VE filled of fall-related visual perturbations found in the scientific literature to induce realistic falls. Establish partnerships with nursing homes and residential homes to gather data from older adults. Chapters 4, 6, 7 and 8 address this objective by performing experimental protocols. KPIs: i) more comprehensive public databases than [31, 33], respecting GPDR-EU; and ii) a VE resembling a home-living scenario with visual perturbations truly capable of induce imbalance.

- **Objective 4: Develop AI-based multifactorial FRA and prediction tools** to continuously assess risky-ADLs, users' QoL, fatigue, gait, and balance indicators, predict ADLs, gait events, future and immediate fall risk, and onset, direction, and type of falls. Tools will attend current human and ambient context, fusing biomechanical, physiological, environmental data. This objective is

tackled in Chapters 4, 6 and 7. KPI: more reliable tools (ACC>98%, timing<100ms) than [25, 26], benchmarked to fall history, clinical fall risk and motor scales.

- **Objective 5: Develop fall prevention strategies for devices' bioinspired control architectures** to generate countermeasures personalised to user's needs and predicted fall onset, considering the literature biomechanical analysis about detection and actuation timings. Chapter 7 describes the first steps towards this objective, presenting the design of a a slip-related fall prevention strategy. KPIs: i) efficient, non-intrusive actuation for 60% fall risk mitigation [38]; ii) Root Mean Square Error (RMSE)<3; iii) Actuation time<100ms.

- **Objective 6: Categorise automatic and ecologically realistic fall-related visual perturbations** with different principles for imbalance induction, covering different types of falls and envisioning a future training rehabilitation tool. Chapter 8 addresses this objective. KPI: sigma < 0.005 to detect significant statistical differences between normal and abnormal situations per dependent variable, using kinematic and physiological data.

- **Objective 7: Exploration of innovation outcomes** to maximise the solution impact considering obtained research outcomes and clinical evidence. KPIs: i) publications; ii) public dataset; and iii) software modules.

The proposed ideas describe the transdisciplinary research adopted in this PhD thesis that will contribute in the near future to prevent and minimise fall incidence rates among the elderly population. The following Research Questions (RQs) are proposed and expected to be answered:

- **RQ1:** What are the main FRA and fall prevention methods implemented in the scientific literature and how input information is obtained and used? This RQ is related to Objective 1 and is answered in Chapter 2.

- **RQ2:** Can an instrumented conventional cane and a cane-type robot detect falls and indirectly gait events? This RQ is related to Objective 4 and is answered in Chapters 4 and 5.

- **RQ3:** What is the best machine learning and deep learning-based strategy, as well as the most suitable features, to implement for real-time ADL and fall events recognition? This RQ is related to Objective 4 and is answered in Chapter 6.

- **RQ4:** Are the biological-inspired Central Pattern Generator (CPG) controllers and the threshold-based algorithms able to effectively track human motion variables and timely detect slip perturbation occurrences, respectively? This RQ is related to Objective 5 and is answered in Chapter 7.

- **RQ5:** Can a VR headset introduce imbalances through visual perturbations, causing postural reactions typical of a fall? This RQ is related to Objective 6 and is answered in Chapter 8.

1.4 Contribution to Knowledge

The monitoring robotic devices presented in this PhD thesis were developed and enhanced to mitigate or reduce the incidence of falls among the community-dwelling older adults. An instrumented conventional cane detects falls and gait events indirectly. A cane-type robot was created, instrumented and equipped with a motion control system. A smart waistband was enhanced based on the team's work [49] to serve as data source for a new FRA strategy. The initial steps were taken in the direction of activity recognition by using data available online and collected from volunteers who are in institutions that support the elderly and are partners of BiRD Lab. These partnerships were established within the scope of this PhD. CPGs were used to detect slip-like perturbations and VR to induce imbalance. This PhD thesis's primary contributions are as follows:

- A set of **reviews** that contributed to expand and clarify the work performed among the scientific literature on the following topics: i) most adopted **FRA methods** using **wearable sensors** to screen high fall risk subjects. This work complemented the previous works of Rucco et al. [26] and Montesinos et al. [25]; ii) assistive robotic devices, namely, **cane-type robots**, **smart walkers** and **powered orthoses** to identify and understand the reasons of implemented **hardware** and **fall prevention strategies**, along with the main results, limitations and challenges; iii) how **real-world fall** data has been **used and obtained**; iv) key experimental aspects adopted to **provoke artificial slip and trip perturbation** distinguishing the application between overground walking and treadmill walking; and v) textbffall-related visual perturbations applied while using an **immersive Head-Mounted Display (HMD)**, along with the limitations found and future direction suggestions. Considering the author's expertise, the reviews mentioned are lacking among the scientific literature (Chapter 2; Objective 1).

- **Partnerships** established with **institutional settings** and data **acquisition protocols** conception and realisation using the developed software and the enhanced waistband (Chapters 3 and 6; Objective 3).

- A **large dataset** with extensive and relevant **kinematic and physiological information** collected during normal and perturbed treadmill walking, as well as during overground walking with VR that allows to study the changes to the human motion induced by **slip-like perturbations** and **visual perturbations** through an immersive HMD (Chapters 7 and 8; Objective 3).

- Two **kinematic data-based approaches**, a Finite State-Machine (FSM) and a AI-based tool, capable of detecting **4 cane events** of an **conventional cane** (Chapter 4; Objective 4).

- A **hardware architecture** capable of responding to different **user's needs** and considering **information from the user** (e.g. gait phase) and the **environment context** (e.g. luminosity) (Chapter 5; Objective 2).
- The implementation of a **cost-effective motion control system** that gathers sensory fusion information acquired by the cane-type robot. It detects the **user's motion intention** and differentiate the various **gait event phases**, i.e., stance and swing (Chapter 5; Objectives 2 and 4).
- The proposal of a FRA tool architecture capable of using several fall risk factors to compute the risk of falling in real-time (Chapter 6; Objective 4).
- The enhancement of a team-owned instrumented waistband for lower trunk inertial data acquisition (Chapter 6; Objectives 2 and 4).
- A **AI-based tool** capable of recognise **16 ADLs** and **4 types of falls** with only **one inertial sensor** at the lower trunk (Chapter 6; Objective 4).
- Evidence highlighting the **effectiveness** of the **CPG controllers** to adapt to steady-state human locomotion variables, and **threshold-based algorithms** to timely detect the occurrence of **slip-like perturbations** provoked during steady-state human locomotion (Chapter 7; Objective 5).
- An **ecological realistic VE** resembling a **home-living scenario** with a wide variety of virtual locations that the participant can be immersed in, as well as a high number of **visual perturbations truly capable of induce imbalance** (Chapter 8; Objective 6).

During this PhD thesis, scientific and technical support was provided to master students of different fields of engineering, contributing to five Master Dissertations on Biomedical Engineering, one Master Dissertation on Industrial Electronics and Computers and one Master Dissertation on Physical Engineering. These Master Students contributed to the work herein presented. Additionally, one Master Dissertation on Biomedical Engineering and one Master Dissertation on Informatics Engineering are currently under co-guidance. Still under supervision were 7 undergraduate/master's students who participated in small internships at BiRD Lab. Furthermore, the work developed in this thesis played an important role in the scientific research and development of two project submissions and in actively specifying one accepted request for evaluation of a research project to the Ethics Committee for Research in Life and Health Sciences (CEICVS) of the University of Minho, as follows.

- **SafeWalk** (2020) - *AI-based user-adaptive robot systems for personalised fall prevention*. Project not approved with Cristina P. Santos as Principal Investigator of the research investigation.
- **Move+** (2021) - *Senior-oriented robotic devices for personalised fall prediction and prevention*. Project not approved with Cristina P. Santos as Principal Investigator of the research investigation.

- Ethics Committee Evaluation (2021) of the project *Robotic system for the prediction and prevention of falls in real time*. Favourable assessment with the reference number CEICVS 063/2021 under the supervision of Cristina P. Santos.

1.5 Publications

The work here described allowed the publication of the following journal articles, conference papers, and book chapters. Contributions as second author or co-author, whether in journal articles, in conference papers or book chapters, relies on the conceptual design of the proposed solution, innovation or strategy, performing the experimental validation, and supporting the paper elaboration and review. Scopus profile recognises a total of 15 publications, with only 4 papers not resulting from this thesis, 29 citations by 25 documents, and an h-index of 3. Google Scholar profile indicates a total of 50 citations and an h-index of 4. The following sources can be visited for further information: i) ResearcherID AAP-9872-2020; ii) ORCID 0000-0003-4177-2587; and iii) SciProfiles: 2035827.

1.5.1 Journal Articles

- Rafael Neto Ferreira, **Nuno Ferrete Ribeiro**, Joana Figueiredo and Cristina P. Santos, "Provoking Artificial Slips and Trips towards Perturbation-based Balance Training: a Narrative Review, "in Safety Science, July 2022 **(Submitted)** [IF(2021) - 6.500; Before the publishing year (2021): Q1 - Public Health, Environmental and Occupational Health, Q1 - Safety Research, Q1 - Safety, Risk, Reliability and Quality].

- Luís M. Martins, **Nuno Ferrete Ribeiro**, Filipa Soares and Cristina P. Santos, "Inertial Data-Based AI Approaches for ADL and Fall Recognition,"in Sensors (Switzerland), vol. 22, no. 11, May 2022. [IF(2020) - 3.576; IF(2021) - 3.847; Before the publishing year (2021): Q1 - Analytical Chemistry, Q2 - Atomic and Molecular Physics, and Optics, Q2 - Biochemistry, Q2 - Electrical and Electronic Engineering, Q2 - Information Systems, Q1 - Instrumentation, Q2 - Medicine (miscellaneous)].

- Rafael Neto Ferreira, **Nuno Ferrete Ribeiro** and Cristina P. Santos, "Fall Risk Assessment Using Wearable Sensors: A Narrative Review,"in Sensors (Switzerland), vol. 22, no. 3, pp. 984, Jan. 2022. [IF(2020) - 3.576; IF(2021) - 3.847; Before the publishing year (2021): Q1 - Analytical Chemistry, Q2 - Atomic and Molecular Physics, and Optics, Q2 - Biochemistry, Q2 - Electrical and Electronic Engineering, Q2 - Information Systems, Q1 - Instrumentation, Q2 - Medicine (miscellaneous)].

- **Nuno Ferrete Ribeiro** and Cristina P. Santos, "Two Fall-Related and Kinematic Data-Based Approaches for an Instrumented Conventional Cane,"in IEEE Transactions on Human-Machine Systems, vol. 51, no. 5, pp. 554-563, Oct. 2021. [IF(2019) = 3.374; IF(2020) = 2.968; IF(2021) =

4.124; Before the publishing year (2020): Q1 - Artificial Intelligence, Q1 - Computer Networks and Communications, Q1 - Computer Science Applications, Q1 - Control and Systems Engineering, Q1 - Human-Computer Interaction, Q1 - Human Factors and Ergonomics, Q1 - Signal Processing].

- **Nuno Ferrete Ribeiro**, Pedro Mouta and Cristina P. Santos, "Two Kinematic Data-Based Approaches for Cane Event Detection,"in Journal of Ambient Intelligence and Humanized Computing, May 2021. [IF(2019) = 4.594; IF(2020) = 7.104; IF(2021) = 3.662; Before the publishing year (2020): Q1 - Computer Science (miscellaneous)].

- **Nuno Ferrete Ribeiro**, João André, Lino Costa, and Cristina P. Santos, "*Development of a Strategy to Predict and Detect Falls Using Wearable Sensors*," Journal of Medical Systems, vol. 43, no. 5, p. 134, Apr. 2019. [IF(2018) = 3.223; IF(2019) = 4.136; IF(2020) = 5.227; IF(2021) = 4.920; Before the publishing year (2018): Q2 - Health Informatics, Q2 - Health Information Management, Q2 - Information Systems, Q2 - Medicine (miscellaneous)].

1.5.2 Conference Papers

- Rúben Durães, **Nuno Ferrete Ribeiro**, Rafael Neto Ferreira, Eurico Seabra and Cristina P. Santos, "*Product Design and Mechanical Validation of a Cane-Type Robot for Fall Prevention*", 2021 IEEE International Conference on Autonomous Robot Systems and Competitions (ICARSC), 28-29 Apr. 2021.

- Pedro Mouta, **Nuno Ferrete Ribeiro**, Rui Moreira and Cristina P. Santos, "*Assistive Smart Cane (ASCane) for Fall Detection: First Advances*", XV Mediterranean Conference on Medical and Biological Engineering and Computing – MEDICON 2019, Coimbra, 26-28 Set. 2019.

- Ana Pereira, **Nuno Ferrete Ribeiro** and Cristina P. Santos, "*A Survey of Fall Prevention Systems Implemented on Smart Walkers*," in 2019 IEEE 6th Portuguese Meeting on Bioengineering (ENBENG), Lisbon, 22-23 Feb. 2019.

- Ana Pereira, **Nuno Ferrete Ribeiro** and Cristina P. Santos, "*A Preliminary Strategy for Fall Prevention in the ASBGo Smart Walker*," in 2019 IEEE 6th Portuguese Meeting on Bioengineering (ENBENG), Lisbon, 22-23 Feb. 2019.

- Pedro Mouta, **Nuno Ferrete Ribeiro**, Luís Gonçalves, and Cristina P. Santos, "*An Overview of Fall-Related Systems Developed in Canes*," in 2019 IEEE 6th Portuguese Meeting on Bioengineering (ENBENG), Lisbon, 22-23 Feb. 2019.

1.5.3 Book Chapters

- **Nuno Ferrete Ribeiro**, Ana Pereira, Joana Figueiredo, José A. Afonso and Cristina P. Santos, "*A Machine Learning Approach for Near-Fall Detection Based on Inertial and Force Data While Using a Conventional Rollator*," in Torricelli D., Akay M., Pons J.L. (eds) Converging Clinical and Engineering Research on Neurorehabilitation IV. ICNR 2020. Biosystems & Biorobotics, vol 28. Springer, Cham.

- João M. Lopes, João André, António Pereira, Manuel Palermo, **Nuno Ferrete Ribeiro**, João Cerqueira and Cristina P. Santos, "*ASBGo: A Smart Walker for Ataxic Gait and Posture Assessment, Monitoring, and Rehabilitation*,"in Gupta, D., Sharma, M., Chaudhary, V., & Khanna, A. (Eds.). (2021). Robotic Technologies in Biomedical and Healthcare Engineering (1st ed.). CRC Press.

1.6 Thesis Plan Outline

This PhD thesis is organised into nine chapters. Chapter 2 comprises five literature reviews. As previously stated, there are numerous actions that may be taken to reduce or avoid falls. Thus, it is necessary to verify the current solutions to assess the risk of falling and to prevent the fall in real time through robotic assistive devices, as well as the mentioned gaps to be filled. The development of algorithms is related to the accessibility to real-world data, so understanding their availability, as well as the work done for this and with this, is vital for the course of this research. Finally, since falls are a sporadic episode in people's lives, it is important to speed up the data collection. The last 2 reviews complement knowledge in this area. Chapter 3 introduces the main functionalities and conceptual design of the project solution. It describes the solution's phases towards the generalised access to safe, equative, and quality healthcare technologies, so the elderly will remain physically and socially active. Chapter 4 describes an instrumented conventional cane capable of detecting cane's falls and events with only an Inertial Measurement Unit (IMU). Two AI-based models and 2 FSMs are described along with their experimental validation. This chapter provides new cane events phases never described in the literature before, and a benchmarking analysis with other solution's lead-times. Chapter 5 details the procedures inspired by Ulrich and Eppinger [50] work and followed from the creation of the mission statement to the first operational prototype of a cane-type robot. Furthermore, the architecture is defined, as is the motion control system, which actuates in accordance with the user's intention. Chapter 6 starts idealising the architecture of a multifactorial FRA strategy, providing information on its 3 phases (Data acquisition, Classification and regression Modules, and FRA estimation and Feedback) and 3 modules (Baseline Risk, ADL Classification and Gait Abnormalities). Moreover, it shows the enhancement of a smart waistband, as well as the first steps towards the ADL Classification Module. Chapter 7 defines a slip-related fall prevention strategy for a PKO. So far, only the detection block has undergone advances that are recorded here. Therefore, it scrutinises the experimental protocol, the importance and application of CPGs and the threshold-based algorithms used for slip-like perturbation detection.

Outcomes are also compared with results found in the literature. Chapter 8 proposes the conception and development of a VE that comply with certain characteristics that are outlined (e.g. ecological validity), and is used as a platform to introduce visual disturbances to the participant through the headset. Visual disturbances created are described, as well as the experimental protocol. Finally, a statistical analysis helps understanding the effect of the visual perturbations on the participants. Chapter 9 summarises the thesis' significant results and contributions, as well as future research and technological development potential.

Chapter 2

Research on Fall Prediction and Prevention

2.1 Motivation and Research Scope

FRA has recently been a major topic of fall-related research. Wearable sensors, in addition to simplistic questionnaires, have been employed to improve the impartiality of this evaluation. However, standard methods must be defined to reflect the multifactorial causes of fall incidents while addressing the variability of the existing created systems. As a result, it is vital to determine the various specifications and needs of each FRA method. On the other hand, assistive robotic devices emerged to prevent falls from happening in real-time. Scientific literature addresses several solutions according to the end-users' level of mobility, showing robotic canes, smart walkers and wearable robotic devices. Thus, it is imperative to understand these device's specifications, as well as their limitations and future challenges.

Real-world datasets are extremely valuable and hard to obtain, specially with robotic assistive devices, for many reasons [31]: i) falls occur much less frequently than other events. On average, an elderly person falls once or twice a year; ii) ensuring that the volunteer uses the equipment correctly is also quite complicated, e.g. because it is not possible to keep a constant watch; iii) volunteers report fall events, which can be biased, as the volunteer may forget or consider that it is not necessary to report the event; and iv) taking into account the previous reasons, identifying fall events based only on the signals from the sensors can lead to labelling errors. Despite all the difficulties highlighted, it is only with real-world data that the existing bias on the literature can be eliminated and allow the development of algorithms.

Due to the low amount of data, researchers have been fighting this shortage using alternative methods. Scientific literature disclosures several alternatives to cause slips and trips with higher frequency in laboratory conditions that mimic the characteristics of real gait disturbances. Only in this manner can data from participants at LOB events be collected. VR can also be a way of inducing imbalance. Commonly

used to manipulate visual feedback to produce conflicts between visual, somatosensory, and vestibular information, VR therapies have been introduced in the field of neurorehabilitation, especially in patients who suffered from stroke or Parkinson's disease and in children with cerebral palsy [51–53]. These studies follow the paradigm of Perturbation-based Balance Training (PBT), adding the perturbation on the VE to cause imbalance.

2.2 Review: FRA Using Wearable Sensors

Recent reviews on FRA have presented and examined several approaches towards fall risk analysis. Reviewing the FRA approaches using wearable sensors in terms of sensor technologies commonly used, their number and location, and performed tasks in a protocol [26]; studying the most significant and strong associations between combinations of feature categories, tasks performed and sensor locations to ascertain subjects as faller or non-faller [25]; or even studying the relationship between the different fall risk factors and highlighted current work and challenges on fall prediction systems [19] are examples of the most recent works performed in this particular area. The analysis within these articles, however, was conducted without identifying the various FRA methodologies, such as long-term or real-time FRA. Consequently, identifying trends is less trustworthy than doing separate analyses for each FRA method discussed. FRA from both long-term and real-time perspectives necessitates various specifications and setups, as well as varied and individual analyses. For example, a certain type of sensor put on a specific part of the body may be generally applied for one FRA approach but not for another. Furthermore, none of the prior evaluations established the validation processes used to evaluate the FRA systems described in the literature. Thus, the aim of this review is to find evidence on the following topics: i) "Which are the main types of FRA methods using wearable sensors in literature studies?"; ii) "What types, number, and location of wearable sensors were adopted in the literature studies?"; iii) "Which tasks or clinical scales were performed during experimental protocols for data acquisition?"; iv) "Which algorithms are used in the scientific literature for the classification of fall risk?"; and v) "How was the validation of FRA systems performed using wearable sensors?". The first, fourth, and fifth questions provide unique analysis regarding the mentioned review articles [19, 25, 26]. On the other hand, the first question has not been addressed previously, while the third question offers a technological description of the sensors used in FRA systems. This enables additional comparison with past review studies to see whether sensor specification trends are maintained or updated. The fourth question provides an overview of the tasks or clinical scale methods used to collect data.

2.2.1 Search Strategy

An electronic systematic search was accomplished in IEEE, Scopus, Web of Science, and PubMed databases on the topic of FRA of towards the elderly population using wearable sensors. On IEEE the keywords used were: (aged OR elderly OR geriatric OR old) AND fall risk AND wearable sensor. The terms (aged OR elderly OR geriatric OR old) AND (wearable sensor OR wearable device) AND fall risk AND (gait OR posture OR walking) were used in the other 3 databases. In order to provide an overview of the most recent and emerging trends of FRA using wearable sensors, the search was conducted considering all articles that were published after 2015. Articles were excluded if: i) the system described in the study presented any kind of non-wearable device; ii) a FRA method was not applied or described; iii) there was a lack of information on either the sensor system or its placement on the body; and iv) previous versions of a study.

2.2.2 Search Results

A total of 332 articles were found and 223 remained after removing duplicates. Further, a careful reading of the title and the abstract of those articles enabled the exclusion of articles that clearly did not perform FRA or were a review. Following this procedure, 48 articles remained for full text reading. In order to screen the most important ones, eligibility criteria were applied to the selected papers. A total of 16 articles were selected for further analysis. Figure 5 depicts the Preferred Reporting Items for Systematic Reviews and Meta-Analyses (PRISMA) flowchart regarding the previously described search strategy. A group of nine studies [54–62] assessed fall risk from a long-term perspective based on clinical established scales

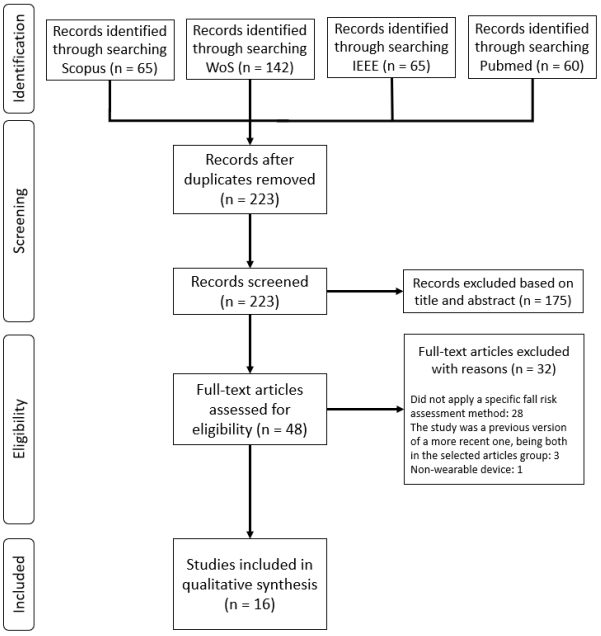

Figure 1: PRISMA Flowchart of the Review on FRA using Wearable Sensors.

(56%). In addition, 25% of the selected manuscripts [63–66] considered FRA from a short-term or real-time approach by developing a system and an algorithm able to identify pre-fall/unbalanced situations and consequently detect fall risk events. Lastly, three studies [67–69] (19%), which followed different approaches to assess fall risk, were identified and included in "Other Methods".

2.2.3 FRA Based on Clinical Scales

Vieira et al. [61] developed a gamified application for the elderly to independently measure the BBS score at home by means of a custom-made sensor containing an accelerometer and a gyroscope. Shahzad et al. [57] estimated the BBS score from data acquired from a single accelerometer. Tang et al. [55] performed a study to obtain the BBS and Mini-Balance Evaluation Systems Test (BESTest) scores for each subject with a sensor apparatus composed by a SmartShoe, which comprised a pressure sensitive insole with three pressure sensors and an accelerometer, as well as an hip accelerometer. Yang et al. [60] conducted four environment-adapting TUG in order to assess fall risk in a more comprehensive way than standard TUG by adapting gait in complex environments. During the trials, subjects wore a Smart Insole in each foot, with a sensing device composed by 16 pressure sensors array along with an IMU Saporito et al. [58] attempted to predict a remote TUG score based on data recorded from three days of free-living conditions by means of one accelerometer and one barometric sensor. Buisseret et al. [59] assessed subjects' fall risk based on the TUG test score and data acquired from an accelerometer, a gyroscope and a magnetometer during the 6-Minute Walking Test (6MWT). Dzhagaryan et al. [62] developed a wearable system, the Smart Button, capable of providing an automated mobility assessment of TUG and 30-second Chair Stand (30SCS) tests from data collected by an IMU with an accelerometer, a gyroscope and magnetometer sensors. In both studies conducted by Rivolta et al. [54, 56], the Tinetti test score was predicted for each of the test subjects by means of data collected from a single accelerometer.

2.2.3.1 Sensor System Characteristics

All the studies used at least one accelerometer, which underlines the importance of the use of acceleration data to characterise the score results from clinical standard scales. The use of gyroscope sensors was highlighted in four articles [59–62]. This search revealed that accelerometers and gyroscopes were the most widely used sensors for this FRA method. The magnetometer sensor is also included in the sensing device of three studies [59, 60, 62] and is used along with both acceleremeter and gyroscope sensors. Beyond inertial sensors, pressure sensors were used in two studies [55, 60]. Concerning the sensors' sampling frequency, all the studies acquired data from sensors at 100 Hz or less except Tang et al. [55], which used 400 Hz, and Vieira et al. [61] that did not mention the frequency adopted. However, in the data processing stage, Tang et al. [55] downsampled data from 400 Hz to 25 Hz.

Most of the studies used a small number of three sensors or less. However, Tang et al. [55] and Yang et al. [60] used 9 and 38 sensors, respectively. In their setup, Yang et al. [60] used 32 pressure sensors and 2 IMU's (with accelerometer, gyroscope, and magnetometer). Tang et al. [55] sensing apparatus consisted on six pressure sensors and three accelerometers. Within these manuscripts, almost all sensors were placed in the insole of the test subjects, thus the high amount of sensors did not compromise the wearability of the system. All the single sensor solutions that assessed fall risk through clinical-based scales used accelerometers [54, 56, 57]. The most widely used two-sensor combination for FRA is accelerometer and gyroscope, which is line with the search results of Rucco et al. [26]. In addition, four articles used the accelerometer and gyroscope combination [59–62], with Buisseret et al. [59] and Vieira et al. [61] using only data from those two sensing modalities.

Furthermore, five studies described the sensor placement on the chest [54, 56, 58, 61, 62], two on the waist/lower back [57, 59], two on the feet [55, 60] and one on the right hip [55]. Both studies that considered the feet to place the sensors used pressure sensors [55, 60]. Additionally, eight studies [54–59, 61, 62] considered at least one upper body part to place the sensors, in which seven of them only considered upper body parts [54, 56–59, 61, 62]. The chest and the lower back were the most used upper body locations. Therefore, the upper body contains the preferred locations to place the wearable sensors in FRA based on clinical scales.

2.2.3.2 Clinical-Based Scales Adopted

The variety of clinical-based scales adopted in the literature towards FRA is shown by the 6 different scales included in the group of 9 studies. TUG was the most selected scale [58–60, 62] and BBS was the second most adopted [55, 57, 61]. The Tinetti test was implemented in both studies conducted by Rivolta et al. [54, 56] and Mini-BESTest, 6MWT, and 30SCS were included in one study each [55, 59, 62]. In addition, three studies conducted two different clinical scales [55, 59, 62]. While the majority of the studies [54–56, 59–62] collected data from activities performed during the clinical scales experimental protocols to assess fall risk, some collected data from activities outside the clinical scale protocols. For instance, Shahzad et al. [57] attempted to predict BBS score of test subjects by means of data collected during a routine which included a group of simple physical movement activities, namely the TUG test, five times sit-to-stand test, and alternate step test. Further, in Saporito et al. [58] data collected from subjects during 3 days of free-living conditions was used to predicted TUG time score.

2.2.3.3 Algorithms for the Classification of Fall Risk

In this FRA method, four studies implemented machine Learning models [54, 55, 57, 58], two considered a deep Learning approach [56, 59], two adopted threshold-based algorithms [59, 61], and two studies did not

perform this classification [60, 62]. All four studies which applied machine Learning used linear regression-based models to predict clinical scale scores. Shahzad et al. [57] used linear regression machine learning models to estimate the scores of the BBS test from the information provided by a single accelerometer positioned in the lower-back. In the same study, researchers opted to choose machine learning models that could be applied in small datasets and found that linear least square and Least Absolute Shrinkage and Selection Operator (LASSO) regularised linear regression outperformed Decision Tree (DT)-based models, especially the LASSO one. Saporito et al. [58] also adopted a regularised linear model for the estimation of a TUG score, by means of signals collected from an accelerometer and a barometer in free living conditions for 3 days. Moreover, Rivolta et al. [54] applied a multiple linear regression model in order to predict the value of the Tinetti test scores assigned to the subjects by a clinician, using data obtained from a single sternum-mounted accelerometer. Tang et al. [55] applied a linear kernel support vector regression to predict clinical scores of BBS and Mini-BESTest from pressure and acceleration sensors data.

Considering the use of Deep Learning, Rivolta et al. [56] attempted to estimate the Tinetti test scores based on gait and balance features obtained from a single low cost acceleration sensor, considering a two-fold problem: i) a binary classification problem to dichotomise individuals at score 18 as High and Low Fall risk; and ii) a regression problem in order to estimate the gold standard Tinetti score assigned to each subject. Based on the performance results, the Artificial Neural Networks (ANN) provided better classification outcomes than the linear model. Buisseret et al. [59] implemented a Deep Learning model, as well as a threshold-based algorithm in order to predict the risk of falls based on the TUG and 6MWT. Therefore, a 6-month prediction of subjects' fall risk based on prospective fall occurrence as the start of the study was performed in three different classification ways: i) a threshold-based approach considering only the time taken to complete standard TUG; ii) another threshold-based approach (TUG+) considering the previously described time and kinematic parameters computed from IMU sensor data; and iii) a Deep Learning Convolutional Neural Network (CNN) network that receives the raw IMU data only. The authors verified that both TUG+ and the AI algorithm enhanced the performance in several classification metrics of the faller status of the subjects regarding the standard TUG alone. Vieira et al. [61] also implemented a threshold-based approach in order to assess the score of BBS through accelerometer and gyroscope measures. The researchers established reference values concerning each of the movements performed during the test in order to assign their respective classification. The works developed in [60, 62] assessed the performance metrics of the features calculated by their systems against ground truth measures of video and optical Motion Capture (MoCap) system, respectively, rather than classify subject's fall risk.

2.2.4 FRA Based on the Detection of Fall Risk Events

Four manuscripts [63–66] addressed FRA from a real-time perspective, focusing on the detection of fall risk events during the performance of activities. Saadeh et al. [63] used the data collected from an acceleration sensor to distinguish between ADL and pre-fall events. Their system achieved a timely prediction of fall events, activating a fall risk alarm before the fall occurrence. Rescio et al. [65] described an Electromyography (EMG)-based system capable of detecting and recognising fall risk events. Leone et al. [66] also presented a FRA system based on EMG capable of recognising pre-fall events. Later, the authors developed a smart sock system, each one equipped with two EMG sensors, able to detect unbalance events associated with a potential fall risk [64]. One important aspect analysed by each of the four studies was the lead-time. This time, which was used to study system's detection performance of fall risk events, was considered with two different meanings. Saadeh et al.'s investigation [63], as well as both studies conducted by Leone et al. [64, 66], evaluated detection performance of the system considering the lead-time as the time between the detection of the unbalance event and the impact of the fall. Saadeh et al. [63] mentioned that their system could predict a fall event with a lead-time between 300 ms and 700 ms before the fall impact. Leone et al. [66] claimed a mean lead-time of 775 ms of their system and, in a later study performed by the same authors [64], a smart sock EMG system was able to detect unbalance conditions with 750 ms of mean lead-time. However, Rescio et al. [65] interpreted lead-time from a different perspective, by considering it to be the time delay between the onset of the perturbation and the instant when the perturbation was detected. The authors claimed that their system was able to detect a perturbation 200 ms, on average, after its onset. EMG-based systems were used in three studies [64–66] to detect pre-fall scenarios or unstable situations associated with fall risk. On the other hand, Saadeh et al. [63] described the detection of fall risk events based on accelerometer data.

Considering the experimental protocol, Rescio et al. [65] instructed subjects to simulate a series of events in a random order: i) being at idle position or walking; ii) perform some common ADL such as bending, lying down, standing up or sitting down; and iii) unstable situations provoked by a tilting platform which simulated LOB. Saadeh et al. [63] collected data and combined it with MobiFall dataset [70] resulting in a total of six different examples of falls and 11 ADL events. ADL included events that have a higher chance of being classified as false positives/falls such as: i) jumping and jogging, as they are abrupt events that are alike to a fall event; ii) stepping in a car or sitting on a seat; and iii) performing standing or walking tasks and ascending or descending stairs. In addition, forward lying falls, back chair falls, front knees falls, and side falls were considered. Leone et al. [66] also developed a dataset consisting of not specified ADL and fall events caused by a movable platform to train and test their algorithm. Later, Leone et al. [64] performed a similar work where they specify the ADL: i) walking; ii) sitting down on a chair; iii) bending; and iv) lying down on a mat. Additionally, forward, lateral, and backward falls were induced by the same movable platform described in [66]. Within the four studies that assessed fall risk from a real-time

perspective based on the detection of fall risk events, three adopted machine learning models [63, 64, 66], whereas the remaining study used a threshold-based model [65].

2.2.5 Other FRA Methods

There were other approaches also identified to assess the risk of fall. Selvaraj et al. [69] highlighted the importance of analysing the foot clearance during stair negotiation, as reduced values of this metric have an explicit mechanism linked to falls by increasing the chance of tripping. They used an IMU-based wearable system on the subjects foot during the protocol. Annese et al. [68] underlined the complexity of FRA and the need to perform it in a multifactorial approach in an everyday life monitoring scenario in order to accurately predict future falls. They used EMG and Electroencephalography (EEG) data as input for their approach. Finally, Parvaneh et al. [67] explored the relationship between fall risk and the number of Premature Ventricular Contractions (PVC) episodes per hour, by using an Electrocardiography (ECG).

2.2.6 System's Validation

From the 16 selected studies, only 11 performed the validation of their FRA system [54–60, 63–66]. The validation carried out on the FRA systems varied across these different studies. The fall risk outcome of the system was compared against reference measures in order to compute the system's performance metrics. Seven studies [54–59, 63] validated their FRA systems using data collected from elderly patients, while the remaining four manuscripts used data from young subjects [60, 64–66]. In addition, the number of subjects enrolled in the experimental protocols was usually equal or below 30 subjects [54, 55, 57, 60, 64–66]. Only four studies [56, 58, 59, 63] included data from more than 30 subjects in their validation process. Saadeh et al. [63] was the only study that performed an external validation, i.e., used data collected outside the study's experimental protocol to validate the system. As well as the data collected from 20 subjects (aged between 65 and 70) within their study, these authors also used data from 57 subjects (aged between 20 and 47) from the MobiFall dataset [70]. The remaining studies performed only an internal validation, i.e., validate the system using only data collected within the same study. Cross-Validation (CV) was the most used validation method using both K-fold [57, 65, 66] and Leave-One-Out (LOO) [54, 55, 58]. The Holdout validation method was used in three studies [56, 59, 64]. Saadeh et al. [63] did not explicitly mention the validation method used. Lastly, Yang et al. [60] performed validation without using an algorithm. Their validation process consisted of comparing the features extracted from their smart insole system during the performance of four environment-adapting TUGs against video ground truth references. Concerning the references measures for classification, five studies [54–58] used the clinical scale scores obtained at the baseline assessment as the reference measures for comparing the algorithm's classification outcome. The algorithms developed by these 5 studies attempted to estimate the baseline clinical scale scores based on the wearable sensor data collected from the subjects. A group

of four studies [63–66] labelled the data based on the activities performed. Thereby, data samples were labelled as fall risk/pre-fall or normal/ADL events and were used as the reference values to compare against the algorithm's outcome. The ACC, Sensitivity (SENS), and Specificity (SPEC) were the most used performance metrics to validate FRA system's performance. Nevertheless, the mean error is also used by some studies that predicted clinical scale scores [55, 57, 58].

2.2.7 Clinical Highlights and Future Directions

Several reasons may contribute to the emergence of wearable-based FRA solutions: i) the advances on the current used sensing technologies; ii) the used algorithms; or iii) the introduction of innovative wearable sensors that record meaningful data for this assessment. Regarding this last topic, the advances of physiological sensors can play an important role by providing meaningful metrics underlying a subject's biomechanical reactions to falls. Future work on the FRA field may focus on a multifactorial approach to assess the risk of fall, comprising meaningful data provided by wearable kinematic, kinetic, and physiological sensors [19]. Nevertheless, it is essential to perform a trade-off between the number of sensors used, which should be the lowest number possible, and the system's algorithm performance, that should be as high as possible. FRA systems must be user-centred designed so that the user feels compliant with the designed sensor system, in order to be able to use it for long periods of time without any issues [19]. It is also necessary to plan and perform a suitable and reliable validation of the performance of the FRA systems [71]. Hence, future work should also focus on the identification of gold standard external validation sources, i.e., public datasets, in which systems could be benchmarked. This would provide a reliable comparison between the different literature FRA systems. In this regard, as these systems are intended to be used by the elderly or subjects with mobility deficits, an effort should be performed to validate the systems with data collected from these target populations.

2.3 Review: Robotic Devices for Personalised Fall Prevention

High fall risk individuals are constantly threatened by the unpredictability of the occurrence of gait perturbations, which can happen in a wide range of scenarios during the everyday living. Although these subjects are able to produce reactive responses to counteract the LOB, they are generally not agile and strong enough to avoid falling [40]. According to the overwhelming prevalence and harmful consequences associated with the occurrence of slips or other types of fall, recent literature has attempted to implement fall prevention strategies to mitigate fall incidence among the elderly. Thus, different assistive devices have been robotised personalising the fall prevention techniques according to the user needs and level of mobility. This review aims to present current fall prevention solutions for robotic canes, smart walkers and wearable assistive devices (except exoskeletons), as well as their limitations and challenges.

2.3.1 Search Strategy

An exhaustive literature review based on three databases was conducted to have a better knowledge of robotic canes: Scopus, Web of Science and IEEE. In a primordial phase, an iteration table was created for each database, with a set of keyword combinations in order to obtain the best search terms for a successful review. The chosen keyword combinations were “Robot cane” OR “Robot walking aid” OR “Cane type robot” for Web of Science and IEEE Xplore, and “Robot cane” OR “Robot walking aid” OR “Cane-type robot” OR “Cane-type robot” AND NOT “sugar cane” for Scopus. A comprehensive survey was also carried out on Scopus and Web of Science to identify smart walkers who have fall prevention or detection strategies. The following keywords were used: ”Walking support”AND fall, ”Smart walker”AND fall, ”Smart rollators”, and ”Walking-aid”AND fall. Due to the limited number of wearable robotic devices for fall prevention, specially to prevent slips, a more cursory investigation was conducted. The points of interest during the analysis of the systems were the following: i) the sensors used and their location; ii) the strategy and algorithm implemented to prevent falls or imbalance events; and iv) the algorithm developed.

2.3.2 Search Results

Taking into account the research on robotic canes, a total of 1506 results were found using the mentioned keyword combinations. The review of these articles was performed based on the PRISMA flowchart, as illustrated in Fig. 2 [72]. After removing 423 duplicates and 1026 articles based on title and abstract, resulted in 57 full-text articles assessed for eligibility. Following a complete reading of the eligible articles, 17 were excluded for not meeting the proposed eligibility criteria, which revealed that they were not relevant to the study in question. This selection concludes with 40 articles included in the final review, however only 9 articles present fall prevention strategies. To round out the information, 8 more articles on smart walkers and 3 articles on wearable robotic devices for slip avoidance were included.

2.3.3 Robotic Canes

To protect the user’s safety, the robotic cane must intervene to prevent a fall when an emergency situation is detected. To accomplish successful fall prevention, efficient approaches must evaluate numerous characteristics within a small time frame capable of giving the opportunity to the user to regain the balance, namely: i) an analysis of the direction of the fall; ii) the relative position and orientation of the cane at the beginning and conclusion of the fall; and iii) the interacting forces applied to the cane. Electronic sensor-based devices are implemented in these robotic canes to acquire important information of: i) the user, such as the user’s gait status and gait phase recognition; ii) the robot-user interaction by detecting the user intention of movement with forces applied on the cane; as well as iii) important information about

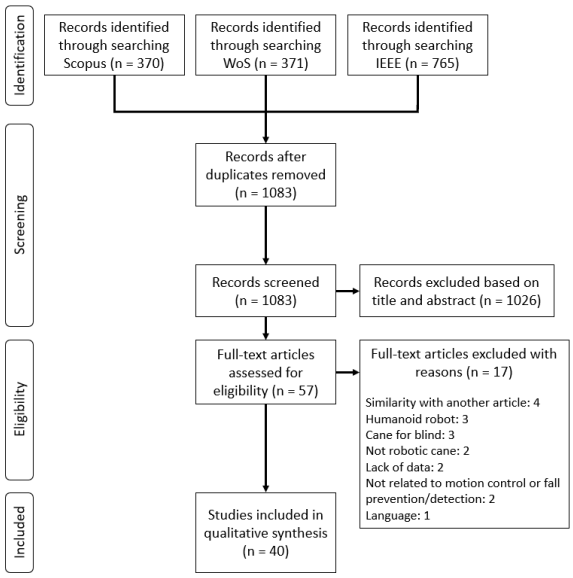

Figure 2: PRISMA flowchart of the Review on Robotic Canes.

the cane itself, such as the cane relative position, velocity and orientation. The following sensors are commonly implemented: i) axial force/torque sensor; ii) IMU; iii) Laser Range Finder (LRF); iv) force sensor; v) tilt sensor; vi) camera; vii) ultrasonic sensor; and viii) infrared sensor.

Four canes implemented fairly similar fall prevention approaches [43, 73–75], since they shift the robotic cane to a favourable and strategic position based on the user's attitude and the direction of the fall. As a result, the users will be able to support their body weight on the robotic cane, allowing them to maintain their balance and prevent falling (Fig. 3.a). In the case of canes made by [43, 74, 75], which have a universal joint for the first two and a revolution joint for the last, the angle of the robotic cane rod can be altered and regulated to give extra help. This strategy can strengthen the stability of the cane during the fall, preventing it from toppling over owing to a strong shove. According to Di et al. [43, 76], the optimum method for preventing falls using a cane's tiltable rod is to place it with the falling direction and the tilted direction of the cane stick in the same line but in the opposite direction.

Canes from Fujimoto [77] and Van Lam [78] are based on the inverted pendulum model in order to have a robotic cane in self-balance. Basically, when the user applies forces in the cane, as in a fall event, the cane will assure a favourable position to aid the user throughout the fall. This procedure is accomplished by moving the cane in the direction of the applied forces, allowing the cane to retain its balance and remain upright. Cane from Fujimoto [77] employs the angle of the cane in respect to the plane of displacement as a key parameter, whereas cane from Van Lam [78] uses the sensing forces applied to the cane's rod as its main parameter (Fig. 3.b). These canes, which must self-balance to remain upright, have minimal strength, instability, and safety, making them unsuitable for older users and those with restricted mobility.

The apparent dynamics of the robotic cane can be altered to prevent the user from falling by changing the braking torques of the wheels. Braking system of the Suzuki's cane [79] limits the speed of the movable

a) b)

Figure 3: Fall prevention methods. (a) Movement of the robotic cane to a favorable and strategic position [43]. (b) Cane self-balance and its capability to maintain balance and move alongside the user [78].

base, so assisting and preventing the user from falling. This passive system is innately safe since they cannot move accidentally; nevertheless, due to the absence of active movement when a fall is detected, it may not be optimal for fall prevention. Because it can only keep the cane from moving, there may be times when it needs to shift position in order to provide a steady and firm support to the user, ensure the balance and stability of the system's Centre of Mass (CoM), and avoid the fall. Although Ito's cane [80] is a prototype with certain drawbacks in terms of its not-so-sturdy structure and motion control, which requires the user to lift the 1.2 kg cane during walking, it proposes a novel way for ensuring cane stability when walking in unstable and irregular circuits. Overall, this walking assistance technology, which also attempts to avoid falls, has limited capacity to give security and stability to sustain the body weight in a fall event.

2.3.4 Powered Orthosis

Wearable robotic devices can also stop falls from happening, particularly slips. It does, however, demand certain requirements for detection and actuation. Wearable robotic devices must have technology capable of detecting perturbations in milliseconds, as well as a motorised joint with time-effective actuation. In the literature, there are some examples related to fall prevention. Monaco et al. [40] developed an Active Pelvis Orthosis (APO) to aid with balance recovery following unanticipated slip disturbances. The scientists based their approach on the idea that increasing stiffness at the hip joints could aid participants in recovering from treadmill slip-like disturbances. Their system presented: i) an assistive torque with the ration of 0.2 Nm/kg and duration of 0.25 s; and ii) LOB detection time between 0.3s and 0.4s. Hopf oscillators were integrated in the detection system. Perturbations were recognised by comparing the actual APO's hip angles to the hip angles predicted by a pool of adaptive Hopf oscillators in real time [13]. The error between both signals was used as input for an adaptive-threshold algorithm, i.e., the responsible for the detection of perturbations.

With the same purpose, Mioskowska et al. [37] presents a wearable knee assistive device capable of actively extend the trailing leg's knee by means of a knee brace once a slip perturbation has been detected. The idea is to quickly restore foot contact with the ground and thus extend subject's BoS. The

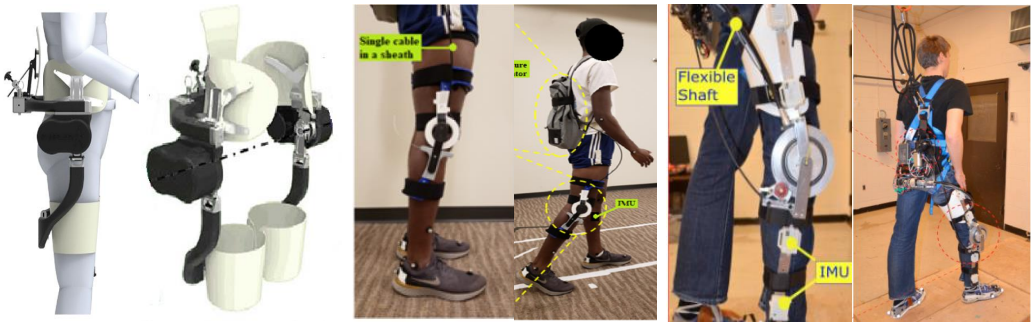

(a) (b) (c)

Figure 4: Literature slip-related fall prevention actuation systems. (a) Monaco et al. [40]. (b) Mioskowska et al. [37]. (c) Trkov et al. [81]

average actuation time for device extension was 0.082 and 0.072 seconds, respectively, from the initial 90 to 0 degrees and 60 to 0 degrees. Furthermore, the technology was demonstrated to stretch a human knee more than 30 degrees in 0.4 seconds. There was no indication of detection time.

Like Mioskowska, Trkov et al. [81] developed a Robotic Knee Assistive Device. They do, however, provide assistive knee torque to the leading leg rather than the trailing leg, as Mioskowska did [37]. The magnitude of the desired torque (up to 40Nm) is established by the linear feedback between the actual and desired knee angle positions and velocities, i.e., operates with an impedance and torque feedback control. It can generate the maximum torque magnitude within less than 0.2 s. Despite the absence of detection timings, the authors reveal that this device employs IMU data as input to the detection algorithm. Figure 4 depicts a general overview of the actuation system from the 3 previously described studies.

2.3.5 Smart Walkers

Through the search process just a few smart walkers were discovered. Stereo cameras, LRF or force sensors are the main information collected to be used as input in these algorithms. RT Walker [82–84], a passive device equipped with rear wheels with powder brakes, was the subject of experimental tests with different sensors. In [82], two LRF were used to create a 7-link human model, which allows the generation of a stability region considering the support polygon formed by the walker and the user's feet. One LRF was located at the same height as the user's hip to measure the distance along the V direction between the walker and the user. The other laser was placed at the base of the walker and measure the distance between the user's leg and the walker. Further in [83], two stereo cameras tracked the head, hands, shoulders, and hip to get the Three-Dimensional (3D) upper body model to classify activities including falls. The upper body centroid position extracted by a depth camera was then used to categorise falls regarding their direction [84]. A Hidden Markov Model (HMM) detected 98.75% of the falls.

Other studies used similar sensors to gather data for their algorithms. Mou et al. [85] used a LRF and force sensors on the handle to classify three kinds of gaits (festinating gait, Freezing of Gait (FOG)

and normal gait). When a sudden push is detected, the walker stops. Azqueta-Gavaldon et al. [86] used depth cameras to measure the distance between the user's leg and the rollator. Healthy subjects simulated forward falls, namely freezing of limbs, stumble, and LOB. When the distance between the user and the rollator is higher than a threshold, the rollator stops, preventing a fall (brake activation: 80-90ms) with an overall ACC of 95%. Xu et al. [42] also used a LRF and force sensors on the handle. However, the Support Vector Machine (SVM) was the approach used to classify the state of gait and, consequently, detect a possible fall. If the user is falling the walker stops moving.

Irgenfried et al. [87] developed a walker only with a 6D-force/torque sensors, which information is used as input to a mathematical model of the human body. Data from simulated falls revealed a peak in the sensor values that can be used to detect a possible fall. Once again, the authors suggested stopping or slowing down the walker. Contrarily, Huang et al. [88] used wearable and non-wearable sensors to detect possible falls. The user is instrumented with IMU in the lower limbs and trunk, while the walker is equipped with force sensors on the handlebar. This combination of information allows estimation of the position between the midpoint of the feet and the Centre of Pressure (COP). Different types of falls were simulated and when the possible fall is detected, the walker brakes and stops.

2.3.6 Clinical Highlights and Future Directions

Studies about robotic canes present some limitations. Clinical gait experiments involving the elderly or those with conditioned mobility are lacking, demonstrating that the systems developed were not tested in the real environments. Furthermore, only one cane offers an active fall prevention method with a mechanism that uses cane movement that does not require the user to wear wearable sensors. Another significant drawback is that the sensor systems of many robotic canes in the literature do not identify the user's gait phases, which is an important element for gait monitoring and possibly fall detection. Considering powered orthoses, the ideal scenario would include the assistive torque supply to all the lower limb joints from both legs upon a slip. Trkov et al. [81] and Mioskowska et al. [37] assisted only one joint. In fact, such an approach would increase the computationally and mechanically complexity of the fall prevention strategy possibly contributing to an ineffective fall prevention. However, scientific literature is poor regarding real-environment tests, mechanical information about the actuation units, importance quantification of each joint in the biomechanical response to a slip event. Smart walkers' prevention strategy consisted in stop the robotic device when the possible fall was detected. Although it ensures safety for forward falls, it is required to investigate lateral and backward falls to mitigate fall occurrences. Tests in a real setting are necessary, just like with robotic canes and powered orthoses. Furthermore, it is feasible to confirm that there are just a few available options for these robotic devices on the market.

2.4 Review: Real-World Falls

To face the dataset problems mentioned, at least two projects, both funded by the European Commission, focused on data collection from daily-life activities from elderly in the hope to obtain data from real-world falls: the SensAction-AAL [33] and the FARSEEING [31]. The SensAction-AAL project intended to assist older people by maintaining independent mobility and daily life activities, and reduce the consequences of falls and injuries. They introduced smart body fixed sensor-based technology allowing medical professionals to initiate interventions in the home environment. In 2013, the FARSEEING project took place to collect more real-world falls from a wide community of elderly people. A total of 10 partners distributed in 5 European countries worked together to collect data from older adults in their own environment by using an inertial-based wearable system at lower trunk and/or thigh. The main goal was to collect also data from falls for further investigation on prediction, identification and prevention of falls. Fall signals were recorded with a Samsung Galaxy S3 smartphone worn in a belt or a uSense sensor device attached with sticky tape. The smartphone or sensor device was worn at the lumbar position L5, close to the CoM. Both devices have similar measurement characteristics: all signals contained triaxial accelerometer (both systems: ±2 g), gyroscope (uSense: ±250°/s , smartphone: ±2,000°/s), and magnetometer data (both systems: ±1,200 μT) sampled at 100 Hz. This review aims to understand what works have been developed with real-world fall data and scrutinise them to understand crucial topics for future investigation.

2.4.1 Search Strategy

A comprehensive search was accomplished in order to understand for what purpose the data on real-world falls are used among the scientific literature. Thus, the following topics were covered: i) what systems were used to collect real-world fall data as well as their technical characteristics (e.g. sampling frequency, number and types of sensors and systems, system location on human body, battery life); ii) how raw data is processed and what features are estimated; iii) how and what algorithms or methods are implemented considering the article's purpose; iv) how the experimental protocol was designed, i.e., for how long a subject was accompanied, how the fall was reported or what was the eligibility criteria used to select volunteers; and v) what researchers did to validate approaches and/or algorithms. On December 9th, 2020, the search was completed in the IEEE Xplore Digital Library, Scopus and Web of Science with the keywords ("Real-World Fall"OR "Natural Fall"OR "FARSEEING"OR "SensAction-AAL"OR "Real fall") AND ("Fall Detection"OR "Fall Prediction"OR "Fall Prevention"OR "Fall Prevention"OR "Falling").

2.4.2 Search Results

A total 460 articles were found. As eligibility criteria, articles were selected if they presented the use or collection of real-world falls data. A total of 13 articles respected the mentioned criteria and were included in

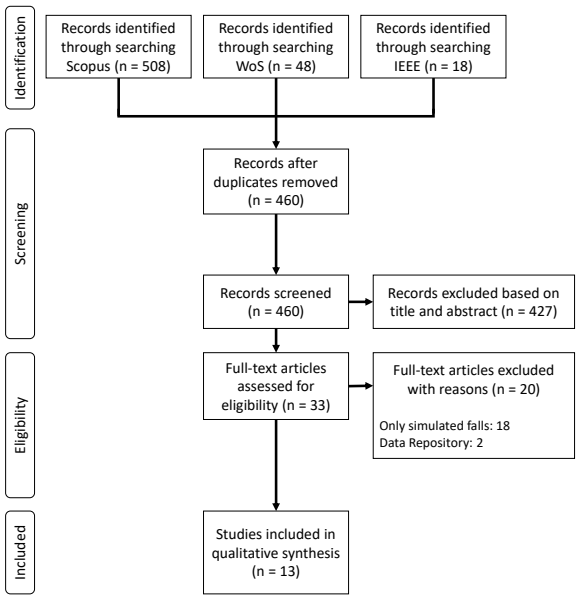

Figure 5: PRISMA Flowchart of the Review on Real-World Falls.

this analysis. The following figure depicts the article selection process based on PRISMA for this review. The included articles reveal four different purposes: i) design, improvement and/or benchmark of fall detection algorithms [89–98]; ii) quantify the trunk and neck's involvement in stabilizing the head during falls [99]; iii) analyse the characteristics of the on-ground and recovery phases after a fall [100]; and iv) compare the accelerometer signals between real-world falls and simulated falls [101]. The next subsections will be responsible for deepening the analysis of each one of the purposes presented by the selected articles.

2.4.3 Fall Detection Algorithms

The non-use of real-world fall data is commonly considered as a limitation by authors that developed fall detection systems. This limitation is based on the hypothesis that fall data from healthy subjects collected in controlled environments are not representative of real-world fall data [31]. The dataset used for the development of this type of algorithms generally presents a large number of falls than normal, in addition to the fact that several other daily activities are not considered and that can be confused with falls. Different purposes can be found on this type of articles: i) performance benchmark of existing algorithms; ii) development or improvement of algorithms; and iii) comparative analysis to find the most relevant features and/or machine learning algorithms. Ten of the thirteen selected articles address algorithms for fall detection, although with different purposes. Three articles benchmark the performance of published fall detection algorithms when applied to real-world fall data [89, 94, 95].

2.4.3.1 Performance Benchmark of Algorithms

Four articles benchmark the performance of published fall detection algorithms when applied to real-world fall data [89, 94–96]. Bagalà et al. [89] benchmark the performance of thirteen fall detection algorithms with data from twenty-nine real-world falls collected within the scope of the SensAction-AAL European project. They directly used the data as input to the published threshold-based algorithms, estimated their performance and compared the results obtained with real-world falls and those obtained by the authors who developed these algorithms. As a main result, the algorithms performance was much lower than the values obtained on simulated falls. The SENS and SPEC averages of the thirteen algorithms were 57.0%±27.3% and 83.0%±30.3%, respectively. Aziz et al. [94] performed a similar approach, but this time focused on a single machine learning algorithm, i.e., the SVM, since its performance is higher when compared to other algorithms, e.g. [94] performed a similar approach, but this time focused on a single machine learning algorithm, i.e., the SVM, since its performance is higher when compared to other algorithms, e.g. DT or K-Nearest Neighbours (KNN). A total of five young adults (30.8±4.1 years) and nineteen older adults (87.4±6.1 years) went about their daily-life activities while wearing seven and four tri-axial accelerometers, respectively. These sensors were mounted on the ankles, thighs, waist, sternum and head for young adults, and on the ankles, waist and sternum for the other group. Data from falls was exclusively obtained from older adults that were resident at New Vista Long-Term Care facility in Burnaby, British Columbia. Falls were confirmed through a surveillance system with 48 cameras. As features, the authors used the means and variances for each of the Anteroposterior (AP), Mediolateral (ML) and V axes over 2.5 s time window, and results demonstrate that the implemented system was able to detect 8 out of the 10 falls in older adults using signals from a single accelerometer (waist or sternum). Moreover, the system showed lower False Positive Rate (FPR) than the existing fall detection systems. Silva et al. [95] combined the real-world FARSEEING dataset with a dataset of simulated falls and non-falls from young volunteers to train a set of supervised classifiers for discriminating between falls and non-falls events. Following the experimental protocol described by Noury et al. [102], these authors collected simulated falls and non falls using a smartphone inside the trousers' pocket from the volunteers. After resampling FARSEEING data to 100Hz and oversampling real-world samples in the train set, they used the following algorithms: KNN, DT, Random Forest, Multi-layer Perceptron and AdaBoost. As features, they computed the mean, standard deviation, median, median deviation, maximum, minimum, energy, Root Mean Square (RMS), inter quartile range, histogram (10 bins), skewness and kurtosis. As main outcome, they confirm that a model trained with simulated falls generalise better when tested with real falls, than the opposite. Yu et al. [96] opted for a HMM to detect falls automatically using a single motion sensor. They used data from FARSEEING database and from ten college students that simulated falls. The younger group used tri-axial accelerometers (±4g; 12.5Hz) at 5 different locations: i) neck (necklace pendant); ii) waist (keychain); iii) chest (left shirt pocket); iv) right side of body (right trouser pocket); and v) left side of body (left trouser pocket). Their results

significantly outperform benchmark systems, which reveals the advantage of sensor orientation calibration. The algorithm achieves a higher positive predictive value (0.981) when using data from the younger group when compared to the value obtained (0.786) when using the data from FARSEEING database. With regard to the limitations of these studies, Bagalà et al. [89] mentioned that the recorded real-falls were from a rare disease population, which cannot be representative of a comprehensive reality. At the same time, tested algorithms are based only on waist or trunk accelerations, which do not represent an exhaustive analysis of the diversified set of published fall detection algorithms. Aziz et al. [94] collected data from more body locations. However, they do not use the same number of sensors in both groups of volunteers. Moreover, they only use one machine learning classifier. This decision was based in only one study among the scientific literature. They also claim that the occurrence of false positives could be related to: i) the relatively similar number of non-fall trials and fall trials simulated in the laboratory experiments; and ii) to non-reported fall events from older adults. Silva et al. [95] performed a transfer learning approach to find the best subset of features and to compare the different machine learning algorithms. They point the lower number of fall samples collected for this work as a limitation, which they claim they surpassed with the oversample process. Finally, Yu et al. [96] also believe that an extensive dataset from real-life senior subjects might improve fall detection results.

2.4.3.2 Development and Improvement of Algorithms

One article [92] used real-world fall data to develop new algorithms for fall detection and other improved a threshold-based algorithm [90]. Palmerini et al. [92] developed a new wavelet-based approach for fall detection. These authors used the same dataset as Bagalà et al. [89] to focus on the detection of the impact phase of a fall. The data were divided into 90% for training and 10% for testing. Subsequently, a 10-fold CV was performed to assess the wavelet-based approach performance that use the acceleration signals the acceleration sum vector as inputs. As a main outcome, it outperforms an Area Under Curve of 0.918. Finally, Soaz et al. [90] used accelerometry-based fall data collected by the Sylvia Lawry Center for Multiple Sclerosis Research and data from simulated events to assess the upper limit of their threshold-based algorithm with multiple features (e.g. gravity acceleration component, acceleration, magnitude of the acceleration vector, angle formed by the V axis of the upper body and the ground, sum of the windowed standard deviation). For data collection, they used the Actibelt, which is a custom-built 3D accelerometer (ADXL 345 BCCZ Analog Devices) that presents high resolution (13-bit), measurement up to ± 6 g, and a sample frequency of 100 Hz. These studies present similar limitations than those discussed previously. Palmerini et al. [92] considered the sample size was small and the recorded real-world falls were mainly from a rare disease population as well as Bagalà et al. [89] mentioned. Soaz et al. [90] also believe the dataset should contain more various types of real fallings, which restricts the ecologic validity of their result.

2.4.3.3 Comparative Analysis

A total of four articles performed a comparative analysis to find the best subset of features as well as the best algorithm. Caya et al. [97] implemented supervised machine-learning algorithms (e.g. DT, Discriminant Analysis (DA), Logistic Regression Analysis, SVM, KNN, and Ensemble classifier) to detect falls using acceleration data from the waist. They used data from FARSEEING database, and fifteen volunteers simulated movements described by the FARSEEING database. The data were computed in features such as mean, standard deviation, variance, kurtosis, skewness, Principal Component Analysis (PCA). The best result was achieved with the Quadratic SVM with an ACC of 95.4% using all features mentioned. Bourke et al. [91]extracted temporal and kinematic parameters for fall detection using exclusively data from the FARSEEING database. Their purpose is to understand what information is important for fall detection and help future algorithms to improve their performance. They computed several features and performed several statistical tests, namely, Kolomogorov-Smirnov test for the distribution of the parameters, and the T-test or the Wilcoxon rank sum test were used to verify significant differences in the listed parameters between falls and ADL sequences. As relevant features, they present the upper and lower impact peak values, posture angle change during the fall and time of occurrence. Bourke et al. [93] also applied a machine learning approach to understand what combination of machine learning techniques and features can result in a better performance for fall detection. Once again, they used only data from the FARSEEING database and computed several features. As main result, a DT presented the best result when employing ten different features (0.88 and 0.87 of SENS and SPEC, respectively). Palmerini et al. [98] recently tested several machine learning algorithms (Naïve Bayes, logistic regression, KNN, random forests, and SVM) using features inspired by a multiphase fall model and a machine learning approach. These authors used a five-fold CV to assess the different algorithms and realised that the SVM is the best algorithm, present a SENS higher than 80%. Caya et al. [97] faced a different limitation from those presented so far, i.e., possible bias in the fall report. The fall and non-fall activities were mainly described by the fallers and the witnesses. On the contrary, the use of surveillance cameras eliminates this risk, although it can interfere in the voluntary's privacy [94]. Also, Palmerini et al. [98] indicated that fall reports did not always align perfectly with the patterns observed in the signals, and they admit the possibility of unreported falls among the ADLs dataset. Bourke et al. [91] only mentioned the non-use of gyroscope sensor data as limitation of their study.

2.4.4 Head Stabilisation

Kuo et al. [99] quantified the neck's involvement in stabilising the head during real-world backward falls in long-term care captured on video. A total of twelve falls from twelve residents in a long-term care (6 female and 6 male; 84.4±7.2 years; 164.7±9.6cm; weight: 56.6±13.3kg) were used for this study and in all of them the head impact was avoided. Further, the authors tracked landmarks on the legs, torso, and head

using an open-source software, namely, the Kinovea. They obtained the position of landmarks, the velocity, acceleration, the spring-dashpot moments, and torso, neck and pelvis angles. With all features computed, the authors implemented a model named Simplified Dynamic Fall, which is capable of reconstruct fall kinematics. As main results, they verified the following values for neck stiffness, damping, and target posture averaged: 24.00±6.17Nm/rad, 0.38±0.16Nms/rad, and 76.2±14.7° flexion, respectively. The stiffness and target posture suggest that the participants actively contracted their neck muscles to maintain the head upright. Thus, the neck strength is extremely important to avoid head impact during a fall. Despite this conclusion, the authors mentioned that the formulas used may be a limitation for this study.

2.4.5 On-Ground and Recovery Phases

Schwickert et al. [100] used fall data from FARSEEING database to perform a statistical analysis to the sensor's characteristics of the on-ground and recovery phases after real-world falls. The authors estimated the trunk pitch angle and used it with the acceleration signals as features for the statistical analysis. Falls with successful recovery, where an upright posture was regained, were different from non-recovered falls in terms of resting. A resting duration longer than 24.5 s (area under the curve = 0.796) after the fall impact was a predictor for the inability to recover standing. Fall signals with and without successful returns to standing showed different patterns during the phase on the ground. The authors mentioned the small sample size and group typology as main limitations. The number of falls should be higher for more strong conclusions, and the subjects were selected from groups with moderate and high fall risk, which do not represent a distributed sample of the community-dwelling.

2.4.6 Comparison of Accelerometer Signals

Klenk et al. [101] compared acceleration signals from simulated and real-world falls. This work was the first article in the scientific community using real-world fall data. These authors collected data from four patients (68.8±4.5 years) suffering from progressive supranuclear palsy, and eighteen students (24.1±1.91 years) recruited to simulate falls. Jerk and variance were computed to be used as input for Analysis of Variance (ANOVA) for statistical analysis. The present findings demonstrate differences between real-world falls and fall simulations, i.e., significant variation. Once again, the recorded real-world falls were from a rare disease population that cannot be generalised to the older population at large. The small size of the dataset is also considered a limitation.

2.4.7 Clinical Highlights and Future Directions

The state of the art reveals a strong tendency for the application of real-world fall data in fall detection algorithms. Ten in thirteen articles compared the performance of existing algorithms with simulated and

real-world falls, developed or improved algorithms, or performed a comparative analysis to find the most relevant subset of features and/or machine learning algorithm [89–98]. A transversal conclusion to several studies is the decrease in the performance of existing algorithms when using real-world fall data [89, 94–96]. This proves that simulated fall data collected in controlled environments does not represent real-life situations. Thus, other authors developed or improved algorithms using real-world fall data [90, 92]. Despite achieving interesting performances, they still have the use of small datasets as limitation. Moreover, comparative analyses suggest SVM as the preferred machine learning algorithm for detecting falls when using real-world fall data [91, 93, 97, 98]. On the other hand, three other articles also carried out analyses on head stabilization during falls [99], on the characteristics of the on-ground and recovery phases [100], and on the accelerometer signals from simulated and real-world falls [101]. Again, the small sample size is pointed as a limitation. More real-world falls should be used to have stronger conclusions. Articles prior to the publication of the FARSEEING database, refer to the importance of the existence of an open accelerometry database of real world-falls for a continuous and independent refinement and validation of fall detection and prevention algorithms [89, 90, 101]. These articles were published between 2011 and 2012 and, at the time, the SensAction-AAL European project was the only known project that provided real-world falls. However, the recorded real-world falls were from a rare disease population that cannot be generalised to the older population at large [101]. Once available, the FARSEEING database provided data for seven selected studies [91, 93, 95–98, 100]. However, it is constantly indicated that the sample provided by the FARSEEING database is small and that better conclusions can be drawn from a larger population sample. Future directions include: i) differentiating falls with immediate recovery, falls with recovery after a certain period, and falls with no recovery at all, or even different severity levels after the fall [98]; ii) more complex models [99]; iii) increase the number of real-world falls and non-fall activities [96, 97, 100]; iv) use other features [97]; v) the distribution of falls and non-falls in real-life should be reflected in the data used for training a classification model [94]; and vi) use gyroscope data [91].

2.5 Review: Provoked Falls

Data scarcity leads to a hunt for alternate solutions, which accelerates technological development. Different sorts of perturbations are employed, and they should be similar to the most important causes preceding fall occurrences in the real-world setting. Slips and trips are the most prevalent occurrences preceding falls [103, 104]. Thus, investigations that induce artificial perturbations frequently depend on the administration of these two types of gait perturbations. Slips occur when the contact between the subject's foot and the floor lacks a sufficient Coefficient of Friction (COF) [105], whereas trips occur when the motion of the swing limb is abruptly disrupted, which can be caused by objects while walking [106].

Previous review studies have addressed different perturbation methods. McCrum et al. [107] investigated the various gait perturbation strategies used in PBT to enhance reactive balance recovery and fall

rate in healthy older individuals. However, by excluding younger adult participants, additional strategies than those employed in older adults may be overlooked. Moreover, Karamanidis et al. [106] wrote a review study that focused on the balance training following slip- and trip-like PBT during treadmill locomotion, however insufficient information is supplied regarding how these LOBs occur during overground walking. This review aims to find the different methods used to provoke slip- and trip-like perturbations to healthy adults during treadmill and overground walking. Hence, the following RQs were addressed: i) "Which methods and walking conditions are used to provoke slip- and trip-like perturbations?"; ii) "Is it preferable to deliver perturbations during treadmill or overground walking?"; iii) "Is it preferable to use a single-belt or a split-belt treadmill to perturb walking?"; iv) "What procedures are implemented to maintain responses to perturbations unbiased?"; v) "Which limb is generally used to apply the perturbations?"; vi) "Which was the participants' walking speed during the trials?"; vii) "What are the main sensor systems used to collect data during perturbation-based protocols?"; and viii) "Are there benefits to apply both slip- and trip-like perturbations?".

2.5.1 Search Strategy

A comprehensive search was performed in the scientific literature in Pubmed, Web of Science, CINAHL (EBSCO), and Scopus databases. This search was carried out using the set of keywords: (gait OR walking OR walk OR locomotion) AND (perturb* OR trip* OR slip* OR balance loss OR dynamic stability OR static stability OR waist pull OR provoked falls) AND (training OR exercise OR adaptation OR adaptive OR repeated OR repetition OR rehabilitation OR task OR responses OR adjustments) AND (age OR ageing OR aging OR aged OR elderly OR old OR older OR senior). The systematic review of McCrum et al. [107] served as inspiration to build the set of keywords. For this review, only articles published since 2016 were considered to find updated trends or evidence regarding gait perturbation paradigms. The eligibility criteria were applied in order to obtain the set of articles that: i) included only slip and/or trip-like perturbations in the experimental protocol; ii) delivered the perturbations unexpectedly; iii) only included healthy subjects; and iv) did not use an assistive robotic device during the experimental trials. Beyond these conditions, the criteria used for title screening were also applied during the abstract's reading.

2.5.2 Search Results

A total of 3622 articles were gathered from the aforementioned databases and 2288 remained after duplicates removal. Afterwards, the papers obtained were screened based on their title. A group of 338 articles resulted from the screening procedure. The article titles in which it was not clear that the conditions stated above were respected were included in the abstract screening. This following selection was based on the careful reading of the abstract of each remaining paper. A group of 110 articles was then obtained through the screening procedure. Since it is not possible to ascertain if the papers fulfilled the eligibility

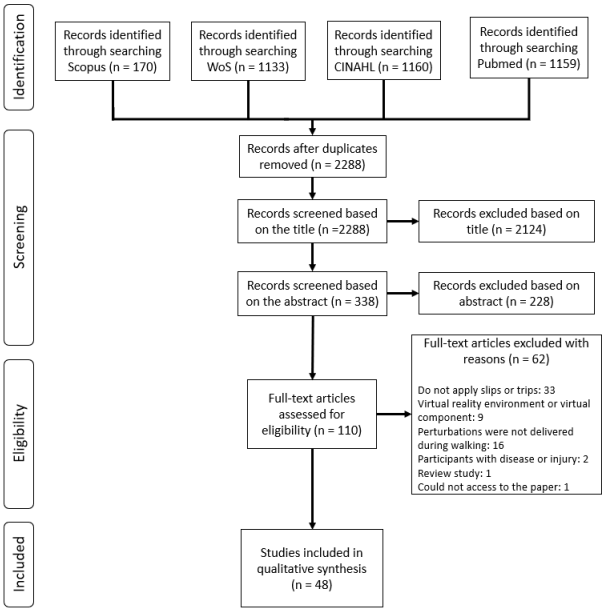

Figure 6: PRISMA Flowchart of the Review on Provoked Falls.

criteria previously defined by only reading the title and the abstract, the remaining articles were read and carefully analysed in order to exclude those who did not respect at least one of the above mentioned conditions. After this analysis, a final group of 48 articles was obtained. Figure 6 depicts the PRISMA flowchart concerning the previously described literature search. From the 48 included studies, slip-like perturbations (40 studies) were more prevalent than trip-like perturbations (15 studies). In addition, 7 studies performed both slip- and trip-like perturbations.

2.5.3 Perturbation Methods

Slip-like perturbations were applied during both treadmill and overground walking with the latter (29 studies) being more prevalent than the former (18 studies). Slips were provoked during treadmill walking by abruptly changing the belt's acceleration to generate an anterior displacement between the BoS and the CoM. This observation is consistent with the findings of Karamanidis et al. [106]. On the other hand, overground walking slips were delivered by movable platforms, slippery solutions, and novel robotic devices. McCrum et al. [107] discovered the widespread usage of movable platforms to cause slip perturbations. The slip-like events were often applied during the Heel-Strike (HS), which is in line with Lockhart [105]. Trip-like perturbations were also elicited during treadmill or overground locomotion. Treadmill walking trips were caused by changing the belt's acceleration, using a brake-and-release system or a tripping device, as Karamanidis et al. [106] verified. On the other hand, overground walking trips were caused by triggering an obstacle release, manual placing an object along the walkway, or using a novel robotic device. Trips were mainly applied during the swing phase of gait.

2.5.4 Treadmill vs Overground Walking

In both slip- and trip-like perturbations, overground walking perturbations outperform treadmill perturbations. Because slips and trips occur while overground walking, the walkway perturbations may be more realistic than the treadmill-based ones. Recent research, however, has attempted to verify perturbation delivery during treadmill locomotion against overground walking [108, 109].

Liu et al. [109] observed that individuals that received baseline overground walking perturbation training had a lower fall incidence and a higher reactive stability against an overground slip applied 6 months after the perturbation training sessions than the group that underwent the baseline treadmill perturbation training. Nonetheless, the treadmill perturbation training group showed higher stability measures and a lower fall incidence than the control group (treadmill training without perturbations), indicating that treadmill perturbation training results in long-term relative preservation of fall resistant skills. Treadmills also allow for the collection of multiple and continuous walking patterns over long periods of time [110], and allow the modulation of the perturbation intensity [111].

2.5.5 Single-Belt vs Split-Belt

Both single and split-belt treadmills have been used to apply treadmill gait perturbations. Single belt treadmills were used in 14 studies [108, 109, 111–119], while split-belt treadmills were adopted in 8 [120–127]. Split-belt treadmills, as opposed to single-belt treadmills, allow researchers to analyse kinetic data from each foot independently by incorporating force sensors into each of the belts. Furthermore, the use of gait perturbations is becoming more standardised and consistent across multiple test participants, allowing to define: i) more accurately the limb that is going to be perturbed; ii) specific velocity profiles for each belt to conduct the perturbation; and iii) automatic onset of the perturbation based on kinetic data from the targeted limb [121, 126]. These features turn the split-belt treadmill better suited to delivering realistic perturbations.

2.5.6 Unbiased Perturbation Response

The authors used several strategies to lessen the predictability of the perturbation events delivered. In general, all of the studies said that the perturbations were meant to be unexpected, and they advised their subjects to react appropriately and strive to regain equilibrium whenever a perturbation was administered. As a result, trials to familiarise participants with the perturbations were not conducted in order to decrease participants' learning effects and gait adaptation to the perturbations. Previous research revealed that after the initial perturbation exposure, participants change their gait characteristics in order to adapt to the perturbation circumstances [128, 129]. Some authors, for example, only tripped or slipped their participants once [35, 115, 123, 128, 130–136].

2.5.7 Common Perturbed Limb

The perturbations have been used in studies on one or both legs. Some works, however, did not specify which leg or legs were affected [111, 118, 128, 130, 137, 138]. The perturbation was administered to only one leg in the majority of the investigations (35 studies). The perturbations were delivered to the right and left legs in 22 and 8 papers, respectively, whereas the 5 remaining investigations detailed perturbation delivery to the dominant limb. It is also worth noting that two of the eight studies that only affected the left leg classified that leg as the participant's non-dominant limb. There is clear evidence that the perturbations should be applied to the right limb rather than the left. This might be connected to the fact that the vast majority of people have right-side dominance [139].

2.5.8 Walking Speeds

Subjects were instructed to walk at a self-selected speed on 23 of the 41 studies that included trials under only one walking condition, either treadmill or overground locomotion, 10 studies applied a fixed walking speed across all participants, 2 studies described the application of a normalised walking speed specific for each subject, and 6 studies did not mention the walking speed adopted. The seven studies that applied perturbations while on the treadmill and overground walking revealed various velocity paradigms for each walking condition. For example, Yang et al. [113] and Lee et al. [119] described the use of 1.2 m/s treadmill speed and a self-selected speed while walking along the walkway. Other studies either reported self-selected walking speeds on both walking circumstances [108, 109] or did not describe the overground walking speed [114, 119, 140]. Regardless of the walking condition used, the majority of the authors advised their participants to walk at their own pace. This is consistent with the findings of McCrum et al. [107]. In the overground walking studies [128, 131–134, 141–150], subjects chose their own comfortable speed, whereas in treadmill walking studies, participants were instructed to either ambulate at their own self-selected speed [116, 118, 125, 130, 137, 151] or to choose a speed from four available options (1.2, 1.0, 0.8, or 0.6 m/s) [111]. Although walking at that comfortable pace simulates more realistic walking conditions, it is more difficult to provide perturbations that are equally taxing to all individuals.

2.5.9 Monitoring Systems

The Optical MoCap devices were the most used sensor systems (45 out of 48 studies). Data from these systems were used to compute subject's stability through the computation the CoM position and velocity [108, 120, 123, 125, 128, 140, 143, 152–154] and for the analysis of spatial-temporal gait parameters [121, 124, 146, 150, 154], upper limb segment angles [120, 125, 154], lower limb segment angles [121, 141], joint angles [35], and joint moments [141, 153]. Force data were acquired in 32 studies by force plates either installed beneath treadmill's belts [120, 124] or embedded in some position along

a walkway [146, 153]. These sensors are commonly used to detect the reliable timing of perturbation application rather than to collect data for further analysis [120, 126, 154, 155]. Participants in five trials were instrumented with wearable inertial sensors to collect data from different human body segments [112, 136] and to feed gait event detection algorithms [149]. Lastly, EMG sensors were considered in all studies, since it may provide useful information about muscles activated during imminent fall risk situations [156]. This information helps to understand how to perform a certain motor task [157], and promote an evidence-based fall prevention treatment [64].

2.5.10 Multiple Perturbation Application

Six of the included studies [125, 126, 149, 152, 158, 159] gave each subject both types of perturbations. If the study's focus is on understanding PBT, using both forms of perturbations may be more appropriate than applying only one type [125, 126, 152, 159]. The use of just slip-like perturbations, according to Okubo et al. [152], may cause people to acquire recovery techniques including the anticipatory adaptation of anterior shifting the CoM, which may increase the danger of tripping. Therefore, these COM predicted modifications must be reduced by the combined use of both slips and trips in order to prepare people for real-life disturbances. Furthermore, in order to simulate more realistic perturbation circumstances, research [159] used slips and trips in a mixed sequence. This would guarantee more organic responses to the imposed gait perturbations, similar to the situation in real life. Nevertheless, a more complicated experimental approach can result from include both kinds of perturbations.

2.5.11 Clinical Highlights and Future Directions

This review examined the present state-of-the-art in the delivery of artificial slipping and tripping disturbances. Slip perturbations were provoked during treadmill walking by changing the belt's acceleration or during overground locomotion by using: i) a movable platform; ii) a slippery solution; or iii) novel robotic devices. Trips were provoked during treadmill locomotion by: i) changing belt acceleration; ii) using a brake-and-release-system; or iii) using a tripping device. Overground trips were elicited by: i) triggering an obstacle; ii) manually placing an obstacle along the walking path; or iii) using a novel robotic device. Despite the fact that most studies induced perturbations during overground walking, treadmill devices' capacity to produce highly standardised perturbation delivery and gather continuous walking patterns over long periods of time has highlighted their usage. Split-belt treadmills appear to be more successful in causing perturbations than single-belt treadmills. Each research tried to generate settings that would reduce participants' awareness of the perturbations as well as learning effects to counteract the perturbations. There was clear evidence for perturbations being sent to the right limb rather than the left.

It is recommended that future research choose the perturbed leg based on side-dominance. In most research, participants were instructed to walk at a self-selected speed, albeit this technique does not

ensure that the perturbations provided are equally difficult for all people. In order to offer participants with comparable dynamic settings, authors are advised to compute subject-specific gait speeds for this purpose. The majority of the sensor systems employed to gather data throughout the tests were optical MoCap devices. Future studies are advised to make use of EMG sensors in light of the pertinent data they offer in order to better comprehend and quickly identify human reactions to gait disturbances. Additionally, applying both slip- and trip-like perturbations during the same experiment would cause the LOB to respond in a more realistic and natural manner, resulting in a more effective PBT than if only one kind of perturbation were used. The distance between falls in the lab and in real life may be shortened by the reliable use of either slip- or trip-like perturbations to simulate actual LOB occurrences.

2.6 Review: Virtual Reality Role in the Perturbation-Based Training

Age-related decline only emphasises the importance of creating and implementing effective VR balance training programmes that target posture and balance control through effective sensory integration. This integration involves quick recalibration of visual, vestibular, and somatosensory information for fall avoidance [51]. There is extensive evidence that the proprioceptive and exteroceptive feedback associated with the execution of skilled tasks induces profound cortical changes associated with motor learning and that humans can transfer motor learning to a real-world environment because it uses visual, sensory, and auditory feedback [160]. Furthermore, it provides a chance to raise the duration, intensity, and mass practise required to induce neuroplasticity, as well as significantly increasing the participant's motivation [161].

The present review aims to find studies that use immersive VR through a HMD to introduce sensory disturbances in subjects, triggering dynamic or static anticipatory and compensatory postural behaviours. Thus, it will be possible to answer the following questions: i) "Can a virtual reality headset introduce imbalances through visual perturbations?; ii) Can they cause postural reactions typical of a fall?"; and iii) "Which visual perturbation challenged the participants' balance the most?".

2.6.1 Search Strategy

A literature search was carried out in the IEEE Xplore, Scopus, Web of Science, and PubMed databases. Combinations of the following keywords were used for each database: "virtual reality" OR "virtual environment" OR "immersive" AND "perturbation". No filters were applied in each database to restrict searches. The studies were chosen under the following inclusion criteria: i) the study was conducted using a HMD; ii) sensory disturbances were delivered to the participants; iii) physiological, neuromuscular, or kinematic data were reported to study participant's reaction to perturbations.

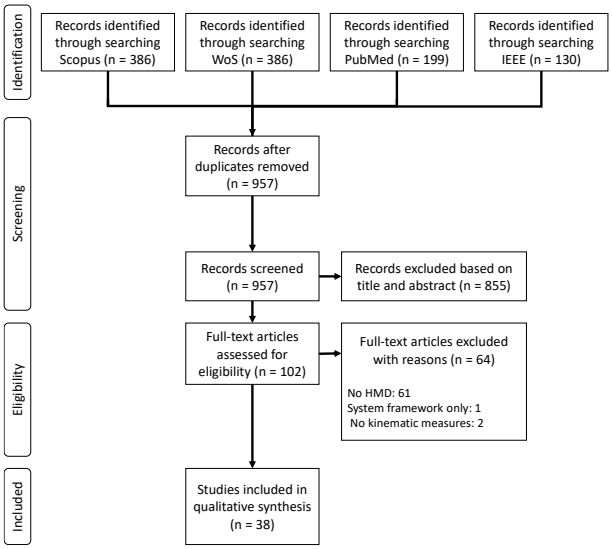

Figure 7: PRISMA Flowchart of the Review on VR-based PBT.

2.6.2 Search Results

The initial search resulted in a total collection of 1101 publications. From this total, 386 publications were imported from Scopus, 130 from IEEE, 386 from Web of Science, and 199 from PubMed. As duplicates, 144 were identified and removed while 855 publications were excluded by title or abstract for not meting the inclusion criteria. Of the 102 complete articles or conference papers that remained, 51 were excluded for using VR that they consider immersive but that does not use HMDs. Thus, 42 publications underwent a full reading, a process that excluded 6 articles for not evaluating the subjects' physiological, kinetic or kinematic parameters after disturbances. In this full reading process, 2 articles were included that fulfilled the inclusion requirements, by references. Altogether, 40 articles were included in the subsequent analysis. Figure 7 depicts the PRISMA flowchart.

2.6.3 Studies Goals

All studies aim to investigate compensatory reactions induced by visual perturbations. Some channel this analysis of postural adjustments to understand differences introduced by advancing age or by diseases. Others analyse these postural reactions when visual information discordant with proprioceptive information is introduced, when placing the participant in threatening situations, or to perform an objective balance assessment, or balance training. The objectives of the studies are mostly divided into two aspects: gait analysis or standing postural analysis. Both can study anticipatory and compensatory reactions to visual disturbances introduced by an optical flow in the VE. More specifically, 18 studies attempt to understand changes in gait patterns, 8 of which during overground walking [30, 162–168] and 10 during treadmill walking [169–178] while the remaining studies analyse postural reactions in upright stance to visual perturbation [179–199], either in bipedal stance or one leg stance. Whether walking or standing upright, the

analysis is carried out without exception when the participant is exposed to visual or physical disturbances of different types, namely: i) continuous and multidirectional; ii) transient; iii) discrete; iv) rotations around the axes (single or multi-axes); and v) dissonant or concordant proprioceptive and visual information.

2.6.4 Visual and Physical perturbations

Given the restriction of the use of VR through an HMD, the most common type of disturbance induced in the subjects was visual disturbance, also called optical flow [200]. It induces modulations in gait patterns and in postural control performance [201]. Can be stabilising when appropriate or destabilising when conflicting. During locomotion, there is a decreased stabilisation pattern due to artificial changes in the optical flow [202, 203]. These visual disturbances create the illusion that a correction is necessary. This perception of the need for correction makes the responses to visual disturbances highly idiosyncratic, while the responses to mechanical disturbances are very consistent. This inter-subject variability makes the introduction of visual disturbances a good way to assess the risk of falling, since the reaction reveals the dependence on visual feedback. Visual processing is a critical component of balance and gait stability [204]. For this reason, all studies use visual disturbances that consist of a change in the HMD display. However, some studies combine optical flow with a physical disturbance. Depending on the objective, these disturbances can be concordant or dissonant. In most articles, visual disturbances consist of rotations or tilts on the Roll, Pitch and Yaw axes, translations on the AP, ML and V axes, or overlapping oscillations in the visual field, in the AP or ML axis directions. Moving items in a virtual world can also be regarded a visual disturbance since they change the sensory feedback information. Lubetzky et al. [194, 195] used animated objects with variable speeds to trigger participant's postural changes. Virtual vertigo situations are a threatening condition that alters balance in a static position or during gait, increasing the weight of proprioceptive and vestibular reflexes [205]. Two studies also used a visual field perturbation to simulate a fall on stairs: instantaneous translations on the V axis of the VE, which transported the subject from the top of a staircase to some steps below. Finally, several authors have combined physical and visual disturbances to examine the interaction between distinct sensory systems, i.e., they have changed the stiffness of the gait support surface, in accordance with the visual feedback or not.

2.6.5 Virtual environments

Most of the VEs were created with VR game engine softwares, mainly Unity and Unreal Engine. The headsets used in the selected articles have inertial sensors that measure the position and rotation of the head. To avoid cybersickness, they always change the VE in real time in response to head movement, with a high refresh rate. The researchers' VEs are mostly realistic enough to make the experience immersive and provide a sensation of presence. Oldest VEs have monochromatic representations: two simulate a simple corridor and the other only shows moving patterns. Only two studies did not create a VE. Instead, they

captured video in real time from a webcam mounted on the HMD and used that as a VE. As a general rule, researchers did not use the subject's own representation in the form of an avatar in real-time. However, this synchronisation is significant. If 3D objects are presented in a dynamic, consistent, and precise manner, the VE is an ecologically valid platform for presenting dynamic stimuli in a manner that allows for both the veridical control of laboratory measures and the verisimilitude of naturalistic observation of real-life situations [206].

2.6.6 Protocol specifications

The diversity in the intervention duration or the exposure time to VR scenarios has already been pointed out as a limitation in several literature reviews that investigated the use of VR for rehabilitation [161, 207, 208]. The selected studies for this review follow the same trend. However, many of the authors do not disclose the duration of the intervention. Some reveal the duration of exposure to the VE and whether there are pauses between trials to minimise the effects of exhaustion or lack of concentration. In the studies included in this work, the same trend can be seen. In addition, as the objectives are generally to study compensatory adjustments triggered by visual perturbations, many of the authors do not even disclose the duration of the intervention. Some reveal the duration of exposure to the VE and whether there are pauses between trials to minimise the effects of exhaustion or lack of concentration. It is common to find familiarisation periods to get the participant used to the HMD and the VE.

Regarding the studies populations, 22 of them used only healthy young adults for the experiments, while 5 studies used healthy older adult participants only. In 4 studies, healthy young people were assigned to the control group, while older adults participated in tests with VR. Only one paper does not specify the type of subjects, nor their demographic characteristics. The scarcity of control groups is evident, being a common practice only in studies with pathological subjects. Four studies with participants diagnosed with vestibular deficits were discovered in this pathological population. Other pathological individuals with Alzheimer's Disease, Parkinson's Disease, Mènière disease and glaucoma were also tested with VR.

2.6.7 Clinical Highlights and Future Directions

There is an increasing interest in using VR to study balance. Because of the technological properties that allow the user to sense a high level of presence and immersion, HMDs are an excellent technique of introducing visual disturbances. Furthermore, it takes very little physical space, minimal knowledge from researchers, and the price tends to fall, making them highly appealing for this sort of study. As can be seen, these studies are mostly concerned with the human body's equilibrium. Postural balance is explored in both quiet stance and gait. It would be intriguing to mix static and dynamical analysis, bringing research closer to the real-world settings that a subject faces on a regular basis. A person's equilibrium might be jeopardised when walking or standing. The level of complexity and detail of the researchers' VE falls short

of the computer resources and technologies now available, which allow the production of ultra-realistic scenarios. As a result, the sense of presence and immersion was significantly raised, perhaps eliciting more genuine emotions. Non-tested stimuli in these research include audio stimuli and tactile feedback which could upgrade the experience's immersiveness. Other limitations include: i) small sample size of subjects; ii) lack of control groups and non-random allocation; iii) failure of follow-up measures; iv) instead of the elderly, the most examined demographic is young and healthy people; v) space restrictions, which lead some authors to use treadmill instead of overground walking tests; and vi) gather data not available online.

Chapter 3

Project Conceptual Design

This chapter describes the conceptual design and functionalities of senior-oriented assistive devices with fall prediction and cross prevention capabilities. The state of the art described in the previous chapter constitutes a fundamental piece for the establishment of this proposal. The numerous gaps and challenges highlighted in the area of fall prevention and prediction, as well as future directions, drive the present project to mitigate or reduce the incidence of falls, specially among the elderly population, using cutting-edge technology. The solution is divided into two forms of action: i) short- and long-term assessment of the risk of falling, which help elderly, caregivers and clinicians to act on a day-to-day basis and will more objectively support clinicians decisions and diagnosis, removing subjectivity between assessments; and ii) prevent the fall from occurring or minimising their effects through robotic assistive devices, interrupting the chain of negative effects (e.g. injuries, fear of falling, social isolation).

3.1 Introductory Insight

For elders to be physically and socially active, this solution strives to provide them with access to excellent, affordable, and safe healthcare technology. By preventing age-related motor deficiencies on a variety of levels, it will support sustained development in the health and social spheres. The risk of serious damage from a fall is highest in seniors, and it rises with age. Thus, the main goal of the project is to reduce the number of falls and injuries connected to falls by implementing proactive and senior-focused fall prediction and prevention strategies. It suggests a set of senior-oriented robotic devices for personalised fall prediction and prevention on the elderly with varying degrees of motor impairment, hence enhancing their wellbeing. The capacity of technology to support elderly people while they perform ADLs in natural settings will be crucial for a continuous diagnosis and evaluation, in an uncontrolled environment, where the user

is comfortable and where falls really happen. The user is therefore not prepared for the test and the risk calculation takes into account the environment and activities that are really dangerous. Furthermore, users will be able to monitor their risk of falling during the day and motivate themselves to modify their behaviour, and be alerted about risky situations and ADLs, which contributes to minimise fall incidence and their consequencesWith this ongoing user-centred care, it is anticipated that seniors' fear of falling would reduce and their confidence in carrying out their daily tasks will increase. This will encourage increased physical exercise, which will boost social inclusion and motor autonomy.

Through digital solutions, the project aspires to securely include elders in physical activity to support an active and healthy life. They will make recommendations for ADLs to complete or avoid, aiming for a long-lasting behaviour modification in accordance with risk factors, reducing the likelihood of falls. Additionally, they will share eHealth targets to proactively lessen functional ability impairments in elders. Parallel to this, apps will be developed with a focus on the technological limitations of the aged, enabling high adoption rates and enhancing the seniors' tech abilities in light of the expanding demand for digital solutions in health and care. Impact on physical exercise will have a positive ripple effect on social and mental wellbeing, enhancing QoL. It is crucial to ensure that the offered technologies, respecting the user privacy, will enhance physical and cognitive abilities to retain the functional capacity that permits well-being in older age and full involvement in society, in accordance with the United Nations Decade of Healthy Ageing. Daily support and improved physical fitness made possible by the technology developed by this research may avoid fall-related injuries, cardiovascular and neurological disorders, with anticipated advantages on lower healthcare costs, sustainable lives, and an extended healthy life expectancy. The clinical decision for a cost-effective, early evidence-based diagnosis and more successful individualised therapies will be supported by advancements in continuous objective motor and FRAs. Continuous monitoring in natural settings paves the way for new diagnostic possibilities and may help to foresee fall risk circumstances and subsequent health consequences, hence promoting long-term health and social care. Overall, it helps to provide elders with sustainable, individualised care that may support their continued independence, health, and physical activity. Its socioeconomic influence extends to all ageing societies.

3.2 Project Conceptual Design

In order to address these issues in the field of fall detection and prediction, this PhD thesis seeks to develop and validate real-time fall prediction and prevention algorithms using diversified human gait monitoring systems. This innovative technological solution presents two approaches to the identified challenge. Firstly, the evaluation of the falling risk, whether short or long term, will be handled with a view to its real-time application. To that purpose, and in order to conduct a successful evaluation, the following steps must be taken: i) real-time assessment of gait and balance; ii) recognise ADLs; iii) use multifactorial user's information; iv) predict long-term fall risk more regularly , i.e., perform future fall prediction at shorter

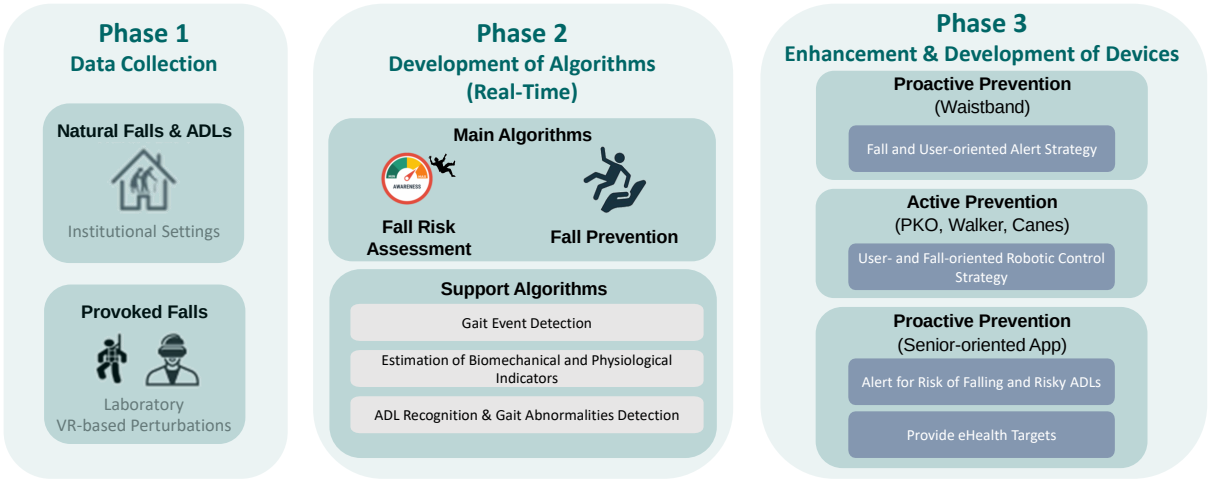

Figure 8: Schematic of the Project Phases. Phase 1: Data collection in real-world settings and controlled environments. Phase 2: Development of algorithms to assess fall risk and prevent falls. Phase 3: Enhancement and development of devices to prevent falls actively and proactively.

intervals to follow-up older adults gait and balance evolution; and v) correlate the assessment result with QoL and ADLs. Secondly, based on the user's continuous monitoring, it is necessary to implement an active daily assistance that includes: i) proactively correcting gait and balance by warning the user through vibrotactile biofeedback; ii) alerting for gait and balance abnormalities; iii) preventing falls through robotic assistive devices; and iv) providing medication, physical exercise, and nutrition recommendations. Both approaches require the collection of multimodal data through literature-driven experimental protocols to be used for the validation of several algorithms, allowing the senior-oriented robotic devices enhancement and development. Thus, the project solution is separated into three crucial phases, as depicted in Fig. 8: i) Data Collection, ii) Algorithm Development, and iii) Devices Enhancement and Development. The descriptions of each of these phases may be found below.

3.2.1 Data Collection

Phases 2 and 3 will only be possible with experimental protocols that allow the collection of data from several sensors. Experimental protocols will necessarily be designed, considering the good practices of the scientific literature. Preliminary phases will rely on healthy subjects to carry out the experimental protocols at BiRD Lab - University of Minho, with the aim of accelerating the process of developing algorithms or tools that can be later implemented in robotic assistive devices , as well as to aid in understanding the biomechanical response to a risky scenario, making it easier to find fall prevention solutions. These experimental protocols were submitted and approved by the University of Minho Ethics Committee and involved human activity in different dynamic environments, from ADLs to the provocation of falls by various mechanisms, whether physical or virtual. Chapters 4, 7 and 8 contain this type of protocols in order to have a first working version of the algorithms to be implemented in the developed prototypes.

It is also expected to collect information from the target population in order to develop, enhance and validate user-centred systems and algorithms. To this end, during the PhD thesis, contact was established with several health care institutions in order to establish a formal partnership with the BiRD Lab. This partnership aims exclusively at contributing to the scientific community, specifically the elderly population, where the institutions are committed to: i) belonging to a panel of stakeholders, where they can suggest improvements to the solution; and ii) facilitate access to volunteers of interest. Contacts focused on the district of Braga and the partner institutions are as follows: i) v*Fundo Social - Braga*; ii) *Centro Social e Paroquial de Sobreposta*; iii) *Centro Comunitário de Prado - Cruz Vermelha Portuguesa de Braga*; iv) *Associação de Reformados ValeD'este - Celeirós*; v) *Estrutura Residencial para Pessoas Idosas de S. José - Póvoa de Lanhoso*; vi) *Casa do Professor - Braga*; and vii) *Associação Cultural e Recreativa de Cabreiros*. It is intended that the elderly can perform various protocols safely. Until the date of this dissertation, seniors from the first 5 mentioned institutions participated in a study that aims to collect data from ADLs for its recognition using AI-based tools (Chapter 6).

3.2.2 Development of Algorithms

The second phase is extremely crucial in the entire project, as it will allow the practical implementation and validation of the devices considered in the solution. As data is collected, this phase progresses in parallel. Thus, this phases proposes three major contributions. First, identify which physical activity parameters predict the risk of falling. The different systems to be used in this project, from those developed by the laboratory to commercial systems for validation, will be able to provide biomechanical indicators (spatial-temporal parameters, joint angles) and physiological indicators (from EMG, EEG, heartbeat and Galvanic Skin Response (GSR) data). Second, provide, adapt and evolve robotic or biofeedback assistance according to each user's outpatient response, fall risk level and QoL. This assistance will be oriented to the user's mobility needs in order to achieve a global recovery of the balance function. Third, it will allow customising fitness programs through mobile applications that provide eHealth physical activity targets to guide each patient's ADLs. An objective assessment will allow to intuitively and in real-time adjust the fall prevention measures according to the ambulatory response of the user, as well as support the clinical diagnosis and the evaluation of the rehabilitation progress [19].

As main objectives, it is intended to develop: i) intelligent and advanced tools to recognise human activity [39], estimate the risk of imminent and prospective fall from the fusion of quantitative and qualitative information with baseline and context sensitive information, and predict the beginning of the fall, its type and direction; ii) portable motion analysis laboratory with diagnostic tools to provide an objective and real-time assessment of the user's motor condition, fall risk level and QoL; and iii) a biofeedback and action system to encourage user participation, ensure bidirectional interaction between the device and the subject, as well as prevent falls and their consequences. During this PhD thesis, algorithms were developed

for: i) the detection of falls and cane events with an instrumented conventional cane (Chapter 4); ii) the detection of gait phases and motion intention for a cane-type robot (Chapter 5); iii) recognition of activities with a smart waistband equipped with a single IMU (Chapter 6); and detection of slip-like perturbations (Chapter 7).

3.2.3 Development of Devices

The research solution considers a set of BiRD Lab devices that will be assigned to each subject according to their level of mobility, ensuring a focus on the user needs. The novelty is that each user receives personalised assistance according to his/her disability/limitation and need to use the device with the best benefit ratio. Each robotic device will be equipped with appropriate and identified fall prediction and detection strategies to enable users to manage various types of unexpected disturbances. Thus, the research solution innovatively interconnects the following wearable and non-wearable systems with the algorithms described previously : i) a smart waistband; ii) a smart walker; iii) a PKO; iv) an instrumented conventional cane; and v) a cane-type robot. Not all devices were used or addressed during this PhD thesis. The smart waistband was enhanced so that it could be used at the partner institutions to collect data from seniors (Chapter 6). On the other hand, an instrumented conventional cane and a cane-type robot were developed from the scratch (Chapters 4 and 5, respectively).

These devices will have proactive and active prevention actions. As a proactive prevention, it was stipulated as fundamental the construction of an alert strategy oriented to the fall and to the user. For instance, the waistband will collect kinematic information from the trunk that, together with clinical, demographic and physiological information, will be able to estimate the risk of falling and alert the user and caregivers in real time if the fall risk is high or a gait abnormality is detected. Thus, this device must be instrumented with vibrotactile motors as an actuation mechanism. Previous and promising results from the BiRD Lab team were achieved through the application of vibrotactile biofeedback on a waistaband proper for parkinsonians with FOG [49].

On the other hand, robotic assistive devices, i.e., the smart walker, the PKO and the cane-type robot are assist-as-needed fall prevention solutions, which are therefore considered as active prevention actions since they can avoid falls from happening. The smart walker is intended to support balance by adjusting its trajectory of movement, as well as to alert about fall risk situations or the occurrence of falls. The cane-type robot will operate similarly to the smart walker, since it will also provide balance support, and an alert in case of risky situations or even falls. This device will perform, as illustrated in the literature, a positional adjustment to ensure support for the user. The system will monitor the user primarily and exclusively through sensors installed in the cane, making it a wholly non-wearable system. In contrast, the PKO, as a wearable robotic device, will present a distinct prevention strategy from the other two devices. This will automatically adjust the joint angle, being a custom adjustment depending on the type of disturbance

(e.g. slip or trip). Previous team work reflects the physical support validation through the use of the smart walker [209] and the PKO [46] for other research purposes.

The development of mobile applications will be able to establish a real-time connection between the elderly, caregivers and clinicians, allowing information to flow in a timely manner, which contributes for proactive prevention actions. Thus, seniors will be able to have daily information about their activity, get advice on possible risk activities and set eHealth targets for active life and for training. On the other hand, caregivers will receive alerts of high risk of falling or the occurrence of falls and will be able to receive, like seniors, advice on possible risk activities that they may instill in the elderly. Finally, clinicians will have access to quantitative and objective assessments of gait and balance of daily activity, as well as ongoing assessment of fall risk.

3.3 Research Hypothesis

The research activities that were developed within the scope of this project are based on the following technological and clinical hypotheses.

- This investigation is based on the hypothesis that the user's kinematic parameters make it possible to timely recognise and predict the occurrence of abnormal situations such as fall events in the most varied situations, i.e., during and between modes of locomotion [210–212] (Objectives 3-6; Chapters 4-8).

- Previous team work supports the hypothesis that the information from the moments before the fall, namely until the last step before the fall, is considered as high risk of falling information. This knowledge might be used to strengthen AI-based algorithms and provide devices the capacity to anticipate high-risk fall scenarios [36] (Objectives 4 and 5; Chapters 4, 6 and 7).

- This project considers the hypothesis that biomechanical and physiological parameters objectively monitored by sensory systems are correlated with qualitative clinical scales commonly applied in motor diagnosis to assess the risk of falling [25]. As an alternative to the subjective measures currently being used, it is intended to offer a set of objective and unified metrics for the objective evaluation of the level of risk of falling (Objective 4; Chapter 6).

- Another hypothesis refers that less concern about falling leads to greater physical activity on the part of patients/users. Greater confidence can naturally result in a better mood and better performance of gait and/or ADLs, which lowers the risk of falling [23]. This lower concern may be related to the use of robotic assistance devices that contribute to a sense of security [213] (Objectives 2-5; Chapter 4-7).

- The project considers the existing hypothesis that VR technology has the potential to impair balance and may facilitate the collecting of fall data [30, 214–216] (Objectives 2 and 6; Chapter 8).
- The project is based on the clinical hypothesis that training reactive recovery responses after sudden disturbances during gait may be more effective for fall prevention than conventional methods [107]. That is, therapies focused on testing and training individuals through the application of sudden disturbances may provide more information and benefits for the reduction and prevention of falls. This process relies on repetition to train the subject's reflexes. Thus, it is crucial to collect different types of data related to the subject and his gait when applying disturbances (Objectives 2 and 6; Chapter 8).
- The senior population's fear of falling is correlated with activity limitations and more unstable cognitive and physical abilities. Therefore, it is assumed in this study that fear of falling, as a significant predictor of the risk of falling, is linked to health-related QoL [217, 218] (Objective 4; Chapter 6).

3.4 Outcomes

The health market, namely health institutions, and policy makers (e.g. governments and ministries of health), that seek to enhance treatment offered, are the major targets of the project's outcomes. The aging of the population, and the consequent increase in the prevalence of neurological diseases such as Parkinson's disease, Dementia, Cerebrovascular Accidents, has resulted in a high number of people with mobility impairments and a consequent increase in the risk of falling and a decrease in QoL. In this respect, there is a general need for the development of wearable and non-wearable robotic assistance devices, such as those that are planned to be researched and developed in this project, that allow increasing users' QoL with the delivery of health care while minimising costs. This research solution was designed to intervene within the scope of motor assistance and support for hospitals, nursing homes or other clinical units. The target population is the elderly and neurological patients with a wide spectrum of motor disabilities. Through robotic devices that can provide early warning in order to reduce falls and encourage active and healthy ageing, this solution will be able to aid the gait of the elderly. To this purpose, it offers a variety of devices that are appropriate for every level of functional mobility, making it possible to modify support in accordance with the patient's level of impairment at the time in the future. The population's ageing has the tendency to increase the number of prospective consumers. In the long-term, this technology is easily adaptable to provide daily support with ADLs and continuous gait monitoring without requiring a face-to-face examination with the health services. Without the requirement for the patient to physically travel to the location of medical help, the data might be seen by a health expert in real time or offline, facilitating the diagnosis and the user's QoL. The following outcomes, with possible effect, are expected to be attained over time: i) recovery of balance in real time; ii) FRA in real-time; iii) new objective metrics; and iv) adaptability and

personalisation of assistance according to the level of mobility. Thus, it is expected to obtain the following technological results: e) an assisted-as-needed robotic technology; ii) non-intrusive sensory systems; iii) advanced parameter estimation tools based on kinematic and physiological information; iv) advanced clinical decision support tools; v) an open-source database; vi) an intelligent fall prediction tool; vii) sensory feedback and biofeedback systems; and viii) a personalised and interoperable technology. This PhD thesis intends to take the first steps towards the presented outcomes of the research solution.

3.5 Conclusions

This PhD thesis aims the development of cutting-edge technology solutions to detect and predict falls, with the goal of reducing the occurrence of falls, particularly among the senior population. Three major phases were selected and presented: data collecting, algorithm development, and device development. During the initial phase, the collection will mostly take place at institutions such as day care centres and nursing homes. However, because falls occur infrequently, options that speed the gathering of kinematic and physiological data near to real-world falls are required. As a result, algorithms capable of being deployed in various devices geared toward seniors based on their level of mobility will be developed. Finally, various hypotheses were advanced to support the investigation described in the next chapters, as well as the expect long-term outcomes.

Chapter 4

Instrumented Conventional Cane

This chapter starts with an introductory insight into the relevance of stimulating the usability and acceptability of canes among the elderly to reduce the incidence of falls. It presents the design, development, and validation of: i) an AI-based framework that determined the best models and features for four classification problems: fall event, fall phase, fall category and cane event; and ii) two FSM that combined accelerometer and gyroscope's data to detect the cane's fall and four cane events, respectively. Both approaches are efficient, automatic, user-independent, and perform real-time classification.

4.1 Introductory Insight

Stimulating the usability and acceptability of canes within the geriatric community is crucial for fall prevention. Clinical evidences support the prescription and use of canes to increase the user's balance and reduce the fall risk [219], having a direct and beneficial physical and psychological impact on user's health [220]. Canes can increase older adult's confidence and safety, which consequently increases the levels of activity, balance, stability and independence [213, 220]. For instance, Dogru et al. [221] verified that BBS scores are higher while using the cane than without it. However, the non-use of a cane is still a problem within the geriatric community. Forgetfulness, inaccessibility, feeling of oldness, the thought of no need, inappropriate device prescription, lack of user education, or use of unprescribed devices are pointed as reasons for abandoning canes [213, 220]. Luz et al. [213] evidenced that most of the falls at home occur with the absence of the assistive device, and result in more severe injuries for the people who do not have their cane with them. To fight the non-use of this assistive device, it is suggested to develop and test strategies capable of improving usability and acceptability, involving environmental reminders and using cutting edge technology to develop new canes [213]. Currently, monitoring systems, e.g. fall detection systems,

are commonly supported by the advantages of few wearable sensors placed at the user's trunk [26, 222]. However, placing sensors on various parts of the body may be uncomfortable and difficult to wear, lowering usability, especially for the elderly or patients who are undergoing rehabilitation that need as much freedom of movement as possible [223]. Towards usability and acceptability, technology-based canes have been developed, robotised, and equipped with: i) fall detection systems, allowing fast interventions after a cane's fall and saving human lives [224, 225]; and ii) gait or cane event detectors to indirectly assess human gait, fostering a more efficient functional motor recovery when applied in the design of personalised gait therapies that shape the therapeutic assistance accordingly to the user's needs [226–228].

Fall detection systems in conventional canes present some methodological drawbacks. Firstly, the majority of the studies use simple threshold-based algorithms to detect cane's falls [224, 229–231], which suffer from high FPRs in real-life situations, and do not combine information from different sensors, using data from only one inertial sensor. The accelerometer data is the most used information to detect cane's falls [224, 225, 229, 230], but Almeida et al. [231] proved the gyroscope can be used for the same purpose. Mouta et al. [225] have shown that the acceleration vector module reaches high values at each ground contact, which can be understood as a false positive by threshold-based algorithms. Thus, the use of a single sensor may be insufficient for fall detection and some redundancy is required. Secondly, the number of participants represents also a concern for the feasibility of the results. Usually, only 3 or 4 subjects perform a small group of fall representative activities [224, 229, 230]. Moreover, Mouta et al. [225] used only the SVM to detect cane's falls using the entire information as input. This machine-learning classifier may not represent the most suitable machine learning model for this problem, and, on the other hand, using the entire information may affect the use of the model in real-time. Most of the studies about inertial sensor-based instrumented canes implemented fall-related algorithms that estimated orientation or even contact-phases [225, 232]. Considering gait segmentation, no previous study correlated the sensory information of the cane with the movement of the human foot during the gait. This chapter addresses this question and, in addition, examines a greater number of cane events than just verifying whether the cane is in contact with the ground or not [232].

4.2 System Overview

The proposed system (Fig. 9.a) collects cane's acceleration and angular velocity data at 200 Hz. It comprises a 9-axis Motion Processing Unit (MPU-9250) near the cane's handle which was configured as follows: $\pm 8g$ for the accelerometer and $\pm 300^{o}/s$ for the gyroscope [225]. The IMU's location is based on Chen's work [224]. These authors verified that the amplitudes of the acquired data in the upper part of the device were higher than in other locations, which contributes for a more discriminative characteristics of the signal. Both physical quantities were measured on three directions: AP, ML and V. These specific kinematic data were used as inputs for both approaches due to their usability and operability in daily scenarios. A

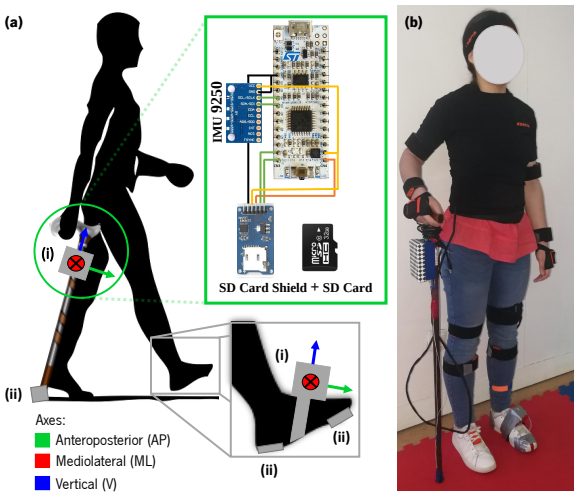

Figure 9: System overview: a) Developed system used for data acquisition with: i) an IMU and ii) FSR; b) Subject with all systems and equipped with the *MVN BIOMECH* (Xsens, Netherlands).

Force Sensitive Resistor (FSR) was placed at the cane's tip as a ground truth mechanism to detect cane's "Stance"and "Swing". Additionally, the subjects were equipped with a MPU-9250 and two FSR on the opposite side of the cane [233], i.e., the left foot as depicted in Fig. 9, to study similarities between cane and foot's data. Both IMU are connected via I2C protocol to a STM32F4 microcontroller and collected data is stored into a SD Card.

4.3 Ambulation with a Cane

A proper locomotion with a cane improves balance, helps in weight distribution, and requires the use of the cane on the opposite side of the affected leg and in tandem with it so as to simulate normal gait [233]. There are two ways of walking with a cane, namely, two and three point gait [234]. Two-point gait is characterised by the movement of the cane and the affected leg forward in unison. Consequently, cane and foot events occur approximately at the same time. While in three-point gait both legs and the cane move forward individually at different times. Thus, since both approaches use only inertial data from the cane, it was only possible to detect the following cane events, which are related to gait events only if the user performs a two point gait, as depicted in Fig. 10.a: i) First Ground Contact (FGC) - the event which equals to the first ground contact of the cane and it is similar to HS; ii) Maximum Support Moment (MSM) - occurs when the cane fully supports the subject's body weight and corresponds to the Middle Mid-Stance (MMSt); iii) Full Cane Off (FCO) - moment in time that the cane base lifts entirely from the ground and corresponds to the Toe-Off (TO); and iv) Cane Middle MidSwing (CMSW) - phase in which the swinging cane passes the opposite stance limb. The opposite side foot is in Middle Mid-Swing (MMSw).

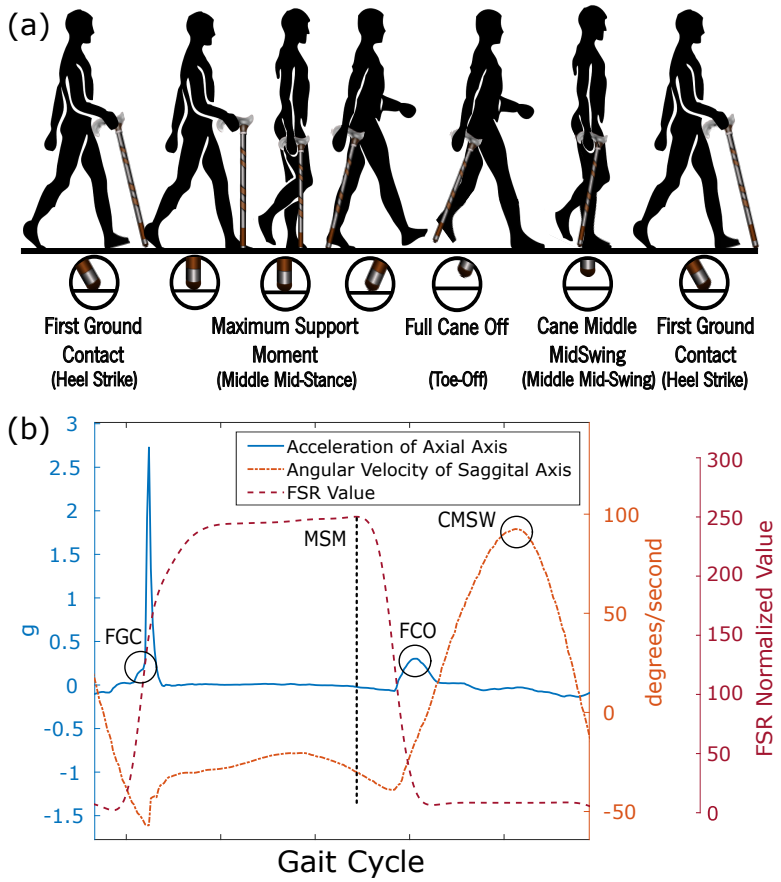

Figure 10: Cane events matched to: a) the respective human gait events during one gait cycle of two point gait. b) inertial and force data from the cane.

4.4 AI-based Framework - Comparative Analysis

This section describes the methodologies adopted and the equipment used to build the AI-based framework. The AI-based tool is constituted by four accurate classifiers. For each classification problem, a comparative analysis, which strategy is illustrated in Fig. 11 and implemented in Matlab (2019a, The Mathworks, MA, USA), was performed to determine the most suitable AI-based classifier and the subset of features that allow the best performance. It compares different techniques with the same kinematic data and describes the conducted stages during training and testing. The proposed framework is explained in the following subsections.

4.4.1 Feature Calculation

The *Feature Calculation* (Fig. 11) aims to obtain a *feature table* that includes filtered acceleration and angular velocity data, and several features extracted from this filtered data (Table 1), resulting in a total of 165 features. All features are calculated per sample. There are three types of features that use initial filtered data as input to estimate a new sample: i) features that require only one sample from initial data

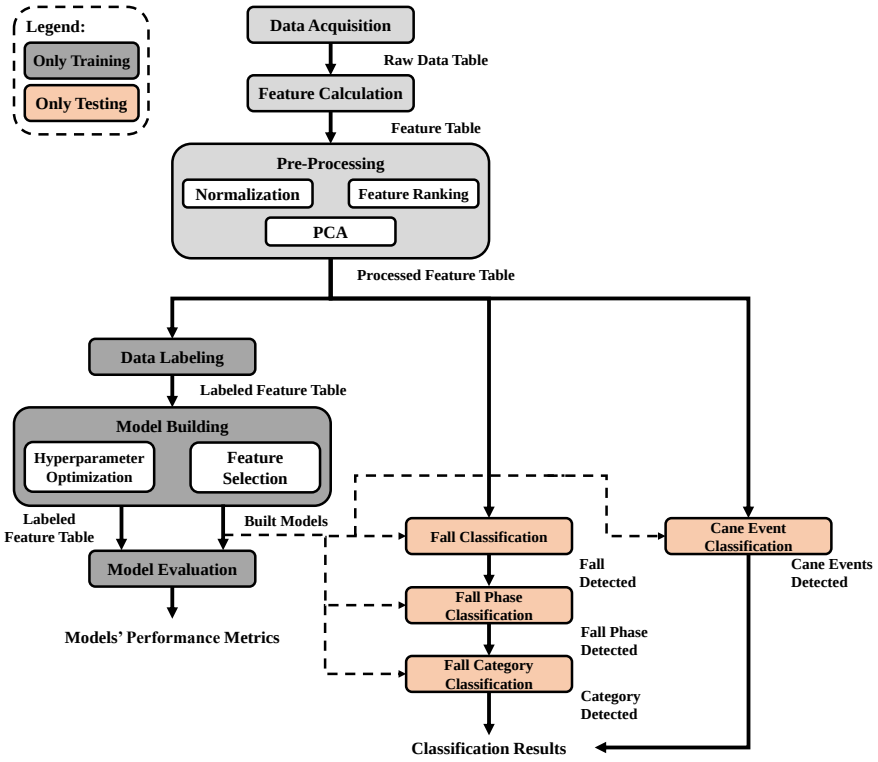

Figure 11: Schematic of the machine learning-based framework for fall-related purposes.

(e.g. the Sum Vector Magnitude (SumVM) and the Dynamic Sum Vector); ii) features that require only the current and the previous samples from initial data (e.g. the Resultant Angular Acceleration (RAA) and the Acceleration Exponential Moving Average (EMA)); and iii) features that use a larger time window from initial data. The current sample and the 4 previous samples were used from initial data, i.e., a time-window of 5 samples, to estimate the new sample of the output feature (e.g. Minimum, Maximum, Mean, Variance, Standard deviation, Skewness, Kurtosis, Velocity and Peak-to-Peak Values (PPV)). The dependence on past samples requires feature estimation within each activity. The first 10 samples of each activity were removed in order to ensure that all features had a value. Previous studies used these features [235–240].

4.4.2 Pre-Processing

The *Pre-Processing* is responsible for feature normalisation and for identifying discriminative features to help building the AI-based models. As first step, features were normalised by the subject's height since the anthropometric scaling features reduce the variability of the *feature table* [241]. Further, a 1st order low-pass filter (exponential smoothing) with 0.5 as the smoothing factor and a cut-off of 10 Hz was applied to cane's data [242]. Appendix A.1 provides instances of the collected data. Additionally, the min-max scaling [0;1] technique was used to normalise each feature, ensuring a low computational cost when building the models [243]. Furthermore, features were ranked by using the following ten feature selection methods that rank features in descending order according to their relevance [244]: i) Infinite Latent Feature Selection

Table 1: Feature Table

Feature	**Feature description**
1-3	Acceleration (AP, V, ML)
4-6	Angular velocity (AP, V, ML)
7, 8	SumVM of acceleration and angular velocity*
9-11, 17-19, 25-27, 33-35, 41-43, 49-51, 57-59	Skewness, Kurtosis, Minimum, Maximum, Mean, Variance, Standard deviation of acceleration (AP, V, ML)
13-15, 21-23, 28-30, 36-38, 44-46, 52-54, 60-62	Skewness, Kurtosis, Minimum, Maximum, Mean, Variance, Standard deviation of angular velocity (AP, V, ML)
12, 16, 20, 24, 31, 32, 39, 40, 47, 48, 55, 56, 63, 64	Skewness, Kurtosis, Minimum, Maximum, Mean, Variance, Standard deviation of 7 and 8
65-70	Correlation between axes - accelerometer and gyroscope (V-ML, V-AP, ML-AP)
71-73	Acceleration after high-pass filter (AP, V, ML)**
74-80	SumVM of acceleration raw data*, Dynamic Sum Vector*, V Acceleration*, Total Angular Change, RAA**, Activity Signal Magnitude Area (ASMA)**, Signal Magnitude Area (SMA)
81-83, 89-91, 97-99, 105-107	PPV, RMS, Ratio Index (RI), RI of PPV of acceleration (V, ML, AP)
84-86, 93-95, 101-103, 108-110	PPV, RMS, RI, RI of PPV of angular velocity (V, ML, AP)
87, 88, 94, 96, 100, 104, 111, 112	PPV, RMS, RI, RI of PPV of 7 and 8
113-120	Quaternions**, Roll**, Pitch**, Yaw** and Absolute V acceleration*
121, 125, 126, 130, 134	SumVM of resultant angle change*, Maximum RAA, Sum of Flutuation Frequency, Resultant of Average Acceleration*, Resultant of Standard Deviation*
122-124, 127-129, 131-133, 135-137	Resultant angle change**, Flutuation Frequency, Resultant of Average Acceleration**, Resultant of Standard Deviation** (AP, ML, V)
138-146, 156	Slope**, Fast Change Vector, SumVM of horizontal plane*, EMA**, Rotational Angle using Acceleration**, Z-score*, Magnitude of Angular Displacement*, Acceleration and Angular Velocity Resultant of Delta Changes**, Cumulative horizontal displacement
147-155, 157-165	Gravity Component*, Velocity, Displacement, Cumulative horizontal sway length, Mean sway velocity, Displacement Range (V, ML, AP)

* - First type of features; ** - Second type of features; Excepting features 1-6, the remaining features require the mentioned time-window of 5 samples.

(ILFS); ii) Infinite Feature Selection (INFS); iii) Correlation-based Feature Selection (CFS); iv) Extended CFS (ECFS); v) Minimum-Redundancy Maximum-Relevancy (mRMR); vi) Relief-F; vii) Mutual Information Feature Selection (MutInfFS); viii) Multi-Cluster Feature Selection (MCFS); ix) LASSO; and x) ANOVA base method with mRMR. This last method uses mRMR to provide a first rank. Then, ANOVA starts on the highest-ranked feature and evaluates which classes are distinguishable for the feature using the feature's mean and variance per class until there are a set of features that distinguish between all classes. Consequently, it were compared the effects of the rankings on the models' performance.

The PCA, a feature extraction method, was adapted in this study to provide a ranking to the features from Table 1 as presented in Fig. 12. The Principal Components (PC) that correspond to a cumulative percent explained of 70% were selected [245]. Further, a resultant and proportional PC is obtained and used to rank features. PCA was also used to reduce the computational cost of the machine learning framework. Instead of using all 165 features, it was only used the features which have a PC value greater than $\frac{1}{165}$ and multiplied that number by 2. This means that a higher number of features was selected to realise the study than those with great contributions to the variability of the data. The success of this procedure will be determined by achieving the best performance with a lower number of features than the number stipulated here. Both feature selection methods and PCA (both purposes) were performed for each classification problem.

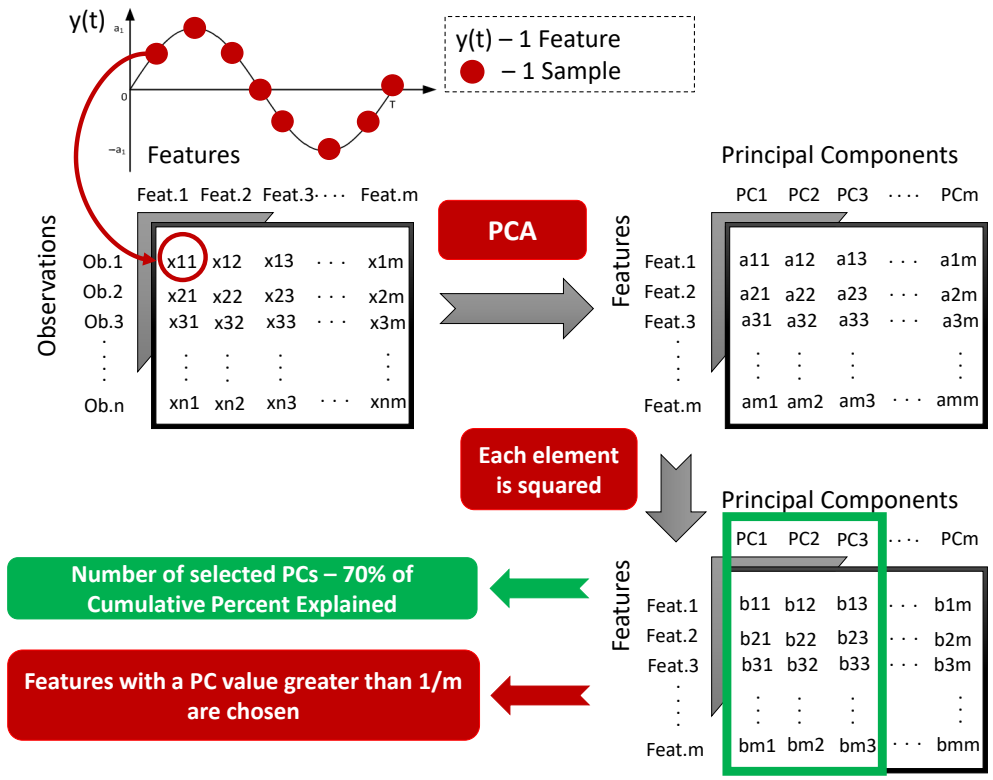

Figure 12: PCA-based procedure to rank and obtain the most crucial features and limit the computational cost of the study.

4.4.3 Data Labeling

The *processed feature table* (Fig. 11) was labeled using the cane's acceleration data, the biomechanical human model from the MVN BIOMECH (Xsens, Netherlands) (Fig. 9.b) and the cane's FSR to determine the beginning of the fall in the activities where the subject fell with the cane, as well as the cane events mentioned previously. The *labeled feature table* resulted from this process. According to the work of Chen et al. [224], using only acceleration data, it is possible to divide the fall of a cane in three major and distinct phases: i) Collapse; ii) Impact; and iii) Shock. During the collapse phase, the cane starts to fall towards the ground. This phase is characterised by an approximation of the three acceleration axes to zero until impact. Then, an abrupt polarity inversion of its vector in the direction of the trajectory is verified. Since the cane is a lightweight object, after impact, it usually suffers rebounds which characterises the shock phase. Inactivity comes next along with frequently unpleasant consequences for older adults. Cane's FSR detected FGC, MSM and FCO events, while MVN BIOMECH was used to determine the CMSW. When the FSR signal is 70% higher than its minimum, a FGC event is detected if the derivative of the FSR signal is positive, and a FCO event is detected if the same derivative is negative. MSM is detected when FSR signal reaches the maximum value. Finally, the CMSW is detected through video of the biomechanical model when the MVN BIOMECH extra unit passes the opposite stance limb. These events correspond to a specific sample in time data. Therefore, once an event is detected, the following samples had the same label until next event. Figure 10.b depicts the match between cane events detected by ground truth systems and the cane's inertial data.

Further, the *labeled feature table* was organised into 4 databases (A, B, C and D) depicted in Fig. 13, one for each classification problem (Fig. 11). Database A contains 2 classes: fall and non-fall. This first model will determine if the cane is falling or not. The databases B and C contain only data from falls, however, database C only contains data from activities where the subject fell forward and to the sideways. Database B contains three classes: the collapse, impact and shock phases. On the other hand, Database C was examined with different combination of classes (forward, right and left) and fall phases. Finally, database D contains the four cane events mentioned: FGC, MSM, FCO and CMSW.

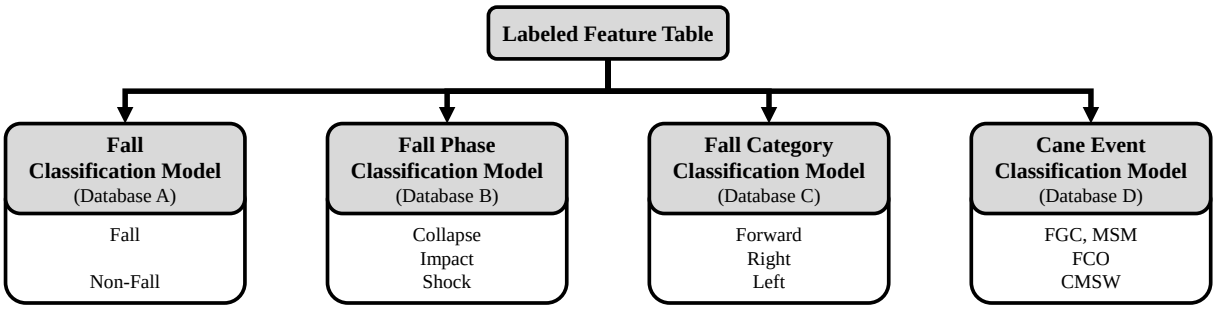

Figure 13: Identification of databases per classification model and respective classes. Database A receives data from all activities, databases B and C only from cane's falls, and database D from walking activities.

4.4.4 Model Building and Evaluation

The process explained here is responsible for building the four classification models for the AI-based tool (Fig. 11), and involves the optimisation of the models' hyperparameters. A total of 8 classifiers were compared, namely DA with linear and quadratic approaches; KNN with linear, inverse and squared inverse distances; Ensemble Learning; DT; SVM with linear, polynomial and gaussian kernels; and a Long Short-Term Memory (LSTM), a CNN and a Convolutional Long Short-Term Memory (CLSTM) neural networks. The first 5 classifiers were compared to obtain the best set of features. Then, it was compared the model's performance with the neural networks' performance for the same set of features. This comparison aims to identify the better-suited classifier for fall event, fall phase, fall category and cane event, aiming a low-cost computation. Figure 14 depicts the entire process for obtaining the classifier with best performance for each classification problem. Initially, it was performed the Hold-Out (HO) method to split $\frac{2}{3}$ of data for training and $\frac{1}{3}$ for testing. With training data, for each classification problem, it was performed an initial 5-fold CV with 1 repetition to find the machine-learning classifier with best performance between DA, KNN, DT, Ensemble Learning and SVM, with a specific subset of features. Further, the process was repeated for the selected classifier using 10 repetitions and performed the hyperparameter optimisation. Test data was further used to evaluate the classifier. The neural networks were also trained using only the subset of features determined previously. Then, test data was used to evaluate the neural networks, allowing a

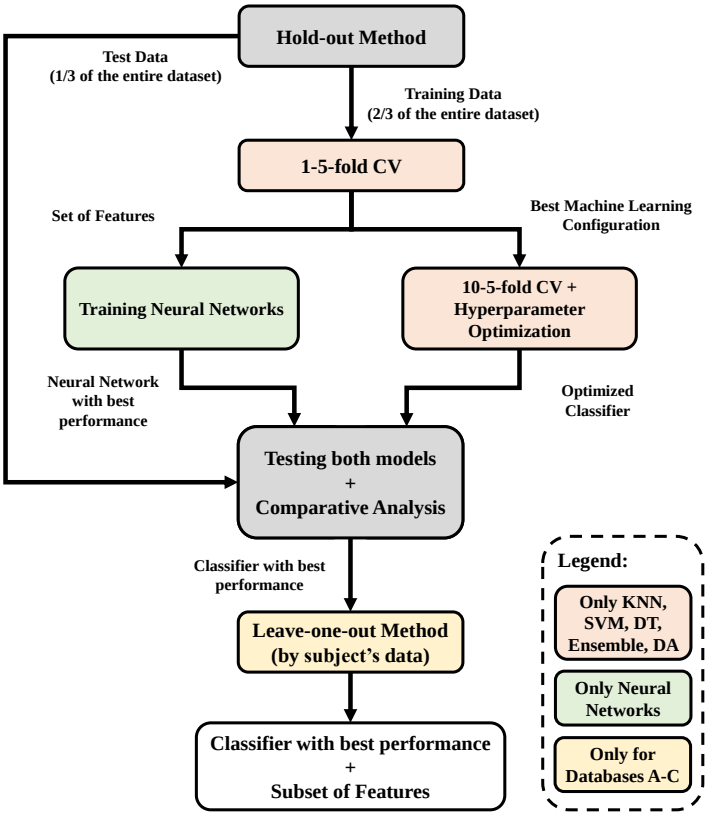

Figure 14: Schematic of the procedures performed to build and evaluate the classifiers.

comparison between classifiers. The model with best performance was further evaluated with the LOO CV method (only databases A to C). One subject was left out and trained the model with the other 10. The process process was repeated 11 times to leave all subjects out once. This method evaluates the generalisation capability of the final classification models [241]. Thus, it is possible to obtain the machine learning classifier with best performance and a specific subset of features. All models were built to be used in real time. The Mathew's Correlation Coefficient (MCC) was used as evaluation performance metric, since it presents good representative properties of unbalanced classes, which happens in this study. The ACC was also computed for benchmarking the literature's findings, as well as the SENS, the SPEC, the False Negative Rate (FNR), the FPR and the F1-Score. These evaluation performance metrics were used for both comparison and reporting of models' performances [246].

4.5 Fall-Related Finite-State Machine

The FSM combines the accelerometer and gyroscope information to detect cane's falls differently from the existing threshold-based algorithms from literature. Mouta et al. [225] verified that an acceleration-based lower-threshold is capable of detecting cane's falls before the impact. However, a possible recovery of the subject's balance between the detection moment and the impact could result in a false positive. Thus, gyroscope data is here used to confirm the impact on the ground. This FSM, represented in Fig. 15, shares some procedures already described, such as data normalisation, filtering and data split for training and test. The test data from the HO method and the LOO CV were also used to asses the FSM. Training data was used to obtain the upper and lower thresholds. Once the SumVM of acceleration crosses the lower threshold, a cane's fall is validated when the SumVM of angular velocity surpasses the upper threshold in less than 1 second later.

4.6 Cane Event Finite-State Machine

Correlation methods (Spearman and Pearson's Correlation Coefficients) were used to compare inertial data from aligned cane and foot strides and understand which sensors' signals are correlated. This analysis shows that the cane pattern indirectly reflects the human gait and thus events can be detected and used as indicators of the associated human walking gait events. It also helps choosing which signals to use in the FSM to establish the rules for cane events. Thus, it was created a FSM for cane event detection based on the team's work [247]. The number of conditions were reduced from 6 to 4 to match with the previously described cane events (Fig. 10.b) and implemented a real-time high pass filter (derivative filter with α = 0.995) to remove the baseline of the inertial data and simplify the decision-making rules. Moreover, foot and cane strides were aligned offline since not all subjects performed a two-point gait with the cane. Table 2 contains details about the FSM decision rules which are based on curve tracing techniques, namely,

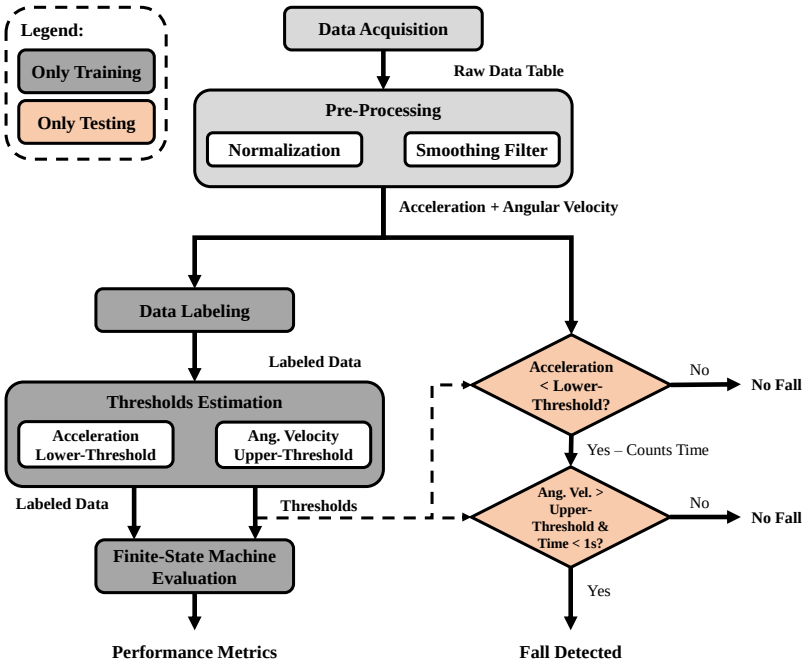

Figure 15: Schematic of the FSM for fall detection.

adaptive thresholds crossing, local extrema detection (i.e., maximum and minimum), and the evaluation of signal derivatives. These rules were implemented based on inertial data from male and female healthy-bodied young subjects. Despite presenting changes in spatiotemporal gait parameters, elderly, according to the literature, are expected to have a similar gait pattern [248].

Instead of just using information from gyroscope, accelerometer data were also included to help FGC, MSM and FCO detection. Generically, it was defined: i) FGC as the instant in which the acceleration suffers a polarity inversion due to the impact on the ground and the angular velocity is within a range empirically determined ($FGC\_GYR_{thr} \pm FGC\_GYR_{std} = -35.75 \pm 22.93^{o}/\text{s}$) after the maximum value has occurred. The acceleration is also within a range empirically determined ($FGC\_ACCEL_{thr} \pm FGC\_ACCEL_{std} = -0.09 \pm 0.23g$); ii) MSM was defined as when the angular velocity is within a range empirically determined ($MSM\_GYR_{thr} \pm MSM\_GYR_{std} = -17.06 \pm 10.58^{o}/\text{s}$), the derivative of the gyroscope signal is negative, the accelerometer signal is negative for ten samples, after 43% of the size of the previous stride; iii) FCO was determined as the maximum detected above an adaptive threshold (MAX_ACC_{thr}), i.e., a local maxima, after 55% of the size of the previous stride; and iv) CMSW was determined similarly to the FCO, however using the angular velocity data to detect a maximum above an adaptive threshold (MAX_GYR_{thr}). The rules are also accompanied by conditions dependent on stride time, i.e., adaptive intervals where the events shall occur. This implies robustness to the algorithm for changes in gait speed. The FSM approach shares some procedures already described for the AI-based framework, such as data normalisation, filtering and division for training and test. Training data was used to establish threshold values for decision rules, while test data was used to evaluate the FSM.

Table 2: Decision Rules with Adaptive Thresholds in Generic Form

State	Decision Rule
1 - FGC	(FGC_GYR_{thr} - FGC_GYR_{std} <$gyro_n$ <FGC_GYR_{thr} + FGC_GYR_{std}) AND (FGC_ACC_{thr} - FGC_ACC_{std} <acc_n <FGC_ACC_{thr} + FGC_ACC_{std}) AND (acc_n >0) AND ($acc\_derivative_n$ >0) AND ($acc\_derivative_{n-1}$ <0) AND ($acc\_derivative_{n-2}$ <0)
2 - MSM	(MSM_GYR_{thr} - MSM_GYR_{std} <$gyro_n$ <MSM_GYR_{thr} + MSM_GYR_{std}) AND ($acc_{n-9:n}$ <0) AND ($gyro\_derivative_{n-2:n}$ <0) AND ($Index$ - FGC_{index} >0.43 × $STRIDE\_TIME_{Prev}$)
3 - FCO	(acc_n >MAX_ACC_{thr}) AND ($acc\_derivative_n$ <0) AND ($acc\_derivative_{n-1}$ >0) AND ($Index$ - FGC_{index} >0.55 × $STRIDE\_TIME_{Prev}$)
4 - CMSW	($gyro_n$ >MAX_GYR_{thr}) AND ($gyro\_derivative_n$ <0) AND ($gyro\_derivative_{n-1}$ >0) AND ($Index$ - FGC_{index} ∈ [0.7 × $STRIDE\_TIME_{Prev}$: 1.3 × $STRIDE\_TIME_{Prev}$])

4.7 Validation Approaches

The proposed system was calibrated before data collection while the participant and the cane were in the upright standing position for 3 s to remove the data offsets. All subjects used the cane in their preferred hand and they were allowed to rest as much as they wished and when they wished. All participants provided written and informed consent, respecting the ethical conduct defined by the University of Minho Ethics Committee that follows the standards set by the declaration of Helsinki and the Oviedo Convention. The AI-based framework and both FSM were validated through three protocols. The first protocol validated the fall-related classification problems (Fig. 16). Further, cane event detectors were validated using repeated measures of healthy gait patterns recorded in (Fig. 17): i) controlled; and ii) real-life situations.

4.7.1 Fall-related Protocol

This protocol included 11 able-bodied subjects with a mean age of 24.20±2.60 years old (22-29 years), a mean height of 1.73±0.09 m (1.51-1.83m) and a mean weight of 70.80±8.23 kg (52-80kg). Further, the subjects performed randomly a total of 7 activities three times each. The selection of activities was based on the work of Noury et al. [102] where it is suggested a list of scenarios that must be addressed for the evaluation of fall systems. The experimental protocol was divided in activities with and without falls. Activities without falls consisted in walking at a comfortable pace with the cane. These activities included three walking circuits: i) walk approximately 10 m forward, rotate 180^o, and turn back to the original position (Fig. 16.a); ii) walk approximately 10 m forward, turn right and walk 4 m (Fig. 16.b); and iii) similar to the second circuit, however the subject turned left (Fig. 16.b). Activities with falls included falls only from the cane and falls with the cane and subject simultaneously. Activities where subjects did not fall were the: i) cane's free-falling (Fig. 16.c); and ii) thrown out the cane (Fig. 16.d). These activities are representative of falls in transitions between locomotion modes such as sit-to-stand and stand-to-sit, and

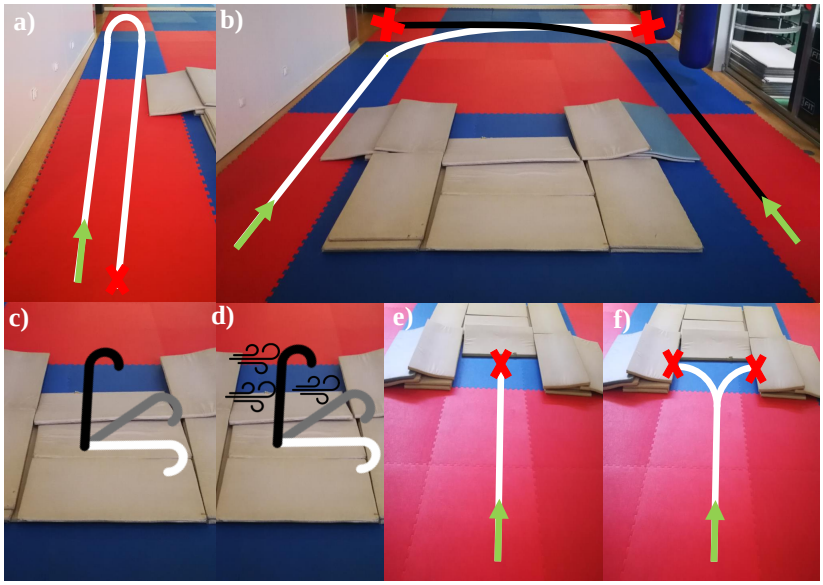

Figure 16: Activities performed during experimental activities: a) Walk forward and turn back; b) Walk forward and turn right or left; c) Cane free falling; d) Thrown out the cane; e) Falling forward; f) Falling sideways.

even fainting. Two other activities involved subjects and cane's falls: i) falling forward (Fig. 16.e); and ii) falling sideways (Fig. 16.f). A total of 132 falls were recorded with 66 only performed by the cane (Fig. 16.c and 16.d), and 66 combining the subject and cane (Fig. 16.e and 16.f): 33 were forward, 21 to the left and 11 to the right. The backward falls are missing in our experimental protocol because it was hypothesise that cane's users generally walk with their torso slightly flexed forward and, consequently, this type of fall occurs less frequently.

4.7.2 Controlled Situations Protocol

A total of 7 able-bodied subjects (5 males and 2 females) with a mean age of 23.29 ± 1.16 years old (22-29 years), a mean height of 1.70 ± 0.09m (1.51-1.81 m) and a mean weight of 69.57 ± 9.06 kg (52-81 kg) participated in this study to validate cane event detection in controlled walking situations by testing the effect of variations in the ground surface and gait speed (Fig. 17). The participants carried walking experiments on an instrumented split-belt treadmill at different speeds (1.0 and 1.5 km/h) and slopes (0%, and 10%). Three gait trials were randomly conducted for the following scenarios: 30 seconds walking without inclination and speed of 1.0 km/h; and 30 seconds walking with an inclination of 10^o at the same speed (1.0 km/h). Besides, the participants were told to carry walking trials at changeable speeds to approximate a real-life environment. In this case, the subjects walked for 60 seconds and changed gait speed every 20 seconds according to the provided instructions (increasing from 1.0 km/h to 1.5 km/h and decreasing again to 1.0 km/h).

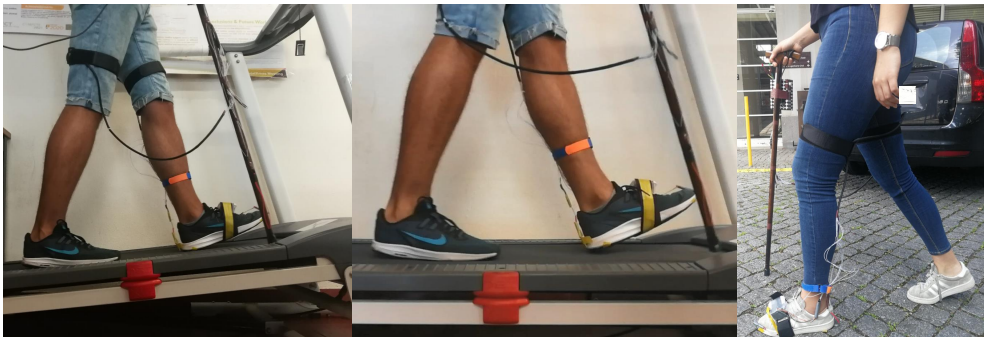

Controlled Walking Situations: Treadmill with & without Inclination

Level-ground walking: rough surface

Walking in Staircase

Walking in Inclined Surface

Level-ground walking: flat surface

Figure 17: Validation of the cane event detection approaches under controlled and real-life walking conditions (flat and rough level-ground, inclined surfaces and staircases).

4.7.3 Real-Life Situations Protocol

These trials were also considered to assess human locomotion in various conditions, including 7 able-bodied subjects (5 males and 2 females). They presented a mean age of 24.14±0.83 years (23-25 years), a mean body mass of 70.85±5.25 kg (61-75 kg), and a mean height of 1.75±0.04m (1.70-1.81 m). Since human gait is very dynamic in the real-world frequently including different gait speeds, surfaces and surface inclinations, the proposed approaches were verified in uncontrolled indoor and outdoor conditions. Three gait trials were randomly conducted for the following scenarios, which are illustrated in Fig. 17: forward level-ground walking on a 20 m flat surface; forward level-ground walking on a rough surface (urban ground) along 30 m; descending and ascending an inclined ground (approximately 10^o) and a 10 m rough surface; and climbing a staircase of 8 steps with standard dimensions (a height of 17 cm, depth of 31 cm, and step width of 110 cm). For each condition, the participants were asked to walk at a comfortable speed to achieve proper ambulation with a cane.

4.8 Pre-impact fall detection time

Both the Fall Event Classification Model and the fall-related FSM are designed to detect a cane's fall during the collapse phase. Thus, since the collapse phase occurs before the impact, it is important to understand how long in advance both tools can predict the impact. Pre-impact fall detection times from the fall event classification model and the FSM were assessed using test data split by the HO and LOO CV methods. Inertial-based wearable systems have been widely explored for pre-impact fall detection. These systems allow protection during falls since they detect in advance the occurrence of a fall impact with a short lead time, usually presented in milliseconds [210]. The majority of studies present lead-times shorter than 400 ms and use simple threshold-based algorithms with high values near or equal to 100% of ACC, SENS and SPEC. Bourke et al. [249] presented a mean of 323 ms only by using accelerometer and gyroscope data from the chest. Liu and Lockhart [250] also used inertial information, however the mean lead time was lower (255ms). Regarding machine learning-based strategies, Shan and Yuan [251] trained a SVM classifier using data from a tri-axial accelerometer at the subjects' posterior waist and achieved a mean lead time of 203 ms. Martelli et al. [252] used a neural network instead and presented a higher mean lead time (351 ms). Nyan et al. [253] developed a strategy based on the characteristics of angular movements of the thigh and torso segments. Their system presented also high ACC and a mean lead-time of 727 ms before impact. To the best knowledge of the authors, no study on the pre-impact fall detection time was ever performed for conventional canes only instrumented with inertial sensors. Pre-impact fall detection systems implemented in canes can be combined with existing wearable systems capable of actuating with e.g. wearable airbags for a more reliable detection.

4.9 Fall Detection: Results and Discussion

4.9.1 PCA Outcomes

For a cumulative percent explained superior to 70%, it was verified a similar number of PC and minimum individual percent explained between different databases. Only training data split from HO method was used. Moreover, the number of features with a PC value greater than $\frac{1}{165}$ is equal between databases A and B (31) and lower for database C (26). Once performed the PCA, the number of features for the AI-based framework has been reduced. Instead of using the 165, the 62 first ranked features by any feature selection method were used for the 2 first classification problems and the 52 first features for the third classification problem. Table 3 resumes the information of the PCA-based procedure.

Table 3: PCA outcomes for computational cost reduction

Database (Model)	Cumulative % Explained	PC (Min. % Explained)	Features
A (Fall Event)	70.87%	13 (>2.50%)	31
B (Fall Phase)	70.90%	14 (>1.82%)	31
C (Fall Category)	70.45%	13 (>2.01%)	26

4.9.2 Fall Event Classification

The 5-fold CV with one repetition revealed that KNN presented the best performance among the used classifiers (MCC = 99.88%; ACC = 99.98%) while using the first 32 features ranked by the Relief-F method. Ensemble learning presented closer but lower results (MCC = 99.69%; ACC = 99.96%) with the first 28 ranked features by the Relief-F method. Even with the first 55 features ranked by the same feature selection method, DT presented lower results (MCC = 99.20%; ACC = 99.90%); as well as the Gaussian SVM (MCC = 96.52%; ACC = 99.57%) with the same 32 features that KNN used; and the Linear DA with the first 46 features ranked by the MutInfFS method (MCC = 92.28%; ACC = 99.06%). The KNN and the respective set of features went through a 5-fold CV with 10 repetitions to assess what influence more repetitions could have on the model's performance. For this particular case, increasing the number of repetitions did not worsen the CV results. Instead, when using HO Test Data, the model presented lower results (MCC = 93.76%; ACC = 99.24%). Hyperparameter optimisation did not improve the model's performance. Using the first 32 features ranked by the Relief-F method, the LSTM presented slightly better results while using HO Test Data (MCC = 93.81%; ACC = 99.26%) when compared to the KNN's performance. Although it identified all the 41 falls included in the test dataset, these errors frequently happen at the beginning of the fall's collapse phase where the model has some short-time misclassifications due to indecisions or simply a delay. The remaining neural networks presented lower results when compared to KNN. Although CNN presented an almost 5% difference in MCC value (MCC = 88.92%; ACC = 97.64%), the CLSTM only presented a 1% difference (MCC = 92.72%; ACC = 99.13%). Thus, LSTM is the model with better performance for fall detection among all tested classifiers. The LSTM was further subjected to a LOO CV, presenting results in accordance to what was mentioned before (MCC = 93.97% ± 2.12%; ACC = 99.24% ± 0.28%). Table 4 depicts the subset of features found for each classification problem where the respective model presented the best performance. Features are presented in descending order according to the ranking. Table 6 contains the main results.

4.9.3 Fall Phase Classification

KNN presented the best performance among the used classifiers during the 5-fold CV with one repetition (MCC = 98.25%; ACC = 99.60%). This result was obtained while using the first 17 ranked features by the mRMR method. Ensemble learning with the first 21 features ranked by the same feature selection method,

was the classifier with the closer results to the KNN (MCC = 97.59%; ACC = 99.45%). More repetitions in the 5-fold CV are considered irrelevant for the model's performance (MCC = 98.13%; ACC = 99.58%). The use of HO Test Data revealed a considerable decrease in the model's performance (MCC = 83.30%; ACC = 94.73%). These results already account the hyperparameter optimisation, which slightly improved the performance. Misclassification occur mostly in the Impact phase since it presents a low proportion of data when compared to other phases. The precision of the Collapse, Impact and Shock phases were: 96.84%, 73.31% and 94.57%, respectively. It was chosen the LSTM for fall phase classification because it presented better performance results than KNN for the same features while using HO Test Data (MCC = 86.93%; ACC = 95.91%). Each phase presented higher precision values: Collapse - 97.94%; Impact - 83.01%; and Shock - 95.80%. CLSTM also presented close results to LSTM and slightly better than KNN (MCC = 85.96%; ACC = 95.79%). Once again CNN presented lower results than KNN and the other neural networks (MCC = 79.42%; ACC = 93.92%). When subjected to a LOO CV, LSTM presented results in accordance to what was mentioned before (MCC = 87.82% ± 2.53%; ACC = 96.50% ± 1.39%). Table 7 presents the main results.

4.9.4 Fall Category Classification

For Fall Category Classification, the classification of the following classes presented the best possible results: i) Forward+Right; and ii) Left. This can be connected to the fact that all subjects involved in the study used the cane with their right hand, which affected the falls to the right side since they avoided fall over the cane. This produced falls closer to forward falls, while falling to the left was more discriminative. Besides, the number of falls to the left are twice the number of falls to the right. Additionally, this classification problem only accounts for the collapse and impact phases. During shock phase, the cane suffers more rotations due to the consecutive impacts on the floor. KNN presented the best performance during the 5-fold CV with one repetition (MCC = 100%; ACC = 100%). With the first 40 features ranked by the Relief-F method. The second model with better results was the Ensemble Learning (MCC = 99.94%; ACC = 99.97%), requiring the first 45 features ranked by the same feature selection method. Increasing the number of repetitions did not alter the outcome, however, when using HO Test Data, the model's performance decreased drastically (MCC = 43.70%; ACC = 74.54%), which may indicate overfitting during the 1-5-fold and 10-5-fold CV. These results already account the hyperparameter optimisation. Regarding the neural network classifiers, CLSTM presented the highest results (MCC = 42.58%; ACC = 74.11%), however, they are lower than those presented by KNN. Both LSTM and KNN presented MCC values lower than 40% (39.57% and 35.75%). LOO CV only reinforced the negative results (MCC = 26.29% ±18.12%; ACC = 73.08% ±15.10%). Fall Category Classification results are expressed in Table 8. All confusion matrices are available on Appendix A.2.

Table 4: Features ranked in descending order per classification problem

Classification Problem	FSM	No. of features	Ranked features
Fall Event	Relief-F	32	95, 134, 137, 135, 89, 94, 28, 44, 4, 136, 36, 40, 38, 118, 96, 46, 48, 77, 30, 116, 117, 26 , 8, 32, 133, 130, 42, 143, 93, 124, 114, 6
Fall Phase	mRMR	17	147, 27, 134, 39, 137, 113, 114, 136, 35, 34, 135, 144, 25, 26, 141, 132, 46
Fall Category	Relief-F	40	132, 131, 137, 136, 115, 144, 134, 135, 113, 133, 130, 95, 116, 119, 118, 117, 114, 36, 44, 4, 28, 94, 70, 38, 106, 46, 103, 30, 127, 111, 158, 5, 97, 40, 29, 8, 93, 110, 164, 37
Cane Event	Relief-F	32	118, 38, 116, 132, 91, 46, 131, 137, 136, 6, 135, 115, 30, 25, 134, 141, 41, 122, 130, 71, 133, 95, 119, 144, 33, 1, 28, 36, 44, 4, 85, 94

4.9.5 Fall Detection Finite-State Machine

Similarly to the AI-based framework, the FSM detected correctly all falls (41 for HO Test Data and 127 falls for LOO). Considering the HO Test Data, the FSM (MCC = 92.88%; ACC = 99.15%) presented results closer to the LSTM (MCC = 93.81%; ACC = 99.26%). The LSTM presents better results for the LOO CV than for the HO Test Data (MCC = 93.97% ± 2.12%; ACC = 99.24% ± 0.28%). On the other hand, the FSM performance for the LOO CV slightly decreases (MCC = 92.21% ± 2.39%; ACC = 99.03% ± 0.38%). Results of the FSM performance are in accordance to the literature (Table 9). ACC and SPEC values are near-perfect results. However, the SENS is lower because the tool detects the fall collapse phase with some delay. Upper and Lower Thresholds (Fig. 15) obtained when using HO Training Data and during LOO CV are represented in Table 5. The threshold values are similar in both situations.

Table 5: Normalised Upper and Lower Threshold values obtained for the FSM

Threshold	HO Test	LOO
Upper Threshold	0.1766	0.1840
Lower Threshold	0.0381	0.0378

Table 6: Fall Event Classification Model's performance

Model	Method	ACC (%)	SENS (%)	SPEC (%)	FPR (%)	FNR (%)	F1 Score (%)	MCC (%)	Build (s)	Classify (s)
KNN	10-5-fold	99.98± 0.002	99.89± 0.02	99.99± 0.001	0.01± 0.001	0.11± 0.02	99.89± 0.01	99.88± 0.01	0.993	0.0593
KNN	HO Test	99.24	92.15	99.74	0.26	7.85	94.14	93.76	4.965	0.0573
LSTM	HO Test	99.26	90.19	99.9	0.10	9.81	94.11	93.81	4187	0.1444
LSTM	LOO	99.24± 0.28	91.36± 4.65	99.83± 0.25	0.17± 0.25	8.64± 4.65	94.25± 2.07	93.97± 2.12	4291	0.1439

Table 7: Fall Phase Classification Model's performance

Model	Method	ACC (%)	SENS (%)	SPEC (%)	FPR (%)	FNR (%)	F1 Score (%)	MCC (%)	Build (s)	Classify (s)
KNN	10-5-fold	99.58± 0.04	98.05± 0.18	99.69± 0.03	0.31± 0.03	1.95± 0.19	98.41± 0.14	98.13± 0.17	0.291	0.0063
KNN	HO Test	94.73	84.80	95.95	4.05	15.20	86.74	83.30	1.455	0.0060
LSTM	HO Test	95.91	87.30	96.75	3.25	12.7	89.54	86.93	1043	0.1246
LSTM	LOO	96.50± 1.39	89.32± 3.37	97.60± 1.33	2.40± 1.33	10.68± 3.37	89.93± 1.68	87.82± 2.53	1246	0.1241

Table 8: Fall Category Classification Model's performance

Model	Method	ACC (%)	SENS (%)	SPEC (%)	FPR (%)	FNR (%)	F1 Score (%)	MCC (%)	Build (s)	Classify (s)
KNN	10-5-fold	100	100	100	0	0	100	100	0.247	0.0039
KNN	HO Test	74.54	91.59	46.14	53.86	8.41	81.81	43.70	1.455	0.0042
CLSTM	HO Test	74.11	91.78	44.55	55.45	8.22	81.61	42.58	475	0.0041
KNN	LOO	73.08± 15.10	80.98± 14.01	45.25± 31.09	36.57± 28.16	19.02± 14.01	78.94± 12.24	26.29± 18.12	1.723	0.0044

Table 9: FSM performance for different methods and data

Method	ACC (%)	SENS (%)	SPEC (%)	FPR (%)	FNR (%)	F1 Score (%)	MCC (%)	Build (s)	Classify (s)
HO Test	99.15	87.77	99.95	0.05	12.23	93.13	92.88	0.147	0.0017
LOO	99.03± 0.38	87.36± 4.36	99.89± 0.19	0.11± 0.19	12.64± 4.36	92.48± 2.38	92.21± 2.39	0.165	0.0012

4.9.6 Pre-Impact Fall Detection Time

Generally, the LSTM presents higher lead-times than the FSM (Fig. 18). This can be justified by a higher value of FNR presented by the FSM. This means it detects the fall closer to the impact than the LSTM. With lead times of 446±210 ms (HO Test Data) and 373±158 ms (LOO CV), the LSTM detects earlier a fall event than the majority of the existing studies on wearable systems and with a higher number of different activities during the experimental protocol. On the other hand, the FSM only surpasses some studies [250, 251], presenting lead times of 285±206 ms (HO Test Data) and 266±93 ms (LOO CV).

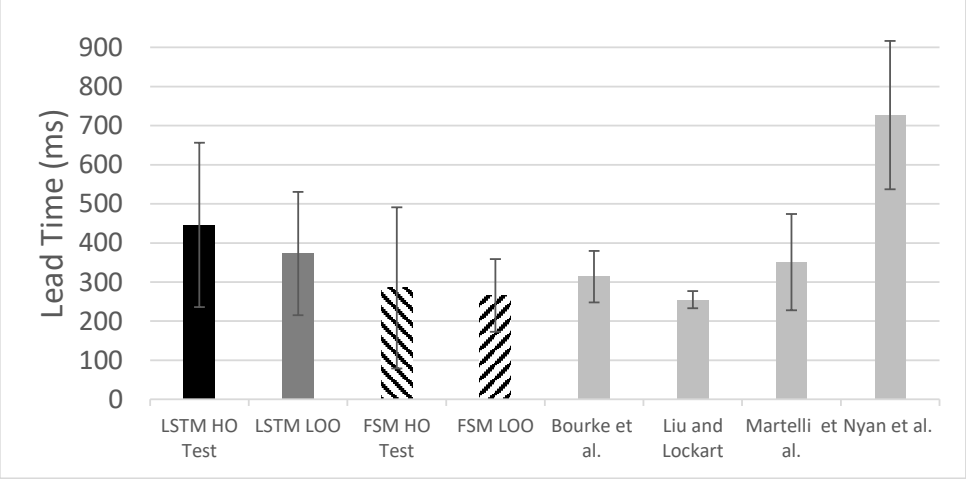

Figure 18: Comparision of pre-impact fall detection times and ranges between both approaches and literature results.

4.10 Cane Event Detection: Results and Discussion

4.10.1 Correlation between Cane and Foot Signals

Filtered inertial data from cane and foot strides were compared and the acceleration V (Pearson = 0.56± 0.23; Spearman = 0.67±0.18) and angular velocity ML (Pearson = 0.60±0.27; Spearman = 0.47±0.23) were the signals with higher correlation coefficients. Both signals present a large correlation according to the Pearson's correlation coefficient, and a strong (acceleration V) and moderate (angular velocity ML) correlation according to the Spearman's correlation coefficient. The rest of the signals present a small or very weak correlation with values closer to 0. Acceleration AP and angular velocity V present positive values, while Acceleration ML and angular velocity AP present negative values. It was opted to employ the acceleration V and the angular velocity ML for decision rules as a result of these findings (Table 2). The angular velocity ML is commonly used among state-of-the-art FSM [247].

4.10.2 PCA Outcomes

For a cumulative percent explained superior to 70%, it was verified that 14 PC are required. Moreover, the resultant PC evidenced that there are 35 features with a PC value greater than $\frac{1}{165}$. Once performed the PCA, to reduce the computational cost of the comparative analysis (Fig. 11), the number of features has been reduced, i.e., instead of using all the 165 features, only the first 70 features ranked by any feature selection method were used. Only training data from the HO approach was used in this study.

4.10.3 Cane Events Classification and Detection

The 1-5-fold CV results revealed that **KNN** presented the best performance among the used classifiers (MCC = 98.35%; ACC = 98.95%) while using the first **32 features** ranked by the **Relief-F method**. Ensemble learning presented closer but lower results (MCC = 98.01%; ACC = 98.73%) with the first 24 ranked features by the Relief-F method. DT presented lower results with the first 19 features ranked by the same method (MCC = 95.45%; ACC = 97.06%); as well as the Gaussian SVM (MCC = 89.04%; ACC = 92.54%) with the same 32 features that KNN used; and the Quadratic DA with the first 18 features ranked by the mRMR method (MCC = 72.51%; ACC = 81.37%). The KNN went through a 5-fold CV with 10 repetitions and it was discovered that increasing the number of repetitions had no effect on the outcome CV results (MCC = 98.34±0,02%; ACC = 98.95±0.01%). However, when using Test Data, the model presented lower results (MCC = 77.97%; ACC = 85.29%). KNN hyperparameters are: i) distance - Minkowski; ii) distance weight - Inverse; iii) Exponent - 0.5; and iv) Number of neighbours - 1. Using the first **32 features** ranked by the **Relief-F method**, the LSTM stood out among the neural networks in the 10-5-fold CV, however it presented lower results when compared to KNN (MCC = 90.94±0.23 %; ACC = 93.86±0.18 %). While using Test Data, the CLSTM presented the best performance (MCC = 84.44%;

Table 10: Algorithms Performance in Controlled Situations Considering the Maximum Timing Error

Cane Events	CLSTM					FSM				
	ACC (%)	Delay		Advance		ACC (%)	Delay		Advance	
		%	ms	%	ms		%	ms	%	ms
FGC	99.27	37.28	31.79 ± 35.32	43.46	51.31 ± 55.19	92.37	10.92	27.03 ± 19.27	85.84	77.59 ± 51.35
MSM	96.53	43.96	84.04 ± 62.26	49.10	94.01 ± 54.54	84.15	21.43	98.56 ± 50.88	77.92	91.00 ± 53.17
FCO	99.78	14.39	18.62 ± 10.99	38.21	32.92 ± 38.69	97.26	86.48	16.97 ± 22.33	13.52	40.10 ± 41.79
CMSW	99.87	38.23	28.71 ± 23.17	29.87	29.75 ± 20.28	99.49	19.54	6.51 ± 4.24	64.78	36.51 ± 38.32

Table 11: Algorithms Performance in Real-Life Situations Considering the Maximum Timing Error: Level-Ground Surfaces

Cane Events	CLSTM					FSM				
	ACC (%)	Delay		Advance		ACC (%)	Delay		Advance	
		%	ms	%	ms		%	ms	%	ms
FGC	99.87	38.40	21.56 ± 8.70	36.00	28.67 ± 18.04	98.21	1.82	40.00 ± 3.71	98.18	102.04 ± 46.00
MSM	98.40	52.85	94.62 ± 49.88	40.65	95.90 ± 50.32	84.91	44.44	88.75 ± 64.60	53.33	74.38 ± 55.94
FCO	100	16.94	21.43 ± 23.03	33.06	16.83 ± 4.97	100	100	13.11 ± 10.66	0	-
CMSW	100	60.18	35.29 ± 25.76	14.16	23.44 ± 12.21	100	8.06	8.00 ± 4.47	77.42	26.46 ± 25.47

Table 12: Algorithms Performance in Real-Life Situations Considering the Maximum Timing Error: Inclined Surfaces

Cane Events	CLSTM					FSM				
	ACC (%)	Delay		Advance		ACC (%)	Delay		Advance	
		%	ms	%	ms		%	ms	%	ms
FGC	99.82	46.00	23.48 ± 20.14	46.00	83.48 ± 55.93	90.63	10.34	33.33 ± 5.77	89.66	106.15 ± 51.11
MSM	99.27	52.00	139.92 ± 9.42	42.00	135.00 ± 8.97	81.25	50.00	113.46 ± 60.43	42.31	46.36 ± 44.11
FCO	100	18.75	25.00 ± 16.77	25.00	15.00 ± 3.68	100	96.88	12.26 ± 6.43	0	-
CMSW	100	40.00	26.67 ± 25.50	33.33	58.00 ± 41.61	100	27.03	10.00 ± 8.50	54.05	32.25 ± 29.93

Table 13: Algorithms Performance in Real-Life Situations Considering the Maximum Timing Error: Stairs

Cane Events	CLSTM					FSM				
	ACC (%)	Delay		Advance		ACC (%)	Delay		Advance	
		%	ms	%	ms		%	ms	%	ms
FGC	100	19.74	21.00 ± 7.61	65.79	90.00 ± 55.47	100	17.65	40.00 ± 21.79	82.35	84.29 ± 60.28
MSM	85.53	32.31	117.14 ± 28.46	64.61	126.07 ± 16.13	43.75	50.00	125.00 ± 17.66	50.00	66.67 ± 36.86
FCO	99.82	21.62	16.88 ± 5.12	40.54	17.50 ± 5.69	93.75	93.33	73.21 ± 75.84	0	-
CMSW	100	36.76	48.60 ± 49.23	38.24	40.96 ± 28.95	100	25.00	41.00 ± 77.73	35.00	25.00 ± 19.79

ACC = 89.41%). LSTM presented similar results to the CLSTM neural network (MCC = 84.44%; ACC = 89.09%). On the contrary, CNN presented results lower than the other classifiers (MCC = 68.69%; ACC = 79.32%). Thus, CLSTM is the classifier with better performance for cane event classification among all tested classifiers. Through all test results, the FNR (>11.84%) and FPR (>4.11%) present significant values mainly due to delays and advances in detecting events. Table 14 contains the main results for this classification problem.

The ACC, the percentage of occurrence and duration of delays and advances in the controlled (Table 10) and real-life situations (Tables 11, 12 and 13) were further studied to assess the versatility and time-effectiveness of the model. The time-effectiveness was only inspected for correct detections. Timing errors greater than 150 ms (10% of the mean stride duration empirically determined) were considered as a

Table 14: Cane Event Segmentation Performance

Model	Method	ACC (%)	SENS (%)	SPEC (%)	FPR (%)	FNR (%)	F1 Score (%)	MCC (%)	Build (s)	Classify (s)
KNN	1-5-fold	98.95	98.73	99.63	0.37	1.27	98.72	98.35	0.564	0.0574
KNN	10-5-fold	98.95 ± 0.01	98.72 ± 0.01	99.63 ± 0.003	0.37 ± 0.003	1.28 ± 0.01	98.72 ± 0.01	98.34 ± 0.02	1.003	0.0587
KNN	HO Test	85.29	83.31	94.46	5.54	16.69	83.47	77.97	5.237	0.0577
LSTM	10-5-fold	93.86 ± 0.18	93.15 ± 0.24	97.70 ± 0.07	2.30 ± 0.07	6.85 ± 0.31	93.23 ± 0.20	90.94 ± 0.23	4751	0.1222
CNN-LSTM	HO Test	89.41	88.20	95.89	4.11	11.84	88.46	84.44	4687	0.1083
FSM	HO Test	87.49	84.67	94.85	5.15	15.33	86.04	81.32	0.157	0.0023

misdetection. It was confirmed that the CLSTM can detect event transitions with an ACC higher than 99% for FGC, FCO and CMSW in both situations. The lower ACC of MSM event (85.53%) is exhibited on stairs. However, the remaining ACC values are greater than 96.53%. Advances (<135.00±8.97 ms) and delays (<139.92±9.42 ms) are generally higher than those obtained by [247].

4.10.4 Cane Event Finite-State Machine

The FSM presented an ACC of 87.49% when using Test Data (segmented outcomes), which is very close to the result presented by the CLSTM (89.41%) and suggests feasibility to this proposed method that only uses two features (Table 14). Considering the versatility and time-effectiveness of the FSM, and the maximum timing error of 150 ms previously defined, it was verified that CMSW is the event with higher ACC values for controlled (ACC of 99.49%) and real-life (ACC of 100%) situations. This event is followed by the FGC (ACC >90.63%) and FCO (ACC >93.75%) events. The FGC is better detected in stairs and level-ground surfaces, while the FCO is detected accurately (100%) in inclined and level-ground surfaces. As well as the CLSTM, the FSM has more difficulties in detecting the MSM event, especially on stairs where the ACC was 43.75%. On the other situations the ACC is within 81.25% and 84.91%. Advances (<106.15±51.11 ms) and delays (<125.00±17.66 ms) are also generally higher than those obtained by [247]. However, the CMSW is the only event detected by the FSM with shorter mean advances and delays values for all situations when compared to the CLSTM results. The remaining values of advances and delays are similar. The FCO is never detected in advance for level-ground and inclined surfaces.

4.11 Conclusions

The AI-based tool correctly classified fall events and phases commonly encountered in daily life exclusively from data coming from an instrumented conventional cane. On the other hand, fall category classification presented weak results possibly due to a low amount of data, presenting over-fitting during training. The most effective AI-based model for the following classification problems are (Table 4): i) fall event: LSTM using the first 32 features ranked by Relief-F method; ii) fall phase: LSTM using the first 17 features ranked by mRMR method; and iii) fall category: KNN using the first 40 features ranked by Relief-F method. Moreover, the tool correctly classified cane events and proved to be an accurate, time-effective, low-cost,

low computation strategy for real-time gait analysis. Therefore, it can be used either in gait assessment or rehabilitation tasks. The most effective AI-based classifier was the CLSTM using the first 32 features ranked by Relief-F method. The first and third classification problems share 22 features, more than half of the features, as they use the same feature selection method. In contrast, since the fall phase classification uses a different method, it only shares 7 features with the fall event classification and 9 features with the fall category classification. All three classification problems share 6 features with great variability in amplitude and frequency between normal walking and fall events: 46, 114, and 134-137. These 6 features are thus able to detect normal walking and fall events. The resultant of standard deviation and its value for each axis (features 134-137) use acceleration data to estimate the standard deviation till time and can detect specific variations during fall events. The mean of the angular velocity in the ML axis (feature 46) and the second quaternion (feature 114) may be selected because of the relevance of movements around the ML axis. The fall-related FSM presented close results for fall detection when compared to the Fall Event Classification Model. Both tools can detect the occurrence of a fall with short lead times before the impact. However, the LSTM is more prone for this function since it presented higher lead times: 446±210 ms with test data from HO method and 373±158 ms when applying the LOO CV method. Based on the obtained results, the LSTM has better performance than the FSM. However, this requires a further study to assess the computational load in an appropriate processing unit for real-time classification and understand how it influences the lead-times for both approaches.

A correlation analysis between inertial data from the cane and the foot shown a large correlation for the acceleration V and the angular velocity ML. The angular velocity ML is commonly used in FSM for wearable systems. It was decided to use both signals and the Cane Event FSM performance was closer to the CLSTM performance. Only the MSM event presented significantly lower results, especially while on stairs. Based on the results, the CLSTM is preferable than the FSM for this purpose. Due to its low computational cost, the FSM can be implemented in a microcontroller like the one used in this study. However, further studies can improve the FSM performance, especially the detection of the MSM event, by testing new rules and using features from the first 32 ranked by the Relief-F method (Table 4). Both FSM are recommended for a stand-alone version where the data remains in the embedded system of the cane. The PCA-based procedure used to reduce the computation cost of the AI-based framework can be thus considered as successful since the best performance of the models was achieved with less features than those stipulated by this procedure.

This study contributes to the state-of-the-art with two versatile fall-related tools capable of detecting the fall of a cane and two cane event detection tools capable of discriminate four events. The AI-based tool was also designed to detect the fall phases and their category. Relevant features were found and they can now be studied for further improvements regarding the fall and cane event detection in conventional canes. There is also evidence that kinematic data from a cane are appropriate for predicting falls before their occurrence and segment data between events.

Chapter 5

Cane-Type Robot

Still within the scope of stimulating the usability and acceptability of assistive devices, this chapter aims to prove an innovative and cutting-edge technology-based concept by obtaining a functional prototype of a cane-type robot. These type of robots have been researched extensively in the scientific community. However, mechanical validation and optimisation of the prototype design are lacking, which could prevent these devices from reaching the market. Because this device is more sophisticated than a conventional cane, it requires a series of chores to achieve an optimal result, which are detailed in this chapter: i) gather relevant information about consumers' needs and target specifications from scientific literature and international standards; ii) present the cane-type robot prototype developed based on the information collected; iii) mechanically validate the prototype by performing mechanical simulation tests in the SolidWorks software; iv) implement a low-level hardware and software architecture to manage the sensory and the actuation units; v) implement a high-level hardware and software to manage the low-level information and actions; vi) implement motion control strategies; and vii) validate the implemented functionalities.

5.1 Introductory Insight

To conceive, design, and commercialise a product, a series of phases from a specific and detailed development process must be followed (Fig. 19) [50]. As a result, the creation of a cane-type robot followed the ideas of this generic development process in order to produce a valuable and unique device capable of overcoming the mentioned drawbacks in subsection 2.3 of the state of the art. **Quality assurance** and **coordination** are the two main reasons why a well-defined development process is beneficial when creating a new product. For the **quality assurance**, the development process outlines the steps it will

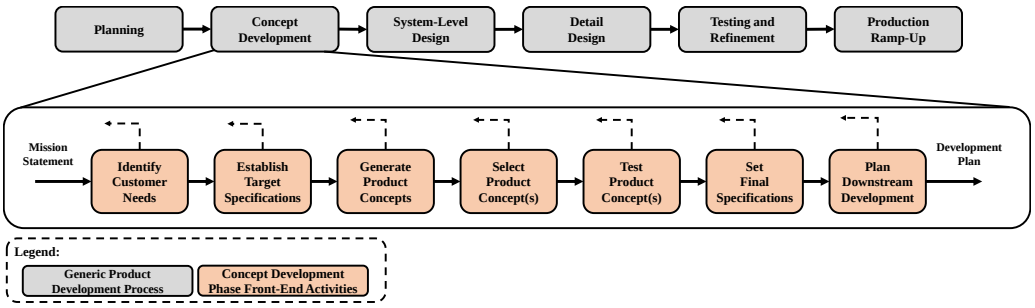

Figure 19: The generic product development process while detailing the concept development process.

take and the checkpoints it will encounter. Following the development process is a way to ensure the quality of the final product when these phases and checkpoints are appropriately chosen. Second, the clearly described development process serves as a master plan that outlines the tasks of each person on the development team, including when and with whom they will need to exchange information and materials.

As shown in Fig. 19, the generic product development process is divided into six stages. The process starts with a **planning phase**, which serves as a bridge between advanced research and technology development activities. The mission statement is the result of the planning phase, and it is the input required to begin the concept development phase, as well as a guide for the development team. The product launch marks the end of the product development process, when the product becomes available for purchase in the marketplace. The needs of the target market are recognised during the **concept development phase** (Fig. 19), and alternative product concepts are produced and reviewed before one or more concepts are chosen for further development and testing. A concept is a description of a product's shape, function, and characteristics that is usually supported by a set of specifications, a competitive product analysis, and a business case for the project. Finally, **system-level design**, **detail design** and **testing and refinement** phases complete the generic product development process explained by Ulrich and Eppinger [50] before product launch. They are responsible for, respectively: i) the definition of the product architecture, decomposition of the product into subsystems and components, and preliminary design of key components; ii) the complete specification of the geometry, materials, and tolerances of all of the unique parts in the product and the identification of all of the standard parts to be purchased from suppliers; and iii) the construction and evaluation of multiple pre-production versions of the product.

The cane-type robot evolved through the many phases outlined previously until it reached a functional prototype with an innovative, cost-effective, and intuitive motion control system that recognises user movement intentions and identifies the user's gait phases. Current literature cane-type robots present some drawbacks: i) only were tested with forward falls [74]; ii) were designed and limited to move in a pre-planned walking path [254], specially when the user is walking forward [255]; iii) requires previous data from the patient gait to detect falls [73, 79]; and iv) requires wearable sensors information (e.g. force sensors) to counteract fall occurrence or imbalance [43]. Large dimensions them awkward or impossible to use in small places, and high weight makes transport and storage difficult [77, 78, 256, 257].

5.2 Mission Statement

The mission statement helps to better grasp the cane-type robot's significance and it is composed by different steps [50], including: i) defining a description of the product; ii) indicating the target market for the product; and iii) determining some premises for the robotic cane, so that the final concept works according to the user. The core market for this product is those with restricted mobility, which can be caused by stroke, Parkinson's disease, or other types of restricting health issues, and includes people of all ages. The cane-type robot must be able to overcome the accompanying gait issues while also assisting in the prevention of falls. The benefit proposition is linked to a real-time fall prevention strategy, i.e., the ability to avoid a fall and the negative effects that come with it. In this case, the key market for this gadget is people who have trouble with their balance. Because various risk factors contribute to falls, it is possible to include every customer who may require balancing assistance. The secondary market caters to the seniors in institutions and people undergoing rehabilitation. Although falls are not specific to the elderly, age has been identified as a significant risk factor, with a definite correlation established between ageing and higher rates of falls. The goal of choosing a market in institutions and rehabilitation centres is to set a starting point for the cane-type robot as a market product, allowing for a study of the product's performance before developing further functionalities for real-world applications. The cane-type robot is a handheld gadget featuring smooth and intuitive motion control, as well as integrated real-time fall detection and prevention strategies. The cane's character as an assistance device, which is a product held in one hand, determines the handheld assumption. Furthermore, according to Afzal et al. [258], the user-cane contact is critical because the application of haptic light touch enhances balanced posture by assisting the human brain in producing better upright balance and giving lateral stability while walking. Finally, it is hoped that the final design adapts to the user's stride, physical attributes, health issues, and needs. The cane-type robot's mission statement is stated in Table 15. This device presents the following main functionalities: i) gait analysis through the estimation of gait parameters; ii) fall detection using an optical system; iii) fall prediction by implementing a FRA tool and acting mechanically to avoid a fall; and iv) context awareness by collection information from the environment.

Table 15: Mission Statement

Product Description	Cane with built-in real-time fall prevention strategy.
Benefit Proposition	Prevent falls and avoid injuries related to fall events altogether.
Primary Market	Consumers with balance impairments.
Secondary Markets	Institutionalised elders. Rehabilitation patients.
Assumptions	Handheld. Built-in fall detection and prediction systems with a fall prevention strategy.

5.3 Consumer Needs

Consumer needs are a key resource for judging the prototype's actual utility during product development phases such as defining the product's target criteria, concept generation, and selection. [259]. A need is considered as an attribute of a potential product that is desired by the consumer, i.e., the potential end-user of the cane-type robot prototype [50]. Although the process of recognising customer needs is not a perfect science, the information acquired is always valuable, even if it does not allow for the identification of every demand. To reduce the inherent risk of building a new prototype, a modified strategy for gathering consumer demands was used at this stage [50]. Instead of conducting interviews, focus groups, or other methods, it was performed a literature search for typical uses, likes, dislikes, and suggested improvements and needs associated with canes in general, which is presented below. By combining the results of numerous studies, it was possible to avoid issues such as the financial expense of focus groups, the time spent on interviews, and the project's innovative component, while gaining a broader perspective on the subject as a consequence of the greater number of perspectives considered.

Affordability refers to how much money the user has to spend on the cane's purchase, upkeep, and/or repair [260, 261]. According to a recent survey, the most prevalent cause for unmet mobility equipment needs, such as canes, is cost [262]. If the cane is easy to set up and use that means the user can assemble the product quickly, or it already comes assembled within an adequate package, learns how to correctly use the device faster, or with less training required [263]. The gadget may be carried and utilised in several locations at the same time. It responds to the user's input and is compatible with a variety of different devices [260, 261]. The cane should be the right height, with an ergonomic handle, and be light to maximise physical comfort and effectiveness during sporadic moments where it is necessary to transport the device anywhere else (e.g. change floor level) [77]. On the other hand, the device must have the enough weight to be stable enough when support is required [43].

The user will not experience any physical discomfort as a result of using the device. The height of the cane and how it is adjusted are critical for avoiding bad postures and a higher risk of falling [264]. Using varying shapes, sizes, and textures, the handle should be customised to accommodate different hands with different ailments, such as arthritis [265]. A light triggering mechanism must be implemented to provide better visibility to the cane's user and improve its safety. Inadequate lighting results in poor visibility which leads to a direct association with the risk of falling [266, 267]. Also to increase user's safety, vibrating motors should be integrated into the cane, with the purpose of notifying and adjusting irregular gait through vibratory signals [268]. Typically, assistive devices incorporate haptic feedback in the form of mechanical vibrations to assist blind users or even parkinsonians [269]. In addition, the device should be lightweight to make it easier to use during the user's daily routine and to prevent injuries [263]. The cane must be both safe to use and supportive to the user [270]. Given the device's intended use, the consumer must have an easy access to the product in the market [271]. However, there are still certain

Table 16: Primary and Secondary Needs for Canes and Their Relative Importance

No.	Primary Needs	Secondary Needs	Imp.
1	Affordable	Cheap; maintenance-free; covered by financing programs; has no hidden costs and a cost-free warranty.	3
2	Easy to set up and use	User-friendly interface and easy to learn; automatically turns on; independent operation; already assembled; easily transported; equally easy to use in both hands.	2
3	Correct height	Height is adjustable; already with the correct height.	5
4	Ergonomic	The handle is adjustable to the hand; has the correct size and shape accordingly to the user; pleasing texture.	5
5	Safe	The cane provokes no physical reactions; can be used everywhere; illuminates dark places; alerts the user for irregular gait.	5
6	Lightweight	The cane weight does not provoke fatigue.	5
7	Stylish	Design compatible with the consumer's ideals; customizable.	1
8	Offers support	Supports a body weight percentage; helps the user to walk.	4
9	Easily obtained	Simplified procurement process.	1
10	Effective	Accurate fall prevention, motion intention and gait phase detection. Control units sufficiently capable of executing the required algorithms. The cane meets the consumer's needs.	5
11	Durable	Cane lasts at least or longer than the expected life. Battery enough for a gait therapy session.	3
12	Reliable	The cane is breakdown free; no special condition needed; remains dependable under repeated use; no damage if not properly operated.	5

personal aspects that could influence how the cane is used. Reduce social stigma can start in the design process by developing more trendy and fashionable devices that are compatible with the user's personality and lifestyle [272], resulting in increased psychological comfort whether using the device in public or in private [260]. The cane needs also to be effective, durable, and reliable. The cane's use will improve the consumer's living situation by increasing functional capacities and/or independence, preventing falls and injuries, detecting user's motion intention and gait phases, and addressing the user's needs for such a device [260]. Moreover, the cane-type robot should be able to move effectively in any direction without changing orientation, being also capable of changing to any desired orientation while in motion. High- and low-level control units must be powerful enough to meet these needs for real-time usage. The gadget must be able to function for an extended period of time, with repeatable use resulting in predictable results [271]. This initial prototype's battery life ought to be sufficient for gait therapy sessions. In future prototypes, the battery should ideally last enough time for continuous and daily usage and assistance.

Table 16 divides consumer needs into two categories: primary needs, which are the most general, and secondary needs, which describe demands in greater depth. It was feasible to assign a level of importance to each primary need in collaboration with ORTHOS XXI dedicated personnel. This firm is engaged in

the production of orthopaedic and hospital equipment. This ranking is based on a numerical scale of 1 to 5, with 5 being the most important and 1 being the least important. Along with the design, this allows for proper trade-offs and resource usage. Because this is the initial prototype, functional needs took precedence over other needs, and they are the ones that will be examined in the following section.

5.4 Target Specifications

Target Specifications are a set of individual specifications that describe what the product has to do or accomplish. A specification is made up of a metric and a value, which can take many different forms, such as a number, a range, or an inequality, and is always accompanied by the appropriate unit [50]. This gives instructions on how to build and engineer a cane-type robot. They do not explain how the customer's needs will be met, but they do indicate what will be done to meet the needs identified in the previous section. They are preliminary specifications that convey hopes, aspirations, and goals for a marketable product. Appendix B lists all target specifications defined for the cane-type robot.

5.4.1 Affordability & Set-up and Use

Because there is now no commercial cane-type robot on the market, assessing or determining a price is rather difficult. However, there are other fall-related market solutions. The prices of the Dring and iStand canes are 129€ and 136€, respectively [273, 274]. They are, however, traditional cane concepts with sensors for post-fall detection. Hip protectors are only capable of minimising fall impacts since they are based on pre-impact fall detection algorithms. Helite Hip'Safe, for example, is a 649€ wearable airbag [275]. Although complicated literature solutions for the cane-type robot can increase the final price, new prototypes must be designed to lower manufacturing costs so that the product can compete with the presented solutions, relying on instrumentation and usage simplicity with technological assistance, e.g. detection of user's motion intention, gait phases and fall prevention strategies.

5.4.2 Support, Height & Ergonomics

During the gait cycle, canes only support a portion of the user's weight, and the weight transferred to the cane changes as the user walks. When the cane is entirely upright, the maximum force is imparted to it [276]. The weight of the cane is determined by the user's weight, but even more so by their condition; for example, users in bad health require more help [276]. According to Youdas et al. [277], the body weight percentage value is 25%. However, the International Organisation for Standardisation (ISO) 11334-4:1999 [278] specifies a static loading test with a specified loading force of 1000 N ± 2 % with a minimum value of 350 N ± 2 % to determine with greater certainty whether the cane can withstand large loads. The cane is inspected to ensure that it is not damaged to the point where it is unsafe to use, and that no portion of

the device is cracked or broken [278]. The weight of the final prototype, on the other hand, was set at a maximum of 6 kg (skeleton, wheels, DC motors, battery and other hardware) , since the cane will be used primarily on the ground. Otherwise, for conventional canes, literature proposes a weight lower than 1.2 kg because it can cause injuries in the user's arm and shoulder [80]. Towards human-robot interaction during gait to assess the influence of the weight on the device, mechanical simulation tests are required to understand how the cane deforms during this interaction. This allows for a better understanding of where and how force sensors can be used and, consequently, obtain input information for low- and high-level algorithms. Firstly, considering that the transfer of body weight supported on a single tip cane is 29 kg [276], deformation tests were specified with V forces of 300N (≈30.6 Kg) applied on the handle to simulate this event. Another smaller value of force (100N) was applied separately in the AP and ML directions.

When compared to previous robotic devices, this gadget should be easier to transport in circumstances where climbing or descending stairs is required. The weight is also crucial for DC motor dimensioning, which involves determining the torque and angular speed of the shaft. Walking speeds greater than 1.3 m/s, according to Quach et al. [279], increase the chance of falling. As a result, the maximum lateral speed was set to 1.3 m/s. The parameters for lateral acceleration, rotational speed, and rotational acceleration were set to 1 m/s^2, 1.3 rad/s, and 1 rad/s^2, respectively, with the help of Orthos XXI, so that the device can operate effectively to prevent a fall.

Another reality is that wrong cane length can cause a significant alteration in the user's gait biomechanics [264]. A lengthy cane causes more postural sway, necessitating postural modifications to maintain balance [280]. It alters the angle at which horizontal forces are applied, increasing the risk of slipping, sliding, or tipping over [264]. When using a short cane, the user leans toward the cane and bends forward when the device is placed forward, putting more strain on the lumbosacral region [281]. When the user stands upright, the top of the cane should match the distal wrist crease [264]. Studies demonstrated that this procedure allows 15° to 30° degree angle of elbow flexion which is biomechanically ideal [282]. The ISO 11334-4:1999 specifies a minimum height of 350 mm and a maximum height of 1100 mm for canes, which is normally adjustable for the user [278].

The handle of the cane is also very significant because the user grips it frequently while using it. The length of the handle, i.e. the dimension of the handle measured lengthwise, is defined as 100-150 mm to suit the user's palm [283]. According to ISO 11334-4:1999, however, this value is determined by the user and cane height, with a range of 65–110 mm [278]. A range of 25–45 mm should be considered for the handle width, i.e. the size of the handgrip measured horizontally at the thickest point, to allow the thumb to just cover the end of the index and middle fingers [283]. A similar range can be found in the ISO standard (25-50 mm). The range of handle slope is 0° to 15° [151]. The surface on the handgrip should not have sharp edges or high spots, which can decrease the comfort, strength, security of grip, and potentially cause injuries [284].

5.4.3 Safety, Durability & Effectiveness

Under normal circumstances, the cane must not cause harm to the user. All portions of the cane must be free of burrs, sharp edges, or projections that could harm clothing or cause discomfort to the user, according to ISO 11334-4:1999 [278]. In this context, international standards specify the need for three tests, using ISO11334 and ISO24415 as examples [278, 285]. The **stability test** is performed to evaluate the tipping angle and it is divided into two components: inwards and outwards. Both tests are carried out by applying a static force of 250 N ± 2% to the handgrip's midpoint and tilting the plane while simultaneously recording the highest angle obtained by the plane when the walking stick is tilted. In the inwards test, the angle must be at least 2 degrees, while in the outwards test, the angle must be at least 5 degrees for a tripod walking stick and 7.5 degrees for a quad-cane [278]. The **separation test** is only applicable to walking sticks which are joined together by two or more parts only when the joint is not part of the height-adjustment mechanism. It involves pulling on the lower and top sections of the walking stick with a 500 N ± 2 % force. That force should be increased progressively over 5 seconds, up to the maximum force, and held there for 10 seconds. A positive result indicates that the canes' top and lower halves cannot be separated [278]. Because cane-type robots lack tips, the **friction test** cannot be used [285]. Light triggering mechanism must illuminate the user's path with low luminosity up to 5 meters in order to safely and early find obstacles and environment hazards [286]. Additionally, users must perceive vibrations for alerting tips. ISO 11334-4:1999 specifies a **fatigue test** when it comes to durability. A cyclic force of 450 N ± 2 % is given to the handle, with a minimum of 157.5 N ± 2 %, at a frequency of 1 Hz for 200 000 cycles. The cane must not be damaged to the point that it becomes unsafe to use, and no part must break or crack [278]. The cane-type robot's battery life must be at least 1 hour to ensure a gait therapy session [287]. The cane-type robot's effectiveness relies on several factors. First, the device must run the algorithms in real-time without deficient delays. It also must present high performances for fall prevention (≥ 84%) [224], motion intention (>95%) and gait phase detection (>95%). The last two functionalities must be as accurate as possible to also guarantee the user's safety while using the device. Finally and generally, effectiveness also assesses if the cane meets the consumer's needs.

5.5 Concept to Prototype

ORTHOS XXI assisted in the concept development process that might potentially address the same demands and specifications after identifying a set of consumer needs and creating target product specifications [50]. Using Solidworks, a 3D design of the robotic cane was created based on numerous ideas. For this first prototype, it was decided not to employ the ball joint as Yan et al. [288] suggested because it would add to the prototype's costs and could result in even more unexpected alterations, particularly for users who are not accustomed to using a cane. The created prototype, shown in Fig. 20, is separated into

two parts: i) the upper part, which is made up of the cane's handle and trunk; and ii) the lower part, which is made up of the holonomic base, DC motors, and omnidirectional wheels. Robots can be categorised as "holonomic"or "non-holonomic"drive robots depending on how they move. This is decided by how much of the robot's total Degrees of Freedom (DoF) are controlled, and when both are equal, the robot is said to be "holonomic"[289]. These robots can move in any direction without altering their orientation, and they can also do it while still moving [290, 291]. This is crucial for the cane-type robot since it makes it easier to manoeuvre in confined spaces, which has a significant impact on the product's functionality. The cane's upper part was moved to holonomic base CoM to allow the user to get a better grip on the instrument, as well as a higher stability when the user needs support. This concept intends to allow the user to walk in a more natural manner, providing greater comfort to the upper limb. Furthermore, the height of the cane can be easily adjusted, with a range of 846–998 mm, which meets the desired criteria (350–1100 mm). The handle of the cane adheres to the criteria discovered.

Considering the lower part, we reduced the distance between the furthest wheel from the user and the prototype's CoM as depicted in Fig. 20. Thus, the cane-type robot will be able to perform rotations more quickly since this wheel will need to travel shorter distances. This detail can be important for the fall prevention strategy. Moreover, the holonomic base is made of plain carbon steel and it has 3 mm of thickness. The distance between the furthest wheel from the user and the prototype's CoM was lowered in the lower part, as shown in Fig. 20. Because this wheel must travel fewer distances, the cane-type robot will be able to perform rotations faster. This information might be crucial for the fall prevention approach. Furthermore, the holonomic foundation is 3 mm thick and made of alluminium. All the dimensions are depicted in Figure 20. At this stage, the prototype costs are less than 15€ without DC motors, wheels, or hardware.

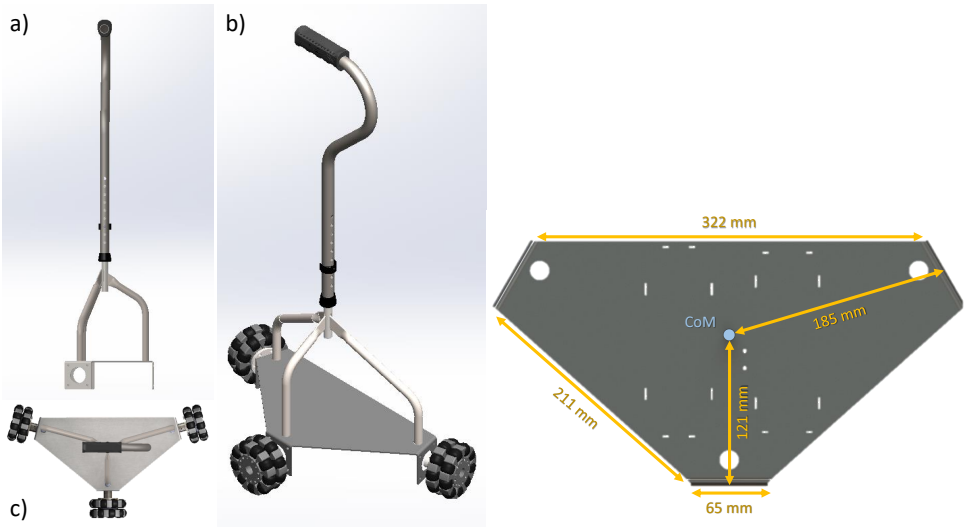

Figure 20: Final render of the cane-type robot prototype on the left: a) front view; b) trimetric view; c) top view. Prototype's holonomic base, its dimensions and CoM position on the right side.

5.6 Mechanical Validation

Simulation modelling must be used to improve some features before generating a physical prototype. This analysis is carried out against the previously stated target specifications, where stress distribution and other computer-aided engineering techniques can help discover and eliminate model flaws, potentially avoiding the need for one or more physical prototypes, saving time and money [50]. Because of their importance, it was conducted the following tests: static load, separation, and fatigue tests. The SolidWorks model was also simplified by deleting the upper part and simplifying the omnidirectional wheels. If the prototype achieves the previously established good results, it is considered validated. Moreover, simulation mechanical tests were performed to measure deformations in the cane's upper part in order to identify higher deformation locations to install force sensors for further advances in the human-robot interaction. The results are summarised below.

5.6.1 Static Load Test

The chosen fail criterion was the von Mises's theory which states that a ductile solid will yield when the energy density reaches a critical value for that material, considering an uniaxial point of view (σ_{VM}=σ_Y, where σ_{VM} represents the von Mises's maximum stress and σ_Y the material yield strength). This yield strength is the point at which elastic behaviour ends and plastic behaviour begins. Plastic deformation occurs when the maximum stress exceeds the yield strength, resulting in some type of permanent deformation. The optimum outcome would be for the maximal von Mises stress to be less than the yield strength [292]. Applying a total force of 1000 N distributed between the three legs, the maximum σ_{VM} is equal to 6.43x10^7 N/m^2 (Fig. 21), which is lower than the plain carbon steel yield strength (σ_Y = 2.21x10^8 N/m^2). Therefore, the $\sigma_{VM} < \sigma_Y$ condition is verified and the holonomic base should not fail due to plastic deformation. Moreover, the minimum Factor of Safety (FOS) is equal to 3.4, the maximum strain is 2.01x10^{-4}, and the maximum displacement is 2.78x10^{-1} mm, which should be negligible since the material always operates in the elastic domain.

5.6.2 Separation Test

The separation test applied a force of 500 N to the lower and upper parts of the prototype. The maximum σ_{VM}, equal to 2.84x10^7 N/m^2, is registered in the connection points between the DC motor and the holonomic base. The chosen material for the DC motor was the AISI 1045 steel, a common material used in gears, shafts, and bolts. This metal has a σ_Y equal to 5.30x10^8 N/m^2 and higher than the σ_Y of the plain carbon steel. Therefore, the $\sigma_{VM} < \sigma_Y$ condition is verified again and there should not happen any failure due to plastic deformation, and no separation between parts of the cane-type robot. The minimum

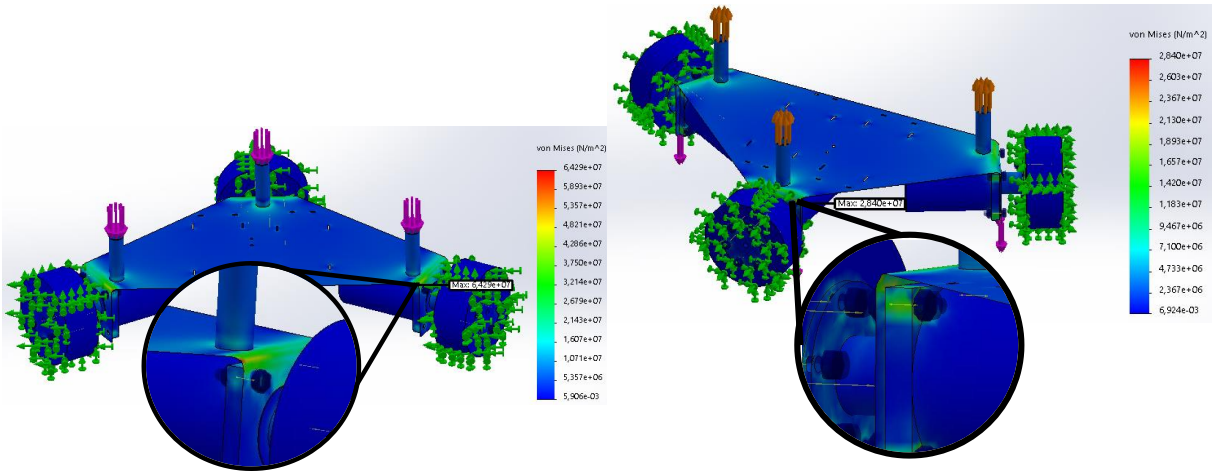

Figure 21: Stress plots obtained in the static load test simulation (left) and in the separation test simulation (right). Regions where the greatest stress occurs are zoomed.

FOS is 7.4, the maximum strain is 1.23x10^{-4}, and the maximum displacement equal to 8.40x10^{-2} mm. Figure 21 plots the stress obtained in the holonomic base.

5.6.3 Fatigue Test

According to ISO 11334-4:1998, a cyclic force of 450 N is delivered to the cane for 200 000 cycles [278]. However, no failures occur with this setup, suggesting that the amplitude of the stress level is less than the endurance limit, within the infinite life area. The fatigue simulation shows that increasing the load scale by a factor of 6 for 200 000 cycles results in the highest damage percentage of 77.32%, which occurs in the region of higher stress reported during the static load simulation. It also shows that the model has a life cycle of roughly 258 700 cycles at 6000 N before fatigue failure. These figures are much in excess of the desired range, and no fatigue failure is foreseen.

5.6.4 Human-Robot Interaction Test

Based on the performed simulations, it was obtained a maximum value of equivalent deformation (ϵ) of 9.909e-4 m and 3.748e-3 m when 100N are applied to the cane's handle in the AP and ML directions, respectively, simulating forward and lateral movement. On the other hand, 300N applied vertically in the cane's handle, simulating a support gait phase, resulted in a ϵ maximum value of 1.590e-03 m. The obtained results are represented in Fig. 22. Considering these findings, it is possible to claim that the material deformation of the of the cane's upper part is too small to be detected by common strain gauges. A common strain gauge has a SENS of about ≈2.0mV/V to 1000µm/m ($\epsilon = 1x10^{-3}$) deformation in a full-Wheatstone-bridge configuration [293–295]. Considering the highest value obtained in the simulations when AP and ML forces were applied, this would result in a value of ≈7.50mV/V for the respective equivalent

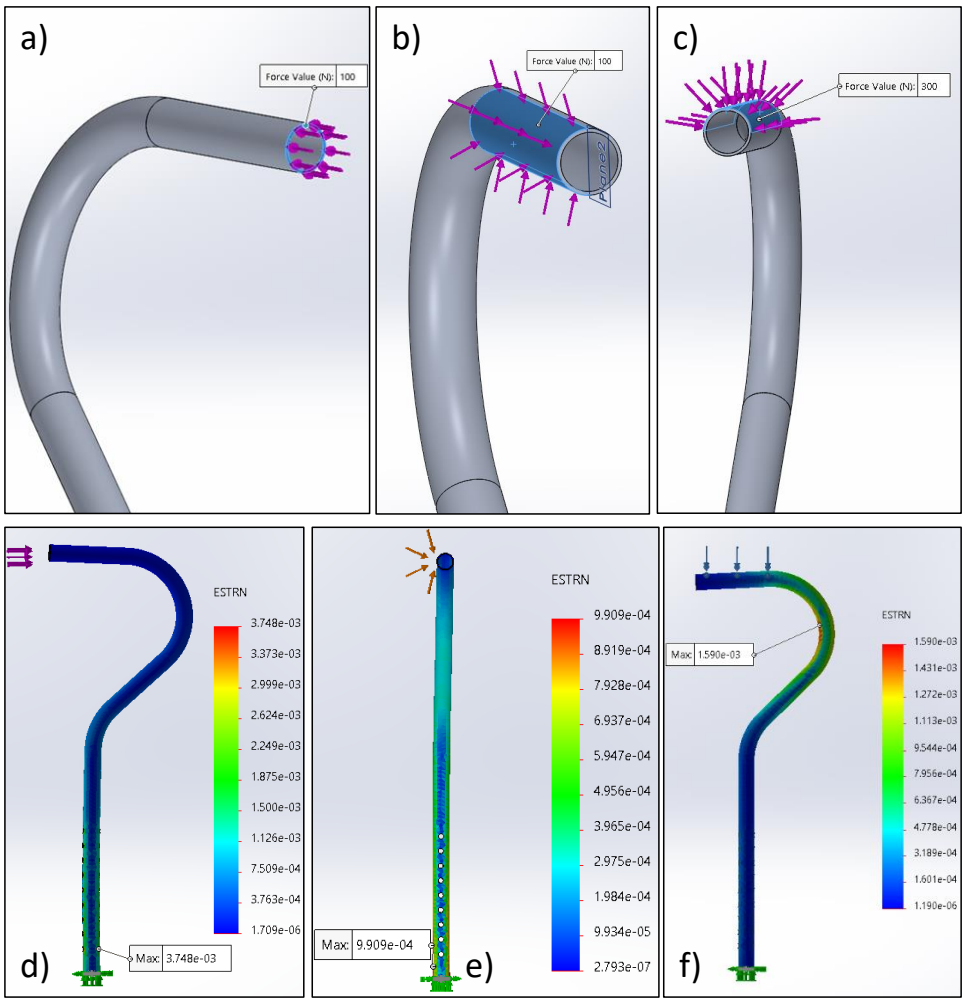

Figure 22: Applied force on the cane handle of (a) 100N in the AP direction; (b) 100N in the ML direction; (c) 300N in the z-axis direction. Equivalent deformation values obtained for applied force in d), e) and f), respectively.

strain. This SENS would result in a signal too small to be feasibly detected by common control unit's analogue ports. It is further suggested the implementation FSR sensors as the sensory device of the motion control system, as they are durable, thin, flexible, widely available and cost-effective sensors with a wide range of force SENS, and capable of detecting the user interaction forces applied in the cane's handle [296].

5.7 Cane-Type Robot Architecture

The cane-type robot is equipped with physical units (hardware) and software tools. The physical units are divided into five categories: i) sensory unit; ii) actuation unit; iii) control unit; iv) storage unit; and v) power unit. An integration unit is also included in the cane-type robot, allowing synchronisation with other technological systems. The control unit will transmit commands to the actuator unit after the information and

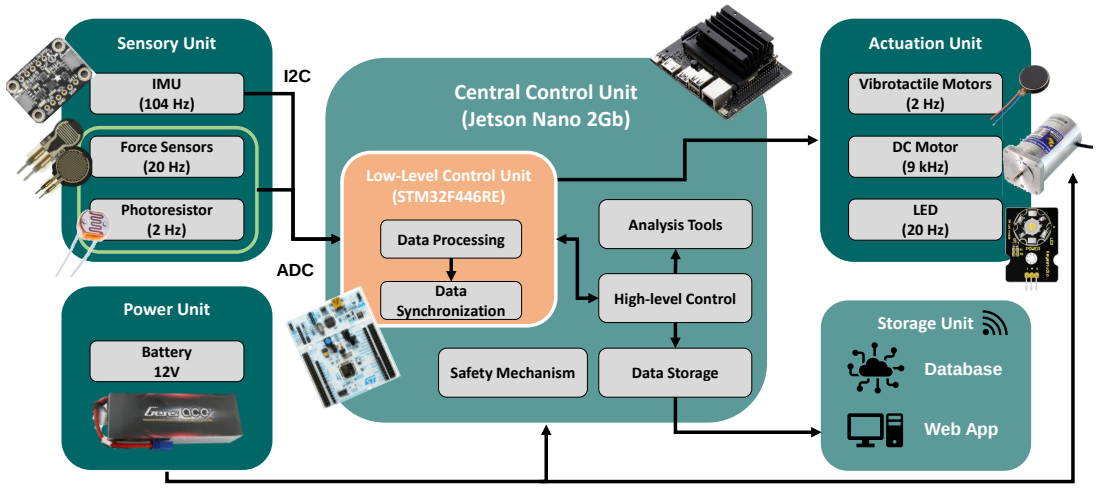

Figure 23: Cane-type Robot architecture with the respective units, components operating frequencies, communication protocols and data control of the electronic system.

data received by the sensory unit has been examined and processed. These orders are intended to trigger action mechanisms in order to ensure the proper operation of the entire cane system, hence ensuring security conditions and corresponding to the user's intentions and commands. The control, storage, and power units are all housed in the cane's holonomic base. The actuation units are incorporated in the holonomic base (DC Motors and a LED) and the cane handle (vibrotactile units), as this is the only point of contact with the user for vibratory sensory inputs. A set of powerful computational tools is referred to as software tools. Both at the prototype level and in the realm of intuitive graphic programmes for cell-phones and desktops, progress is still being made. Figure 23 depicts the fully instrumented cane-type robot architecture that is being implemented.

5.7.1 Central Control and Storage Units

The Control Unit is in charge of processing all of the data collected by the sensors and providing commands to the actuation units. The low-level and high-level control units are divided into two components. It is critical that they have a high processing power, as well as numerous communication channels that allow connecting to all components of the cane-type robot, for all processing to be carried out without errors and swiftly enough to calculate, receive, and transmit all data. The information is transferred between the two control devices using USB connectivity. The low-level control unit (STM32F446RE microcontroller) stands out for its versatility of connections with different components, being also responsible for cane motion control, security mechanisms, and external device synchronisation. It was designed for simpler calculations of acquired data from the sensory unit, and transmission to the actuation unit as well as the high-level control unit. The STM32F446RE microcontroller (Fig. 24.a) demonstrates a high processing power with a maximum clock speed of 180 MHz, as well as a wide range of Pulse Width Modulation (PWM) outputs and

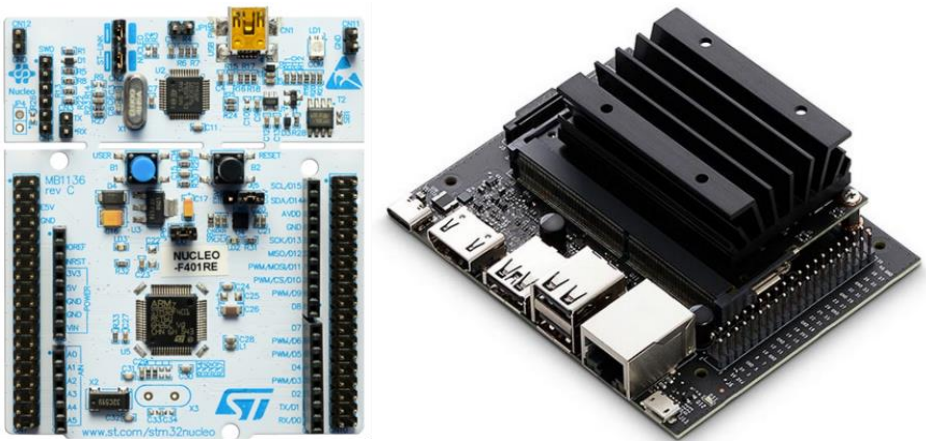

a) b)

Figure 24: Cane-type Robot's control unit: a) STM32F446RE board; and b) NVIDIA Jetson Nano.

3x 12-bit Analog-to-Digital Converter (ADC) (up to 16 channels) with a selectable resolution of 12/10/8/6 bits. It also supports UART, I2C and SPI communication, which allows to perform the necessary communications with several components and units simultaneously. The NVIDIA® Jetson Nano™ 2GB Developer Kit, a compact and powerful computer with great processing power, is used for high-level activities and specially created for real-time usage of AI, being one of the best market solutions for this purpose (Fig. 24.b). It will be in charge of storing data, communicating with the low-level control unit, communicating with the outside via Bluetooth or Wi-Fi, and all analysis tools, such as FRA, processing and calculations for fall detection and prevention, and distinguishing between normal and abnormal walking states. The high-level control unit supplies USB power to the low-level control unit.

5.7.2 Sensory Unit

A set of specifications were developed for the sensory unit's execution, which culminated in its integrated features and high performance. The sensory unit was required to use current, efficient, compact, and low-cost technologies. An **inertial system**, a **context-awareness system**, and a **force system** are all part of the sensory unit. Force sensors, light sensors, and inertial sensors are among the components that make up the sensory unit. The function and context of the sensory unit, which is already or will be included in the cane-type robot, are summarised in Table 17. One of the information that could be received in the sensory unit is context-aware footage from a RGB or depth camera or even lasers, which could be used for gait analysis, FRA, and fall detection. This sensor, however, will not be described in this PhD thesis because it is not included in the current version of the cane-type robot. The **inertial system** is composed by the Adafruit LSM6DSOX + LIS3MD IMU, and it is positioned at the base of the cane (Fig. 25.a). The LSM6DSOX component, which is a 3-axis accelerometer and gyroscope, measures i) the rate of change of velocity along three axes, and ii) detects rotational changes in relation to orientation and calculates angular

Table 17: Contextualisation of the cane-type robot's sensory unit

Purpose	**Information Acquired**	**Parameters**	**Currently Available**
Gait analysis	Acceleration Angular velocity Cane orientation Force Context-aware footage	Gait phases Stride and support phase duration Stride length Support weight User movement intention Velocity	✓*
Fall risk assessment	Context-aware footage	Displacement, velocity and orientation FRA and correlation with the QoL	✗
Fall detection	Context-aware footage	Image processing	✗
Context awareness	Light intensity	Environment luminosity	✓

*- except context-aware footage

velocity along three axes. The LIS3MDL component, which is a 3-axis magnetometer, monitors the relative change of a magnetic field, as well as its direction and intensity. With all these sensors, important inertial information about the cane-type robot will be attained. By combining data from 3 sensors with triple-axis (9 DoF), it is also possible to obtain the movement orientation and direction of the cane, as well as its inclination in relation to a predefined reference plane. The system works at 104 Hz and uses a data rate of ±2G for the accelerometer, ±250 DPS for the gyroscope, and ±4 Gauss for the magnetometer. Given that many falls occur due to low visibility conditions, it was also discovered that none of the robotic canes tested in the state of the art had mechanisms of sensing and action related to brightness. As a means of overcoming this barrier, which increases the risk of cane users falling, it was decided to implement a **context-awareness system** based on a light sensor that aims to detect environmental conditions, specifically the luminosity in the vicinity of the user's circulation. Then, the information is sent to a light triggering mechanism considering the readings obtained, in order to provide better visibility to the cane's user. A photoresistor, also known as a Light Dependent Resistor (LDR), is employed as a light sensor at the base of the cane (Fig. 25.a).

The haptic sensing system and the axial force system make up the **force system**. Firstly, V force detection (i.e., on the axis perpendicular to the cane's displacement plane) is critical for tracking the user's gait. Such parameters enable for the detection of when the cane is being used, as well as the amount of support weight put by the user on the cane, in order to determine which phase of gait the user is in. For the sensing of V forces imparted to the cane, piezoresistive sensors, also known as FSR, are used. Because of its tiny size, the Interlink FSR® Model 402 Short Tail sensor (Fig. 25.b) was chosen as the optimum solution for sensing human-robot interaction forces to be applied in relatively small systems.

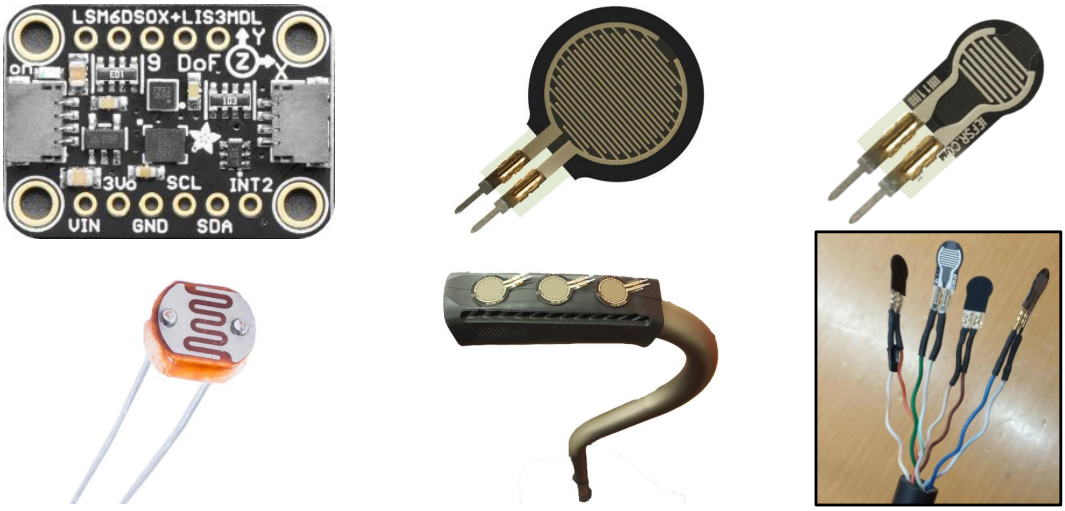

Figure 25: Sensory unit elements already implemented. a) inertial system (top) and photoresistor (bottom). b) Interlink FSR® Model 402 Short Tail sensor (top) and location in the handle (bottom). c) Interlink FSR Model 400 Short Tail force sensor (top) and combinations of four sensors to detect the engagement between the user and the cane-type robot.

Thus, the haptic sensing system creates a map of the forces applied by the user's hand while using the cane and supporting its weight during different gait phases.

An axial force sensor is required to detect the forces of engagement between the user and the device. Through the forces applied to the cane, this sensor can assess the user's intention of movement and so acquire admittance control to move the cane to the desired position and accompany the user while walking. A combination of four force sensors, placed around the cane rod and perpendicular to the horizontal plane, is offered as a solution for the cane-type robot axial force system. The Interlink FSR Model 400 Short Tail force sensors to be used for axial force detection are depicted in Fig. 25.c and have the same characteristics and response as the handle force sensors previously stated for the haptic sensing system. It was used to take advantage of the fact that the cane's rod is separated into two sub-rods, the handle rod (upper part) and the base rod (lower part), which are interconnected to allow the cane handle to be adjusted in height. As a result, by slightly lowering the diameter of the base rod, the four FSR sensors may be placed between the upper and lower rods of the cane, 90° apart in regard to the tube's centre point, as shown in Fig. 26. There is a small space between the two rods in this design, which allows the user to measure the interaction forces applied in the handle of the cane at the position where the four force sensors are situated. The amplitude and direction of the force applied in the cane's displacement plane can be determined using this sensor arrangement, showing the user's intention when manipulating the handle.

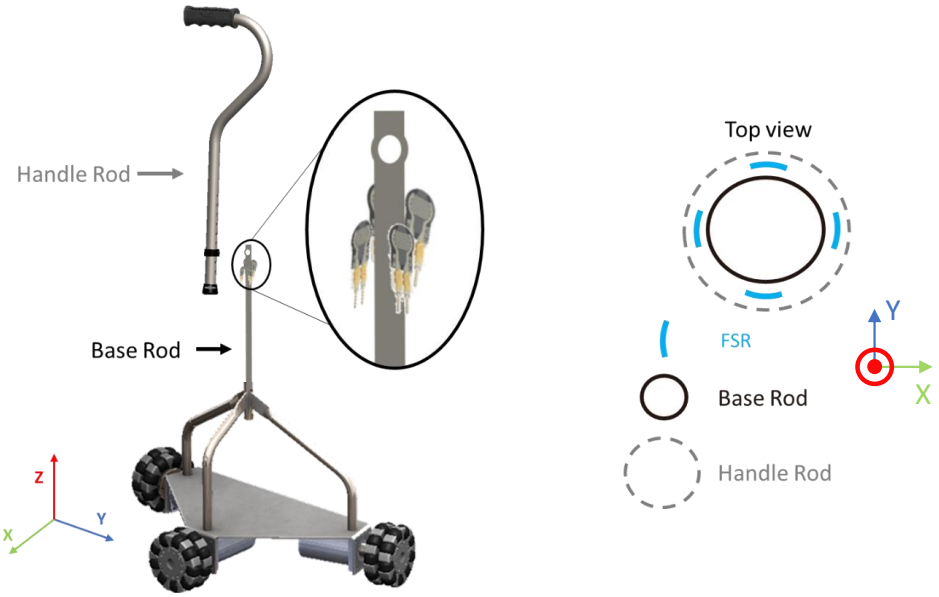

Figure 26: Force sensor configuration to obtain an axial force system. The sensors are placed between the base rod (lower part) and the handle rod (upper part) of the cane.

5.7.3 Actuation Unit

The actuation unit is made up of multiple of systems that manage the interaction between the cane and the user, as well as the interaction between the user and the surrounding environment, and lastly the movement of the cane-type robot. The actuation unit is composed of three main parts: vibrotactile motors, a luminosity device, and DC motors that operate the wheels. The purpose and context of the actuation unit are summarised in Table 18. The cane-type robot is made up of applications that need mobility and physical manipulation and requires close human-robot interaction. A vibratory actuation mechanism was used in the context of robot-to-human communication, allowing direct interaction between the robot and the user. Assistive devices with haptic feedback in the form of mechanical vibrations are typically designed to assist blind people in being steered in a specified direction. Furthermore, vibrational actuations are used as a resource in patients with Parkinson's disease to deal with gait problems and FOG symptoms [297]. These symptoms have a significant impact on patients' QoL since they might cause unpredictably lost movement control and lead to falls. When walking on a treadmill, Wegen et al. [268] found that vibrations supplied to the wrist at a frequency 10% below the optimum stride frequency resulted in lower stride frequencies and longer stride lengths. Vibrotactile motors were integrated into the cane-type robot with the goal of informing and regulating irregular gait through vibratory impulses, allowing for a regulated gait and, consequently, potentially reducing user falls. Vibrotactile feedback is really quite significant given its discretion, lack of habituation, and ability to notify the user without raising stress levels [298]. These motors are housed inside the cane's handle, as shown in (Fig. 27.a), with no physical interference with the user's grip. This allows vibration to be transmitted to the user's hands , i.e., the only point of contact between the user

Table 18: Contextualisation of the cane-type robot's actuation unit

Purpose	**Actuator**	**Parameters**	**Currently Available**
Gait correction	Wheels DC motors Vibrotactile motors	Velocity User alert	✓
Fall prevention	Wheels DC motors	Displacement, velocity and orientation	✗
Context awareness	Light	Environment luminosity	✓

and the device, facilitating robot and human contact. Myles et al. [299] also claim that the hands have the highest vibrational SENS when compared to other parts of the body, which explains the location and mechanism of the haptic feedback system used on the cane-type robot. Because the motors are flat and the tube inside the handle has a round surface, a 3D printed structure has been designed to allow the motors to make full surface contact with the handle tube, allowing full vibration transfer (Fig. 27.a). The vibrating units are 10 mm eccentric rotating mass vibrating motors from Precision Microdrivers (Fig. 27.b), which have an off-center load and vibrate when rotated by the centripetal force [300]. Because of their compact size and closed vibration mechanism, they are ideal for being inserted inside the cane handle while retaining all of their functions. The Texas Instruments Haptic Motor Driver DRV2605L is required to operate the motors (Fig. 27.b), which involves I2C connection and allows the motors to be controlled by PWM signals, allowing the vibration intensity and rotation direction to be adjusted [301, 302].

When the user is operating the cane in poor vision conditions, the luminosity device is responsible for illuminating the outer environment. This actuation mechanism is linked to the photoresistor component of the light sensor. When the control unit senses low light, it activates the appropriate lighting equipment to ensure that the surrounding area is well lit. A high-brightness LED with a huge field-of-view capable of illuminating up to 5 m is employed on the cane's base pointing in the movement direction (Fig. 27.c).

The cane-type robot's omnidirectional mobility is enabled by DC motors, which control its direction, speed, acceleration, and rotation. They are linked to admittance control, which accepts sensory information from the user's intention and regulates the motors to match the movement. A kinematic and dynamic model of the holonomic base was developed in order to calculate torque and angular velocity values for DC motors [303]. The DC motors should have a minimum torque of 1.47 Nm and a minimum angular velocity of 295 rpm, based on a maximum payload of 29 kg [276] and the specifications of mass, velocities, and accelerations criteria defined previousley. Three Rhino Motion Control Solutions NEMA23 (RMCS-2255) motors [304] are integrated into the holonomic base of the cane for this purpose, as shown in Fig. 27.d. These motors feature a high torque (2.94 Nm) and an angular velocity of 300 rpm, which respects the values obtained with the dynamic and kinematic models. They employ an optical encoder, which offers

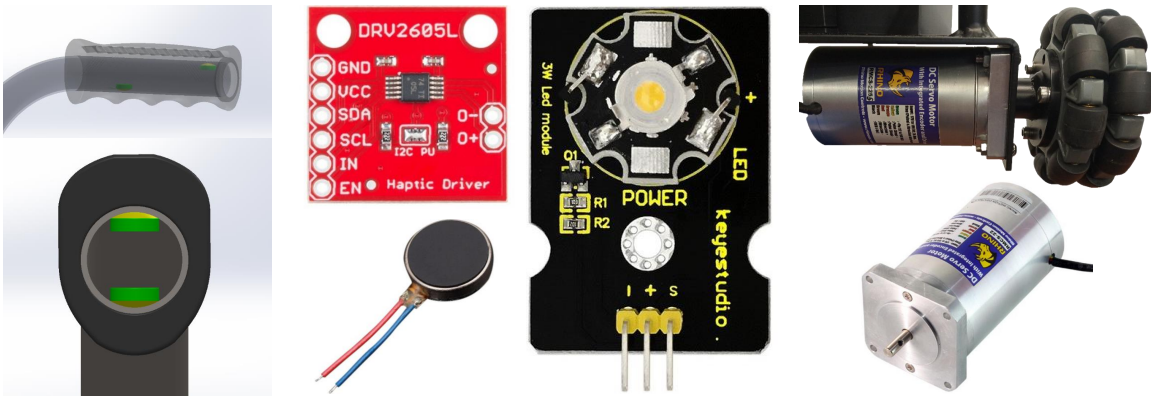

a) b) c) d)

Figure 27: Actuation unit elements already implemented. a) vibrotactile motors position at the cane's handle. b) vibrotactile motor from Precision Microdrivers (bottom) and a DRV2605L driver (top). c) LED. d) NEMA23 (RMCS-2255) motor (bottom) and the same motor installed in the cane with the omnidirectional wheel (top).

better precision and resolution (0.2° per step, 1800 steps per rotation) than a magnetic encoder and can be used in applications with a high magnetic field. Although the motors' technical specifications state that the no-load current is 0.8A and the maximum load current is 7.5A, experimental tests revealed that the values obtained for no-load current at maximum motor speed are on the order of 0.4A. In addition to these figures, it was discovered that the average current consumption of the three motors when walking with the cane-type robot is 3.6A. Their operate voltage is 12V and present a direct replacement for 50W stepper motor and drive. Each DC motor with these specifications costs around 80€.

5.7.4 Power Unit

All the architecture units in this chapter require energy to function. This need a power source that can power the full robotic system. However, not all components use the same amount of energy, necessitating the installation of devices capable of restricting and quantifying the amount of energy given to each component. Furthermore, because improper current and voltage administration can cause malfunction or even permanent irreparable damage to electrical components, an electrical safety scheme is essential to prevent such harm. As shown in Fig. 28, the power unit circuit consists of a battery, DC voltage regulators (+5V and +12V), electric fuses, and a power button positioned at the holonomic base. The Gens Ace lithium-polymer battery [305] has a capacity of 8Ah, meeting the previously identified battery capacity, and a voltage of 14.8 V, accounting for any possible voltage drops during operation. As for the battery type, lithium-polymer was the chosen one because of its higher safety, lightweight (0.74 kg), and low profile (157 x 53 x 43 mm), ideal for the cane-type robot. However, based on the average consumption of the previously indicated DC motors, which are the components that consume the most energy (approximately 7.8A), this battery allows a continuous operation time of 60 minutes on a single charge, approximately,

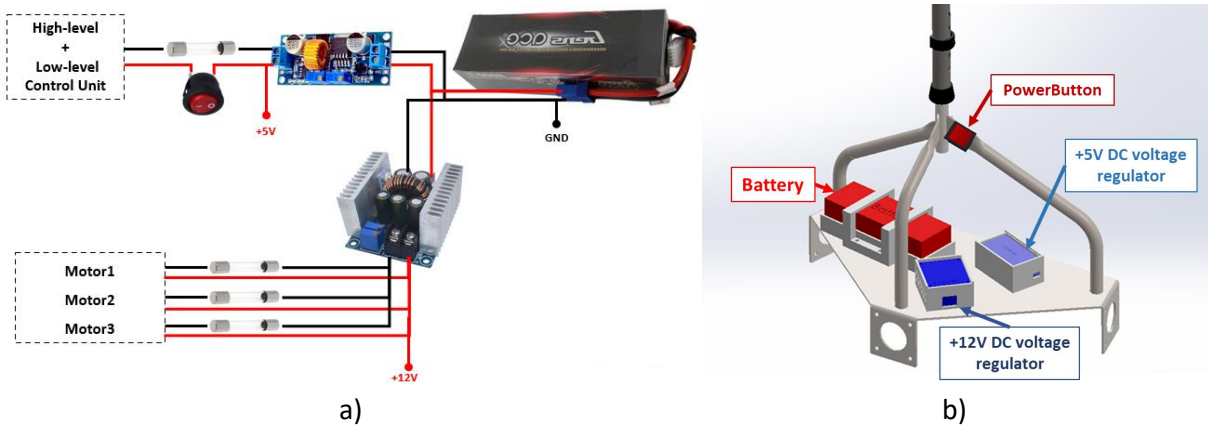

Figure 28: Power unit. a) schematic. b) location of the elements at the cane-type robot.

which meets the target specification identified previously. This finding shows that the cane-type robot can be used, for example, in gait therapy sessions. The DC Voltage Regulator, also known as a step-down, is designed to regulate the voltage from the battery and deliver the proper power to the general circuit, ensuring that the functionality remains steady. A step-down capable of restricting the input signal to 5V at the output [306] is meant to deliver energy to the high-level Control Unit through USB-C, with the low-level Control Unit receiving energy via USB mini-B afterwards. The DC servo motors are powered by another step-down with the option to limit the input signal from the battery to 12V at the output [307]. Thus, this unit powers the architecture elements separately. A current overload, or a sudden increase in the intensity of electrical current flowing through an electrical circuit, can cause overheating, compromising the conductors' integrity and potentially resulting in fire, skin burns, or the destruction of other circuit elements. Electric fuses [308] are employed as safety and protection methods for the cane-type robot circuit to avert such an occurrence.

5.8 Cane-Type Robot Assembly

This subsection aims to synthesise the various units responsible for the cane's overall operation by demonstrating an overview of the connections that encompass the electronic components, in order to gain a better understanding of how the components communicate with one another and which connections are required for information exchange. A Printed Circuit Board (PCB) was developed to serve as a common reference point for all of the cane's electronic components. It houses the low-level control unit, as well as the majority of the system's connections. The power unit is entirely connected to this PCB, as well as the actuation and sensory units. The PCB schematic and board layout were made using the EAGLE software, designing a single-sided PCB, where the conductors are placed on only one surface of the dielectric base, obtaining the dimensions of 125 x 152 mm. The PCB layout and the final print result with the implemented electronic

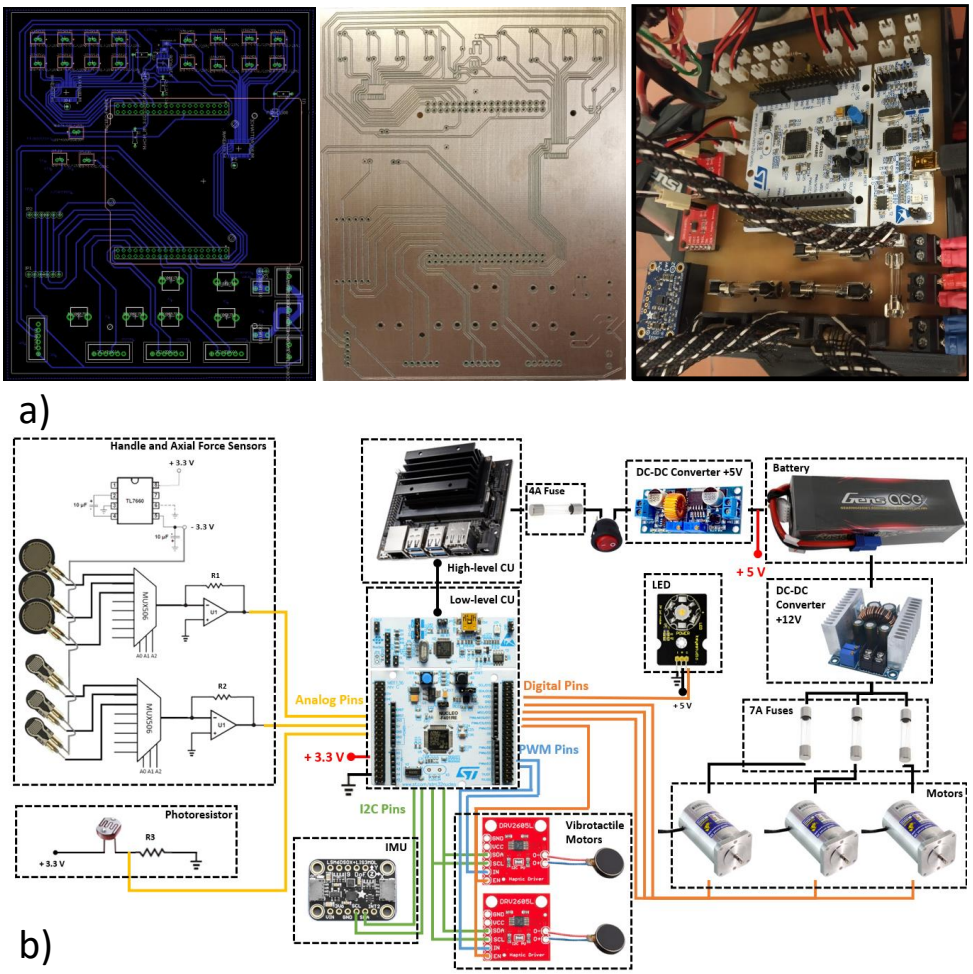

Figure 29: Cane-type Robot. a) PCB virtual board, physical board and final result (from left to right). b) Schematic of cane's hardware.

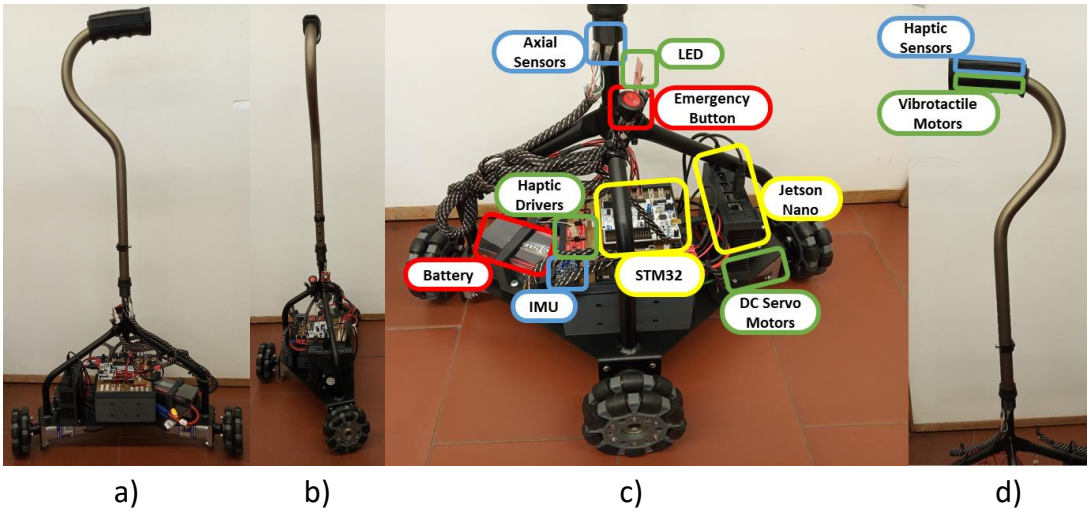

Figure 30: Cane-type Robot. a) Lateral View. b) Front View. c) Lower part instrumentation. d) Upper part instrumentation. (Red – power unit; Green – actuation unit; Blue – sensory unit; Yellow – control unit)

components is illustrated in are shown in Fig. 30.a. Figure 30.a shows a diagram of the components' connections for a better understanding and visualisation. On the other hand, Figure 30.b depicts the current cane-type robot with all components installed and labels all of the robotic cane's electric components. The cane-type robot is reported as having a total of 71 instrumented components, a total weight of 5.5Kg, an average current draw of 7.8A, and a total price of 688.97€. Appendix B presents the main information of each cane-type robot component.

5.9 Cane-Type Robot Motion Control

The motion control is responsible for allowing the cane-type robot to move and manage the device through user input. This must take into account a number of factors in order to provide the end-user with a simple, straightforward, intuitive, and comfortable experience. It must have a controlled gait that always follows the user and has no mobility restrictions, ensuring user safety as a top priority in all conditions. According to state of the art, admittance control [309–311], self-balance control [77, 255], passive control [79], and accompanying control mode [75, 311] were all employed as motion controls. The admittance control method is identified as the most used method among cane-type robots within the scope of motion control. Therefore, this method was incorporated in this work, leading to the instrumentation of specific sensory components into the cane.

5.9.1 Admittance Control Strategy

The proposal of an algorithm that permits operating the cane-type robot by considering the user's gait phase and the forces applied by the user is the initial phase of motion control implementation. The Admittance Control method considers the user's intention while defining the cane's behaviour. There is a whole process that starts with the acquisition of sensory data and continues with the synthesis of signals through signal processing techniques, allowing an analysis and evaluation of how the cane should operate based on all the information obtained, and thus control the motors to originate the movement of the robotic cane through direct kinematics. In order to determine how the robotic cane will operate, the user and cane's movement while walking was idealised, as shown in Fig. 31. According to Nakagawa et al. [310], it is possible to successfully lessen the load applied to the affected leg when a person walks with a cane-type robot by programming it to function similarly to a conventional cane.

The user's feet are aligned with the robotic cane at the start of the gait event, which represents the **standing phase**. The **cane swing phase** follows, in which the cane must comprehend the user's intention to move it forward with a constant speed (25% of 1.3 m/s, i.e., 1.2 km/h approximately) in order to support leg movement during the next gait phases. The **healthy leg support phase** begins with the robotic cane already in a posterior position in relation to the user's feet, where the cane must

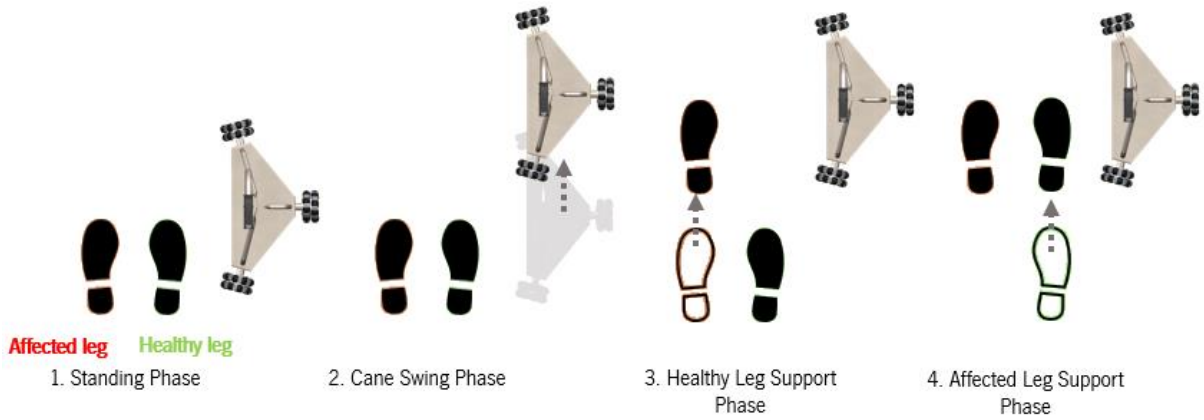

Figure 31: Power unit. a) schematic. b) location of the elements at the cane-type robot.

remain stationary to prevent the user from falling during this gait event to advance with the affected leg while supporting the majority of his weight on the healthy leg. Finally, the **affected leg support phase** occurs, which is the most crucial gait event, during which the healthy leg advances. During this phase, the user leans on the cane to allow the healthy leg to advance, rather than maintaining the body weight on the stationary leg (i.e., the affected leg). The cane remains in a static posture during this process to ensure a steady support for the user. The cane-type robot must comprehend the user's intention of movement in order to carry out all of these sets of procedures correctly. In order to stop the cane from moving, it is also necessary to detect when there was a stronger application of V pressures on the cane, indicating when the user is supporting his body weight on the cane, particularly in the third and fourth gait phases (Fig. 31).

5.9.2 User Motion Intention

The ultimate solution for the cane-type robot axial force system is based on a combination of four force sensors mounted on the cane rod perpendicular to the cane displacement plane in the AP and ML directions. A 3D printing structure, nominated **axial ring** (Fig. 32), made out of a polymer known as Polylactic Acid (PLA), is placed on top of the sensors sensitive area to obtain a better distribution of the applied forces, and also to provide stability by preventing them from moving around [312]. This axial ring, in conjunction with another 3D printing structure known as the **stabiliser ring** (Fig. 32), placed in a higher position of the base rod, has the secondary function of stabilising the upper rod of the cane, reducing and mitigating unwanted and accentuated oscillations resulting from the user's interaction with the cane handle, while allowing the detection of forces applied in the direction of the cane's displacement plane. The user's movement intention can be then classified in a primary phase as "front", "back", "left"and "right", from the relation of the force components obtained by the FSR sensors. If no force is applied, the intention is considered to be "stop". The stabiliser ring allows the user's forces to be transferred to the FSR in the axial ring, acting as the basis of a first class lever system in which the fulcrum is the connector that binds the upper and lower parts of the cane. Figure 33 shows a picture of the interaction of forces in the cane and

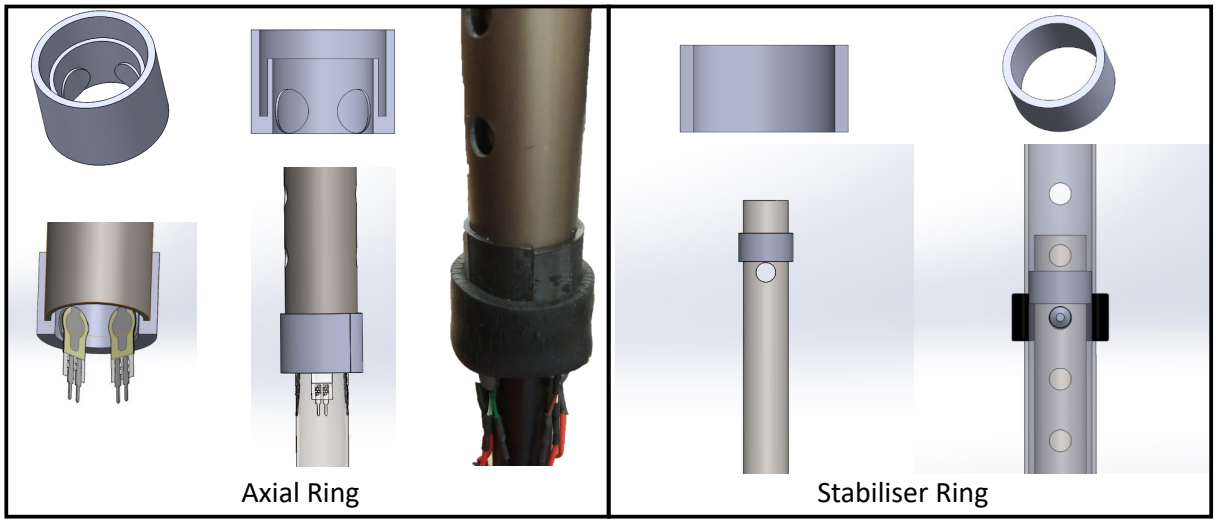

Figure 32: Axial Force System. Left: Configuration of the axial ring fixed to the upper rod of the cane with the FSR sensors. Right: Configuration of the stabiliser ring fixed to the lower rod of the cane. Both rings are in grey.

an illustration of the system's comparison to a lever, as well as an example of motion intention detection when the user wants to go forward and backward.

An experimental test was carried out to assess the motion control system implemented. A total of 6 healthy subjects aged between 22 and 27, with body weight between 48 kg and 95 kg, and with body height between 1.51 m and 1.82 m, performed only the intended action of propelling the cane-type robot forward. Therefore, with the cane immobilised, a brief explanation of the axial force system of the cane was given, and the participant was then requested to pretend to be intending to go forward. The force sensor data were first collected in order to alter the threshold values to match the person's strength and preferred sensitivity. Then, after recording the sensor readings and confirming that they matched the individual's desire to move, this process was repeated 10 times for each participant. A total of 58 correct results were obtained in a total of 60 tests performed, achieving an ACC of 97% for the axial force system (Table 19), which is in accordance with the target specification established previously.

5.9.3 Gait Phase Detection

The proposed solution for generating the haptic sensing system was determined by combining three FSR sensors that are equidistant from each other and situated on the cane's handle. This setup can identify when the user supports his body weight on the cane and identifies the user gait phase by acquiring the interaction forces between the user and the cane-type robot, more specifically the forces applied vertically. Considering the maximum body support weight discussed earlier (25% of the body weight or reach the 30Kg), the haptic sensing system was designed to detect data in the range of 0-300N. A 3D printed PLA structure must be placed over the sensors, covering the handle, with the same function as the axial force

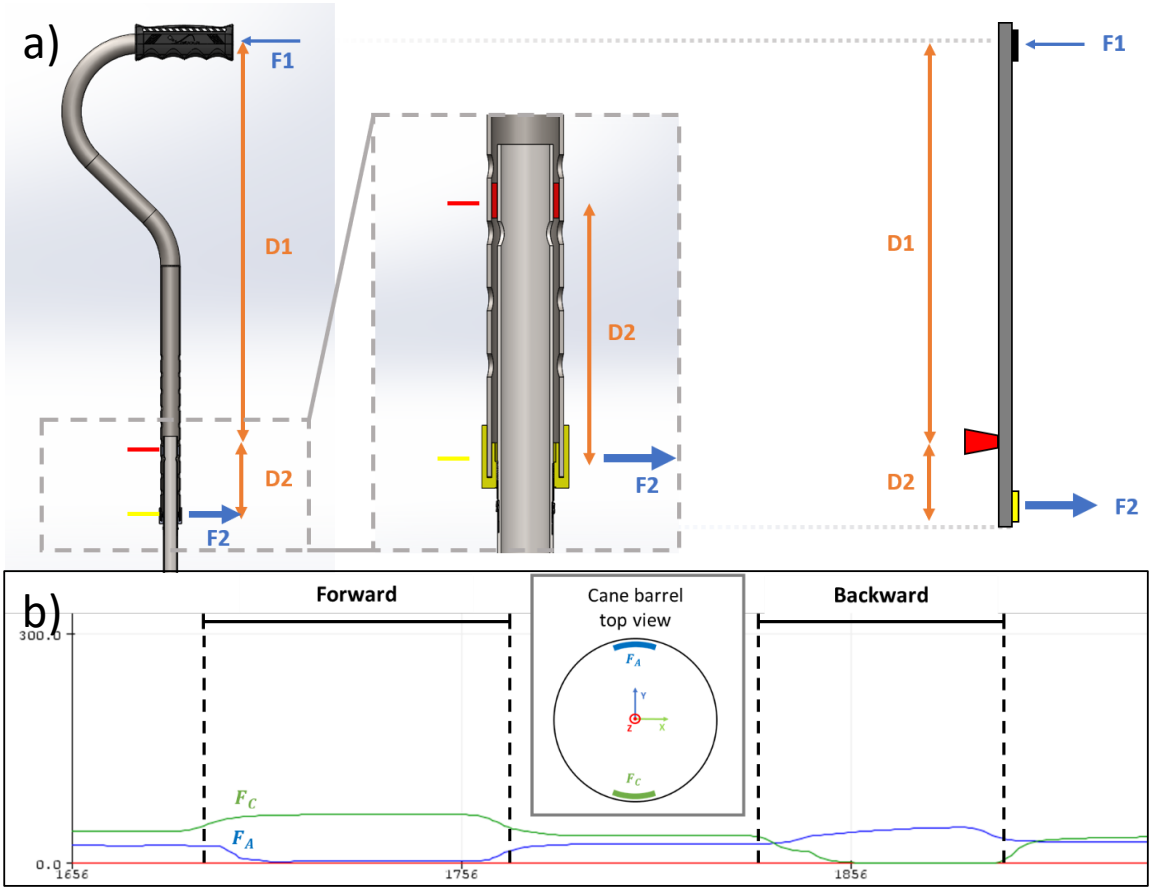

Figure 33: Cross-sectional view of the cane main body structure with the axial ring (yellow) and the stabiliser ring (red) implemented, and the interaction of the forces applied in the handle by the user, with the resultant force in the force sensors. At the right an analogy of the force detection system applied to the cane handle to a first-class lever model. b) Data acquisition by the axial force sensors with force applied in the AP direction, when a participant was asked to move in the forward and backward directions.

sensors discussed previously, in order to increase the distribution of the applied forces, as illustrated in Fig. 34.a. Furthermore, PLA is biocompatible, which means it is not toxic or harmful to human skin. The 3D printed structure also has the same geometric structure as the handle, preserving ergonomics, and the width and height of the cane handle remain within the range of values shown in Table 55 (Appendix B) of the cane technical specifications. Figure 34 depicts a visual representation of the force sensors, as well as the structure that covers the sensors' contact area to improve the distribution of applied force at the cane handle, both virtually (Fig. 34.b) and physically Fig. 34.c. The V forces were also classified into three categories: i) "no touch- no forces are being applied to the cane; ii) "light touch- the user's hand is resting on the cane; and iii) "support phase- the user is supporting their body weight on the cane. Figure 35 depicts a demonstration of the mentioned categories detected by the haptic sensing system.

The same group of subjects also performed a second test to validate the detection of V forces applied in the handle. Once more, the device was immobilised while a brief explanation was given about the different types of force that the cane's handle could detect. Each participant was further asked to simulate

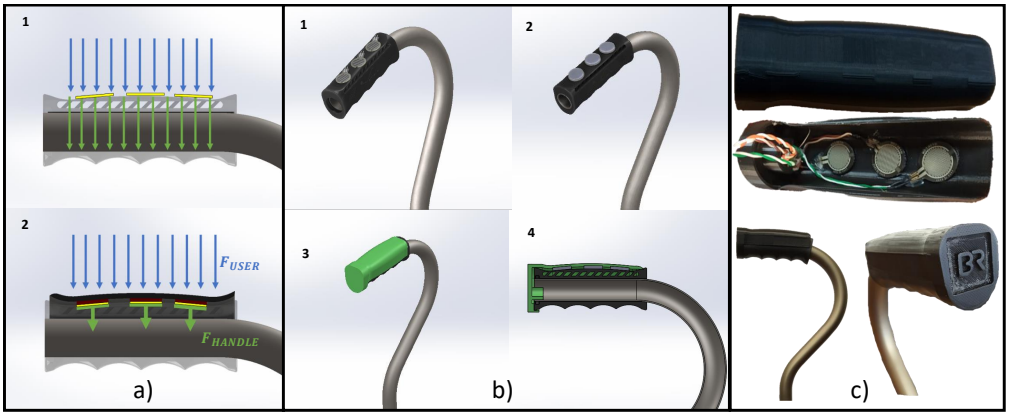

Figure 34: Haptic Sensing System. a) Demonstration of the force distribution on the FSR sensors and cane handle, without (1) and with (2) the PLA structure (Blue - force applied by the user; Green - force applied on the handle; Yellow - FSR sensors; Black and red – PLA structure). b) 3D model representation of the FSR sensors with the PLA structure placed on top of the handle for improved force distribution (1 to 3 - evolution from only FSR sensors to the final cane handle; 4 - cross-section view of 3). c) 3D structure with the three FSR sensors (top) and final result (bottom).

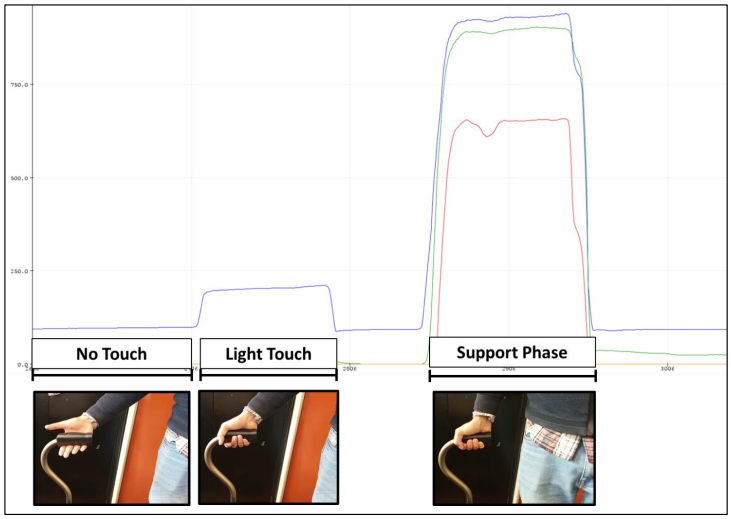

Figure 35: Haptic Sensing System. Force applied in the z-axis direction, when a participant was asked to: stand still, place his hand on the handle, and to lean its weight on the cane.

each of the three categories of detectable forces so that sensory data could be gathered to define the threshold values for each strength category based on the user's weight and structural make-up. Finally, the participant was randomly assigned to apply one of three types of force settings, where the results acquired by the sensors were later checked to see if they matched the action performed. Up until there were a total of 20 outcomes per participant, this process was repeated. A total of 81 correct results were obtained out of 90 tests performed, achieving an ACC of 90% for the haptic detection system (Table 19).

Table 19: Experimental results obtained from the axial force system and haptic detection system

No. of Participant	**Axial Force System**	**Haptic Sensing System**		
	Forward Intention (n/10)	No Touch (n/5)	Light Touch (n/5)	Support Phase (n/5)
1	9	5	5	5
2	10	4	4	5
3	10	3	4	5
4	9	3	5	5
5	10	5	5	5
6	10	4	4	5
Success/Total	**58/60**		**81/90**	
ACC	**97%**		**90%**	

5.9.4 Holonomic Base Movement Control

The cane-type robot is capable of moving in any direction without changing orientation, and also capable of changing to any desired orientation while in motion. This can make it easier to move in narrow, constrained locations while retaining a high level of mobility and stability. Since the axial force system obtains the user's motion intention by detecting the AP and ML forces, it is now necessary to implement a way to transform these interaction forces into the movement of the cane. A kinematic and dynamic model [303] was used previously to dimension the DC motors, calculating the minimum torque and angular velocity. Now, the same model is used to move the cane accordingly to the user's desired direction, while considering the motor's disposition and the direction of the applied force. It is required to have a well-defined reference

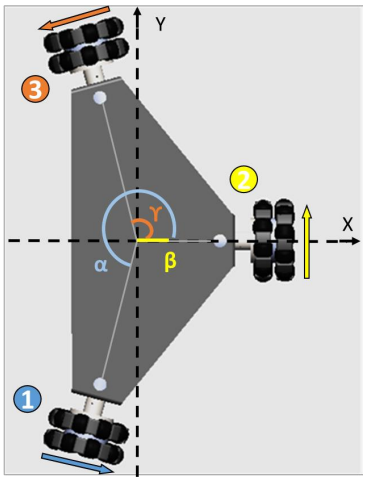

Figure 36: Cane's base with the Cartesian frame of reference located at the cane's CoM.

axis to determine the locations of each motor in respect to each other through a common point as a first step in obtaining the cane kinematic equations. The origin of the axis of the Cartesian coordinate system was defined at the CoM of the cane for ease of calculation, with the y-axis pointing in the AP direction (i.e., forward motion) and the x-axis pointing in the ML direction (i.e., in the direction of motion to the right). This Cartesian reference, as well as the arrangement of the cane's base and the configuration of the wheels and motors, is depicted in Fig. 36 with the appropriate numbers to aid in the kinematic calculations. Then, through the kinematic equation obtained, it is determined the contribution that each motor must have to achieve the desired movement.

5.10 Conclusions

This work contributes to the state of the art with the first advances in the development of a cane-type robot for fall prevention. The construction of the prototype was based on an iterative process that initially took into account the identification of the consumer needs from the literature, namely affordability, ease of use, ergonomics, cane height, safety, mass, style, obtaining the product, effectiveness, durability and reliability. Based on the most important needs for the construction of a first prototype, a survey of metrics was carried out based on scientific literature and international standards, which can translate the consumer's subjective needs into measurable target specifications. Then, the prototype was conceived and generated with the objective of reducing the production costs associated with this type of devices, while maintaining high durability and reliability. Only then can the target audience be more widely reached. The mechanical simulation tests reveal that the holonomic base obtained a positive assessment, having largely exceeded the established specifications. It should be noted that these tests described in international standards are generally applied to different types of walking sticks and that they do not include cane-type robots.

The hardware architecture was then defined, as well as the features and the main functionalities to be implemented that differentiate the cane-type robot from a conventional cane. Subsequently, the control units in responsible of processing all of the data in the cane electronic system were identified. The STM32F446RE is the low-level processing control unit, and the NVIDIA JetsonNano is the high-level processing device, which is dedicated to future fall detection and prevention strategies. Based on the review analysis performed in Chapter 2, the components for the sensory, actuation, and energy units were also identified and implemented. The overall purchase price was €688.97, which included all of the components required for the cane-type robot. Although this price is slightly more than the €650 stated in the target specifications, it is crucial to remember that this version of the cane-type robot is a prototype for a future commercially available product and not the final product. As a result, all parts were obtained in single quantities, and all hardware components are considered experimental, with the potential to be over-engineered later in the design to improve performance while also changing the overall pricing of the prototype. This architecture strives to maximise the efficiency of the control units' processing time by

prioritising the most relevant data, ensuring the user's safety as well as the cane's proper operation.

The goal of the motion control approach to be adopted at the cane-type robot was first specified as obtaining a simple and intuitive system that was also cost-effective. This proposal takes into account the fact that most robotic canes rely on expensive sensors or require significant cane modifications, making them more inaccessible and reducing the number of possible users. Following the development of a workable admittance control approach for the cane based on the gait of a healthy person and a person with an afflicted limb, admittance control was identified as the movement control method to be used. The methodologies indicated in the state of the art, the cane's design, and the previously established mission statements were used to conduct this evaluation. The motion control was then split into three categories: i) motion intention recognition; ii) gait phase recognition; and iii) holonomic base motion control. Considering the performed mechanical simulations, it was determined to use FSR sensors as the motion control system's sensory device for categories i) and ii), since they are durable, thin, flexible, widely available, and cost-effective sensors with a wide range of force SENS. A strategy for improving the gathering of sensory data from the FSR was also presented, which involved a better distribution of applied forces. The sensors were then mounted on the cane rod and positioned on the handle, resulting in an innovative, cost-effective motion control system that did not necessitate major structural alterations to the cane. The movement of the holonomic base was based on the admittance control approach, which permits the transformation of the user's intention forces into cane movement using forward kinematics and matrix equations while taking into account the configuration of the wheels and motors in the holonomic base.

Chapter 6

Fall Risk Awareness Strategy

This chapter provides the groundwork for a tool that can assess a subject's fall risk in real time, taking into account a variety of existing fall risk factors and focusing on the real-time detection of falls and daily activities conducted by the elderly. The idealised FRA strategy included a three-part modular architecture that enables for real-time FRA using simply a waistband with an inertial sensor, a smartband to monitor the heart rate, and a smartphone. Each module must look at risk factors such demographic information, environmental changes, and even geriatric behaviour issues like ADL. The *Activity Recognition Module* was the sole module studied during this thesis. ADL recognition has been a widely discussed topic, with applications in many areas. Data from wearable sensors, particularly positioned at the lower trunk, can be used to recognise ADL, which appears to be a viable solution in uncontrolled environments, and AI-based algorithms are recommended due to their promising results. Thus, this chapter also presents an AI-based framework that performs comparative analyses to find the best classification model and the most relevant features. This framework is fed with data from six public datasets, three team-owned datasets from prior projects, and a new dataset created in collaboration with nursing homes in the Braga district.

6.1 Introductory Insight

Currently, as seen in the state of the art (Chapter 2), only a few studies focus their efforts on a multifactorial FRA tool, analysing only one type of fall risk factor. In addition to this issue, real-time FRA is still a procedure that can be improved, despite the fact that certain research have already demonstrated promising results in this field. The usability of today's methods and hardware is another issue that has to be addressed. These should evolve to be more easily and autonomously used by the elderly, i.e. in a free-living environment rather than under controlled settings, and to reduce the number and size of sensors required,

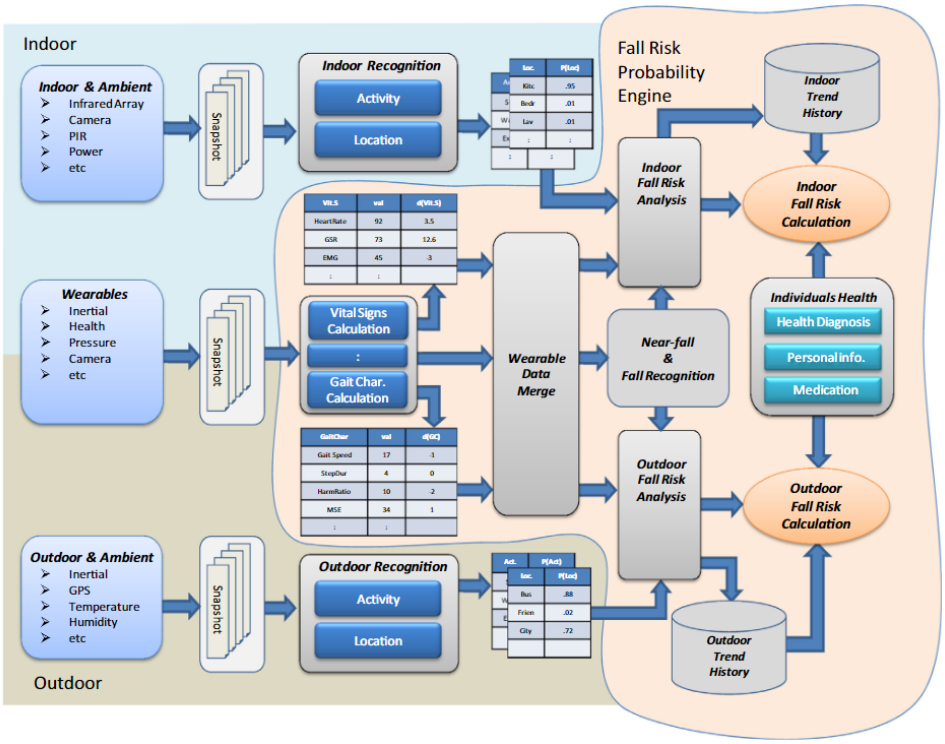

Figure 37: Calculation of fall risk using the fall risk probability engine proposed by Danielsen et al. [24].

making the experience as pleasant as possible for the users. Finally, several of the algorithms studied in Chapter 2 did not have a clear validation strategy or it was poorly distinguished, especially in the immediate FRA. As a result, a mechanism must be implemented that can suppress the previously mentioned FRA drawbacks, allowing the elderly to use FRA instruments on a daily basis. The architecture for a future FRA tool that eliminates the aforementioned disadvantages will be described in this chapter. Danielsen et al. [24] presented a FRA engine in Fig. 37, which inspired the development of the FRA tool discussed in this chapter. These researchers determined what types of data are most important for a multifactorial FRA using wearable and other types of sensors in a daily living setting, and then created an optimal FRA procedure based on their findings.

Considering the scientific literature, a list of requirements that must be met was gathered. Data acquisition equipment and FRA tools will be used by the elderly, who are the major target audience for this technology. Health care providers and nursing home staff should also have access to the tool so that they may provide immediate assistance if needed [313]. FRA is now based mostly on tests and medical evaluations, which only provide an estimate of the risk of falling in relation to the time and conditions of the referred test. Machine Learning is typically used in FRA techniques that include other sorts of analysis, and only one type of data — inertial – is used to generate a binary classification (Faller vs Non-Faller). As a result, ensuring that this instrument is multifactorial is one of the most crucial needs to meet. This implies it must estimate risk based on a range of elements, such as wearable sensor data, clinical test results,

physical or psychological information from users, and information about the surrounding environment. In order to be dependable and easy to use by any subject, the approach must also deliver a genuine fall risk result, in a scale or code that all users can understand, and in real-time (i.e., be user-friendly and subject-independent). It must also be a tool that works with a wide range of data-gathering devices, including instrumented waistbands, smartwatches, canes, and walkers. This necessitates the use of tools such as eHealth platforms, which allow the target audience to see the risk level in an easily understandable manner, as well as the construction of connectivity between the aforementioned data collection and risk analysis devices and other caregiver gadgets. Finally, this strategy must take into account the target audience as well as the time of use. As a result, it must be built in such a way that it can compute a fall risk value with the fewest number of sensors possible, avoiding the use of inconvenient measuring devices and making the use of associated devices more comfortable, avoiding discomfort that could lead to an increase in the risk of falling. As a result, the goals of the strategy presented in this dissertation are as follows: i) the gathering of multifactorial data from a variety of sources, including inertial data, clinical tests, and demographic data on the elderly, as well as data related to the environmental context in which they live; ii) Compute a single fall risk value from the above data on a continuous basis, taking into consideration both immediate and prospective FRA perspectives, as well as the usage of AI-based methods; and iii) in the event of a fall or near-fall situation, such as slipping or other LOB, provide prompt feedback. The following sections will go through all of the steps that were defined to establish an eHealth platform-based strategy capable of computing fall risk in real-time and in a multifactorial manner. The tool's primary requirements will be discussed first, followed by a dataflow overview of the suggested architecture, and the various classification and feedback stages of the idealised tool. Then, the *Activity Recognition Module* is scrutinised in terms of data used and performance.

6.2 FRA Strategy Architecture Overview

With the electronic growth of wearable sensors, as well as the rise of AI technologies capable of evaluating and understanding the meaning of data from sensors, strategies for automatic FRA tools are becoming widely explored [24–26]. They present an architecture that is organised into three distinct operational phases: i) the signal acquisition and processing phase; ii) the signal analysis phase; and iii) the final decision and communication phase [314]. This division is also used in a number of other publications with a similar goal, as indicated in Chapter 2, of calculating fall risk from different data sources [24, 68, 315]. Figure 38 depicts the strategy provided in this chapter, which is based on the type of architecture mentioned previously. The proposed FRA tool's first block (**Data Acquisition & Processing**) defines the different data acquisition and processing methodologies that have been proposed, i.e. signal filtering and feature estimation. The second block (**Classification & Regression Modules**) is created in a modular fashion, with three classification and/or regression modules operating in parallel. The fall risk will be

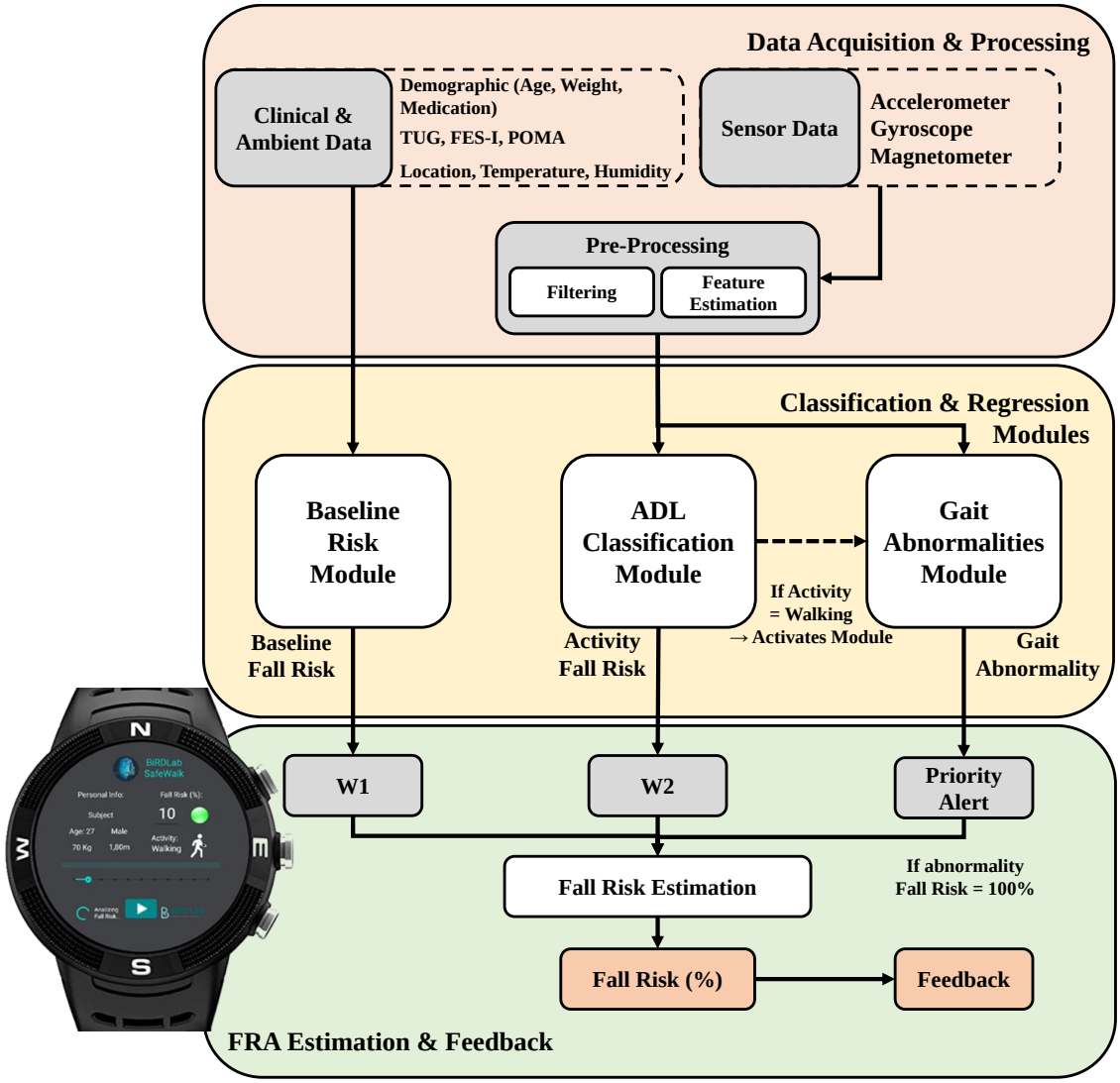

Figure 38: Proposed FRA tool architecture overview. The 3 main phases (*Data acquisition & Processing*, *Classification & Regression*, and *FRA Estimation & Feedback*) should be noted in the different areas, as well as the 3 parallel modules in the *Classification & Regression Modules* phase. Smartwatch eHealth app example for continuous FRA on the left.

estimated, in the third and final phase (**FRA Estimation & Feedback**), based on the results obtained in these three modules, and appropriate feedback should be delivered to the subject, family members, or health professionals in a timely way. The many parts of the proposed strategy would be controlled and connected by an eHealth platform. This platform would also indicate the users' fall risk level in real time, and it would be put on devices like smartwatches (Figure 38), smartphones, or tablets that are utilised by both the elderly and caregivers. The goals, data workflow, and expected outcomes of each block will be discussed in the following subsections, citing the sort of data to be used, as well as the type of processing and mathematical/decision processes that will result in a fall risk value.

6.2.1 Data Acquisition & Processing

One of the tool's prerequisites is to conduct a FRA using a variety of fall risk sources in order to gain a better understanding of all the risk factors that can influence and cause a fall occurrence. Wearable sensors, such as inertial sensors, are the most prevalent for data collecting in FRA, as confirmed by the literature review, and are usually mounted on the subjects' waist [24, 25, 316]. Inertial data of acceleration and angular velocity will be acquired from a waistband placed on the subjects' lower trunk to examine the kinematics of their movement. As a result, information about the subjects' activity and behaviour throughout the day will be available. This information will aid in the real-time monitoring of geriatric movements and the identification of potential danger scenarios associated with elderly behaviour, such as conducting high-risk activities (e.g., climbing stairs) or being out of balance, in the immediate future. In order to have access to information about each user's clinical situation, data should be collected through questionnaires, clinical tests, and medical consultations, and then assessed as needed to perform a FRA that is more focused on the long-term future (prospective), knowing a subject's current physical and psychic skills and what this means for their long-term fall risk. The use of temperature, humidity, and light intensity sensors to collect data about the environment that surrounds the subjects is also suggested in this tool, covering some of the risk factors associated with external characteristics that are not tied to the individual. These three acquisition strategies should yield a diverse set of data from various sources, allowing for multifactorial fall risk analysis. This acquisition must be made by coupling the aforementioned sensors to devices already used in everyday life by the elderly (waistbands, canes, walkers), as well as other small devices used by both the elderly and health professionals (smartphones, tablets, smartwatches), which allow for storage, embedded data processing, and risk calculation, making this FRA tool easy to use and comfortable for all users, whether they are elderly subjects or caregivers. These devices would be linked by the aforementioned **eHealth platform**, which will be in charge of coordinating communication between the devices used by the elderly to perform the FRA and the devices used by caregivers, in order to provide prompt feedback as soon as the elderly devices detect a high risk of falling. It would also store data from the elderly and make it available to caregivers on a constant basis, as well as the various outcomes acquired from the FRA algorithms.

6.2.2 Baseline Risk Module

The *Baseline Risk Module*'s main purpose is to provide a baseline fall risk value based on a patient's clinical data (physical and psychological), test results from medical fall risk scales, or even external factors like location and weather. Table 20 lists some of the factors that will be used in this module. The acquisition and storage of data is the first phase of this block, where much of the data about the subjects can be obtained using simple clinical tests, heart rate measures and questionnaires. Temperature, humidity, and GPS sensors can be used to collect data about the environment and people's locations, and these sensors

Table 20: List of several Baseline risk factors which can be used in the Baseline module of the FRA tool

Risk Factor Group	Factor	Value
Demographic	Age	Numeric
	Weight	Numeric
	Height	Numeric
Clinical	TUG	Numeric/Binary
	POMA	Numeric/Binary
	FES-I	Numeric/Binary
	Fall History	Numeric/Binary
	Heart Rate	Numeric
	Other conditions	Binary
Psychological	Fear of Falling	Numeric/Binary
Ambiental	Location	Binary
	Temperature	Numeric
	Humidity	Numeric

can be linked to assistance equipment used by the elderly on a regular basis, such as smartwatches, waistbands, canes, and walkers. This information can be saved in databases or on electronic devices such as smartphones for eventual use in the FRA tool's second phase. As can be observed in the second column of Table 20, the numerous elements included have a wide range of scales and orders of magnitude, with subjective factors such as clinical tests and the respondents' fear of falling also appearing. As a result, a second stage of this module is required to convert and normalise data from various forms into numeric or binary values so that mathematical models can interpret it. The third and last stage of this module should be the computation of the fall risk value from the converted and normalised data, taking into consideration the aforementioned distinct types and magnitudes of data and their conversion. This value should be determined using regression methods, such as Logistic Regression, according to the line of thought found in the literature [315, 317, 318]. Until any of the parameters change (e.g. subject's weight, new clinical tests results or even changes on the location or temperature during the day), the result obtained should remain constant, creating a baseline fall risk value appropriate to each individual's characteristics and the environmental variables to which each is exposed at any given time. The data flow and the aforementioned processes for this module's proper operation are summarised in Fig. 39.

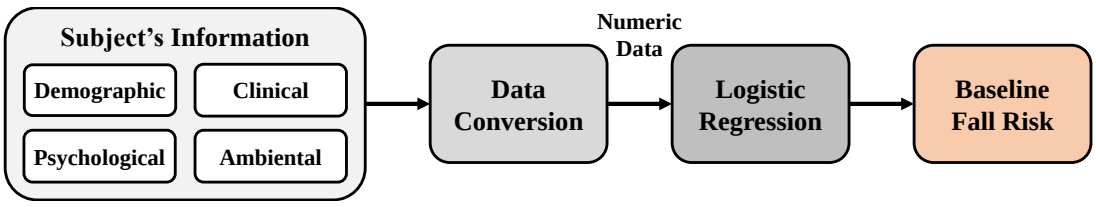

Figure 39: Baseline Fall Risk module Data flow overview.

6.2.3 ADL Recognition Module

An increase in the likelihood of a fall has been linked to particular behaviours, along with other factors. Lord et al. [319] indicate that the effective number of falls reported varies by location and activity, indicating that the issue of daily activity recognition may be a significant area of research for improving FRA instruments. With that in perspective, an ADL classification module will be in constant operation, allowing decoding of the participants' daily activities. This module is included in the proposed FRA tool's second phase, and it will be the chapter's main focus because it is the least researched aspect of the literature when it comes to the integration of daily activity recognition with the risk of falling.

Wearable sensors have been the most widely used type of sensing in recent years for the automatic assessment of the danger of falling in the elderly, as well as for the detection of everyday activities, as indicated in Chapter 2. Additionally, inertial data, acceleration and angular velocity, are the most often used data types for activity recognition. Thus, in the first phase of this block, it is planned that a waistband outfitted with these inertial sensors collects data continuously from the subjects' lower trunks as they freely carry out their daily activities.

The second phase should process the inertial data collected from wearable sensors by computing several features that will be used with AI-based models to identify several postural ADL. Moreover, fall events must be identified, as well as their orientation/category (forward, backward, or sideways). After determining which activity is being performed at a given moment, this information will be used in the following step, where, in addition to some of the demographic data from the *Baseline module*, a fall risk level will be allocated to each activity based on the findings of [319], which show the probability of falling based on the activity and location of the fall, gender and age. Figure 40 depicts a summary of the data flow of these modules.

Despite the module's potential since no other work used ADL recognition in fall risk analysis, it is necessary to validate the data collection methods and determine which features and classification models to employ so that ADL can be recognised with the shortest possible delay between the start of the activity and the classification, as well as with low classification error rates. Furthermore, while studies have shown that the probability of falling varies with activity [319], it also depends on a combination of other factors, necessitating more research on this topic, including extensive prospective work and large datasets of elderly subjects, their falls, and their causes, in order to make a statistical association between a daily activity and the respective risk of falling.

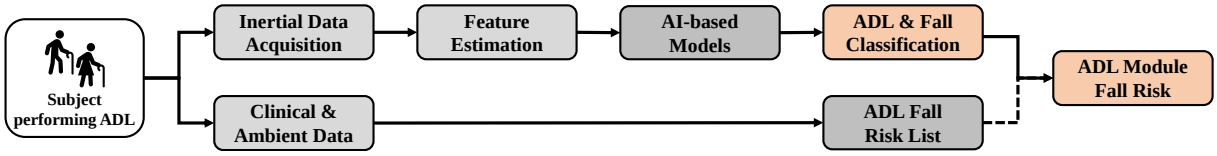

Figure 40: ADL Recognition Module data flow.

6.2.4 Gait Abnormalities Module

The second phase of this FRA tool introduces a final classification module, dubbed the *Gait Abnormalities Module*, with the goal of quickly detecting gait abnormalities. The quality of human gait has been one of the most studied themes in the analysis of the risk of falling [320–322], therefore a complete and real-time analysis of the user's gait is critical for determining an individual's fall risk. Figure 41 depicts a fast overview of its operation. The operation of the *Gait Abnormalities Module* will be based on the results obtained from the *ADL Classification Module*. As a result, when this module detects a walking activity, the *Gait Abnormalities Module* will be activated, remaining in standby when other activities differemt from walking are detected. The approach provided in the *ADL Classification Module* will be quite similar in the general functioning module for the detection of gait abnormalities.

The waistband with inertial sensors will be used to collect data to be used as input for AI-based methods as previously mentioned, but this time they will be used to analyse the users' gait, with the expectation that these models will be able to produce a binary classification of gait quality. It should be characterised as normal if the subject walks within a specified range of normality, or abnormal if the user walks in a pattern that is related to a disability or a temporary LOB, such as a slip or trip [49, 320, 322]. This module is not activated if the subject's gait is judged normal, and it continues to collect and classify the gait until the subject's activity changes. The risk level computation is provided in this situation by the modules *Baseline* and *ADL*. If the subject's gait is identified as abnormal, on the other hand, this block will override the aforementioned risk level computation, boosting it to a maximum value and

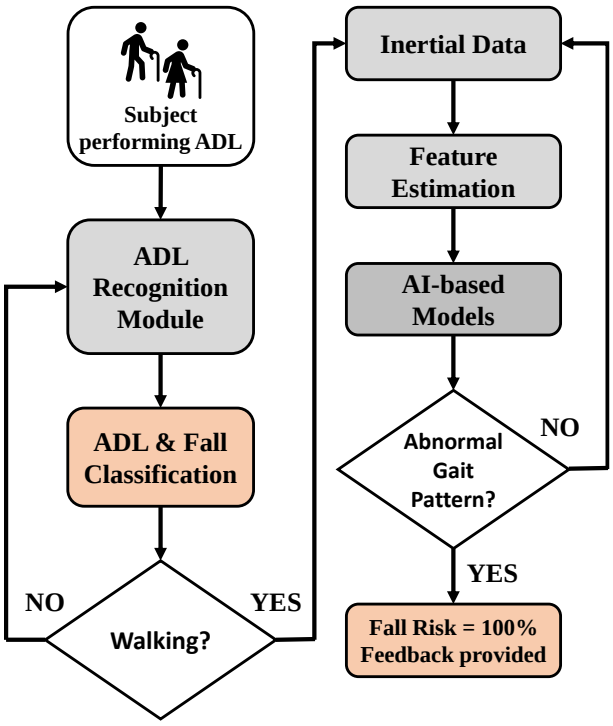

Figure 41: Gait Abnormalities Module data flow.

initiating feedback mechanisms, whether for the subject, family members, or health care providers. The communication between the categorisation algorithms (and their outcomes) and the caregivers' devices would be handled by the **eHealth platform**. Finally, the given method selection was based on the use of the fewest amount of sensors and devices possible for FRA, allowing risk analysis with only a waistband and a smartband/smartwatch. However, in the future, this block should be upgraded to not only perform a binary classification but also a more detailed study of the location of the CoM and COP, for example, perhaps with the addition of instrumented shoes [321, 323, 324], and wearable sensors or other devices.

6.2.5 Fall Risk Assessment & Feedback

The last phase's main function is to combine the results from the previous phase's three modules and generate a fall risk value on a fall risk percentage scale. Obeying that, and considering the risk value acquired, appropriate feedback must be sent to users as well as health professionals in the event that the fall risk is judged high or a fall event occurs (Fig. 38). The methodologies provided in [68] and [315] for determining a fall risk level served as a guide for the presented tool, with weights assigned to each of the existing blocks for fall risk analysis. As a result, the *Baseline Risk Module* was given a 60% weight (W1), while the *ADL Recognition Module* was given a 40% weight (W2). The *Gait Abnormalities Module* is not included in the fall risk calculations, but it is configured as a priority module, so that when an abnormal gait is detected, it takes precedence over the others, raising the fall risk level to its maximum. Thus, the fall risk value will be generated in real-time as a result of the following Equation 1, taking into consideration the results of the two previous modules that are used to assess the risk of falling:

$$\text{Fall Risk (\%)} = (\text{Baseline Fall Risk} \times \text{W1}) + (\text{ADL Fall Risk} \times \text{W2}) \tag{1}$$

A set of feedback processes, which are exemplified in Fig. 42, must be triggered if: i) a fall is detected by the *ADL Recognition Module*; or ii) any gait abnormality is detected by the *Gait Abnormalities Module*; or even iii) if the risk level calculated by Equation 1 exceeds a given threshold. Smartphones, smartwatches, and other instrumented support devices can communicate with other devices automatically. These devices must be engaged in the case of a fall or a high fall risk circumstance to offer timely feedback in order to avoid falls or mitigate their consequences. Feedback must always keep the subject informed about his current fall risk and provide warning signals in the event of a high-risk condition (e.g. walking in an area with low light, LOB), such as through graphic or numerical scales, colour codes, or other sensory indicators (e.g. vibrations or warning sounds). The referenced devices must be able to communicate with family members and health professionals as quickly as possible in order to provide the required support and avoid or mitigate the potential effects of falls [24]. This feedback should consist of automatic messages, calls, emails, or even notifications via apps for smartphone or other electronic devices.

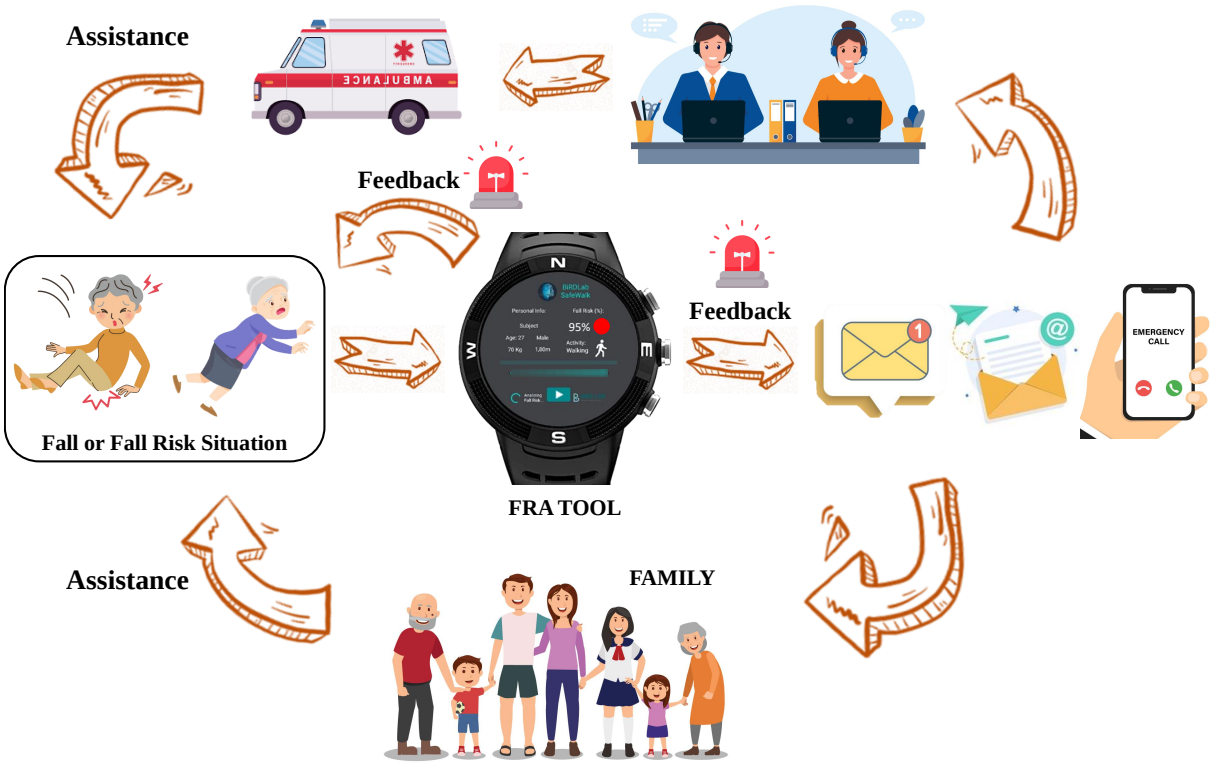

Figure 42: Warning signals and feedback processes implemented in case of a fall event or a high fall risk situation.

6.3 Activity Recognition: Methods & Materials

The *Activity Recognition Module* makes use of a large number of multiple datasets, publicly available or private ones, to validate activity recognition models based on inertial data collected from the participants' waist. Subsequently, after using these data, established partnerships with nursing homes and day centers in the district of Braga were crucial to collect more data based on new protocols considering what is implemented in the scientific literature. Thus, a vast dataset was built from the fusion and normalisation of several ADL datasets. This process has not been carried out before in any other works of the kind, despite its importance being highlighted multiple times [71, 325].

6.3.1 Public & Team-Owned Datasets

Datasets that met certain requirements were searched: i) be publicly available online for download; ii) contain inertial data collected from the lower trunk (back) of at least accelerometers and gyroscopes; and iii) contain postural daily activities and/or fall events. The research carried out resulted in the gathering of the public datasets and the three other team-own datasets, which are described in Table 21. The gathered public datasets were as follows:

1. **Sisfall** [32]: Data acquired with 23 healthy young adults (19–30 years, 149–183 cm, 42–81 kg) and 15 healthy elderly participants (60–75 years, 150–171 cm, 50–102 kg) with a device composed of two types of accelerometer and one gyroscope fixed to the waist of the participants, who performed 19 ADLs and 15 fall types.

2. **FallAllD** [326]: Data acquired from 15 healthy subjects (21–53 years, 158–187 cm, 48–85 kg) who used 3 devices equipped with an accelerometer, a gyroscope, a magnetometer and a barometer. A total of 44 classes of ADLs and 35 classes of falls were performed.

3. **FARSEEING** [31]: Large-scale collaborative database to collect and share sensor signals from real-world falls. Real fall data are acquired from either 2 locations: waist or thigh, and the acquisition devices are equipped with up to 3 sensors, namely accelerometer, gyroscope and magnetometer.

4. **UCI HAR** [327]: Dataset recorded from 30 healthy subjects (19–48 years) by using a waist-mounted smartphone with an embedded 3-axis accelerometer, gyroscope, and magnetometer. This dataset contains six classes of ADLs: walking, ascending stairs, descending stairs, sitting, standing, and laying.

5. **Cotechini et al.** [328]: Dataset acquired from 8 healthy subjects (22–29 years old, 173–187 cm, 60–94 kg) using a wearable device containing a 3-axis accelerometer and gyroscope, tied to the subject's waist, that recorded subject's acceleration and orientation. Subjects simulated 13 typologies of falls and 5 types of ADLs.

6. **UMAFall** [329]: A dataset acquired from a total of 17 healthy subjects (18–55 years, 50–93 kg, 155–195 cm). Accelerometer, gyroscope and magnetometer data were collected from five wearable sensing devices, located on the subject's chest, waist, wrist, ankle and pocket. The participants performed 8 different ADLs and 3 different typologies of falls (except by those older than 50 years, who did not perform falls).

The used team-owned datasets were as follows.

1. **+Sense** [49]: Dataset with data acquired from 10 healthy subjects (44.02 ± 16.42 years, 67.5 ± 16.06 kg, 172 ± 7.93 cm) and 40 subjects with Parkinson's disease (64.00 ± 10.60 years, 69.93 ± 11.41 kg, 165.93 ± 8.65 cm). A waist-mounted waistband, equipped with an accelerometer, a gyroscope and a magnetometer recorded subject's data in walking activity protocols.

2. **SafeWalk** [36]: Dataset acquired with 12 healthy subjects (25.33 ± 6.33 years old, 66.92 ± 10.07 kg, 1.74 ± 0.11 m). Five IMU were attached to the lower back, both back thighs, and to both feet of the subjects, who performed walking trials and front fall events.

3. **InertialLab** [330]: Dataset which includes data from 11 able-bodied subjects (24.53 ± 2.09 years old, 171 ± 10 cm, 65.29 ± 9.02 kg). Gyroscopes and accelerometers were attached to six lower limbs and trunk segments. Walking in varying speed and terrain (flat, ramp, and stairs) and including turns were the activities carried out by the subjects.

The merging of these heterogeneous datasets, which included data from both adult and elderly subjects, as well as healthy and unhealthy individuals, served two aims. Gather a large and diverse dataset appropriate for training AI-based models, and then use them to recognise ADL regardless of the subject's age and health condition. A global dataset containing 6702 files covering a total of 20 ADLs and falls conducted by 180 subjects (age = 33.60 ± 16.84 years, weight = 69.98 ± 10.99 kg, height = 168.99 ± 9.42 cm) was generated. This vast amount of data is crucial for validation purposes since it is far larger than any other dataset used in the AI-based ADL recognition research carried out. Furthermore, the global dataset presents a balanced distribution regarding the subject's gender (Male = 54%, Female = 46%), also containing data from both young adults and elderly people. However, despite the presence of elderly data, the average and standard deviation values show that the global dataset is still made up mostly of young adults, with the percentage of people over 65 years old being just over 20% of the total dataset (37/180 subjects). Due to the great variability found between datasets, it was necessary to pre-process them as

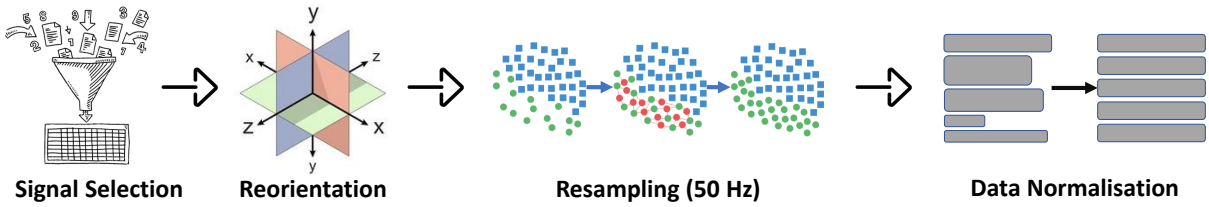

(a)

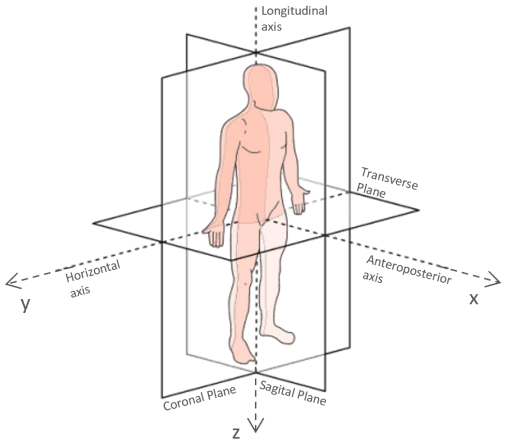

(b)

Figure 43: a) Pre-processing steps implemented before using the datasets for ADL recognition. b) Desired sensors orientation (x, y and z indicate the positive direction of the AP, ML and V axes, respectively).

Table 21: Datasets description regarding sensing methods and location, sample frequency, participants and activities recorded, where: A = Accelerometer, G = Gyroscope, M = Magnetometer, and B = Barometer

DataSet	Availability	Sensors	Location	Sample Frequency	Participants	ADL Falls
SisFall [32] [1]	Public	A, G	Waist	200 Hz	23 subjects <30 year 15 subjects >60 years	19 ADLs 15 Falls
FALLALLD [326] [1]	Public	A, G, M, B	Chest, Waist, Wrist	238 Hz	15 subjects 21–53 years	44 ADLs 35 Falls
FARSEEING [31] [1]	Public	A, G, M	Waist, Thigh	20 Hz 100 Hz	20 subjects [2]	Real falls
UCI HAR [327]	Public	A, G	Waist	50 Hz	30 subjects 19–48 years	12 ADLs
Cotechini [328] [1]	Public	A, G	Waist	33,33 Hz	8 subjects	5 ADLs 13 Falls
UMAFall [329]	Public	A, G, M	Waist, Chest, Wrists, Ankle, Front pocket	20 Hz	17 subjects 18–55 years	8 ADLs 3 Falls
+Sense [49]	Private	A, G, M	Waist	100 Hz	10 Healthy 40 Pathological	1 ADL
SafeWalk [36]	Private	A, G, M	Waist, Thighs, Feet	30 Hz	12 subjects 25.33 ± 6.33 years	1 ADL Falls
InertialLab [330]	Private	A, G, M	Waist, Thighs, Shank, Feet	200 Hz	7 subjects 23–26 years	5 ADLs

[1] Several activities in these datasets were grouped into one single class of basic activities.
[2] Only data from 3 subjects were suitable to use.

depicted in Fig. 43.a. First, only data corresponding to the acceleration and angular velocity of the sensors located in the subjects' waist were considered. Then, the sensor reorientation method was applied so that the axis orientation corresponded to the one depicted in Fig. 43.b. Finally, all datasets underwent a re-sampling process, so that the sampling frequency was normalised to 50 Hz, and a normalisation process per dataset. The datasets, whether public or private, contain the great majority of ADLs used for activity recognition in the literature. Therefore, a total of 20 labels, including periodic activities, static postures, transitions between postures and falls, were used in order to cover all ADLs listed in every dataset. It should be noted that some activities whose labels in public datasets were considered different were recognised as the same activity in this work, since their basic body movement is similar, e.g.,the cases of Sisfall's activity of sitting in high chairs or low chairs were included in the "Stand to Sit"class; or even cases of standing in different places, such as in the room and in the elevator, were all included in the "Standing"class. Table 22 lists the ADLs that were adressed in this work. A study carried out on how the ADL were distributed showed that the global dataset is unbalanced, with a greater tendency toward cyclical activities, such as walking or lying (29.73% and 18.52%, respectively), with only a small percentage of transitions between activities and fall events, such as syncope, which is the activity with the least amount of data in the constructed dataset (0.27%). Figure 44 shows the percentage amounts of each activity.

Table 22: Static postures and locomotion daily activities, postural transitions and fall events selected to be recognised by the AI-based models

Periodic Activities & Static Postures	**Transitions**	**Fall Events**
Walking	Lying to Stand	Forwards
Standing	Stand to Sit	Backwards
Sitting	Sit to Stand	Lateral
Lying	Stand to Pick to Stand	Syncope
Upstairs	Stand to Lying	
Downstairs	Change Position (Lying)	
Jumping	Turning	
Jogging	Bending	

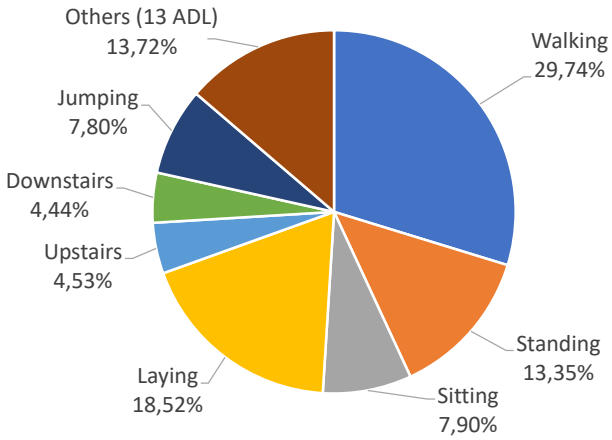

Figure 44: Percentage of each activity present in the global dataset. The activities are named according to Table 22.

6.3.2 Data Acquisition in Nursing Homes

At this stage, an initial version of the FRA strategy was implemented offline with the use of public and team-owned datasets. However, it is critical to develop or improve a system capable of collecting data in order to create a new and robust dataset. A waistband with an inertial sensor was improved, and smartphone apps were developed for use in data collection sessions with older people in nursing facilities. This proof of concept is also an essential first step for the development of the remaining blocks of the FRA tool, since this block is shared by all FRA modules. Thus, this section will address the process of enhancement of a previous team-own instrumented waistband and smartphone applications for data acquisition, as well as a data acquisition protocol, which was carried out with the following three nursing homes, namely: i) *Fundo Social - Braga*; ii) *Centro Social e Paroquial de Sobreposta*; and iii) *Associação de Reformados ValeD'este - Celeirós*. The materials used to the construction of the waistband will be identified, as well as the data collection protocol.

6.3.2.1 Waistband Enhacement

The waistband used in nursing homes to collect data was based on a version designed by BirdLab members and was equipped with electrical components to collect gait data from parkinsonic participants [49]. For waist-located inertial data acquisition from ADLs performed by the elderly in nursing homes, the previous sensing system (**MPU-6050**) was changed for an inertial sensor (**LSM6DSOX**), miniaturised (15x20x2 mm) and light (10 g), integrating a 3-axis accelerometer (±16 g) and gyroscope (±2000 °/s). An ultra-low power high-performance three-axis magnetic sensor (**LIS3MDL**) was also added. As can be seen from Fig. 45, the sensing system is located in a central region of the outer part of the waistband, connected by a cable to the control unit.

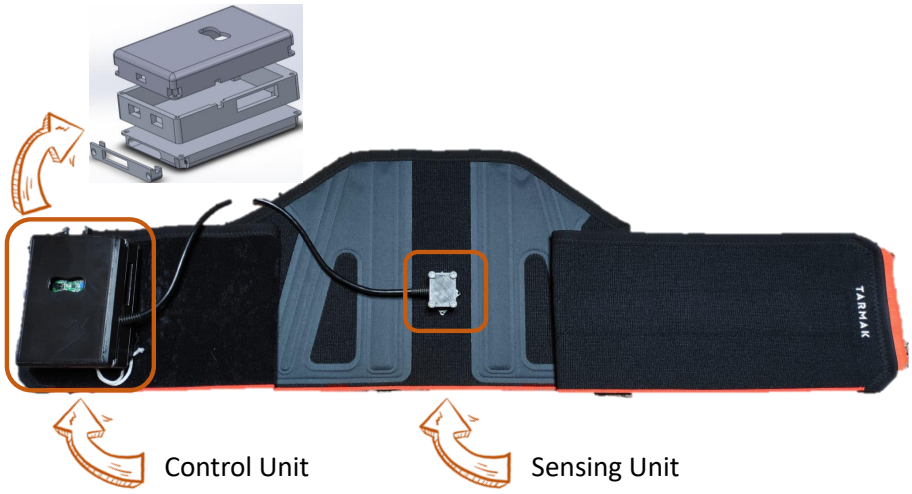

Figure 45: The instrumented waistband developed for data collection in nursing homes. 3D Solidworks assembly of the control unit box on top.

A control unit, which includes the STM32F4 Discovery as a processor, allows the communication between all the components, sending the necessary commands for the sensory unit to start and stop the data collection, and saving the collected data in a file once the acquisition is finished. The inertial acquisition takes place at a sampling frequency of 100 Hz, sufficient for the acquisition of human movement, without loss of information [331]. The files containing the inertial data acquired by the sensory unit are stored on a USB pen drive with a capacity of 32Gb. To power the system, the power-bank Turbo 3000 (5 V; 2 A; 3000 mAh; 75 g) is used. The system has an eight-hour autonomy, allowing for daily monitoring sessions over long periods of time. Furthermore, a new Bluetooth module (HC06 Bluetooth module) was also included to allow a better connection between the waistband and external devices, such as smartphones. The last improvement implemented in this waistband was related to its fabric, which was modified in order to be more easily adjustable to the subjects' abdominal perimeter, since the previous version of the waistband, despite being elastic, was one-size-fits-all and could cause discomfort. All the referred components are depicted in the diagram presented in Fig. 46.

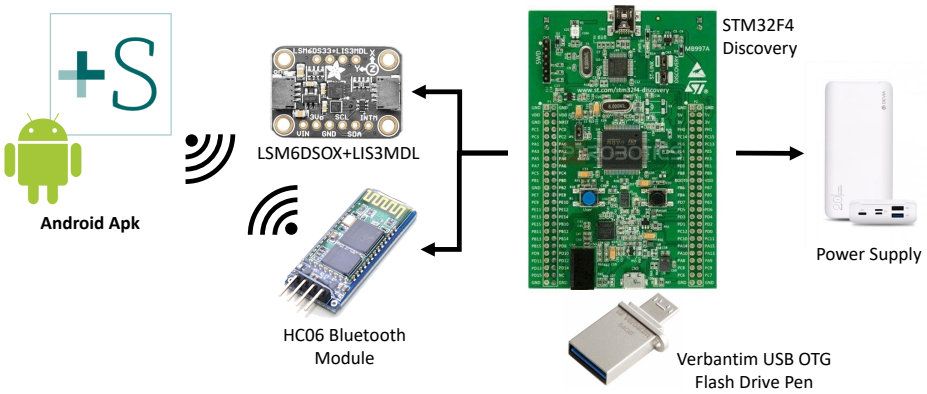

Figure 46: The waistband component's system overview, illustrating the central systems with the respective components and interfaces between them.

Two graphic applications for smartphones, capable of communicating with the control unit via Bluetooth, were created in Android Studio to facilitate: i) the data acquisition; and ii) the labelling process. The first smartphone application (Fig. 47.a) was previously developed by BirdLab members for the last version of the waistband. However, it was altered to send the initial timestamp for further synchronisation with other devices, as well as to allow an intuitive beginning and ending of the data acquisition and saving the file containing the inertial data from ADLs. The second application (Fig. 47.b) helps labelling data, through simple clicks, during the acquisition by saving the start time of several ADLs into a text file. The text file's name can be changed by the user. It also includes an embedded timer so that the person in charge of data collection may keep track of how long each activity takes.

6.3.2.2 Data Acquisition Protocol

The data acquisition experimental protocol was elaborated in collaboration with Doctor Gorjão–Clara, specialised in the field of geriatrics, in order to define several inclusion and exclusion criteria, the ADL to be realised by the selected subjects, and the conditions under which data acquisition must be done. Based on the exclusion criteria outlined, seniors with the following conditions were excluded: i) dementia (Mini Mental State Examination (MMSE)≤15); ii) severe depression (Geriatric Depression Scale (GDS) ≥ 11); iii) physical disabilities (unable to walk without walking aid, Functional Ambulation Categories (FAC) < 4); iv) orthopedic, cardiac, or respiratory diseases that affect locomotion; v) Morbid obesity (Body Mass Index (BMI) ≥ 30); and vi) Fear of falling moderate-high (Short Falls Efficacy Scale – International (FES-I) ≥ 14). Clinicians, nurses and caregivers of nursing homes performed the various tests and clinical scales mentioned above in order to identify possible participants for data collection. After getting the clinical FRA from the several above mentioned clinical scales and the demographic data (age, height, body mass and gender), a total of 25 subjects were selected to perform the experimental protocol whose age ranged from 55 to 95 years old (77.64 ± 10.20 years), with a body mass between 42.7 and 97.5 kg (66.45 ± 14.19 Kg) and a height of 49 to 172 cm (159.52 ± 7.08 cm). This group of participants was further divided

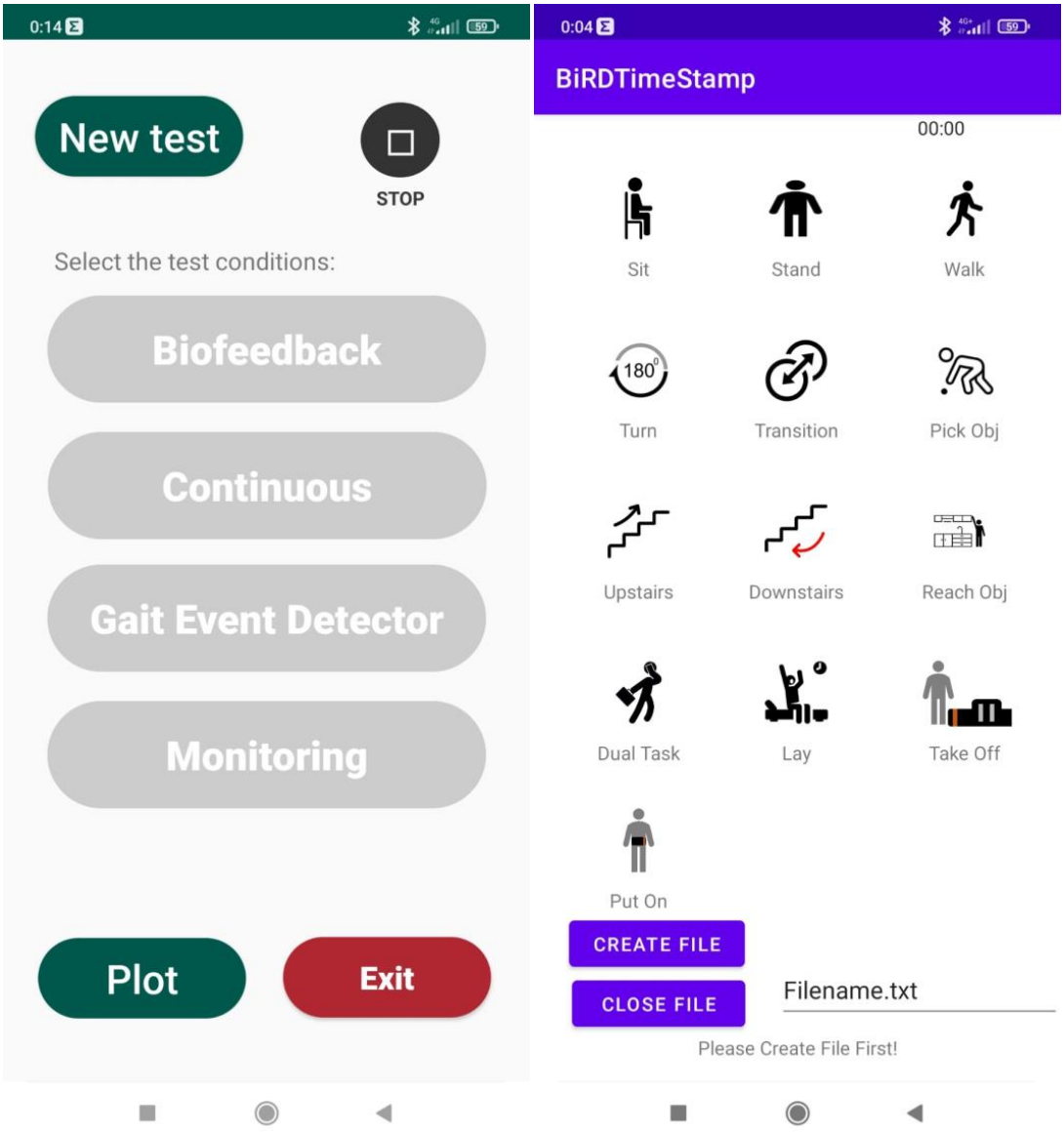

(a) (b)

Figure 47: a) Data acquisition App. b) Data labelling App.

into fallers and non-fallers considering their fall history. The activities available on Table 23 were carried out in two different protocols (circuit of activities and repetition of isolated activities) and the inertial data was gathered under controlled conditions to ensure the individuals' safety at all levels. The placing of the waistband on the individuals was the initial stage for collecting inertial data. The inertial sensor must be aligned with the spine in the central region of the subjects' waist (Fig. 48.a). Then, each subject completed the set of activities shown in Table 23 in the form of a circuit (Fig. 48.b). Each participant performed the circuit once at a comfortable pace. Each activity had a duration of at least 2 minutes, with the exception of the Sit-to-Stand, Stand-to-Sit and Lay down transitions. The circuit was the following: Sit – Sit to stand (not with a specific time) – Stand – Walk – Pick objects from the ground – Walk – Climb stairs (not with

Table 23: Set of ADL that elderly subjects performed under controlled trials

Code	Activity
ADL001	Walking
ADL002	Sitting
ADL003	Standing
ADL004	Walking Upstairs
ADL005	Walking Downstairs
ADL006	Sit in a regular height chair, wait a moment, and up
ADL007	Sitting a moment, lying, wait a moment, and sit again
ADL008	Standing, pick something from the ground, and getting up
ADL009	Gently jump without falling (trying to reach a high object)
ADL010	Being on one's back change to lateral position, wait a moment, and change to one's back (Lying)

a specific time) - Descend stairs (not with a specific time) – Walk – Reach high objects –Walk (dual task: answering the telephone/talk with a person) - Stand – Lay down. The responsible for the test delivered voice orders to the participants to change their activities while they were performing the circuit, noting the start time of each activity in the mobile app to capture the timestamps. In addition, if any of the volunteers showed signs of exhaustion, the test was interrupted to give them time to recover. Finally, after the circuit of activities, each volunteer repeated 3 times each activity from the Table 23 separately. These activities were chosen with the target audience (elderly) and their physical constraints in mind. During the realisation of these activities, each subject was accompanied by caregivers and the person responsible for the data collecting. All participants provided their written consent.

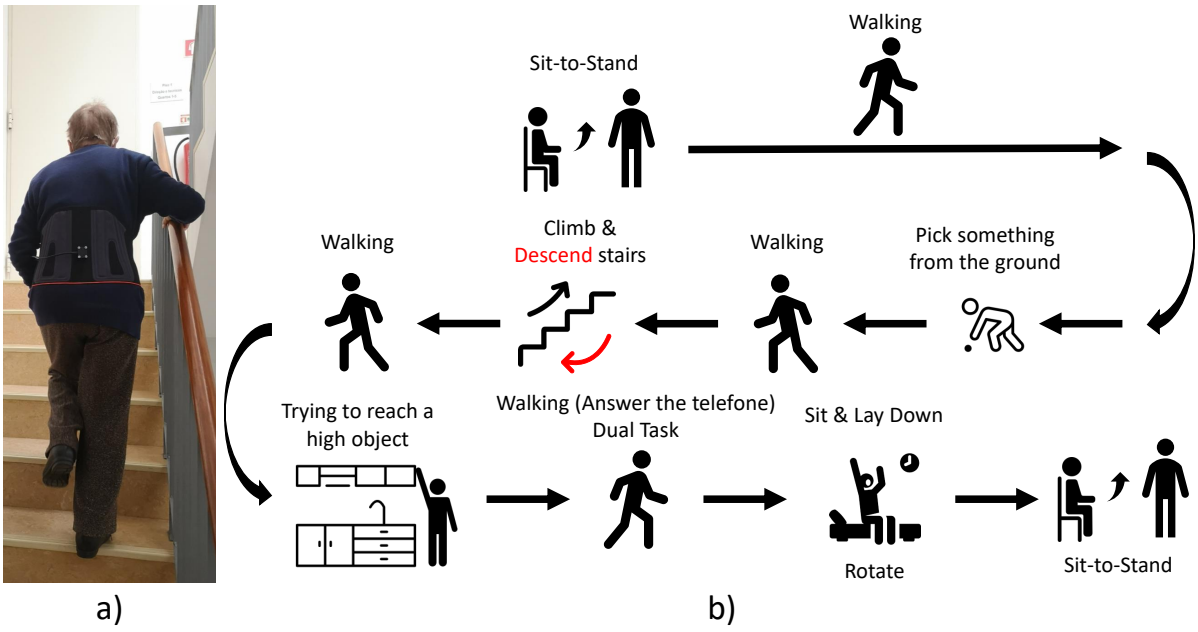

Figure 48: a) Placement of the waistband. b) Circuit for inertial data collection of ADL.

6.3.3 AI-based Comparative Analysis

Two stages make up this AI-based comparative analysis. Data from the datasets in Table 21 were used in the first phase to determine which models and features were optimal that attain the best performance for activity recognition. This initial phase uses a method that is quite similar to the one used in section 4.4. The following processes were performed as mentioned previously but some of them present some exceptions: i) PCA, ii) feature extraction/estimation; iii) feature selection; iv) feature normalisation; and v) model building and evaluation.

This initial approach consisted of training several machine-learning classifiers to identify ADLs and fall events with different feature subsets. The subsets of features with the best performance were then used with several Neural Networks architectures, and their performances were compared with the machine-learning classifiers. Finally, for the best machine-learning classifier and neural network, a study to assess the influence of the window size used for feature extraction on the classification model's performance was carried out. It should be noted that all operations were performed on the global dataset without the use of any noise filters or other sorts of processing, i.e., the raw inertial data were directly implemented in the referred procedures. All the processes used for the development, validation and evaluation of these ADL recognition algorithms were implemented offline using the Matlab 2021b version on a Lenovo Legion Y540: processor—intel core i5, 9th Gen; graphics card—NVIDIA® GeForce® GTX 1650; memory—8 GB DDR4 at 2666 MHz and SSD PCIe of 512 GB.

Feature extraction was achieved through the sliding window method, where a signal is segmented into several windows of equal size, on which different features can be calculated. The most used sliding windows' size corresponded to approximately 1 second for this type of activity classification, and the overlap between consecutive windows can vary from 50% to 87% [332–334]. Within the scope of the activity recognition, firstly, a one-second window was selected for the comparative analysis, which corresponds to a 50-sample window, with an overlap of 80%. In addition to the initial window size, 4 other different sizes were explored in the window size study: 0.5 s; 1 s; 1.5 s; and 2 s. The overlap was kept at 80% for all tests, despite the literature suggesting that it can also have a high impact on the classification performance and computational cost for real-time applications [334, 335]. The segmentation in windows with a size of 1s and an overlap of 80% resulted in a total set of 666,660 windows for the models' training and evaluation. Similarly, for a window size of 0.5 s, 1.5 s, and 2 s, a total of 1.366.289, 435.111, and 318.516 windows were obtained, respectively. Thus, for each window, several features, such as the averages, maximums, minimums, and standard deviations of each of the acceleration and angular velocity signals, among other metrics, were extracted, making a total of 199 features calculated - a higher number than used previously in Section 4.4. A summary of the extracted features can be seen in Table 58 (Appendix C). The window labelling was carried out according to the Mode Labelling Method, where the label of a given window would be the mode of the labels present in that window's samples [335].

Table 24: Specifications for the use of the Deep Learning models

Specification	Value
Epoch Number	100
Hidden Layers	150
Batch Size	64
Optimizer	Adam [336]
Learning Rate	0.001 (Constant)
Loss Function	Cross-Entropy

The remaining methods were implemented in a similar way. PCA was performed as previously, but now for 199 features. The same feature selection methods were used, as well as the same machine-learning classifiers and neural networks, excepting the BiLSTM. Initially, the HO method was used to split 70% of the created dataset's data for training and 30% for testing. The machine-learning classifiers were used to obtain the subset of the most relevant features by performing an initial five-fold CV with one repetition and using only training data. Once determined the subset of the most relevant features, a five-fold CV with ten repetitions was performed to the four best classifiers from the previous step in order to evaluate the generalisation capabilities of each model. The two best classifiers from this step were chosen, and its hyperparameters were optimised through a grid-search process. The optimised machine-learning classifiers and the neural networks architectures were further trained with all training data and tested with the test data from the HO method and the final performance of each classifier was compared in order to choose the best AI-based classification models. During all of the operations, test specifications such as the loss function used, number of epochs, the optimiser employed, number of hidden layers, batch size and the Learning Rate were kept constant for all the architectures. Table 24 provides a summary of all these characteristics and respective values. Furthermore, the time required to perform the training and testing of the KNN and Ensemble Learning classifiers for each of the window sizes was also computed. This exercise had the objective of investigating the possibility of using one of the algorithms that presented better performance in real-time situations.

Finally, the data collected in institutions from the target population were used as input for the models that presented the best performance. This information went through the same pre-processing steps as the previously used public and team-owned datasets (Fig. 43). However, only the following conditions were tested: i) window size of 1s; ii) overlap of 80%; iii) normalisation between 0 and 1; and iv) Mode Labelling Method. Initially, the HO method was used to split 90% of the created dataset's data for training and 10% for testing considering the labels proportion. This process implies that a model is trained and tested with data from the same subject (Subject Dependent). This process is very similar to the one used previously with public and team-owned datasets, having only changed the percentages of data for training and testing. The LOO approach was then used. Of the 25 older adults, 24 were chosen to train the models and one was set aside for model evaluation - the process was repeated until all subjects had been tested once.

As a result, the model is tested using data from people who did not appear in its training set (Subject Independent). As mentioned previously in Chapter 4, LOO method evaluates the generalisation capability of the final classification models [241].

6.4 Activity Recognition: Results

6.4.1 PCA Outcomes

The scree plot determined that 11 PC were necessary for a cumulative percent explained greater than 70%. Furthermore, the resulting PC demonstrated that there were 55 features with PC values greater than 1/199. After performing the PCA, the number of features were reduced to lower the computational cost of the comparative analysis, i.e., instead of using all 199 features, only the first 110 features were used and ranked by the feature selection method included. Only training data split from HO method were used.

6.4.2 ADL and Fall Events Classification

The results attained from the five-fold CV with one repetition disclosed the Ensemble Learning classifier as the one that presented the best performance among the used classifiers (MCC = 85.78%; ACC = 94.59%) when using the first 65 features ranked by the PCA method (Table 57 - Appendix C). With the first 85 features ranked by the Relief-F (Table 57 - Appendix C), KNN produced similar but inferior results (MCC = 85.10%; ACC = 93.63%). DT performed worse with the first 74 features ordered by the same technique (MCC = 70.65%; ACC = 88.22%); and Quadratic and Linear DA had the worst performance results with the first 55 and 66 features ranked by the Relief-F method, respectively. The two best classifiers went through a five-fold CV with ten repetitions, and we realised that increasing the number of repetitions did not change significantly the CV results either for the Ensemble Learning (MCC = 85.79%; ACC = 94.59%) or KNN classifier (MCC = 85.05%; ACC = 93.62%). From this second CV stage, the Ensemble Learning using the first 65 features ranked by PCA and the KNN using the first 85 features ranked by Relief-F were chosen for the next phases. Table 25 presents the main results for the two phases of the CV process.

When using test data from the HO data split method, the two best classifiers presented slight improvements in their performance in comparison to the results shown in Table 25. However, the Ensemble Learning model presented lower results (MCC = 88.36%; ACC = 95.44%) than the KNN classifier (MCC = 93.19%; ACC = 97.27%) when tested with unseen data, contrary to what was verified during the CV process. After the optimisation stage, KNN hyperparameters were: i) distance—minkowski; ii) distance weight—squared inverse; iii) exponent—0.5; and iv) number of neighbors—1. Ensemble Learning hyperparameters were: i) Method—Bag; and ii) number of learning cycles—37. Table 26 depicts the main results obtained for the HO validation process.

Table 25: Comparison of the best classification results (ACC, SENS, SPEC, Precision, F1 Score, MCC), attained after the 5-1 and 5-10 k-fold CV steps for the KNN and Ensemble Learning classifiers

ML Model	Feat. Sel. Met.	CV Step	Nº of Features	ACC (%)	SENS (%)	SPEC (%)	Prec (%)	F1 Score (%)	MCC (%)
KNN	Relief-F	5 Fold (1 rep.)	85	93.63	84.17	99.64	86.80	85.43	85.10
	PCA		85	92.99	84.08	99.60	86.01	85.01	84.63
	FSASL		70	91.49	81.39	99.51	83.66	82.48	82.02
Ensemble Learning	PCA		65	94.59	82.22	99.68	90.54	85.80	85.78
KNN	Relief-F	5 Fold (10 rep.)	85	93.62 ± 0.016	84.12 ± 0.066	99.64 ± 0.001	86.75 ± 0.055	85.38 ± 0.056	85.05 ± 0.056
	PCA		85	92.95 ± 0.021	83.91 ± 0.094	99.60 ± 0.001	85.88 ± 0.085	84.86 ± 0.085	84.48 ± 0.086
	FSASL		70	91.48 ± 0.026	81.40 ± 0.063	99.51 ± 0.001	83.59 ± 0.079	82.45 ± 0.066	81.99 ± 0.067
Ensemble Learning	PCA		65	94.59 ± 0.015	82.18 ± 0.067	99.68 ± 0.001	90.64 ± 0.073	85.79 ± 0.061	85.79 ± 0.060

Table 26: HO test results for the Ensemble Learning with the first 65 features ranked by the PCA and for the KNN classifier with the first 85 features ranked by the Relief-F.

ML Model	Feat. Sel. Met.	Nº of Features	ACC (%)	SENS (%)	SPEC (%)	Prec (%)	F1 Score (%)	MCC (%)
KNN	Relief-F	85	97.27	92.90	99.84	93.79	93.34	93.19
Ensemble Learning	PCA	65	95.44	85.97	99.73	91.67	88.43	88.36

6.4.3 Deep Learning Outcomes

The BiLSTM stood out among the neural networks in both case studies, using the first 85 features ranked by the Relief-F method (MCC = 82.83%; ACC = 92.55%) and the first 65 features ranked by PCA (MCC = 80.52%; ACC = 91.48%). However, in both cases, it presented lower results when compared to Ensemble Learning and KNN. On the contrary, CNN presented the lowest performance results for both case studies, using the first 85 features ranked by the Relief-F method (MCC = 37.87%; ACC = 57.01%) and the first 65 features ranked by PCA (MCC = 24.90%; ACC = 42.67%). Thus, the machine learning-based methods, KNN and Ensemble Learning, were considered the classifiers with better performance for ADL and fall events recognition, among all tested classifiers, being selected for the window size study and classification time analysis. Table 27 contains the main results for ADL recognition when neural networks are used.

6.4.4 Window Size and Classification Time

The results attained in this last analysis, for the optimised KNN and Ensemble Learning classifiers, are depicted in Table 28. It should be noted that the same labelling method was used during the feature extraction step for each window size selected for this analysis. Both tables show a decreasing trend in the performance of the two classifiers as the window size increases from 0.5 to 2 s.

In addition to the results obtained regarding performance metrics, the time required to perform the training and testing of the KNN and Ensemble Learning classifiers for each of the window sizes used in this last study was also computed. This exercise has the objective of studying the possibility of using one

Table 27: Results for the test of the 4 Deep Learning architectures with the 85 first features ranked by Relief-f and 65 first features ranked by PCA

Feat. Sel. Met.	Feature Number	Architecture	ACC (%)	SENS (%)	SPEC (%)	Prec (%)	F1 Score (%)	MCC (%)
Relief-F	85	CNN	57.01	37.06	97.22	54.67	35.47	37.87
		LSTM	92.06	79.58	99.55	84.25	81.02	81.01
		CLSTM	88.84	74.48	99.36	75.24	74.53	74.06
		BiLSTM	92.55	81.14	99.57	85.56	83.14	82.83
PCA	65	CNN	42.67	26.46	96.15	54.49	22.27	24.90
		LSTM	91.46	77.81	99.51	84.38	80.61	80.38
		CLSTM	88.55	74.33	99.35	75.09	74.36	73.88
		BiLSTM	91.48	79.33	99.52	83.32	80.67	80.52

Table 28: Window size comparative study results for the KNN best optimized model with the Relief-F feature selection model

ML Model + FSM	Window Size (s)	Window Overlap (%)	ACC (%)	SENS (%)	SPEC (%)	Prec (%)	F1 Score (%)	MCC (%)
KNN + Relief-f	0.5	80	98.22	95.20	99.90	96.04	95.62	95.52
	1		97.27	92.90	99.84	93.79	93.34	93.19
	1.5		96.30	91.73	99.79	91.15	91.41	91.22
	2		95.33	90.53	99.74	88.51	89.44	89.22
Ensemble + PCA	0.5		96.53	88.94	99.79	94.09	91.29	91.21
	1		95.44	85.97	99.73	91.67	88.43	88.36
	1.5		95.01	85.60	99.71	90.76	87.64	87.62
	2		94.51	85.21	99.68	89.37	86.92	86.79

of the combinations which presented better performance results in real-time situations. Table 29 depicts the results obtained for the training and testing time of each classifier and window size combination.

Through direct observation of Table 29, the KNN classifier has a training time of around four seconds, regardless of the size of the windows. The Ensemble classifier's training time shows an increasing trend as the window size decreases. On the other hand, the time required to test only one window (last column of Table 29) is lower than 4.5×10^{-5} s for every window size tested in the case of the Ensemble Learning classification model. The test time per window for the KNN classifier shows an increasing trend as the window size decreases.

6.4.5 ADL Recognition from Nursing Homes Data

KNN and Ensemble Learning were then selected for this last stage, since they were the models that had previously the best performance. The results attained from the HO method as disclosed the KNN as the one that presented the best performance (MCC = 95.81%; ACC = 99.10%) when using the first 85 features ranked by the Relief- F method. On the other hand, Ensemble Learning showed lower results, although close to KNN (MCC = 95.81%; ACC = 99.10%) when using the first 65 features ranked by the

PCA. These results are in accordance to what was obtained previously with the public and team-owned datasets using only the HO method (Table 26). Table 30 details these results. The LOO approach presented lower results when compared to the HO method. Both models presented similar results in terms of ACC (KNN: 72.74±8.51%; Ensemble Learning: 72.73±13.78%), however Ensemble Learning presented a slight higher value of MCC (KNN: 54.67±8.28%; Ensemble Learning: 59.75±12.87%). Standard deviation values show that Ensemble Learning presents more variability in its outcomes. Table 31 resumes the results of the LOO approach. Table 32 demonstrates this variety in outcomes, with a 60% difference between the best and worst subjects in terms of ACC. Ensemble Learning produces the best and worst performance for a subject for which the model has never seen data.

Table 29: Classification time for the training and testing of the two best combinations of Machine Learning model and Feature Selection Method, for each of the selected windows for the window size study

ML Model + Feat. Sel. Met.	Window Size (s)	Window Overlap (%)	Test Windows	Train Time (s)	Test Time (s)	Test Time per Window (s)
KNN + Relief-f	0.5	80	409,740	4.36	213,588.88	0.521
	1		199,997	4.18	66,782.58	0.334
	1.5		130,421	4.70	12,633.08	0.097
	2		95,482	4.09	6752.47	0.071
Ensemble + PCA	0.5		409,740	829.55	15.99	3.90×10^{-5}
	1		199,997	279.03	8.54	4.27×10^{-5}
	1.5		130,421	145.21	5.68	4.35×10^{-5}
	2		95,482	100.23	3.94	4.13×10^{-5}

Table 30: HO test results for the Ensemble Learning and for the KNN classifier when using data from older adults

ML Model	Feat. Sel. Met.	Nº of Features	ACC (%)	SENS (%)	SPEC (%)	Prec (%)	F1 Score (%)	MCC (%)
KNN	Relief-F	85	99.10	95.61	99.93	96.48	95.71	95.81
Ensemble Learning	PCA	65	97.65	88.96	99.82	94.36	90.27	90.78

Table 31: LOO mean and standard deviation test results for the Ensemble Learning and for the KNN classifier when using data from older adults

ML Model	Feat. Sel. Met.	Nº of Features	ACC (%)	SENS (%)	SPEC (%)	Prec (%)	F1 Score (%)	MCC (%)
KNN	Relief-F	85	72.74±8.51	54.22±8.84	97.25±0.75	60.54±8.78	57.50±8.53	54.67±8.28
Ensemble Learning	PCA	65	72.73±13.78	57.40±12.72	97.24±1.38	69.73±12.27	67.03±6.46	59.75±12.87

Table 32: LOO best and worst test results for the Ensemble Learning and for the KNN classifier when using data from older adults

Subject	ML Model	Feat. Sel. Met.	Nº of Features	ACC (%)	SENS (%)	SPEC (%)	Prec (%)	F1 Score (%)	MCC (%)
Best Subject	KNN	Relief-F	85	84.23	63.03	98.37	75.11	64.62	64.45
	Ensemble Learning	PCA	65	90.47	76.66	98.73	85.06	77.73	78.06
Worst Subject	KNN	Relief-F	85	47.36	42.79	95.01	35.42	35.41	32.63
	Ensemble Learning	PCA	65	29.72	30.54	93.19	36.7	-	27.85

6.5 Conclusions

The architecture and functioning of a simple FRA tool was demonstrated with the aim of eliminating some gaps found in the literature, namely reducing the subjectivity presented in tests and clinical scales, allowing an assessment in real-time and using a wide range of risk factors to carry out the assessment, while still being easy to use and comfortable for the target audience. This tool is based on recent developments in AI techniques and in data acquisition methods from wearable sensors. Thus, all modules can work using inertial data acquired by waistbands or smartwatches, thus making it an easy-to-use and comfortable tool for everyday use by the elderly. With the *Baseline Risk Module* it should be possible to integrate and evaluate different types of risk factors, whether associated with the subjects, such as age, weight, fear of falling or results of clinical tests, or risk factors associated with the surrounding environment, such as location or humidity level. This module will thus make it possible to address the question regarding the need for a FRA tool that assesses the risk of falling in a multifactorial way. Another positive aspect that differentiates this FRA tool from all others is its ability to classify in real-time the ADL that is being carried out, and assign a risk level to that classification. Despite the positive aspects mentioned above and the possibility of suppressing some disadvantages found in the literature, this tool is still require a validation of each module described above. The validation of methods that make use of AI models is a complex process, which requires the use of a large set of data and several processes, in order to find the best method for a given task [71].

Considering the ADL Recognition Module, the first stage presented as result an algorithm capable of recognising ADLs. This algorithm that recognises sixteen ADLs and four different types of fall (twenty classes in total) from several AI-based classification models and feature selection models was built in order to find the combination that presents better performance in this type of classification. The performance of the different combinations was evaluated using the following parameters: i) performance evaluation metrics, ii) subset of features used, and iii) classification time per window of the models. Two different approaches (machine-learning and deep-learning) were investigated and compared: when performing one waist-located inertial sensor-based ADL and fall events recognition. Furthermore, a new procedure of fusion and normalisation of datasets was carried out in order to generate a vast dataset to validate the activity

classification models in order to battle concerns observed in the literature. Taking into account the performance values as well as the classification times found in this work for the machine used, it is concluded that the most effective AI-based classifier was the Ensemble Learning classifier with the first 65 features ranked by the PCA. Moreover, the classification time per window in this combination was lower than the window advance time in every window tested, which represents an encouraging result for the application of this algorithm in real time in the future. The deep learning outcomes were not as good as in the prior procedure; however, their potential was demonstrated, indicating that they could be a good option in the future with the appropriate future work regarding the input data used and its architectures.

Considering the data acquired in institutions and their usage in the best-performing models, it is possible to verify that the HO results, as expected, are in line with those achieved with public and team-owned datasets, because the method is the same, achieving even slightly better results. This could be related to: i) the smaller number of activities to identify; and ii) the slower rate at which the elderly conduct the activities, which could explain why the 1s window with these data produces equivalent outcomes to the 0.5s window when public and team-owned datasets are used. KNN once again outperforms the competition in terms of performance metrics. MCC and F1-Score metrics indicate a need for more data collection, activity balancing, and possibly data processing (e.g. filtering data). Both for the KNN and the Ensemble Learning, the LOO outcomes were much lower than the HO approach. Different ways of carrying out tasks by different subjects, signal noise, and a short amount of data might all excuse this significant drop in performance when a subject-independent analysis is undertaken.

Chapter 7

Knee Orthosis for Real-Time Fall Prevention

The purpose of this chapter is to establish a slip-related fall prevention strategy, which is divided into actuation and detection. The actuation strategy was developed based on human biomechanics responses to slips, with the perturbed (leading) leg's knee joint playing an important part in preventing slip-induced LOB. Thereby, when a slip is detected, this strategy highlights a knee orthotic device that delivers assistive torque to avoid falls. To predict gait parameters, the detection strategy took advantage of the appealing qualities of bioinspired CPG controllers. To identify slips, threshold-based algorithms analysed the CPG's prediction error, which increases when there is an unexpected gait perturbation. As gait monitoring variables, the knee angle and shank angular velocity were used. An experimental protocol intended to induce slip perturbations in human volunteers allowed data from these variables to be collected in order to further verify the perturbation detection system.

7.1 Introductory Insight

Slips have been recognised as the leading cause of falls [337, 338]. Hence, researchers have been examining the biomechanics of slips in order to better understand human reactions to these occurrences and mitigate their negative implications. Slips happen when the interaction between the subject's foot and the floor lacks adequate COF [105]. As a result, the environment has a significant impact on the chance of slipping. These events occur mostly when the foot contacts or leaves the floor, and they resemble crucial body weight transfer circumstances between the lower limbs, particularly when the heel strikes the floor [105]. Slips started at the HS cause a backward LOB by deviating the subject's CoM relative to the BoS. When human sensory systems identify this anomalous deviation, information is conveyed to the motor control areas of the Central Nervous System (CNS) through afferent nerves. The CNS interprets the information

and provides efferent signals to specific skeletal muscles to compensate for the LOB by correctly contracting to keep the body position inside the BoS. The coactivity of recruited lower limb muscles counteracts foot displacement and facilitates slip recovery [105]. The slip perturbation direction is also known as the motion direction, i.e., the AP direction. Only 8.2% of the instability-induced falls are connected to the ML orientation [339]. Cham and Redfern [340] discovered that the predominant reaction to to counteract the LOB caused by a slip at the HS was a rise in both knee flexion and hip extensor moments at the leading leg, which Moyer et al. [45] also verified. This allows to counteract the perturbed foot's sliding action, bringing it closer to the CoM and reducing the body's V decline. Despite primarily considering the recovery biomechanics of the leading limb, Cham and Redfern [340] acknowledged the trailing leg's probable helpful function during a slip. In this context, Moyer et al. [45] emphasised the relevance of trailing leg kinematics in understanding the human biomechanical response to slips. Moyer et al. [45], as in Marigold and Patla [341], found that the higher the severity of the slip, the sooner the swing phase of the trailing foot was terminated by lowering the foot to the ground, using a corrective hip extension, and reestablishing a stable BoS to maximise the odds of recovery. The increase in slip severity also causes the trailing foot to settle on the ground more posteriorly and with a smaller contact area. The time it takes to reverse the swing motion direction after a slip before putting the foot on the ground is critical to slip recovery [120]. If the slip caused only minor discomfort, the trailing limb's swing phase was not disrupted [45]. Moyer et al. [45] discovered evidence of interlimb coordination during recovering from slip events, since the intensity of the trailing leg's reaction was related to the knee moment exerted in the leading leg after the slip. Consequently, interlimb cooperation of both lower limbs is required for effective recovery following a slip incident. In order to slow the sliding motion of the slipping leg and bring it closer to the CoM, an increase in the flexion moment applied at the knee is complemented by an increase in the hip extension moment [340]. In parallel, the trailing leg's reaction is characterised by greater moments at the hip and knee joints [45]. The hip reaction is distinguished by a greater extension moment used to drop the foot

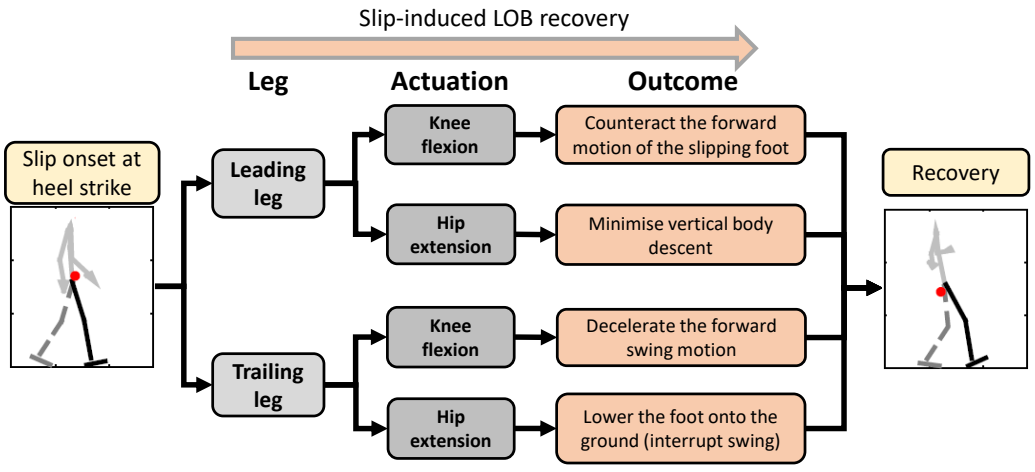

Figure 49: Human biomechanical reactions adopted upon a slip event [120] (red dot = CoM).

into the ground, interrupting the swing phase and reestablishing a stable BoS. To summarise the available literature findings, Fig. 49 displays the primary human biomechanical responses to a slip incident. The following sections will provide a Slip-Related Fall Prevention Strategy and the validation of its detection system. This innovative technique aims to overcome the literature limitations by selecting the actuation leg based on side-dominance and having a real-time detection system with greater performance.

7.2 Slip-Related Fall Prevention Strategy

Two major modules constitute the slip-related fall prevention strategy concept: i) the actuation strategy; and ii) the detection strategy. Each strategy's requirements were developed in order to encourage effective performance from the identification of slip-induced LOB through the successful corrective actuation of the assistive device. Given that the slip-related fall prevention strategy is intended at real-world settings, the sensors used for data collection were thought to be wearable devices or incorporated on the assistive device. Also for the current strategy, only slips caused at the HS were examined, as this gait event was proven to be the most conspicuous and prevalent to onset slip perturbations during walking [105]. In terms of actuation strategy definition, the optimal situation would include the provision of assistive torque to all lower limb joints from both legs following a slip, taking into account the prominent role of the perturbed (leading) and unperturbed (trailing) legs in counteracting slip-induced LOB. However, such an approach would increase the fall prevention strategy's complexity, both computationally and mechanically, perhaps making it useless. As a result, only the leg and joint deemed to be most relevant in counteracting slip-induced LOB would get assistive actuation. Trkov et al. [81] and Mioskowska et al. [37] actually only assisted one joint with their slip fall prevention device. Thus, in order to define the strategy's assistive device, it is critical to answer the following questions: i) Which leg has a more significant role in preventing slip-induced LOB?; ii) Which lower limb joint has a more determinant role in preventing slip-induced LOB?; and iii) Which joint moment characteristics should be applied to the actuation joint? The definition of the detection strategy is based on the usage of bioinspired controllers that can learn and modify their output to practically periodic inputs. These controllers are well-suited for monitoring human locomotion characteristics and offer benefits over conventional training-based algorithms. The signal anticipated by the bioinspired controller will diverge from the actual motion signal in the presence of a gait perturbation. Based on these produced deviations, threshold-based algorithms were employed to detect gait disturbances. However, in order to detect slip-induced LOB, it is vital to objectively pick the variables that will be monitored. Important human motion variables from the literature were considered and filtered to select the most suitable variables to be used by the CPG controller. Finally, the timings allocated to the slip-related fall prevention strategy, specifically the durations attributed to the detection and actuation phases, were established based on literature evidence on biomechanical reactions to slip-like perturbations.

7.2.1 Actuation

The full characterisation of assistive actuation properties is required for successful fall prevention. Given that only one joint will be provided with assistive actuation, it is critical to accurately determine which leg and joint exhibit the most appropriate reactionary response to counteract a slip-induced LOB. After identifying a joint, the assistive actuation characteristics and the assistive device were determined. The assistive actuation features recommended for the present slip-related fall prevention strategy are shown in Fig. 50. This decision was made based on the evidence gathered from the literature, which is explained further below.

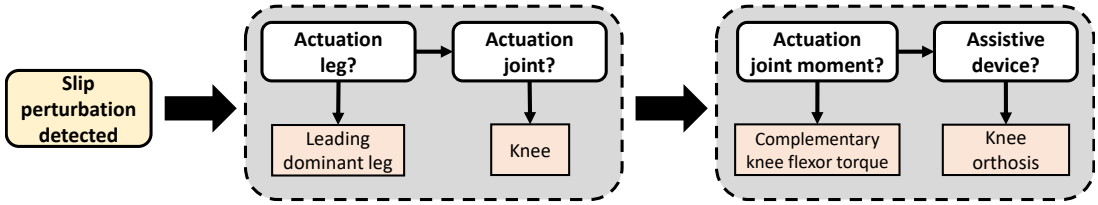

Figure 50: Assistive actuation strategy features.

7.2.1.1 Actuation Leg

Two factors must be considered while choosing the actuation leg: i) the perturbed leg; and ii) the subject's side-dominance. For the first criterion, evaluate the system's actuation in either the leading or trailing legs. The option for the second criterion is whether to actuate on the dominant or non-dominant legs. Previous research has highlighted the importance of both the leading [340] and trailing [45] legs in terms of balance recovery following a slip perturbation at the HS. The leading leg's duty is mainly to move the anteriorly displaced BoS closer to the CoM as a result of the sliding action of the foot [340]. In the event of a more severe slip, the trailing leg's task is to break the swing phase by lowering the swing limb onto the ground to give support and prevent the body from collapsing [45]. The interlimb coordination of both legs' corrective responses is responsible for the total recovery response to slip disturbances [45, 133, 144, 342]. However, the leading leg's corrective reactions are thought to be the most important since a large number of studies choose to examine them over those that research the trailing leg's responses [45, 340, 343]. Yang et al. [344] discovered that slip outcomes were crucially affected by the leading leg before to the trailing limb's recovery landing, implying that slip-induced falls can be avoided by individually managing the leading leg [142]. Thereby, the actuation on the leading leg may address the slip at its source by reducing the distance between the CoM and the BoS, so reducing the severity of the slip. As a result, the actuation leg was chosen to be the leading leg. Nevertheless, the leading leg might be either the right or left leg. The side-dominance or laterality, i.e., the preference for one side of the body over the other, should be examined. This results in bilateral asymmetries during healthy gait. The "functional asymmetry"theory, on the other hand, indicates that this asymmetry may be related to the task discrepancy between the two lower limbs. According to

this idea, the dominant lower limb is more responsible for propelling the body forward, whereas the non-dominant lower limb is more responsible for providing support [345]. The laterality may influence the reactions adopted to both standing [346] and walking [347] corrective reactions towards perturbations since fall risk increase when the non-dominant leg was perturbed [348]. Thus, the non-dominant leg is more used and equipped to give body support than the dominant leg.

7.2.1.2 Actuation Joint

To prevent slip-induced LOB, the knee appears to be the most important lower limb joint. Sawers et al. [144] discovered that during slip trials, patients who fell had a delayed knee muscle activity start time in the leading leg when compared to participants who recovered. These findings showed that the capacity to coordinate muscle activation around the knee in a timely manner might be critical in preventing slip-induced falls. Sawers & Bhatt [349] also discovered that individuals who recovered from slips had greater neuromuscular control variety and complexity, which is based on the synchronisation of knee muscle activity in perturbed and unperturbed legs. Furthermore, the critical role of knee joints in preventing slip-induced falls has been demonstrated both experimentally [340] and analytically [344]. As a result, the conceptualised fall prevention strategy would emphasise the knee joint as the actuation joint for slip fall prevention.

7.2.1.3 Actuation Joint Moment

The principal answer to slip-induced LOB is to increase the knee flexion moment, which is proportional to the severity of the slip [45, 133, 340]. This joint moment increase lets the slipping foot to slow down its sliding motion and lessen its anterior displacement, bringing it closer to the CoM. As a result, literature data suggests that the torque used to bend the knee allows for control of crucial factors for preventing slip-induced falls, such as heel acceleration [350] and the shank-to-ground angle, i.e, the angle created by the shank segment relative to the ground [142]. The acceleration of the heel in the direction of motion at the HS is thought to be a key predictor of slip incidence [105, 350], being used in experimental research to assess the severity of slips [45, 351]. Beschorner et al. [350] found that the torque exerted by the leading leg's knee affected the heel acceleration during HS.Furthermore, Wang et al. [142] discovered that the leading leg's shank-to-ground angle in the sagittal plane of motion was linked to the forward displacement of the BoS caused by slips and was the most important predictor in LOB prevention.

Despite the fact that high-fall-risk people are often not nimble or powerful enough to prevent falling from slip-induced LOB, they are nevertheless capable of taking some steps to mitigate these gait disturbances [40]. As a consequence, the torque values exerted by the assistive device must be context-dependent, taking into account the reactive torque created by the subject during the gait perturbation in order to calculate the extra torque required to recover from the slip-induced LOB. Hence, the actuation joint would

only receive a complimentary 'delta' torque. In this case, the assistive robotic system would only aid the subject as and when needed, promoting a symbiotic relationship between the human and the robotic system [40]. An orthotic system would be worn on the knee to produce the necessary assistive torque. Previous research on human knee reflexes has demonstrated that providing brief and quick knee torque assistance during walking is safe, indicating that the knee orthosis can be used [352].

7.2.1.4 Assistive Device

The assistive equipment for the slip-related fall prevention strategy designed was a knee orthosis. The SmartOs system, which was developed by a research team at BiRD Lab, includes a PKO. SmartOs is a wearable active lower limb orthotic device that delivers repeated and user-oriented gait training while measuring human motor condition using kinematic and muscular gait parameters. The ankle and knee right-side modules of the lower-limb H2-exoskeleton are currently integrated into SmartOs' architecture (Technaid S.L., Spain). For gait speeds between 0.5 and 1.6 km/h, the PKO aids gait in the sagittal plane of motion. It also has the following embedded sensors: i) an angle position sensor with a resolution of 0.5°; ii) a user-PKO interaction torque sensor with a resolution of 1 Nm (4 strain gauges connected in a full Wheatstone bridge); and iii) a hall effect sensor that measures the motor's angular speed (rpm), current, and torque. The actuation system of the PKO consists of an electrical actuator (flat brushless DC motor EC60-100 W, Maxon) linked to a gearbox (CSD20-160-2A strain wave gear, Harmonic Drive) with a ratio of 160:1, producing an average torque of 35 Nm and peak torques of 180 Nm. The mechanical construction of the PKO is built of type 7005 aluminium and stainless steel, and it has a 4-strap system with two lower straps on the shank and two upper straps on the tight, as shown in Fig. 51 [353]. In accordance with the proposed fall prevention strategy, the PKO would provide participants with an assistive torque anytime a slip-like disturbance is detected.

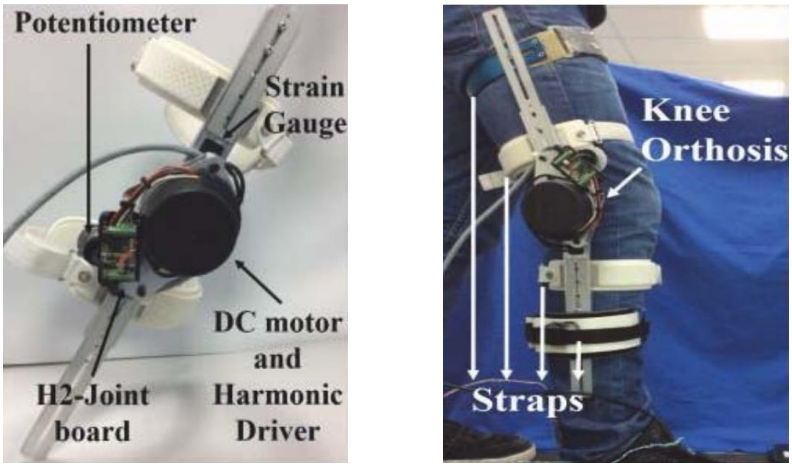

Figure 51: PKO device [353]. (a) Device's elements. (b) Mounted in one subject.

7.2.1.5 Requirements

Previous research proposed and attempted to meet several conditions that the fall prevention system should accomplish. The most often used fall prevention system identified needs were: i) flexible customisation amongst various users [40]; ii) assisted-as-needed behaviour [40, 354]; iii) no (or very limited) disturbance to the subjects, as demonstrated by: a) lightweight and comfortable to wear while walking [37, 40, 81]; b) compact design [81]; c) mechanical compliance between the subject and the exoskeleton [354]; and d) positioning heavy parts of the device away from the actuation joint [37, 81, 354]; iv) high torque development in a short time [37, 81]; and v) adapt to the mechanical needs of the subject's mobility and intents on a constant basis. The fulfilment of these requirements enables the system to ensure a normal gait in the absence of aid and quick assistive torque supply to counteract LOB occurrences in the presence of assistance. Furthermore, in the case of the proposed fall prevention strategy, the actuation of the assistive system must be accomplished within the actuation time period (100 ms).

7.2.2 Detection

The identification of slip-induced LOB needs a careful selection of the perturbation detection algorithm and the motion variables that will be monitored. Figure 52 depicts the properties of the proposed detection approach. Literature studies were used to identify potential motion variables that were then subjected to objective criteria to guarantee that the final monitoring variables chosen highlight visible changes upon a slip without needing time-consuming computation. To collect data from the specified monitoring variables, a slip-like perturbation protocol was developed and conducted, yielding data for testing the perturbation detection algorithm. The suggested detection technique includes: i) a CPG controller that monitors and anticipates the signals of the specified variables; and ii) a threshold-based algorithm for detecting slip perturbations based on the prediction error signal. When the error signal exceeded a certain threshold, a perturbation was recognised.

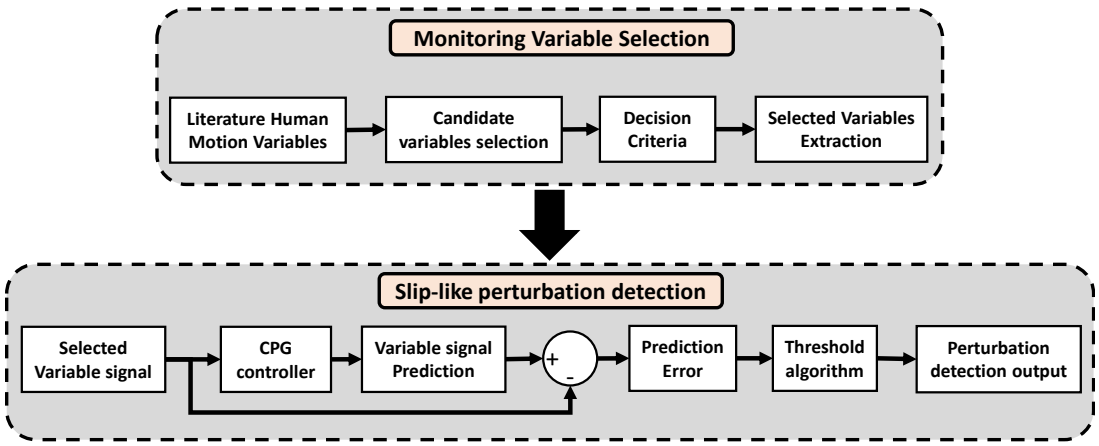

Figure 52: Detection strategy features.

7.2.2.1 Monitoring Variables Selection

The heel acceleration, shank-to-ground angle, and hip angle were identified as relevant kinematic variables. Other variables were also incorporated to increase the number of possibly important kinematic characteristics and undertake a more thorough selection. As a result, the knee angle and shank angular velocity were also taken into account [45, 112, 340, 351]. The following criteria were used to try an objective selection of the most important monitoring variables. As a result, the majority of the criteria were aimed at describing technical aspects of the variables, such as: i) the simplicity of data processing required to extract the variable in real time from sensor data (Criterion 1); ii) based on the scientific literature, the capacity of the variable's signal to efficiently identify gait events (Criterion 2); iii) the number of sensors required to compute the variable, the ease of sensor positioning, and if further instrumentation beyond the assistive device is required (Criterion 3); iv) bibliographical proof of the variable or its corresponding body segment (e.g. knee) being used to research and/or detect human biomechanical responses to slips (Criterion 4). In addition, certain movies from the slip-like perturbation protocol's perturbation trials were visually analysed in order to detect visual modifications in human body segments caused by a slip-like perturbation. This allowed to collect visual signals regarding the changes caused by gait perturbations in the temporal evolution of the variable signal (Criterion 5). Furthermore, an innovation criteria was included in order to account for whether the variable has previously been addressed in a fall prevention strategy in the scientific literature, to the best of the author's knowledge (Criterion 6).

As an outcome, the knee angle and shank angular velocity appear to be the most appropriate variables for detecting slip-induced LOB. Despite the relevance of heel acceleration in slip biomechanics [350], it was overlooked for two reasons: i) the challenge of appropriately positioning and using wearable sensors attached to the heel; and ii) the impact of the foot on the floor puts significant noise into the heel acceleration signal, limiting its usability and capacity to identify gait events. Beschorner et al. [350] gathered the heel acceleration data using reflexive markers, which alleviated the noise problem. The hip angle and shank-to-ground angle variables were also discarded, owing to the necessity to integrate the angular velocity signal in real time to produce the angle signal, which represents computational costs. The encoder from the PKO provides the knee angle, and its extraction would not require any integration and so would not cause any drift issues. Subsequently, the identification of slip-induced LOB was carried out while the knee angle and shank angular velocity variables were monitored.

7.2.2.2 Central Pattern Generators Controllers

Human movement and vital vegetative functions are recognised to be recurrent and cyclic processes. Despite the importance of neuromuscular dynamics and sensory feedback in modulating these rhythmic functions, the functional activity of the neuronal circuits located in the spinal cord, i.e., CPG, is attributed to the foundation of cyclic activity pattern generation [355, 356]. The word "central"means that the peripheral

nervous system and its sensory feedback are not used to generate rhythm [47]. Thereby, the use of biomimetic or biologically inspired CPG controller systems to monitor and regulate human locomotion variables becomes appealing, because such motion is almost certainly controlled by spinal oscillators, i.e., biological CPG [357, 358]. The artificial CPG is thus expected to synchronise with the biological one, which plays a critical role in rhythmic movement support [357, 359]. In terms of rehabilitation, the artificial CPG would provide assistive torque to the controlled joint whenever appropriate, allowing for the compensation of biological CPG deficiencies, such as those caused by a brain lesion, towards healthy locomotion [357]. CPG controllers based on nonlinear Adaptive Frequency Oscillators (AFO) emerge as a dependable method to aid in the detection of abrupt and unexpected gait perturbations [360]. An AFO is a mathematical instrument that can synchronise its output to a frequency component of a periodic or quasi-periodic input signal while learning its key properties like amplitude and phase. A network of AFO, i.e., a CPG controller, may then constantly synchronise with and estimate a periodic or quasi-periodic input signal [359–361]. An unanticipated perturbation during steady walking would cause irregular changes in the input signal, prompting the AFO to search for new signal patterns associated with various frequencies. This would soon divert the input signal from the CPG's expected trajectory, allowing for the early and effective detection of an unexpected gait perturbation [360]. When a perturbation is identified, the artificial CPG activates a robotic assistive system to deliver timely assistive torque at the controlled joints to counterbalance the LOB and encourage an efficient balance recovery [40].

Because human biped locomotion consists of a periodic or quasi-periodic motor activity, it may be decomposed into the sum of periodic or quasi-periodic signals [362]. As such, prior knowledge of the periodicity of human locomotion can be performed by taking advantage of nonlinear oscillators' ability to generate stable rhythmic patterns, i.e., limit cycle behaviour, which is useful for decomposing the respective signals into a sum of sinusoidal waves that can be learned by an oscillator network [359, 361]. The CPG controller must have the same number of AFO as the number of major frequency components required to correctly characterise the input signal, i.e., the learning signal. If the number of oscillators is inadequate to account for all of the essential frequency components of the input signal, the oscillator network will only learn and adapt to the higher-power frequency components [363]. Thereby, the learnt signal generated by the CPG will be a rather approximate approximation of the input signal. Righetti et al. [363] state that if the number of oscillators is more than the number of frequency components to learn from the input signal, one of two things might happen: i) some oscillators will not converge towards any frequency and so contribute nothing to the learned signal; or ii) several oscillators will code the same frequency component and the sum of their corresponding amplitudes will equal the amplitude of the relevant frequency component.

In comparison to other alternative approaches, Ijspeert et al. [364], Tropea et al. [360], and Santos et al. [47] identified some intriguing aspects that make CPG controllers suited for monitoring human locomotion: i) can create stable limit cycles that are resistant to disturbance. If the rhythmic pattern is disrupted, the controller quickly returns to its prior cyclic behaviour; ii) can be userd to control distinct segments or

modules within the same system. The various CPG can be linked together via a phase connection. As a consequence, the CPG model design is ideally suited for distributed implementation [47]; iii) feature a few control parameters that allow them to modulate locomotion based on changes in direction and speed. This characteristic enables CPG to generate online trajectories with smooth modulations even when the control parameters are abruptly changed; iv) allow for reciprocal entrainment between the mechanical system and them; v) do not require any training before implementation, unlike other algorithms, because the algorithm's learning process is integrated into network dynamics. vi) do not have large computing cost since no demanding signal or algorithmic processing is required; vi) offer low computing costs since no intensive signal or algorithmic processing is required. and vii) Once the frequency bandwidth of the regulated signals is known, they may be configured to monitor only these signals (all the higher frequency components can be associated to LOB reactions). Hence, unlike training-based algorithms, the CPG tuning does not need the use of signals captured during sophisticated unexpected gait disruption procedures, as only steady-state walking parameters are employed to tune the system.

7.2.2.3 Threshold-based algorithms

A simple threshold-based approach has been shown to be successful and generalizable for detecting slip-like perturbations based on the error caused between the actual kinematics and the kinematics predicted by an oscillator network [360]. In the presence of a perturbation, the error signal rapidly grows and exceeds the specified threshold values, allowing for early and effective detection of postural changes. This timely identification would allow a powered orthosis worn by the individual to give mechanical help in order to reduce the danger of a fall [40, 360]. In this regard, the capacity of a simple and an adaptive threshold algorithm to identify perturbations was investigated. The simple threshold algorithm began by determining whether the current sample, i, of the error signal was between the set fixed threshold levels. If the error value exceeded one of the thresholds indicating an abnormal condition, a warning was issued and a counter variable, c, was increased. c was otherwise reset. Second, the number of consecutive warnings was checked to see if it exceeded the number of acceptable warnings, r. The variable r was used to enable a more consistent perturbation detection by reducing the amount of false alarms generated by individual samples that exceeded a threshold but were not perturbations. If c is less than r, the algorithm moves on to the assessment of the next sample, $i + 1$. The algorithm, on the other hand, recognised a perturbation if c was equal to or larger than r. The detection time was determined to ensure that the perturbation was correctly detected. To obtain this metric, it is necessary to obtain the time difference between the actual beginning of the perturbation, as determined by pert sample, and the perturbation onset recognised by the algorithm. The detection was considered a false alarm if it was discovered before the perturbation began or later than 1 second after it occurred. The perturbation was declared effectively identified if it was noticed within the 1 second interval following its beginning. This time interval was used as a reference since earlier studies indicated that falls can occur in as little as 1 second [40, 365].

In comparison to the fixed threshold, the adaptive threshold technique follows a similar strategy. Unlike the fixed threshold strategy, this approach allowed for the use of contextual information from prior samples in the setting of threshold values. The mean, μ, and standard deviation, σ, of the m-sized window before the present sample i were acquired in order to compute the dynamic thresholds tailored to each sample. To improve the effectiveness of the subject-specific perturbation detection, the thresholds were additionally determined based on the coefficients a and b assigned to each subject. The coefficients a and b show how the standard deviation, σ, affects the computation of the upper and lower thresholds, respectively. The concept of perturbation detection was identical to the fixed threshold approach once the thresholds were calculated. These algorithms' threshold and window size parameters were set for each participant and are explained further. The variable r was set to 3 in order to identify a perturbation only if three or more consecutive samples exceeded one of the threshold values. Because both threshold-based algorithms do not need knowledge from future samples, they are thought to conduct online perturbation detection in real-world contexts.

7.2.2.4 Requirements

Despite the fact that few research [40] explain the detection of slip-induced LOB, several conditions for the detection stage of the fall prevention strategy were identified in order to validate the perturbation detection performance: i) The detection ACC of actual perturbations must be more than 75%; ii) the real perturbations' mean detection time must be less than the detection time further provided for the fall prevention strategy (360 ms); and iii) the number of false perturbations detected must be smaller than the number of right perturbations detected. Given that this chapter is still in its early stages, the present purpose of this work is to determine whether the perturbation detection algorithm can reach acceptable rather than ideal performance. Hence, satisfying the above-mentioned parameters would demonstrate acceptable performance of the perturbation detection method and open the path for future optimisation of the detection process.

7.2.3 Strategy Timings

As previously stated, the trailing leg plays an important role in preventing slip-induced LOB. A good reaction to a slip perturbation of sufficient severity is characterised by rapidly pausing the forward swing motion of the trailing limb after its lift-off, reversing its direction, and landing the trailing foot posteriorly [45]. Consequently, the time it takes the subjects to reverse the trailing leg's swing motion direction may be connected to the time it takes to identify a slip perturbation. Martelli et al. [120] dubbed this variable reverse time and linked it to the time required by individuals to pick the best biomechanical reaction. They verified that the seniors had a greater reverse time than the younger subjects, although they presented similar spatial-temporal features of the rearward swing motion in response to the slip. As a consequence of

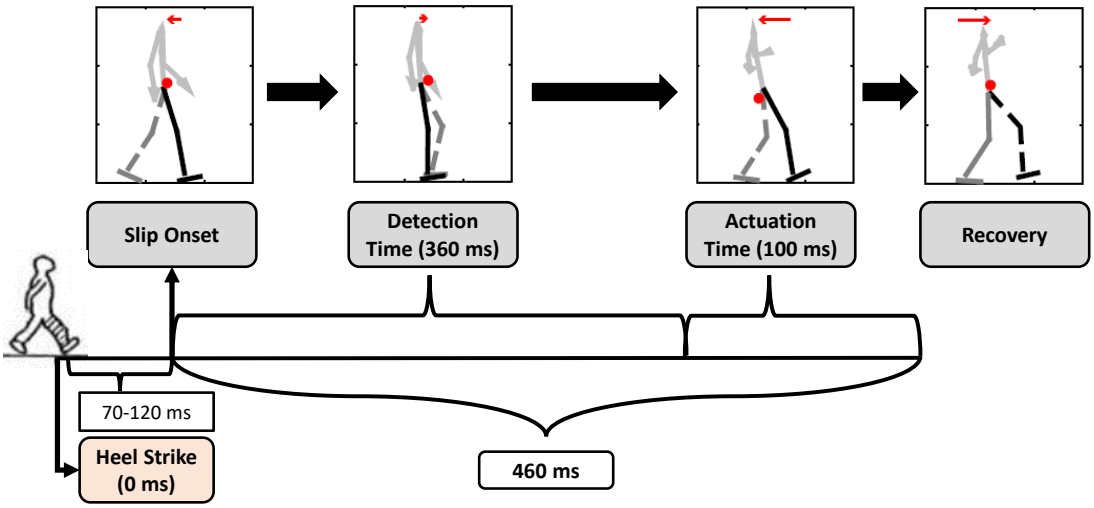

Figure 53: Proposed Fall Prevention strategy timings. The time durations are not to scale.

the provided results and the strategy's targeting of senior people, 360 ms was designated as the maximum time period required to notice the perturbations and thus the system must identify the perturbation before the subject [120]. This immediate identification of the disturbance would allow for the provision of early and appropriate mechanical assistance to assist people in regaining their balance before they are even aware of the perturbation. Furthermore, the actuation time, i.e., the maximum time required to complete the assistive actuation from the instant of perturbation detection, was set at 460 ms since Martelli et al. [347] discovered that the compensatory cycle caused by a slip perturbation lasted 0.46 ± 0.07 s from the moment the perturbation began to the moment the trailing foot landed on the ground. . Because this duration already included the mean time required by the subjects to identify the perturbation occurrence, 360 ms [120], the actuation time was defined as the time interval between the subjects' perturbation detection and the trailing foot striking on the ground. As an outcome, the actuation time was set to 100 ms. Moreover, Lockhart [105] said that hazardous slips that result in falls are most likely to occur between 70 and 120 ms following the HS. As such, the detection and actuation timings are applied after this time interval. Figure 53 summarises the established fall prevention method timings. Table 33 compares the timings provided for the present slip-related fall prevention strategy to the literature timings.

Table 33: Comparison between the timings proposed and the ones obtained for the literature fall prevention strategies analysed. N\A: not available.

Study	Detection time (ms)	Actuation time (ms)
Monaco et al. [40]	350	250
Mioskowska et al. [37]	100	N\A
Trkov et al. [81]	90	N\A
Current proposal	**360**	**100**

7.3 Methods & Materials

To accurately develop and test gait perturbation detection algorithms, it is necessary to acquire meaningful human motion data while dealing with gait perturbations. In order to extract the selected monitoring variables, i.e., knee angle and shank angular velocity in the motion direction, during normal and perturbed walking, a slip-like perturbation protocol was created and carried out. As a preliminary approach of the slip-related fall prevention strategy, older subjects were not enrolled and the PKO was not worn by the subjects during the experiments. However, an acceptable perturbation detection performance using healthy steady-state gait data is required. As a result, the protocol was created addressing some of the limitations mentioned in the scientific literature section 2.5: i) data from slip-like perturbations induced in both legs was collected to account for individuals' side-dominance; ii) one of the walking speeds used during the trials was customised for each subject. This enabled participants to recreate similar dynamic situations while dealing with slip-like perturbations; and iii) data was collected from a variety of sensors, including not only kinematic data but also physiological data. This enabled the creation of a dataset including huge amounts of sensor data, which could then be employed to extensively analyse the motion changes caused by slip-like perturbations. Furthermore, the slip-like perturbations were induced by pulling the participant's ankle anteriorly at the HS or posteriorly at the TO using a rope. Because slip-induced LOBs are primarily initiated during these gait events, they were chosen as the slip onset events. The rope pulling was done manually by an experienced operator.

7.3.1 Participants & Equipment

The experimental protocol included eleven healthy young individuals (age: 24.55 ± 2.15; height: 1.70 ± 0.09 m; weight: 63.25 ± 7.11 kg; males = 6; females = 5) that respected the following inclusion criteria: i) healthy locomotion; ii) total postural balance; iii) more than 18 years; and iv) body mass lower than 135 kg. Subjects were excluded in the following cases: i) presence of a disease or deficit that affects locomotion; and ii) were recently subjected to surgical procedures that affect mobility. All subjects willingly agreed to participate in the experimental studies after providing written informed consent. Each participant completed the Waterloo Footedness Questionnaire to make a qualitative assessment of their preferred foot [366]. To better understand the changes that slip perturbations introduce to human motion, data were collected from a variety of sensor systems, resulting in a massive dataset of kinematic and physiological data.Xsens MVN Awinda (Enschede, The Netherlands) and Optitrack V120 Trio (Corvallis, OR, USA) systems offer data on any changes in motion kinematic parameters that may occur. On the other hand, the remaining sensory systems collect physiological data, namely: i) Delsys Trigno (Natick, MA, USA) - muscles' electrical activity data; ii) RespiBAN (Lisbon, Portugal) - subject's respiration data; and iii) Shimmer GSR (Dublin, Ireland) - GSR and heart frequency rate. A Kinect v2.0 camera (Redmond, WA, USA) also provides video help for labelling occurrences.

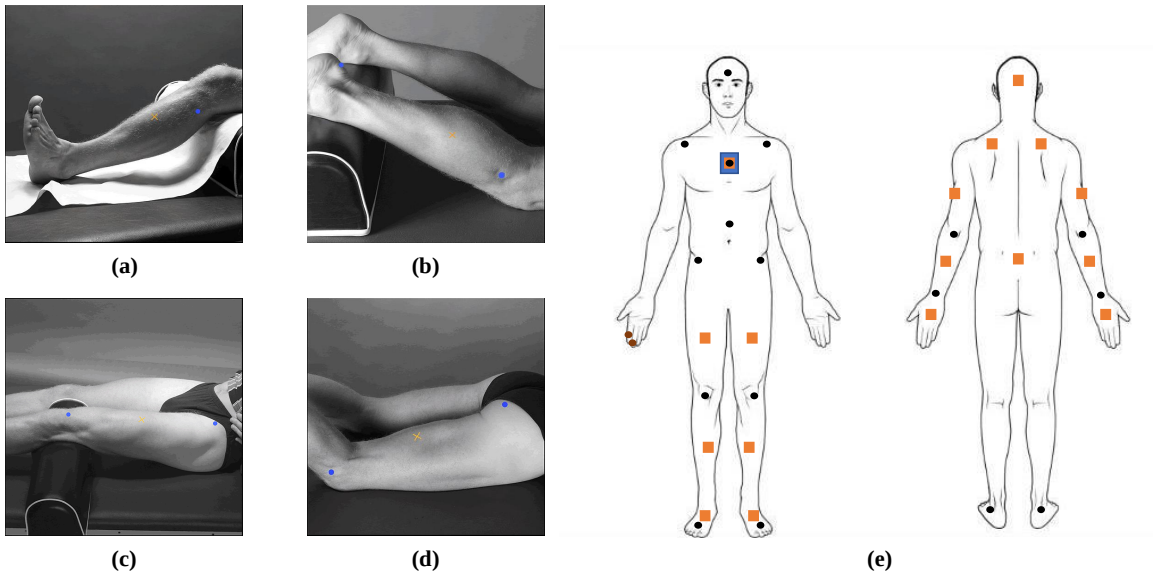

Figure 54: Muscles monitored by the EMG sensors, which were placed on the "x"marks highlighted in each of the 4 subfigures (a-d) and the remaining monitoring systems (e). (a) *Tibialis Anterior*. (b) *Gastrocnemius Lateralis*. (c) *Rectus Femoris*. (d) *Biceps Femoris*. The images were extracted from [367]. (e) Reflexive marker (black dots), IMU (orange squares), RespiBAN device (blue square) and Shimmer electrodes (brown dots) placement.

Subjects were first equipped with eight Delsys Trigno wearable sensors placed in the *Rectus Femoris*, *Biceps Femoris*, *Tibialis Anterior* and *Gastrocnemius Lateralis* muscles from both legs (Fig. 54.a-d), which gathered EMG data at 1111 Hz. To normalise the EMG envelope, this device requires a calibration method that consists of three trials of Maximum Voluntary Contraction (MVC) for each muscle. Participants were further outfitted with the full body configuration of Xsens MVN Awinda (17 IMU), which collected data at 60 Hz. The N-Pose calibration procedure followed the sensor placement. Based on previous research [368], reflexive markers were then implanted in the following bodily landmarks and tracked at 120 Hz by the Optitrack V120 Trio camera bar: i) head; ii) sternum; iii) midtrunk; iv) right and left shoulders; v) right and left elbows; vi) right and left wrists; vii) right and left hips; viii) right and left knees; ix) right and left heels; and x) right and left feet. To reduce noise on the cameras while monitoring the reflexive markers, any existing shiny surface from the subjects' clothing was removed. The video records from the experimental trials were provided by a Kinect camera operating at 30 frames per second. Finally, the RespiBAN system was worn on the upper trunk between the sternum and the Xiphoid process, and the Shimmer GSR device was worn on the dominant forearm with electrodes placed on the index and middle fingers. These devices gathered data at 1000 Hz and 100.21 Hz, respectively. Figure 54.e shows the locations of the wearable sensors used during this experiment. Thereafter, participants wore a safety harness device, which consisted of a vest tethered to a structure in the ceiling by a rope, to prevent irreversible slip-induced LOB from happening. For the subject's safety, the harness rope length was adjusted to register a minimum of 15 cm between the knees and the treadmill belt [158].

7.3.2 SyncLab: Synchronisation Framework

Synchronise data acquisition can be facilitated by the use of an appropriate framework. A logical and intuitive desktop application that allows fast connection with the intended systems, commercial and/or self-developed, represents an automatic and reliable way to ensure a more precise start and stop of data acquisition process. Thus, it is necessary to create an open-source application capable of providing synchronisation between several systems for users who just want to synchronise data in a faster and more intuitive way for their studies and applications. Considering this need, **SyncLab 2021** was created, a C# desktop application for *Windows OS* capable of synchronously start/stop recording and saving data in the computer that runs the app. It contains the following commercial devices, namely Xsens, Delsys Trigno, respiBan, Optitrack, Kinect V2, Shimmer GSR, and at least 3 self-developed systems (Fig. 55). This application only has two simple stages before start and stop recording: i) device selection stage - it displays a list of systems available for synchronisation; and ii) configuration and connection stage - it allows the configuration of some system settings and the serial and wireless connection between the application and the systems to start/stop data acquisition.

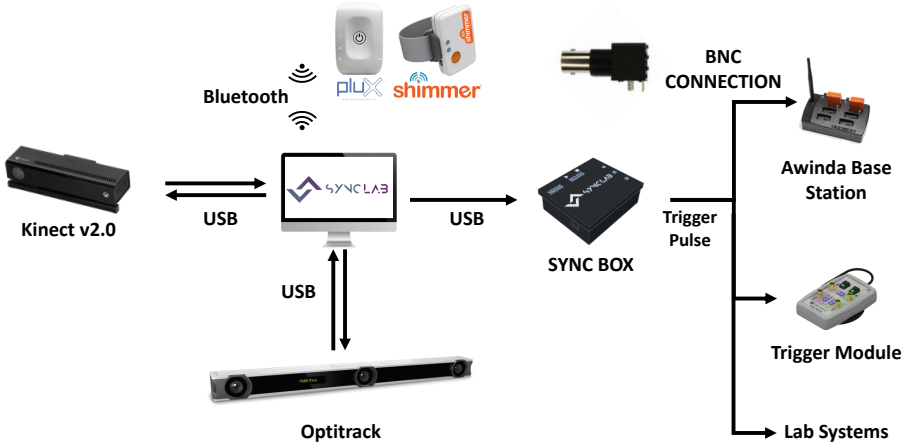

Figure 55: Schematic resuming SyncLab 2021 connections.

7.3.2.1 Software & Hardware Requirements

The open-source desktop application must fulfill the following main requirements based on the user and system needs: i) an easy and interactive way to select which systems will be used; ii) allow to configure the main settings for each system; iii) allow start and stop recording; iv) data collection with Xsens, Delsys Trigno and self-developed systems must be enabled or disabled by 5V trigger pulses (1kHz) through Bayonet Neill–Concelman (BNC) connectors (except for Xsens - 3.3V max.); v) Optitrack must be connected to the computer through USB and the Motive software must be open; vi) Optitrack start and stop commands must be implemented in the desktop app using the NatNet SDK; vii) Bluetooth communication with respiBAN and Shimmer GSR; and viii) the app must be connected and receive data from Kinect.

7.3.2.2 SyncLab 2021 Interface

Once the system requirements were defined, **SyncLab 2021** was designed and developed to fulfilled them. Each requirement has been evaluated and structured to be represented in the application with simplicity, so the user can easily and intuitively interact. When the application is initialized (Fig. 56.a), it is displayed: i) the user's experience level, where the users indicate their expertise on sensor systems as beginner (needs help during the configuration) or expert (needs no help); and ii) icons assigned to the different sensor systems such the users can select which sensors will be used. Upon system selection, the user press the forward button (available on the lower left corner) to reach the configuration panel (Fig. 56.b). It allows the user to correctly establish the connection and configure some systems. For instance, the application allows the user to change the sampling frequency of Optitrack and respiBAN, the record take name from Optitrack, and the folders to save the data when the user selects the Kinect V2 or the respiBAN. Only if the connection is established or the folder to save the data is chosen/created, the application allows the user to move forward onto the next and last panel, the record panel (Fig. 56.c). This last panel depicts: i) the Start/Stop Button - responsible to trigger the systems. Threads are created in cascade, i.e., one thread at a time to send start/stop commands; and ii) the Output Message List - responsible for giving feedback on start/stop data acquisition and alerts of synchronisation problems through text messages.

7.3.2.3 SyncBox

To trigger the data acquisition in Xsens, Delsys or other self-developed systems, **SyncBox** was developed. This equipment includes an STM32F303K8 that establishes a serial connection with the computer where the **SyncLab 2021** is, and 6 BNC female connectors. Both the processor and the connectors are on a PCB. For aesthetic reasons, 3D-printed box was modulated to place the hardware inside (Fig. 55). Based on information from **SyncLab 2021**, **SyncBox** sends the single pulse trigger to the appropriate BNC connectors, which are distributed as follows: i) one to Xsens Awinda Station; ii) two for Delsys Trigger Module (one to start and other to stop); and iii) three for self-developed systems. If the users need more trigger exits, they can use BNC T-adapters.

7.3.2.4 Synchronisation Assessment

The synchronisation times were evaluated by following a strict protocol that focus on answering the following questions: i) Does more systems to synchronise represent more delay time?; ii) How long does each system take to start or shut down? and iii) Does the distance between respiBAN and the computer influence synchronisation times? Thus, 100 starts and stops were performed for 2 to 4 connections (SyncBox, respiBAN, Optitrack, Kinect) and collected information about the time each system takes to start/stop data acquisition after clicking on the Start/Stop button, and the overall time of the recording operation. These commands are sent in cascade, i.e., one system at a time and with this assessment relevant

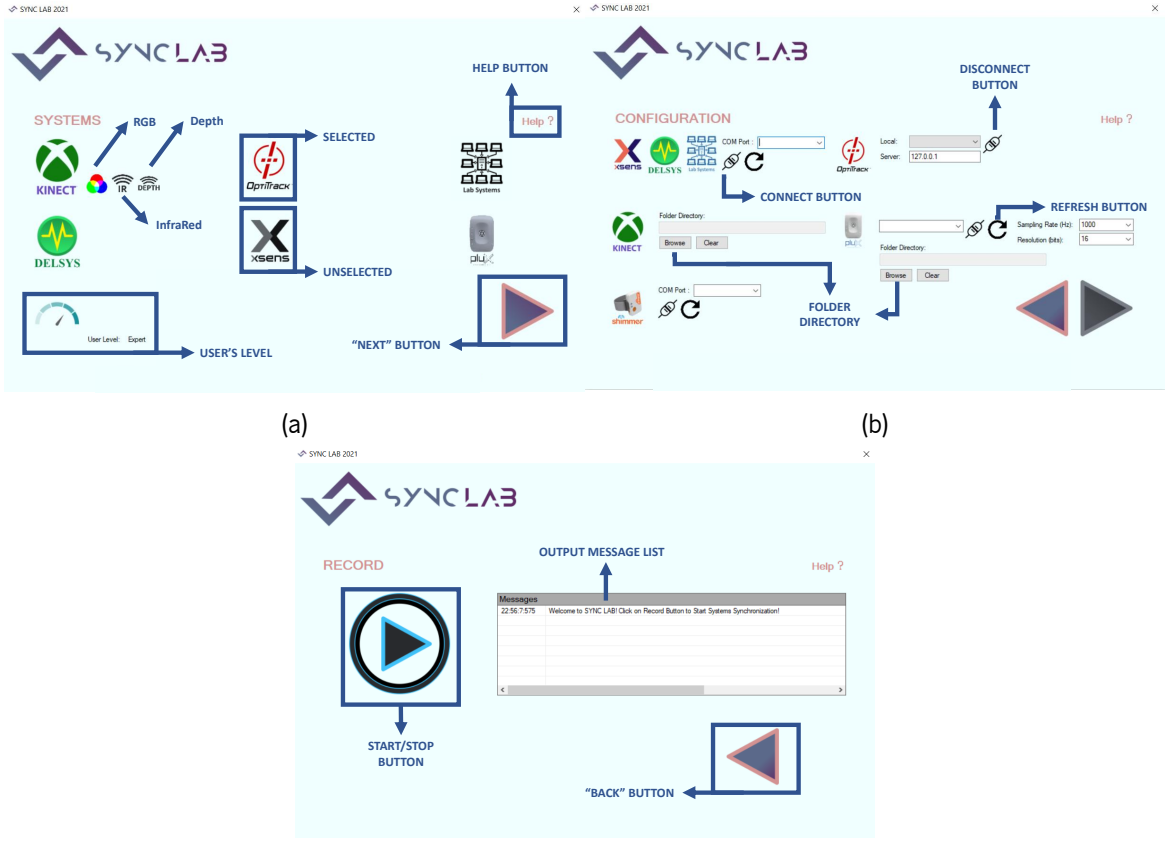

Figure 56: SyncLab 2021 App. (a) First Panel where users can interactively select the available systems. (b) Configuration Panel. (c) Record Panel.

information about the command order can improve the framework's performance. allows us to have a better idea of the framework's ability to synchronise systems and the order of activation and deactivation. The assessment process allows to establish an order in which the systems will receive the command, using the results presented on Table 34. With this information it is possible to minimise the overall time delay of the used set of systems to respond to the start/stop instructions. Results demonstrate that the lag between systems is generally lower than 10 ms (Table 34). Only with four devices the lag was 13.4±12.7 ms. It also appears that Kinect is the system that takes the longest time to respond to the command, specially when stop data acquisition (start: <3.0±2.9 ms; stop: <9.1±3.8 ms). The stop time is higher due to the time delay associated with the generation of an additional file that saves information about each frame captured. On the other hand, respiBAN presents the lowest times and the distance to the computer does not affect the synchronisation times (~0.1 ms). As soon as the wireless connection with respiBAN is established, it starts sending data to the computer. Thus, when the user presses the Start/Stop button, the framework requires only the time necessary to change a Boolean variable. In case of Start, the data is written to a file to be saved. Finally, the time taken to respond to commands by SyncBox (<2.4±2.2 ms) and Optitrack (<5.6±7.0 ms) raises with the increase of the number of devices used.

Table 34: Synchronisation times for each system and for each set during start and stop recording

Set[a]	*SyncBox*	*Opti.*	*Kin.*	respiBAN[b]		Total (ms)
Start Time (ms)						
1	0.7±0.9	0.2±0.4	-	-	-	1.0±1.0
2	0.8±3.4	0.4±0.6	3.0±2.9	-	-	4.3±4.7
3	2.4±2.2	4.4±3.8	1.2±1.8	Tot.	0.10±0.1	7.8±13.9
				1m	0.10±0.2	
				5m	0.10±0.1	
				8m	0.13±0.2	
Stop Time (ms)						
1	0.5±0.8	0.2±0.4	-	-	-	0.7±0.7
2	0.4±0.8	0.3±0.5	9.1±3.8	-	-	9.8±3.9
3	2.2±2.9	5.6±7.0	4.6±6.5	Tot.	0.10±0.2	13.4±12.7
				1m	0.12±0.1	
				5m	0.10±0.2	
				8m	0.10±0.1	

[a] 1:SyncBox+Optitrack; 2:1+Kinect; 3: 2+respiBAN. [b] Different distances to the computer (left) and time (right). CPU:i5-7300HQ; RAM:8GB.

7.3.3 Slip-like Perturbation Protocol

Participants were instructed to manage unanticipated slip-like perturbations during treadmill locomotion, being blind to the protocol to avoid any prior bias in their biomechanical response to the slip-like perturbations. As a result, subjects had no idea when, how, or how many times they would be disturbed. To begin, participants walked on the treadmill without slip-like perturbations while using the whole sensor setup for a familiarisation experiment. To avoid anticipating the commencement of a potential disturbance, subjects were told to fix their gaze on a spot at eye level while walking. During perturbation trials, a trained operator tugged a rope tied to the subjects' ankle during some HS and TO events, i.e., causing an instability comparable to a slip event. Throughout the trials, the rope was always tied to one of the participants' feet, thus they had no idea whether there would be a disruption or not. Each individual was put through eight trials (Table 35) that included every possible combination of disturbed leg (right or left), perturbed gait event (HS and TO), and treadmill belt inclination (0 and 10%). Six sub-trials were conducted inside each trial, where subjects walked at three distinct speeds (1.8 km/h, 5.4 km/h, and a normalised speed) and in two different settings (perturbation or non-perturbation). Normalised speed was estimated using a method based on the subject's leg length in order to reproduce equal dynamic circumstances across all participants. Scientific literature helped defining slow and fast gait speed values [279, 369, 370]. Normalised speed (v) was computed using the dynamic similarity principle, which is stated by the equation below:

$$v = \sqrt{F_r g L} \tag{2}$$

F_r is the Froude number (0.15); g is the gravity accelerations (9.81 m/s^2); and L is the leg length from the prominence of the greater trochanter external surface to the lateral malleolus [347]. The features of each of the six sub-trials are depicted in Table 36. To increase the unpredictability of the slip-like perturbations, these sub-trials were executed in a randomised order. The operator introduced three perturbations in random moments per perturbation trial. Non-perturbation trials lasted an average of 30 seconds, while perturbation trials lasted anything from 30 seconds to 1 minute.

Table 35: Trial's order organisation during the experimental protocol for data acquisition

Trial No.	Perturbed Leg	Perturbed Gait Event (%)	Treadmill Inclination (%)
1	Right	HS	0
2			10
3		TO	0
4			10
5	Left	HS	0
6			10
7		TO	0
8			10

Table 36: Characteristics of the 6 sub-trials performed within each trial

Velocity (km/h)	Perturbation?
1.8	✓
1.8	✗
v	✓
v	✗
5.4	✓
5.4	✗

7.3.4 Data Processing

After acquisition, data were processed using Matlab software to transform data from all of the sensors into a single Matlab table, which required some and varying stages depending on the sensory system and its features. Before Matlab, EMG data collected was normalised per muscle and per subject with the respective MVC information using the Delsys analysis software. Motive software was used to label Optitrack reflexive markers for each trial. Only some of the markers were labelled because some of them experienced frequent occlusions during the treadmill gait, namely: i) head; ii) sternum; iii) midtrunk; iv) right and left shoulders; and v) right and left hips. To create a video for each trial, the frames produced by the Kinect camera were aligned together using *Adobe Premiere Software*. After completing these processes, all data

were ready to be analysed in Matlab and downsampled to 60 Hz because Xsens had the lowest sampling frequency. Further, the timestamps of start and stop data recording provided by the SyncLab Desktop App were used to align data samples from the monitoring systems. This was especially important in RespiBAN and Shimmer GSR devices, which, since they are wireless, did not always start and finish data collection exactly at the same time as the other sensor systems. As a result, data obtained from the various sensors was aligned and had the same number of samples for each trial, allowing information to be concatenated into a single Matlab table. Now is the time to move on to the event labelling process. The events of interest are: i) start of a sub-trial: marked in the frame of the first HS of the foot being perturbed (with the rope) since the subject achieved steady walking during the sub-trial; ii) end of a sub-trial: marked in the frame of the last HS of the foot being perturbed in steady walking during the sub-trial; iii) perturbation onset: marked in the frame where the operator starts to pull the rope to perturb the participant's gait; and iv) end of the perturbation: marked in the frame of the first HS of the perturbed foot after the participant has recovered from the perturbation and regained steady walking. To help the labelling process, videos generated from the Kinect frames for each experiment were uploaded to *Djv software*, which can easily identify the frame number which an event occurred. Thus, it was possible to correlate the identified frame timestamps with data table timestamps from the same trial in order to indicate events because the Sync Lab Desktop App gave the timestamp associated with each Kinect frame. As a result of this labelling process, two columns were added to each trial data table. One column indicates the type of subtrial of the data samples and the other indicates if the data samples correspond to a perturbation or not.

7.3.5 Validation Strategy Proposal

This validation strategy will cover three key study issues for each selected variable: i) determine the best number of oscillators inside the CPG for monitoring reasons; ii) do the Normal Walking Testing; and iii) perform the Perturbed Walking Testing. The slip-like perturbation detection system was validated using data from the knee angle and shank angular velocity. Figure 57 depicts the validation scheme. The perturbation detection algorithm was evaluated for each selected variable using perturbation data from the perturbed and unperturbed legs. The validation strategy was used with data obtained from regular walking trials and perturbation delivery trials while individuals were ambulating on the treadmill with a 0% incline at a normalised speed computed for each subject. The locomotion settings evaluated for this investigation describe a level-ground walking scenario and a velocity that the individuals are likely to use in their daily lives. Hence, data from these conditions were included for analysis, as they are the most likely to occur prior to the occurrence of a real-life slip perturbation for the recruited individuals [337, 338]. Furthermore, according to the literature review, only perturbation trials in which slips were induced during the HS were examined, because this gait event is the most notable for the initiation of real-world slips [105]. As such, each individual had data from six trials: i) four regular walking trials, i.e., without perturbation; and ii) two

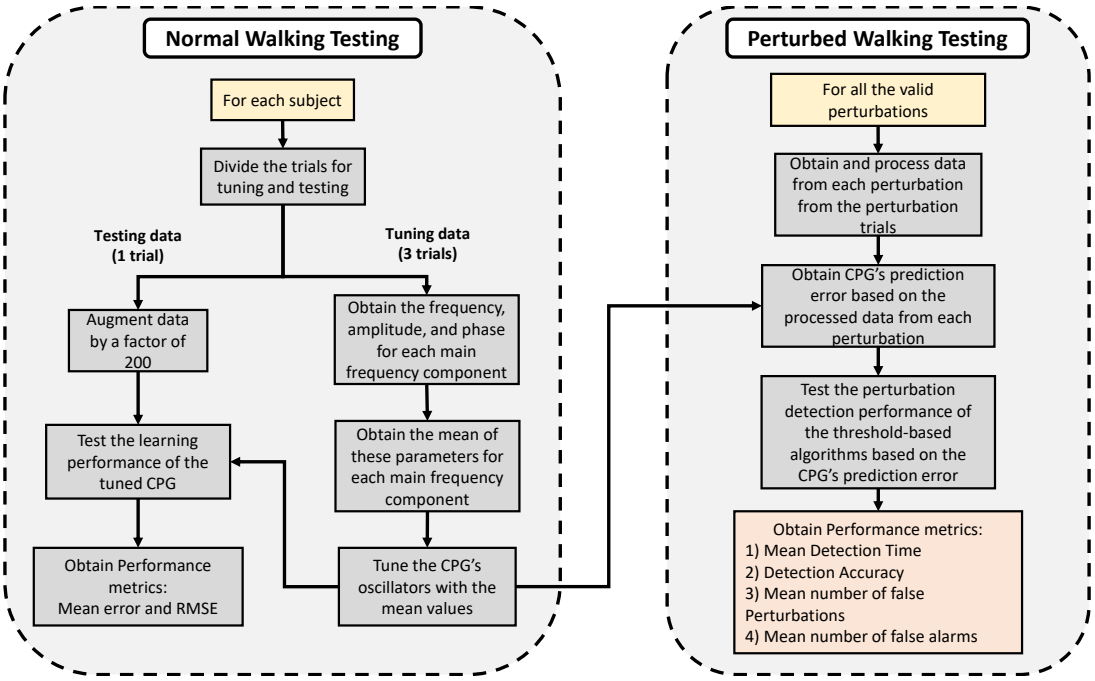

Figure 57: Schematic of the validation strategy for slip-like perturbation detection.

perturbation trials. However, owing to data loss, data from two participants could not be used. There were 23 legitimate slip-like perturbations which were then used to assess the performance. Initially, the collected data were jointly normalised within the interval between 0 and 1. Normalisation was used to adjust the amplitude changes of the kinematic signals to a shorter and equal interval while respecting and keeping the disparities between data from various trials. Data from 3 of the 4 normal walking trials were used to tune the oscillators inside the CPG. The remaining trial data was used to further evaluate the tuned CPG. Two CPG were adjusted and tested for each participant, one using knee angle data and the other with shank angular velocity data. The tuning data was decomposed using the Fourier frequency spectrum to produce the frequency, amplitude, and phase values associated with each relevant frequency component. After obtaining these parameters, the mean of each relevant frequency component was calculated in order to set the start conditions of the CPG's oscillators for each subject. Normal walking testing data were then augmented by a factor of 200 and fed into the adjusted CPG. This enabled the subject-specific adjusted CPG to be tested in tracking the steady-state walking profile of the specified variables. The use of such a large augmentation factor enabled to observe and investigate the CPG's response to input signals over extended time periods. The mean error metrics (Mean error and RMSE values) were used to evaluate the Normal Walking Testing performance across the specified variables. For each selected variable, data from each perturbation were further individually processed and further concatenated between normal walking data from the respective subject. This concatenation process allowed to obtain, for each valid perturbation, steady-state walking data before and after the slip-like perturbation occurrence. The CPG were subject-specifically calibrated during the Normal Walking Testing, allowing simulation data to be

obtained from the CPG's signal prediction when a slip-like perturbation occurred during steady walking. In this regard, for each perturbation, an error signal was generated between the CPG output and the real kinematic signal, which was then used by threshold-based algorithms to identify the perturbation beginning (Perturbed Walking Testing). The mean detection time, detection ACC of real perturbations, mean number of false perturbations detected per each real perturbation identified, and mean number of samples per false perturbation detected (false alarms) were used to assess the threshold-based algorithms' perturbation detection performance. The Matlab programme was used to execute all of the previously stated data processing, while the Simulink software was used to collect the simulation data.

7.4 Slip-like Perturbation Detection Results

7.4.1 Number of CPG Oscillators

The number of oscillators inside the respective CPG must be set in order to adjust the oscillator network according to the selected variables. The examination of the number of main frequency components required to correctly represent the signals of the selected variables allows for the optimal number of oscillators to track each variable. This saves on computational costs caused by the usage of an excessive number of oscillators. First, a spectrum analysis was done to identify the most important frequency components in each changing signal. Appendix D contains examples of regular knee angle and shank angular velocity signals, and their corresponding frequency spectrum. Moreover, two tables depict the first 6 frequency components of both variables highlighting the means of frequency, amplitude, and phase values. After the AFO were tuned with their respective initial parameters, the number of oscillators inside the CPG was altered across numerous simulations to determine the best number of oscillators to follow both variables. The relationship between the error metrics acquired during simulations (mean error and RMSE) and the time required for the last oscillator's frequency to converge (convergence time) was investigated. Tables 37 and 38 provide the results for knee angle and shank angular velocity, respectively. Considering the knee angle variable, this investigation (Table 37) indicates that a greater number of oscillators is usually associated with a decrease in error levels. The greater the number of AFO, which compensates for the incorporation of more frequency components from the variable, the better the approximation of the CPG output to the input signal and hence the lower the error produced. The CPG with three oscillators had the greatest error levels. Nonetheless, the difference in error across all CPG designs was not particularly obvious, as increasing the number of oscillators did not significantly lower the error caused. Regarding the shank angular velocity (Table 38), the largest and lowest error values were produced by CPG designs with three and six oscillators, respectively. However, increasing the number of oscillators did not result in a decrease in error values, since the CPG with 4 oscillators produced lower error values than the CPG with 5 oscillators. In fact, the difference in inaccuracy across CPG designs with 4, 5, and 6 oscillators was barely

Table 37: Performance results of knee angle monitoring for all the tested CPG configurations

Number of oscillators	RMSE	Convergence time (s)
3	0.0482 (0.0659)	instantaneous
4	0.0459 (0.0656)	1868
5	0.0407 (0.0607)	2506
6	0.0413 (0.0635)	5912

Table 38: Performance results of shank angular velocity monitoring for all the tested CPG configurations

Number of oscillators	RMSE	Convergence time (s)
3	0.0615 (0.0869)	instantaneous
4	0.0486 (0.0733)	instantaneous
5	0.0491 (0.0735)	Did not converge
6	0.0451 (0.0685)	5453

discernible. The RMSE values for the CPG with four oscillators (0.0733) and the CPG with six oscillators (0.0685) differed by just around 6.5%. Nonetheless, the RMSE difference between CPG setups with 3 and 4 oscillators was more noticeable, with the CPG with 3 oscillators being 15.7% higher. The results indicate that the fifth and sixth frequency components give insufficient extra useful information. The CPG with four oscillators looks to be the best choice for monitoring the shank angular velocity variable since it has the best relationship between the error metrics produced and the frequency convergence time.

7.4.2 Normal Walking Testing

To compare tracking performance for the knee angle and shank angular velocity variables, the mean error values from all individuals were averaged (Table 39). Only 9 participants were evaluated since data from two subjects could not be used. Although both variables gave a comparable mean RMSE, the average mean error for the shank angular velocity was somewhat shorter. Figures 80 and 81 (Appendix D) depict three different stages of the CPG's output signal (blue) adaptation to the steady-state signal (orange) for knee angle and shank angular velocity, respectively.

7.4.3 Threshold Algorithm Parameters Definition

The thresholds were applied 80 seconds after the simulation start since the error signal began to stabilise at this timing across all individuals. Although the frequencies were thought to achieve instantaneous convergence, as previously stated, the amplitude of the CPG output required longer to adapt to the input signal and so attain steady-state error levels. Then, a pair of upper and lower threshold values were obtained, in which no false perturbations were detected. A considerable variation from the usual gait, which might be caused by a perturbation, would cause the error signal to exceed one of the threshold values, allowing the

Table 39: Mean Error and RMSE values obtained during the normal walking testing using knee angle and shank angular velocity data

Subjects	Knee Angle		Shank Angular Velocity	
	Mean Error	RMSE	Mean Error	RMSE
1	0.0485	0.0664	0,0494	0,0746
2	0.0531	0.0714	0,0488	0,0716
3	0.0505	0.0676	0,0448	0,0676
4	0.0456	0.0605	0,0374	0,0587
5	0.0593	0.0853	0,043	0,0617
6	0.0493	0.0639	0,048	0,0718
7	0.063	0.0909	0,0395	0,0591
8	0.0458	0.0657	0,0583	0,0908
9	0.0523	0.0721	0,0553	0,0873
Mean	0.0519	0.0715	0.0472	0.0715

perturbation to be detected. For the fixed threshold algorithm, the upper and lower threshold values were defined as 0.3 and -0.35 for knee angle, and 0.35 and -0.27 for shank angular velocity (mean values). Additionally, the adaptive threshold-based algorithm was based on the variation of the standard deviation's (σ) multiplier factor and a time-window of previous samples (knee angle: 200 samples; shank angular velocity: 400 samples) to compute signal's mean (μ) and standard deviation (σ) [360]. The upper and lower threshold values were defined for knee angle as $\mu + 3\sigma$ and $\mu - 4.1\sigma$, respectively, while for shank angular velocity were $\mu + 4.4\sigma$ and $\mu - 4.8\sigma$. Comparisons of the threshold parameters indicate that the shank angular velocity signal was given higher absolute threshold values and window sizes than the knee angle variable. This might be because the shank angular velocity signal is more complex than the knee angle signal. As such, the increasing complexity of the shank angular velocity variable during simulations may have increased its respective inaccuracy between the real signal and the respective CPG prediction. In fact, the shank angular velocity variable required one extra oscillator, when compared to the knee angle variable, to achieve comparable RMSE values during the Normal Walking Testing simulations (Table 39). Furthermore, a larger window size was required for the shank angular velocity to accommodate for the signal's increased complexity and fluctuation during the threshold parameters computation.

7.4.4 Online Perturbation Detection

7.4.4.1 Knee Angle

Regarding to the use of knee angle data to detect the perturbations, Table 40 depicts the performances obtained for the fixed and adaptive threshold algorithms. Both threshold methods successfully detected real perturbations with ACC rates greater than 80%. However, a mean of 1.78 and 1.61 false perturbations

Table 40: Knee angle detection performance based on the type of threshold algorithm

Type of threshold	Mean Det. Time (s)	Detection ACC (%)	Mean Number of False Perturbations detected	Mean Number of False Alarms per false perturbation
Fixed	0.52	80.44	1.78	9.29
Adaptive	0.34	84.78	1.61	2.95

were discovered for each true perturbation successfully recognised for the fixed and adaptive thresholds, respectively. Although no false perturbation was discovered in some perturbed walking simulation data, others had a higher false perturbation detection rate, which raised the global mean of false perturbations. The fixed threshold got a significantly higher mean detection time than the adaptive threshold, with a 180 ms difference. Furthermore, the detection ACC was quite greater with the adaptive threshold, by roughly 4%. Furthermore, while the mean number of false perturbations detected by the fixed threshold algorithm was slightly higher, the mean number of samples of each false perturbation detected by the adaptive threshold algorithm (2.95) was significantly lower than that detected by the fixed threshold algorithm (9.29). This implies that after the adaptive threshold method discovered a false perturbation, it quickly ceased detecting it, within a mean of less than three samples. Overall, the adaptive threshold approach outperformed the fixed threshold technique in terms of perturbation detection.

Nonetheless, for each type of threshold technique, the individual detection performance of disturbed and unperturbed knee angle data was assessed, as shown in Table 41. This allowed to determine which leg's data had a more significant detection role. There were few variations in the usage of disturbed and unperturbed knee angle data for the fixed threshold. The altered knee angle data had a shorter mean detection time (by a mean difference of 25 ms) and a lower mean number of both erroneous perturbations identified and false alarms. However, the unperturbed knee angle data had a greater ACC (82.60%) than the perturbed knee angle data (78.30%). The adaptive threshold findings revealed a significant difference between the mean detection time values achieved. A mean duration of 250 ms was required to identify the perturbation beginning in the perturbed leg data, but a mean detection time of 419 ms was seen in the unperturbed leg data. Furthermore, the mean number of false perturbations discovered was significantly lower when utilising perturbed leg data. In fact, fewer than one false perturbation (0.65) was discovered on average for each true perturbation recognised, compared to the mean 2.565 false perturbations detected using data from the unperturbed leg. Furthermore, the mean number of samples associated with each

Table 41: Knee angle detection performance based on the type of leg and type of threshold algorithm

Type of threshold	Leg	Mean Det. Time (s)	Detection ACC (%)	Mean Number of False Perturbations detected	Mean Number of False Alarms per false perturbation
Fixed	Perturbed	0.51	78.26	1.70	8.51
	Unperturbed	0.53	82.61	1.87	10.00
Adaptive	Perturbed	0.25	78.26	0.65	2.60
	Unperturbed	0.42	91.30	2.57	3.03

erroneous perturbation identified (false alarms) was lower for the perturbed leg data (2.60) than for the unperturbed leg data (3.03). However, the ACC of 91.30% obtained with unperturbed leg data was higher than the 78.26% obtained with perturbed leg data. Thus, the adaptive threshold showed a general better perturbation detection performance than the fixed threshold. In contrast, the perturbed knee angle data presented an overall higher perturbation detection performance in comparison to the unperturbed leg data.

7.4.4.2 Shank Angular Velocity

Table 42 shows the performance of the fixed and adaptive threshold techniques for detecting perturbations using shank angular velocity data. The detection ACC of the real perturbations produced by both threshold techniques was less than 80%. Although the fixed threshold attained an overall ACC of 78.26%, the adaptive threshold achieved a much lower ACC of 56.52%. Nonetheless, for each true perturbation successfully recognised, a mean of 5.28 and 3.94 false perturbations were discovered for the fixed and adaptive thresholds, respectively. Despite the fact that no false perturbations were discovered for certain perturbed walking simulation data, some of these data had a greater false perturbation detection rate, resulting in an overall rise in the mean of false perturbations detected. The fixed threshold approach had a much larger mean detection time than the adaptive threshold, with a mean time difference of 192 ms. Furthermore, the fixed threshold algorithm recognised a much larger mean of both erroneous perturbations and related false alarms. This meant that once the adaptive threshold method discovered a false perturbation, it quickly ceased detecting it, within a mean of roughly 3 samples.

Furthermore, the performance of perturbation detection was tested between perturbed and unperturbed shank angular velocity data using the fixed and adaptive thresholds (Table 43). The unperturbed leg data allowed a better detection performance with a much lower mean detection time, significantly greater ACC, and a lower mean number of false perturbations identified per true perturbation detected when using the fixed threshold approach. Nonetheless, the perturbed leg had a lower mean number of false alarms per erroneous perturbation. When the results of the adaptive threshold algorithm were considered, the unperturbed leg data allowed the best performance. This is seen by the reduced mean detection time (266 ms) and substantially greater ACC (73.91%) attained in contrast to the adaptive threshold's mean detection time (486 ms) and ACC (39.13%). Using unperturbed leg data, however, was related with a larger number of false perturbations identified and a slightly higher number of false alarms per false perturbation.

Table 42: Shank angular velocity detection performance based on the type of threshold algorithm

Type of threshold	Mean Det. Time (s)	Detection ACC (%)	Mean Number of False Perturbations detected	Mean Number of False Alarms per false perturbation
Fixed	0.53	78.26	5.28	6.91
Adaptive	0.34	56.52	3.94	3.16

Table 43: Shank angular velocity detection performance based on the type of leg and type of threshold algorithm

Type of threshold	Leg	Mean Det. Time (s)	Detection ACC (%)	Mean Number of False Perturbations detected	Mean Number of False Alarms per false perturbation
Fixed	Perturbed	0.80	73.91	5.87	6.07
	Unperturbed	0.30	82.61	4.70	7.97
Adaptive	Perturbed	0.49	39.13	2.70	2.72
	Unperturbed	0.27	73.91	5.17	3.42

7.5 Conclusions

The studies on human biomechanical responses to slip perturbations reveal that both the leading and trailing legs play an important role in counteracting the slip perturbation. Despite the large number of articles that have examined the slip event and its repercussions on human motion, few slip-related fall prevention techniques have been developed. Thus, a slip-related fall prevention strategy was presented based on the limitations and information available in the scientific literature.

In order to minimise the complexity of the actuation to only the principal joint that counteracts slip-induced LOB, the actuation stage examined the assistive torque supply on a single leg adopting a single assistive device, an orthosis. The strategy emphasised the need of providing a knee flexion moment to the leading leg, which is considered the dominant limb, in the event of a slip-induced LOB caused by a HS. To counteract the slip, the amplitude of the assistive knee flexor torque must be complimentary to the torque created by the subject's knee.

The detection stage addressed the appealing qualities associated with biologically-inspired CPG controllers for monitoring quasi-periodic variables of human locomotion and assisting in the timely identification of gait perturbations. Because CPG do not recognise the irregular patterns presented by the disturbance, the introduction of a perturbation rapidly increases the inaccuracy caused between the monitoring signal and the signal anticipated by the CPG. Simple threshold-based algorithms can then detect the commencement of the perturbation based on the increase in the error signal. In light of the choice criteria used, the knee angle and shank angular velocity variables were chosen as the best kinematic variables for detecting slip-induced LOB. Furthermore, the determination of timings and conditions to be met for both stages based on scientific literature allowed for the conceptualisation of a fall prevention strategy that avoids slip-initiated falls in a timely and effective manner.

Considering the literature evidence found, an experimental protocol was designed in order to collect data from healthy young subjects while dealing with unexpected slip-like perturbations during treadmill walking. This allowed to obtain a vast dataset with kinematic and physiological information concerning subjects' reactions to slip-induced LOB events. Some kinematic features obtained were used for the further perturbation detection algorithm analysis. A novel open-software solution was presented, SyncLab 2021, allowing to sync various systems widely used for human motion analysis, through trigger signals. The

results showed an average delay between systems of few milliseconds, which introduces a significant contribution to easily and intuitively acquire synchronous data from different sensing devices. This software allowed the construction of a more reliable dataset in terms of synchronisation.

CPG with 3 and 4 oscillators were assigned to the knee angle and shank angular velocity variables, respectively, based on a trade-off analysis between the frequency convergence times and the mean error values obtained throughout the simulations. Overall, the CPG configurations chosen based on the preceding research produced output signals with similar shape and phase to the signals from the specified kinematic variables. In terms of perturbation detection, the performance was assessed by taking into account the various combinations of the two kinematic variables chosen, two lower limbs (perturbed and unperturbed), and two types of threshold methods (fixed and adaptive threshold algorithms). In general, the adaptive threshold algorithm performed better than the fixed threshold algorithm. The monitoring of the perturbed leg's knee angle using the adaptive threshold technique resulted in the best overall performance. This combination produced real perturbation detection ACC close to 80% (78.26%), a mean detection time of 250 ms, and a mean number of 0.65 false perturbations identified for each accurate perturbation detected. These findings demonstrated that the perturbation detection method applied performed satisfactorily in terms of detection requirements. However, in order to attain peak performance, the average number of false perturbations identified must be decreased even more.

Chapter 8

Virtual Reality to Provoke Imbalance

State of the art pointed out a lack of datasets regarding real-world falls [19, 371]. Thus, this chapter's aim is to establish a realistic VE with different fall-related visual perturbations capable of disrupting the user's equilibrium, envisioning a future training rehabilitation tool. To answer the proposed RQ5 in Chapter 1, relevant human motion data were collected while coping with visual perturbations induced by a HMD. Therefore, an experimental protocol was designed and conducted to extract relevant information from kinematic and physiological sensors. Data gathering on compensatory reactions when coping with visual disturbances is useful in balance control analysis, the creation of balance training procedures, and, most significantly, combining data from numerous sensors into a big and multivariate dataset. Innovatively, while the occasional use of visual perturbations speeds up the gathering of data about imbalanced circumstances, their ongoing usage encourages the training of postural reactions, contributing significantly for biomechanical studies on how to deal with falls or imbalances. Given the volume of data obtained and the observed disparities in kinematic reactions in the presence of perturbations, statistical analysis was applied by using ANOVAs to investigate the effect of visual perturbations on creating imbalances during gait. Furthermore, the purpose was not to discover gait abnormalities, but rather to determine whether the visual disturbance was an efficient way to create gait variability, which implies imbalance.

8.1 Introductory Insight

Due to the low frequency of natural falls occurrence and the inherent difficulties in collecting biomechanical and physiological data in a non-obstructive and user-friendly way in community-dwelling older adults, the scientific literature shows a lack of public datasets of real-world falls [31–33]. Immersive VR environments with the concepts of **place illusion** and **plausibility illusion** create a medium in which people respond

with their whole body, treating what they perceive as real [372]. As evidenced in section 2.6 of the state of the art, it is thus possible to accelerate the process of collecting data of postural reactions that occur after visual disturbances. The proprioceptive, vestibular, and visual systems all work together to keep the human being aware of its environment, allowing the response to present situations and plan for future changes. Balance control is a complex skill made up of these three subsystems. Immersive VR radically alters how the surroundings are seen, leading to a LOB on its own [216]. Additionally, HMDs are responsible for presenting tricky scenarios endowed with the mentioned concepts of **place** and **plausibility illusions** while increasing the immersiveness of the whole virtual experience [373].

Because of the unique immersive properties of VR, motor rehabilitation is also one of the health fields that is rapidly advancing and has various benefits when integrated with VR systems [374–376]. There are various reasons why training with VR is of greater interest and produces better outcomes in motor learning [377–379]. Repetitive practise, feedback (proprioceptive and exteroceptive), and motivation are the basic principles of motor rehabilitation that may be enhanced with the use of VR [380, 381]. The benefit of repetitive practise in motor learning, which translate into changes in the cerebral cortex, do not occur simply via huge practise. There must be a specified task or target, which the patient must attain through trial and error [381], getting feedback on their performance [382]. Motivation and dedication are required for a repetitive task, which are two common characteristics of a VR user experience [383]. Feedback in VEs can be supplied in real-time in a highly intuitive manner or recognised immediately following a training block. It has been demonstrated that it results in changes in the amount of cortical plasticity and subcortical cells and synaptic connections [384, 385]. However, repetition alone is insufficient to cause changes in the motor cortex associated with motor learning. Increasing a member's frequency of usage does not result in substantial changes. It is vital to do skilled limb motions [386]. Humans may learn motor abilities in a VE and then transfer those skills to a real-world context [387].

Inducing balance disturbances through audiovisual stimuli to impose changes in postural control is the core action point of this chapter, attempting to mimic realistic falls even before performing rehabilitation training. Despite the fact that VR has a wide range of applications and might lead to imbalances while also helping with training recovery as mentioned, the work developed during this PhD thesis essentially focused on developing a **realistic VE endowed with high ecological validity and resembling a home-living scenario** [206, 388] that could trigger postural responses. Scientific literature that used VR headsets and simultaneously introduced visual perturbations (Section 2.6) also found a propensity for each study to solely use one type of perturbation [164, 177, 192]. This might limit the range of compensatory reactions [389, 390]. For this reason, this chapter suggests a wide range of visual disturbances to be given in the VE. These postural reactions induced by imposing a conflict between the visual and proprioceptive systems, are going to be recorded and analysed to cover the gap in existing data regarding real falls. These postural reactivity patterns to visual disturbances are recorded using inertial sensors as a motion tracking system, capturing biomechanical and kinematic data, as well as physiological data such as EMG and

GSR to record muscle and electrodermal activity signals. Moreover, this early study's analysis will make it possible to reduce the amount of visual disturbances that will be included in a future rehabilitation tool.

Thus, this chapter aims to answer the following questions: i) Can a HMD introduce imbalances through visual perturbations?; ii) Can they cause postural reactions typical of a fall?; iii) Which visual perturbation challenged the participants' balance the most?; iv) Which virtual situation placed the participant over the most anxiety?; and v) What influence does the real-time representation of the avatar have in situations of virtual heights? The answers to the first and second questions will be revealed through statistical analysis. Both questions are validated if statistical relevance that distinguishes representative parameters of postural imbalance in gait between undisturbed and disturbed conditions is discovered. In addition, a qualitative comparison will be done between the parameters gathered in this study and those described in studies involving physical disorders. If this comparison reveals parallels, the original question's validity is strengthened. Considering the third question, this study filters the visual perturbations by looking into the most effective perturbations considering the statistical analysis outcomes. This is due to the fact that different visual perturbations will cause distinct postural reactions with variable intensities, activating muscles differently. Moreover,no scientific paper, to the best of our knowledge, has addressed this problem, and a future rehabilitation tool could use this knowledge for a more personalised intervention. Fourth and fifth questions work on anxiety and stress. Using the electrodermal data, one can first identify the events that put the person under stress and connect this state with a deterioration in balance ability. It also provides information about the perceived reality of the VE. Finally, the role of the avatar in stressful conditions is an understudied issue in the literature. Perhaps due to a paucity of studies incorporating the avatar in real time. The answer to this issue will be offered by contrasting vertigo circumstances in which the participant can see their own body and those in which they cannot. If there is statistical significance between these two situations, one can respond whether or not the avatar plays a part in maintaining balance.

Figure 58 outlines the chapter's organisation. The VE as well as the automatic method of adding perturbations are firstly scrutinised. A visual perturbation-based protocol for multimodal data collecting is also discussed, after which the data processing and statistical analysis are detailed. The results of this screening can be used to: i) fine-tune perturbation training and use only the disturbances that are most effective; and ii) extract patterns of kinematic and muscle reactions of interest to do exposure training on particular muscles or compensatory movements, causing an impact on the prevention of falls.

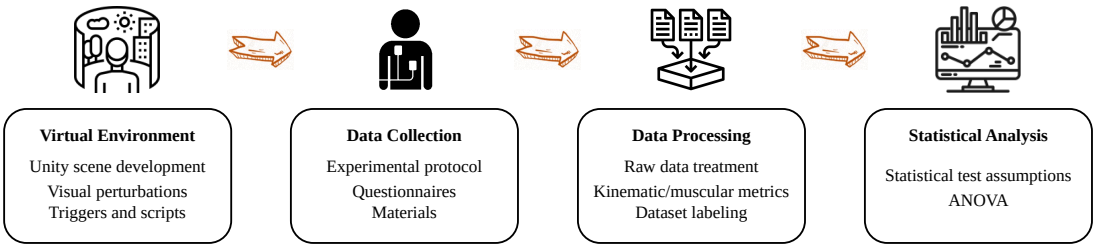

Figure 58: Set of processes implemented within the scope of this work.

8.2 Virtual Environment Design

It is essential to begin by establishing a few requisites that the VE must abide by. A reasonable compromise must be struck between stringent experimental protocols and the addition of naturalistic, dynamic, and contextually embedded stimuli if the objective of future research is to make predictions about real-world fall occurrences [388]. To improve the participant's experience, VE mix appealing surroundings with experimental measurement control. Real-world information differs from laboratory simulated data in three distinct ways, according to Zaki and Ochsner [388]: i) cues are multimodal; ii) they include visual, semantic, and prosodic information; and iii) it is dynamic in the sense that information is presented serially or concurrently. It is embedded in a context that can influence the interpretation of the study. Moreover, some studies in the neuroscience field use uncomplicated stimuli and miss crucial facets of real-world activities and interactions [391].

It is possible to combine laboratory control with ADL by using HMDs to offer virtual settings that digitally mimic real-world tasks [392]. Today, effective administration, stimulus presentation, and computerised logging of participant responses are all made possible by current computational capabilities. Background narratives engage participants and improve the experience since VEs enable experimental control and dynamic stimulus presentation in ecologically realistic settings [393]. Technology advancements that assist in immersing the user in convincing, lifelike sensory illusions are closely related to the future of VR in neuroscience [214]. Verisimilitude, or how closely the test conditions mirror ADL, is one of the criteria for ecological validity, according to Franzen and Wilhelm [394]. Ecological validity describes experimental conditions that are essentially representative of the real world. Compared to environments that merely contain the necessary and sufficient features for an experiment, contextually rich simulations with diverse sensory inputs may be thought to have more ecological validity in VEs [206]. The creation of a VE as close to reality as possible was then the priority of this work to achieve ecological validity and thus ensure: i) transfer of motor skills to the real world and ii) compensatory reactions to perturbation as natural as possible.

It is possible to better investigate human-environment interactions by doing it in a controlled environment by placing individuals in an environment that enhances their presence [395]. Neo et al. [396] have made significant observations about the degree of realism needed in a VE to study human behaviour. The requirement for realistic details and textures must first be assessed. They then emphasise the necessity of context for existence, i.e., the antithesis of an abstract world. Other crucial elements to elicit the most authentic responses from participants are the real-time display of the participant's avatar, ongoing positional tracking of head movement, and sensory input. Only the equipment's rendering capabilities will serve as a limit on how realistic the VE can be made.

The VE was created using Unity 2020.3.2f1 programme [397]. The game engine and Integrated Development Environment (IDE) Unity, often known as Unity3D, was used to create interactive media, most

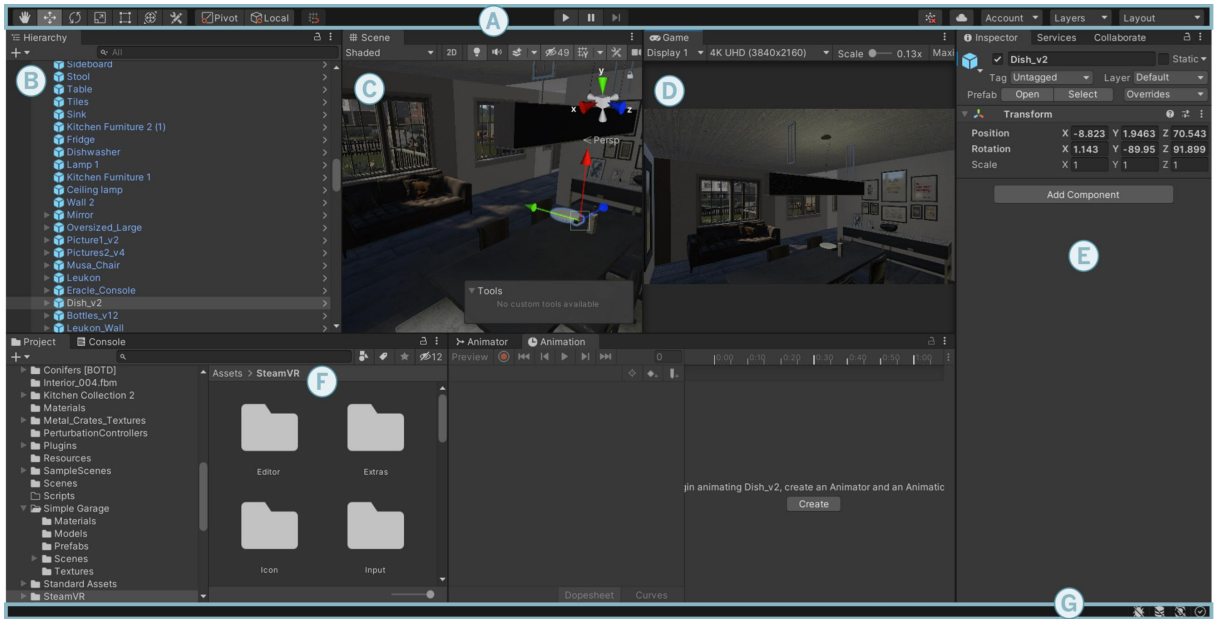

Figure 59: The workspace layout is organised into two main windows for previewing the environment visually, two bars, and three important tabs: A - Toolbar; B - Hierarchy window; C - Scene View; D - Game Preview; E - Inspector; F - Project Window; G - Status Bar.

often video games. The speed with which Unity can prototype is well known. Due to its native C# programming language, which should be familiar to all developers, and its general workspace structure, users generally found Unity to be slightly easier to use than Unreal Engine. With a somewhat steeper learning curve than Unreal Engine, it is a more approachable platform to begin producing on [398]. Figure 59 shows the Unity IDE's default view. The VE structure follows the assumptions that were proposed earlier to elicit natural responses from the participants. A typical suburban block served as the starting point for the base of the VE. The VE was created to be as realistic and comfortable as possible to improve participation. It consists of two fully furnished houses, a suburban block that includes the roads and its integral units, such as parked cars, pavements, and accesses to the houses. The two distinct houses are organised into rooms just as they exist in the real world. These rooms include a kitchen, a living room, two bedrooms, a bathroom, an outdoor area with a pool and garden, and the commuting areas such as hallways and stairs. The created house rooms are depicted in screenshots in Fig. 60. Reproductions of the divisions can be further found throughout the chapter. Additionally, Xsens will enable the real-time representation of a real-time body avatar that is embedded with head motion throughout the immersion, adding sensory input with physical aspects in the real environment.

8.3 Visual perturbations

The most important decision in this VR perturbation-based solution was the selection and implementation of visual perturbations to be used. Once the purpose of the visual perturbations is to produce a postural

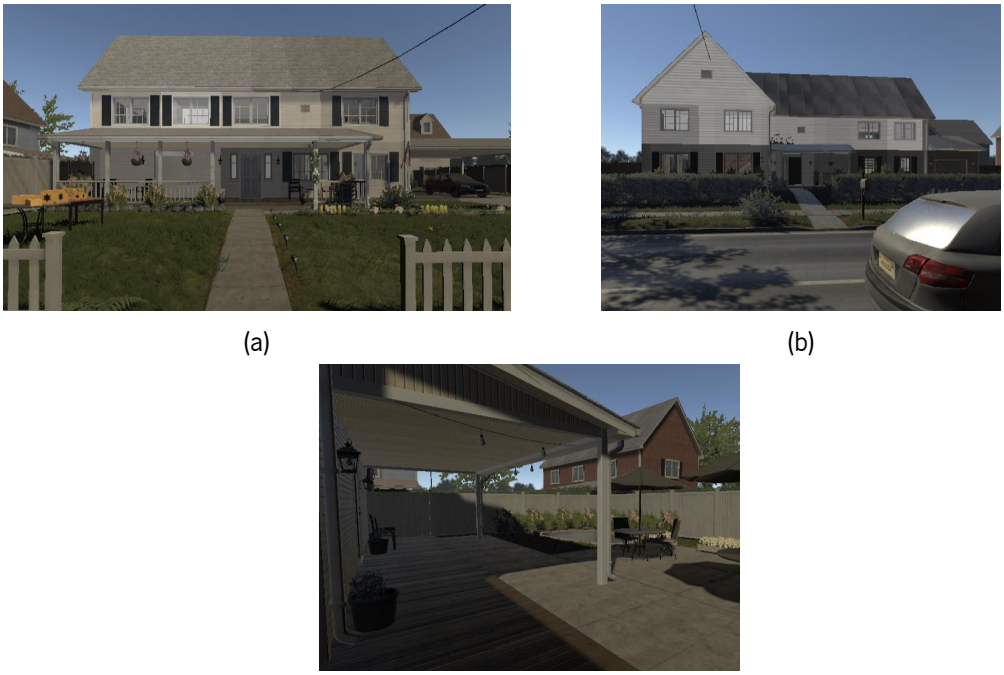

(a) (b)

(c)

Figure 60: Snapshots from the VE. Representations of exterior views of houses. (a) House 1. (b) House 2. (c) House 1 backyard.

reaction as close to a real-world fall as possible, they must elicit all fall categories during normal walking at this stage of the study, i.e., backward, forward and lateral falls, slip, trip, and syncope, as shown in Table 44. This information was obtained from the state of the art (Section 2.6), which enables multiple comparisons at the statistical level. Scientific literature categorises the visual perturbations into: i) translations or rotations on one or several axes simultaneously [164, 171, 172, 174–177, 185, 186]; ii) changes in proprioceptive feedback [168, 179, 190, 197]; iii) visuomotor disturbance introduction [162, 169, 173];

Table 44: List of visual perturbations and corresponding fall categories

Visual Perturbation	**Fall category**
Roll Rotation / ML Translation	Lateral
Object Avoidance	Lateral/Forward/Backward
AP Translation Forward/Backward	Forward/Backward
Pitch Rotation	Slip
Virtual/Real Object	Trip
Vertigo	Fall from heights
RPY Rotation	Syncope

iv) visual field oscillations [30]; and v) predefined trajectories object movement [184, 194]. This categorisation serves to support the choices of the visual perturbations conceptualised, allowing data collection of data that best approximates to an occurrence of these types of falls. The following subsections go into greater detail on the relationships between the type of visual disturbance and the type of fall.

8.3.1 Axis Rotations

The rotation direction for these visual perturbations was expressed using Euler angles. The roll, pitch and yaw angles are formed in three directions in Euler angle notation. A roll perturbation is defined as a rotation about the AP-axis or the coronal plane. A pitch disturbance is caused by a rotation about the ML-axis, which is the same as rotating the sagittal plane. Similarly, rotation about the V-axis would cause a yaw disturbance. Figure 61 specifies the notations used for translations and rotations in the human body's anatomical planes.

Roll rotation is designed to represent a swing from left to right or vice versa in the human body. Bugnariu and Fung [186] use this form of visual disturbance in conjunction with a physical disturbance that is concordant or discordant in vestibular sensory levels. The amplitude of the perturbation used by this author was 8° with a speed of 36 °/s. The stimulus was delivered in each direction independently. This type of rotation was also used by Peterson and Ferris [177] while the subject was attempting to balance by walking on a beam (Fig. 62). This perturbation had a 20° amplitude and a half-second duration. The direction was chosen at random, either Clockwise (CW) or Counter-Clockwise (CCW). Riem et al. [171] applied a roll perturbation in the form of a pseudo random sinusoidal stimulus. The perturbation had

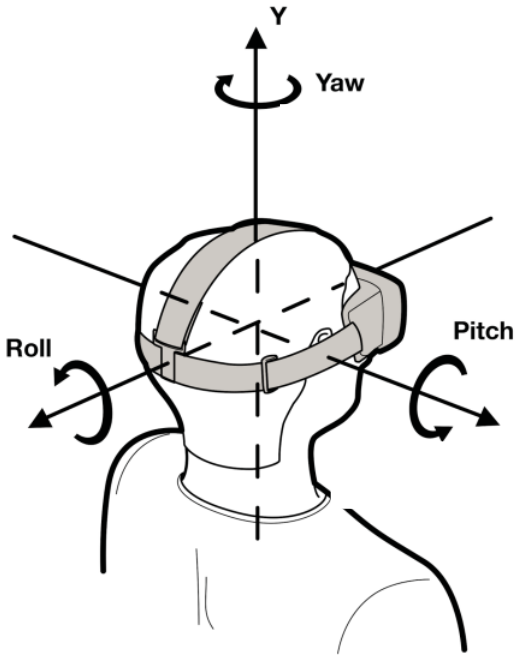

Figure 61: Notation of Roll, Pitch and Yaw angles used for visual perturbations.

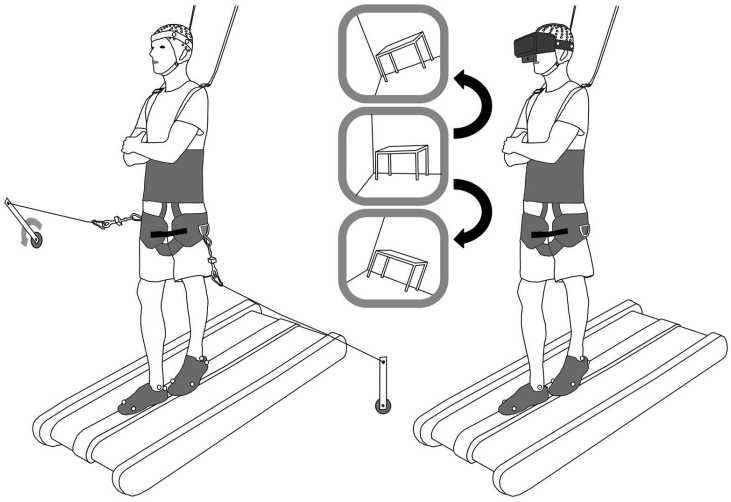

Figure 62: Subject walking on the beam, exposed to pull (left) and visual rotation (right) perturbations. Inset sketches show example 20 degree perturbations in CCW (top) and CW (bottom) directions [177].

three different intensities: 3°, 6°, and 11°. Based on the previous mentioned investigations, Roll-based visual perturbation was used in the created VE along with two directions of rotation (CW and CCW) and three distinct amplitudes (10°/s, 20°/s and 30°/s). Figure 63 exemplifies a CCW with 30°/s. As indicated in the first two entries of Table 45, the rotation speed is constant. These amplitude values were not exactly the same as those found in the literature. Because the literature is lacking in justifying the selection of this type of values, the chosen ones are near and rounded to the tenth, which simplifies the analysis.

Pitch perturbations are also used by Bugnariu and Fung [186]. The intensity and speed are the same. Liu et al. [174] and Parijat et al. [175, 176] performed efforts to address or induce slips virtually. They accomplished this by using a visual perturbation that tilted the VE by 25° at a rate of 60°/s. This perturbation was introduced at the right foot's heel contact. Considering these studies, the VE includes a pitch disturbance with the same conditions (25°; 60°/s) (Fig. 64).

Figure 63: The optical flow undergoes a CCW rotation of 30°/s around AP-axis.

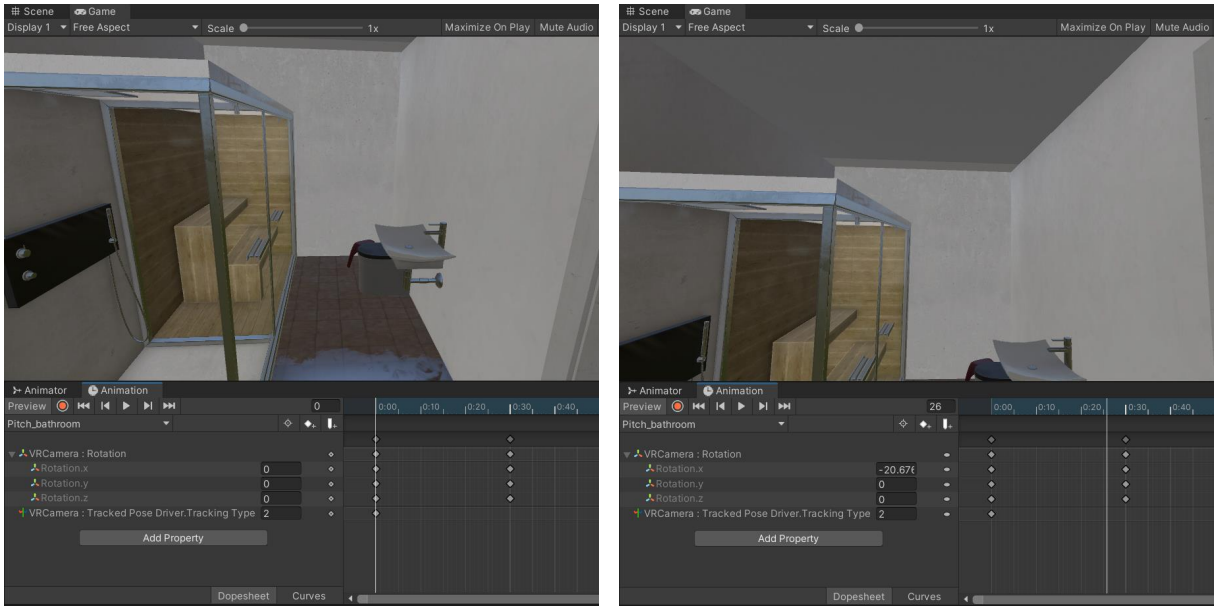

Figure 64: Animation of the pitch rotation. The example in the figure is depicted in one of the places that this disturbance can occur, in a bathroom. This animation is intended to simulate a slip.

Two studies used the visual perturbation around the V-axis, i.e., the yaw perturbation. While the individual walks forward. This perturbation progressively shifts the focus of vision to the left or right over a range of 40°. The purpose of this disturbance was to demonstrate the subjects' response when compelled to glance away from the direction of walking. In these studies [166, 167], the elderly exhibited irregularities in their gait trajectory, whereas the young individuals were able to down-regulate the visual information. Because the participants in this preliminary tests are all healthy young adults, this form of disturbance was not created.

So far, the research reported has only looked at the effect of one rotation. The visual disturbance, on the other hand, can comprise rotations in all three axes at the same time. Three studies [180, 191, 399] look at the risk of falling in patients with bilateral vestibular loss by performing rotations simultaneously. Each axis' velocities were independent and guided by a pseudo random sum of sines. This visual perturbation is related to the syncope event before fall. Syncope or fainting is a temporary loss of consciousness usually related to insufficient blood flow to the brain. This particular event and falls are two prevalent and interconnected geriatric syndromes that cause significant mortality and morbidity among the elderly. These studies inspired the creation of a disturbance that rotated the participant's field of view on all three axes. This disruption is caused by getting up from a physically present chair. The participant is virtually sitting on a bed and must get up. As the participant stands up, he or she experiences a disturbance that mimics a fainting spell or a dip in blood pressure. The amplitude values for each axis were determined base on the work of Chiavorano et al. [180] that used a sum of sinusoids. Figure 65 shows the participant's point of view in the room.

Figure 65: The participant is sitting on a bed with this viewpoint, is instructed to stand up, and undergoes the perturbation that rotates the camera in the three axes.

8.3.2 ML-Axis Translation

Visual perturbations consisting of translations in the ML axis are meant to simulate a physical disturbance that pulls or pushes the body to the left or right mimicking lateral falls. Guzman et al. [164] recreated a school corridor and used continuous oscillations in the ML axis to produce foreground movement, whereas Riem et al. [172] uses discrete shifts with a speed of 1 m/s in the same axis. The participant is standing on a bridge with a pole as a visual aid. The participant viewpoint and virtual position are moved to the left or right, kept for 9 seconds, and then returned to the original viewpoint in the middle of the bridge for one second. Dennison and D'Zmura [185] built a VE that imitated a space station with lengthy corridors. While freely exploring the hallways, a visual disturbance would occur every 2s for 260 ms and pull the participant's body to the left or right. These directions were estimated in relation to the participant's gaze direction. Visual perturbations that pull the participant's body forward or backward are also used in this work. This sort of disturbance is classified as ML-axis translations. With the help of the literature, it was generated a visual perturbation consisting of a bidirectionally moving floor at 1 m/s while the avatar was in the area of the perturbation. Figure 66 depicts the virtual configuration implemented.

8.3.3 AP-Axis Translation

This form of translation is also used by Denison and D'Zmura [185]. These visual disturbances give the subject the sense of being pulled or pushed, imitating a backward or forward fall. Santoso and Philips

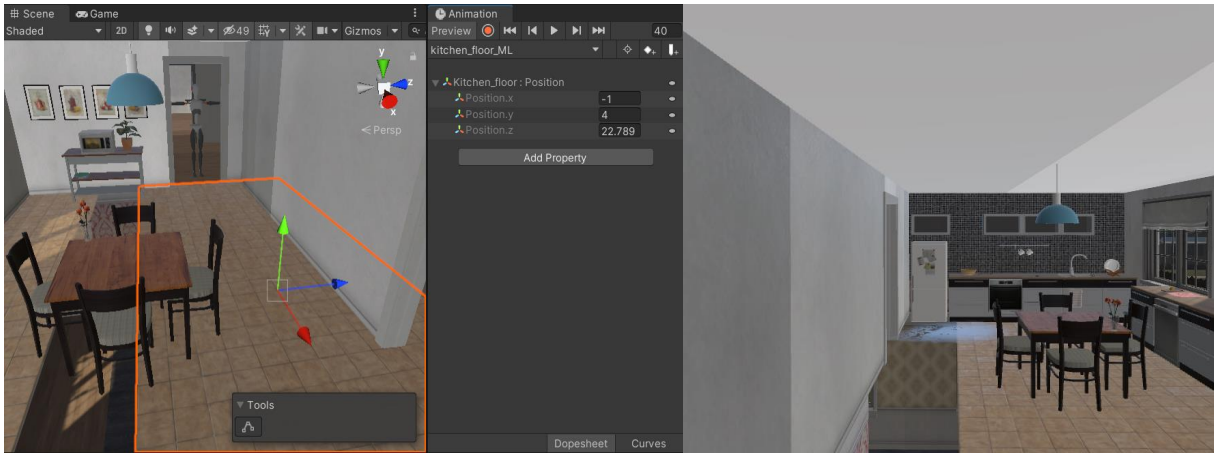

Figure 66: ML floor translation, continuous and bi-directional.

[192] employed the same visual disturbance by abruptly shifting a hallway for three metres in both directions at three different speeds. The axis is positioned in the participant's eye, which is inside a virtual tunnel. The disruption occurs in peripheral vision and is a sum of sinusoids, implying that it is continuous, causing the participant to move forward and backward on the AP axis. Considered the created VE, AP-axis translations in a corridor were the two perturbations devised to cover this type of backward or forward falls. These translations take place in distinct places (a corridor and inside of a bedroom), but they both have a translation speed of 1m/s for 3 seconds and are not bidirectional: one forward, one backward. Figure 67 depicts the VE corridor that will serve as a way for one of these perturbations.

8.3.4 Predefined Trajectories

Programmed trajectories of virtual objects or movements of the background can also be considered a visual perturbation. The participant's point of view is not abruptly altered in this sort of visual disruption. However,

Figure 67: AP-axis Translation Corridor.

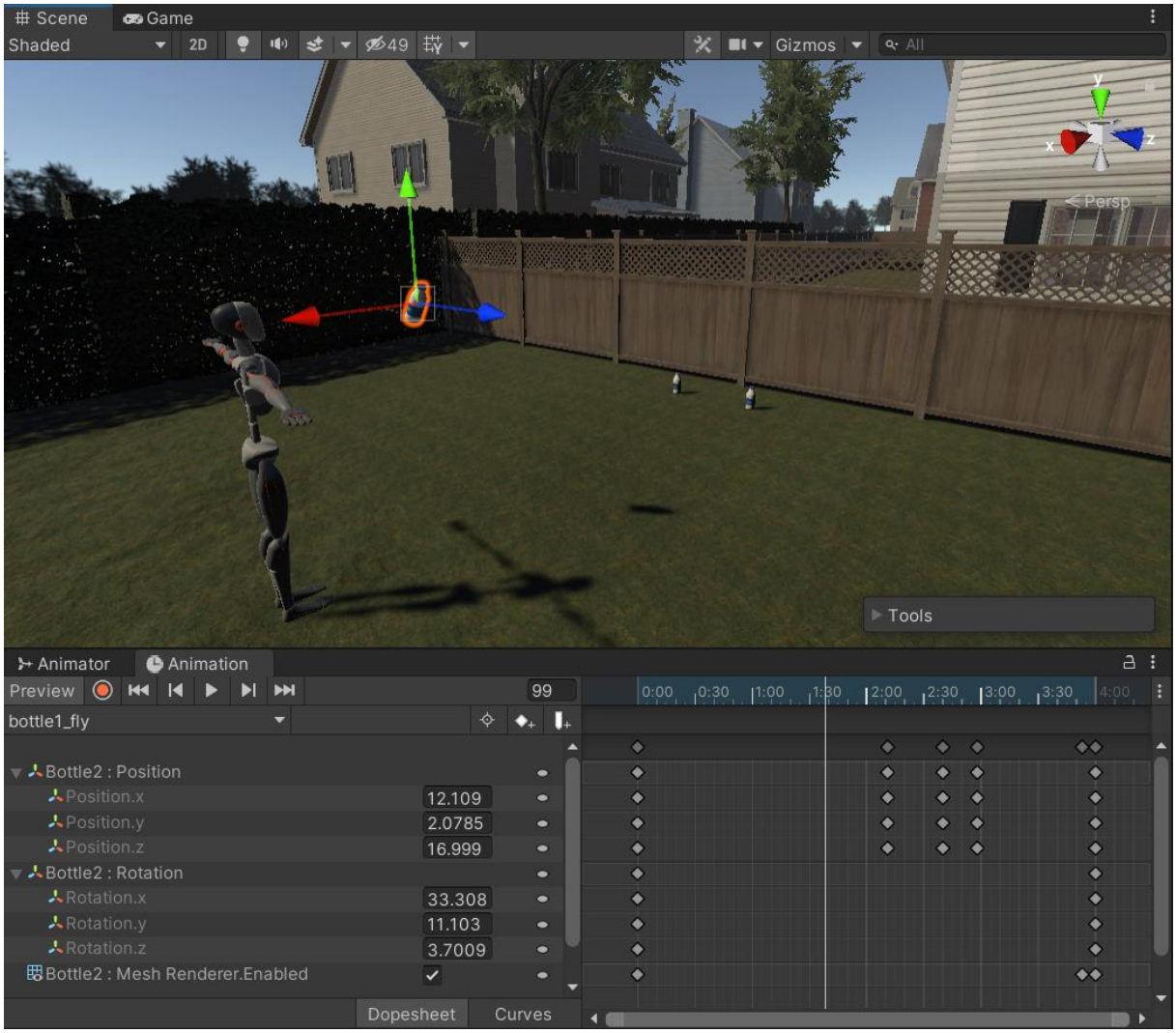

Figure 68: Object avoidance clip animation setup with Xsens Avatar.

while maintaining the viewpoint, one aspect of the scene or the entire scene moves. Ida et al. [184] virtually positioned an object coming from the floor toward the participant. The command was to lift one foot and avoid making contact with the simulated object. Lubetzky et al. [194] employed virtual object movements. A ball flying towards the participant's head, with moving cars and cubes symbolising pedestrians in the backdrop. From the studies that put objects taking off against the participant, the idea of throwing bottles against the participant's head was conceived. Thus, compensatory reactions typical of deflecting an object can be recorded, which can result in lateral unbalance and falling. The visual disturbance is depicted in Fig. 68.

8.3.5 Vertigo

Translations in the V-axis while the subject is placed in a virtual high height can cause fear and anxiety, and has been proven to influence postural control. Four studies [168, 179, 190, 197] used virtual height

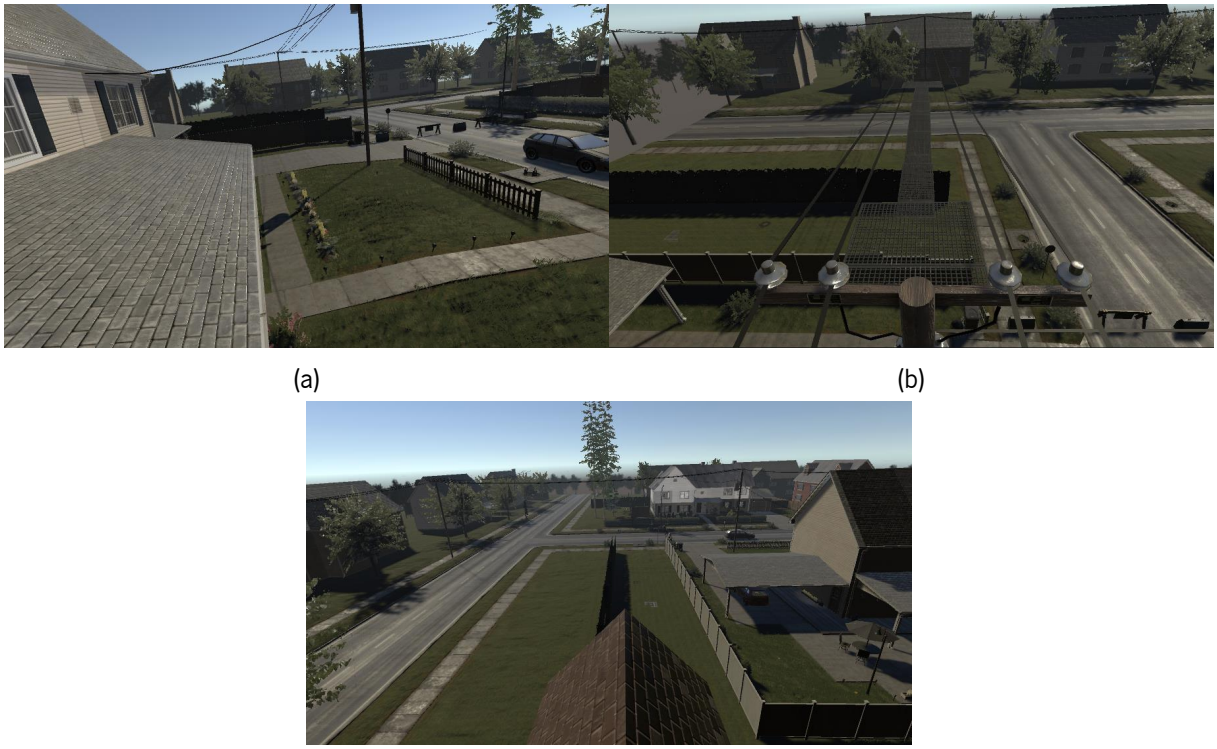

(a) (b)

(c)

Figure 69: Vertigo places. (a) Simple roof. (b) Electricity Pole. (c) Window Roof Beam Walking.

changes to induce vertigo and anxiety in their subjects in order to better understand how these situations affected gait patterns and standing balance. Habibnezhad et al. [168] also investigated the effects of having or not having the real-time depiction of an avatar as the subject walked along a limited route on a scaffold at the top of an incomplete structure. Three unique vertigo scenarios have emerged as a result of these studies. In the VE, the higher locations were used. One of the homes' roofs serves as the initial vertigo trigger (Fig. 69.a). The second requires the users to walk as though they are on a beam to prevent their virtual avatar from slipping off (Fig. 69.c). It is located on another ceiling and has a much smaller walking space. The final site (Fig. 69.b) is situated between two high voltage poles. In this approach, three different vertigo scenarios were produced, each one with a particular feature: a) where the subject may only fall to one side; b) where the subject can fall to both sides; and c) where the subject can fall and slide if the users do not follow the line. The avatar is influenced by gravitational force in the same way as a human body is, in order to increase the participant's fear and stress. Gago et al. [187] and Yelshyna et al. [188] used the V-axis translation to simulate a fall from the top of a staircase. Both studies inspired the idea of inducing a virtual fall in the participant from an upper floor to a lower floor of the house by opening up the floor beneath the participant. This disturbance is called a Free Fall from now on.

8.3.6 Visuomotor Disturbance

Hagio and Kouzaki [162] produced a discordance between the visual and proprioceptive systems by displaying on the HMD a virtual representation of leg height different from the real one, while the participant was traversing an obstacle. A discordant proprioceptive feedback was therefore introduced. This explanation raised the possibility of placing a target in the VE that participants would need to pass. This object would be put in the participant's path on the floor, but it would have a lower virtual height. The participant would attempt to pass the obstacle with the assurance that nothing would hit his foot. Since the height of the real item is bigger than what the subject perceives in the virtual world, it is likely that they may collide in reality. Due to the fact that it would collide with an actual item, this visual disturbance might cause real trips. So, it was defined that the participant is instructed to ascend the sidewalk naturally for this disturbance (Fig. 70). The operator is responsible to timely place a real higher object to cause the trip.

A combination of physical and visual disruption was also developed by Frost et al. [169] and Drolet et al. [173]. By altering the stiffness of the ground using a mechanical device, this perturbation is visual information that is uncorrelated with proprioception. Participants were therefore instructed to go in a straight path on a simulated stone surface that contained random sand or grass fragments. In some circumstances, when the participant walked on a substance they anticipated to be soft, a surface of stone-like hardness was added, producing contradictory sensory information. When the subject was getting ready to land with the leg on a softer surface, this disturbance resulted in alterations in their kinematic and muscle behaviour. Since none of the authors reported any LOB, this visual disturbance had no relevance to the current investigation.

Figure 70: Sidewalk trip induction via visual and proprioceptice mismatch.

8.3.7 Visual Field Oscillations

Because it refers to the superimposition of visual oscillations over the regular flow of vision, the visual field oscillations are distinguished from translations and rotations. A pseudo-random sum of sine waves with four different frequencies made up the oscillations. They can happen in either the ML or AP directions [30]. Due to the minor changes in gait patterns and gait speed observed in the data obtained with this form of perturbation, this type of background oscillation was disregarded. Rotating cameras was preferred. Once all visual disturbances have been discussed and presented, it is important to summarise all information about the visual disturbances implemented in the created VE. Table 45 describes all the visual perturbations choices supported by the literature search mentioned beforehand.

Table 45: Visual perturbations code, name and parameters

Code	Perturbation	Parameters
VP001	Roll Axis Tilt - Clockwise	[10°, 20°, 30°] during 0.5s
VP002	Roll Axis Tilt – Counter-Clockwise	[10°, 20°, 30°] during 0.5s
VP003	Support Surface ML Axis Translation - Bidirectional	Discrete Movement (static pauses between movements) – 1 m/s
VP004	AP Axis Translation - Front	1 m/s
VP005	AP Axis Translation - Backwards	1 m/s
VP006	Pitch Axis Tilt	0°-25°, 60°/s
VP007	Virtual object with lower height than a real object	Variable object height
VP008	Roll-Pitch-Yaw Axis Tilt	Sum of sinusoids drive each axis rotation [399]
VP009	Scene Object Movement	Objects fly towards the subject's head. Variable speeds
VP010	Vertigo Sensation	Walk at a comfortable speed. With and without avatar. House's height
VP011	Axial Axis Translation	Free fall

8.4 Methods & Materials

Using visual perturbations and data gathered from kinematic and physiological sensors, an experimental protocol was created and put into action to create imbalance in the participants. Data collection on compensatory reactions is vital in balance control analysis, designing balance training methods, and compiling data from numerous sensors into a dataset. On the other hand, literature protocols (Section 2.6) presented two main limitations: i) lack of fusion of inertial sensors with physiological sensors for further analyses and conclusions; and ii) introduction of only one visual perturbation. Thus, this protocol attempts to overcome these drawbacks by using various types of sensors used in the scientific literature and introducing a varied list of visual perturbations in a fully immersive VE. This protocol will allow these perturbations to be introduced randomly in an ecologically realistic VE. After data collection, a multivariate dataset will be used to investigate the possibility of using visual disturbances to induce near-fall reactions.

8.4.1 Participants and Equipment

Twelve healthy young subjects (age: 25.09 ± 2.81; height: 167.82 ± 8.40 cm; weight: 64.83 ± 7.77 kg; males = 6; females = 6) were enrolled in the experimental protocol and they respected the following inclusion criteria: i) healthy locomotion; ii) total posture balance; iii) age ≥ 18 years; iv) body mass < 135 kg. Subjects were excluded if they met any of these criteria: i) disease or deficit affecting locomotion; ii) epilepsy, vestibulopathy or other neurological condition resulting in potential instability during trials; iii) have recently undergone surgical procedures affecting mobility; iv) are included in another experimental protocol intervention; v) are under judicial protection/guardianship; and vi) have complications from using VR with a HMD (e.g. motion sickness). All participants provided written and informed consent, respecting the ethical conduct defined by the University of Minho Ethics Committee that follows the standards set by the declaration of Helsinki and the Oviedo Convention. The choice of not to use elderly subjects was not based on their susceptibility to cybersickness. In fact, several studies show that the elderly suffer from less cybersickness than the youngest, and a higher presence attribute is noted [373, 400, 401]. However, aging causes neuromuscular degradations that decrease muscle strength, balance, proprioception and reaction time. Aging may be accompanied by adjustments in muscle activation such as a decrease in voluntary activation. This progressive decline in physical capacities reduces the ability of older adults to perform complex motor tasks and is associated with impaired mobility. For this reason, and to avoid the risk of a fall and injury, older adults were not used in this preliminary study. All subjects must be blinded to the protocol because otherwise it would introduce bias in anticipation to visual perturbations. Due to this, it was also chosen to deliver the visual disturbances in a random sequence and at various locations. The unpredictable and naturalistic elements of the reactions are strengthened since the subjects are never sure when or if they will be disturbed.

Figure 71: HTC VIVE Pro Full Kit.

Table 46: Headset technical specifications

Headset Specs	
Screen	Dual AMOLED 3.5”diagonal
Resolution	1440 x 1600 pixels per eye (2880 x 1600 pixels combined)
Refresh rate	90 Hz
Field of View	110 degrees
Audio	Hi-Res certificate headset
Connections	Bluetooth, USB-C port for peripherals
Sensors	SteamVR Tracking, G-sensor, gyroscope, proximity, Eye Comfort Setting (IPD)

The VR headset was the main equipment involved. It comes with two controllers and two base stations (Fig. 71). The base stations, synchronised wirelessly, are responsible for tracking the headset, which can change the participant's field of view with the movement of the head, and the controllers in a 5 m^2 area. The technical specifications of this headset are described in Table 47. The controllers were used only for setting up the virtual space. The motion tracking system, i.e., the Xsens, was used with full body configuration, which changed the user interaction in the VE. The controllers were deactivated, and if the user wanted to grab or pick some object, the Xsens avatar inserted in the VE allowed that interaction. During the experimental protocol, the following systems were used to capture kinematics, muscle contractions and electrodermal activity: i) Xsens; ii) Delsys Trigno; and iii) Shimmer GSR. A safety harness was used to avoid possible fall injuries. The harness system included a vest that was connected to a ceiling-mounted support via a rope. To ensure that there was at least 15 cm between the knees and the floor, the length of the harness rope was modified. Participants were instructed to lift their feet to apply their entire body weight on the harness system in order to complete this process [158]. SyncLab 2021 was used to synchronise the systems used.

8.4.2 EMG Sensor Location

The selection of EMG sensors location is emphasised. Several studies used EMG in their experimental protocols while causing visual disturbances. By drawing a diagram (Fig. 72) to represent their sensors' locations, it was possible to cross this information with the visual disturbances employed by the same studies. At the bottom of the diagram is the colour code that legends the visual perturbations. Thus, it is possible to instrument the participant with as few sensors as possible, covering the essential muscles for the analysis of different visual disturbances. As an outcome, in order to collect muscle activation data illicited by most compensatory reactions, the following muscles were chosen: i) *Tibialis Anterior* (both legs); ii) *Gastrocnemius Medial Head* (both legs); iii) *Semitendinosus*; iv) *Rectus Femoris*; v) *External Oblique*; and vi) *Sternocleidomastoid*.

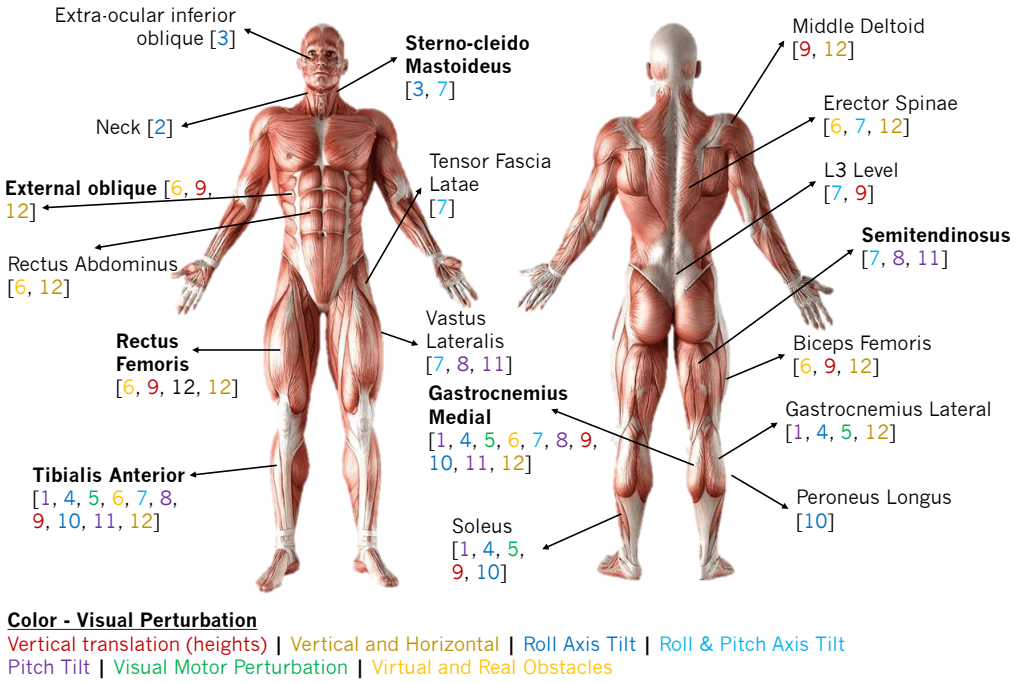

Figure 72: Muscles analysed by the literature within the scope of visual perturbation application. Selected muscles in bold. 1 - Sun et al. 2019 [179]; 2 - Peterson et al. 2018 [170]; 3 - Chiarovano et al. 2018 [180]; 4 - Mohebbi et al. 2020 [182]; 5 - Drolet et al. 2020 [173]; 6 - Ida et al. 2017 [184]; 7 - Bugnariu and Fung 2007 [186]; 8 - Liu et al. 2015 [174]; 9 - Cleworth et al. 2016 [190]; 10 - Peterson and Ferris 2018 [177]; 11 - Parijat et al. 2015 [175]; 12 - Porras et al. 2021 [402].

8.4.3 Balance Perturbation Protocol

VR has advantages for experiment control and repeatability. The design of the experimental protocol brings together four key elements, namely: i) stimulus control; ii) experiment reproducibility; iii) ecological validity and iv) real-world learning transfer. On top of carrying out sequential tasks, the experimental protocol was created. The user's demographic information, including age, height, weight and gender, must be gathered after collecting the written and informed consent. In order to maximise the quality of the electrical signal communicated and to ensure that the EMG sensors were securely fastened to the skin, the locations where the sensors were to be placed were cleansed with alcohol. The participant was then instrumented with the EMG sensors in the chosen muscles. The sensors were firmly glued to the skin. For each muscle, three MVC attempts were done to further normalise the EMG envelope with the help of Delsys dedicated software. Participants were also equipped with the full body configuration of Xsens MVN Awinda wearable inertial system, and the Shimmer GSR device on the dominant forearm with the electrodes placed on the index and middle fingers. The hand dominance was determined using the Waterloo Handedness Questionnaire [366]. Following sensor placement, participants went through the Xsens' N-Pose calibration. Finally, the HTC Vive Pro headset was placed on the participant's head. SyncLab Desktop App assured system's synchronisation.

The subject was advised to: i) ask for help whenever necessary, such as episodes of motion sickness; ii) adjust the distance between the lenses and between the face and the lenses for a proper and more comfortable usage; iii) stay within the playing area restricted by a virtual blue boundary; and perform a familiarisation trial without perturbations while using the entire setup. The familiarisation trial consisted in performing three times the following activities without interruption and visual perturbations while exploring the VE in different virtual locations: walk forward, turn around, and return to the starting location. During the experimental protocol, the subject performed these activities over and over again for almost one hour. The 11 virtual perturbations provided on Table 45 were applied to the subjects. Considering their variants, a total of 35 different situations were considered for this experimental protocol (Table 48). During the entire experimental protocol, each perturbation variant was applied three times, being carried out sequentially and in a distinct order for each subject. The order of virtual perturbations and non-perturbations introduction was created randomly using a Matlab script. Finally, participants were asked to complete the Simulation Sickness Questionnaire (SSQ), a questionnaire about motion sickness during the experimental activity [403]. Igroup Presence Questionnaire (IPQ) was posed to assess the level of immersion and the efficiency of the visual disturbances [404].

8.4.4 Triggers and Scripts

Given the prevalence of visual disturbances, it is essential to fully maximise Unity's capabilities to accomplish the following tasks for a faster execution of the experimental protocol: i) quickly position the avatar in the desired initial position, given that there are multiple initial positions associated with the various visual disturbances; ii) automatically activate visual disturbances when the avatar reaches regions of the VE that have been specifically designated for this purpose; and iii) automatically and temporally record the beginning and end of the various visual disturbances to expedite the labelling process. A system of predefined spaces termed triggers was employed to automate the delivery of the visual perturbations. When the participant enters these spaces virtually, an animation or a visual perturbation seen by the user is activated. The subject will experience visual disruption as long as he or she stays in the area.

Unity's built-in 3D physics engine is a system that simulates aspects of physical systems so that objects can accelerate correctly and be affected by collisions, gravity, and other forces. For this purpose, rigid body collisions and the idea of a trigger need to be described in terms of physics engine principles. A Rigidbody is the main component that enables physical behaviour for a GameObject. With a Rigidbody attached, the object will immediately respond to gravity. If one or more Collider components are also added, the GameObject is moved by incoming collisions. For physical collisions, a GameObject's form is determined by collider components. A cube-shaped collider component called a box collider manages game object collisions. Figure 73 displays an example of a box collider. The box colliders designed to outline the visual perturbation activation zone have a dimension on the x-axis of 2 Unity measurement units, or

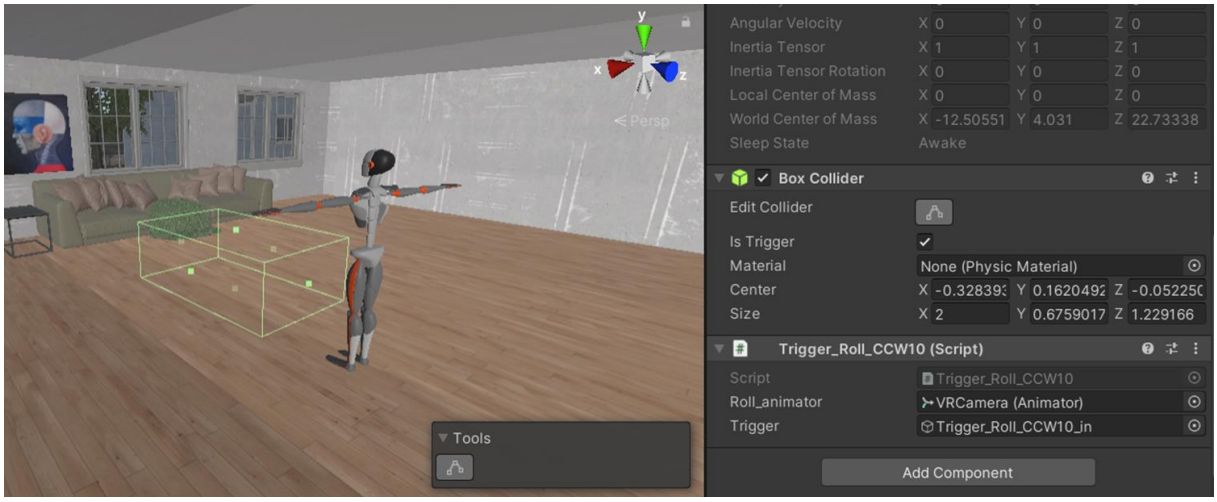

Figure 73: Representation of a box collider (Left). Setting the box collider as a trigger and the associated script visible in the inspector (Right).

2 metres in reality (Fig. 73). The scripting system can detect when collisions occur and initiate actions using the *OnCollisionEnter* function. However, one can also use the physics engine simply to detect when one collider enters the space of another without creating a collision. A collider configured as a Trigger, using the *Is Trigger* property, does not behave as a solid object and will simply allow other colliders to pass through. When a collider enters its space, a trigger will call the *OnTriggerEnter* function on the trigger object's scripts.

8.4.5 Data Processing

Data processing was carried out similarly to the process described in Section 7.3.4. EMG and electrodermal activity data were resampled to 60 Hz, which is the sampling frequency of Xsens and the lowest value among all systems. SyncLab synchronising information helped to combine data into a single Matlab table per subject. Before proceeding to the statistical analysis, data were labelled. Each visual disturbance was assigned a unique number. Except for the trip perturbation, which contains an extra number to identify the foot strike. Uninterrupted walking conditions are also labelled. Table 48 presents the label for each visual perturbation created. The Matlab-generated random sequence with the list of visual perturbations sorted chronologically served as a guide for the labelling process. In addition, the VE was programmed to generate a Log file that records the timestamp of Trigger events This instant of time was compared with the timestamps in the unlabelled dataset. The matching frame was filled with the proper label until the end of the visual perturbation. Some corrections and manual entries of perturbations onsets and finals were necessary. For this, the frames associated with the timestamps were useful for visual inspection in Xsens MVN software. The label plot shown in Fig. 74 helped to correct flaws, as it gives an overview of the perturbations that occurred throughout the experimental protocol.

Table 48: Label encoding

Visual Perturbation	Label	Visual Perturbation	Label	Visual Perturbation	Label
Roll Indoor 1 CW10	**1**	Roll Indoor 1 CW20	**2**	Roll Indoor 1 CW30	**3**
Roll Indoor 1 CCW10	**4**	Roll Indoor 1 CCW20	**5**	Roll Indoor 1 CCW30	**6**
Roll Indoor 2 CW10	**7**	Roll Indoor 2 CW20	**8**	Roll Indoor 2 CW30	**9**
Roll Indoor 2 CCW10	**10**	Roll Indoor 2 CCW20	**11**	Roll Indoor 2 CCW30	**12**
Roll Outdoor CW10	**13**	Roll Outdoor CW20	**14**	Roll Outdoor CW30	**15**
Roll Outdoor CCW10	**16**	Roll Outdoor CCW20	**17**	Roll Outdoor CCW30	**18**
ML-Axis Trans - Kitchen	**19**	AP-Axis Trans - Corridor Forward	**20**	AP-Axis Trans - Corridor Backward	**21**
Pitch Indoor - Bathroom	**22**	Pitch Indoor - Fridge	**23**	Window Roof Beam Walking - Vertigo	**24**
Walking - Vertigo No Avatar	**25**	Simple Roof - Vertigo	**26**	Simple Roof - Vertigo No Avatar	**27**
Pitch Outdoor - Near Car Oil	**28**	Trip - Sidewalk / Trip Shock	**29 / 290**	Bedroom Syncope	**30**
Garden - Object Avoidance	**31**	Electricity Pole - Vertigo	**32**	Electricity Pole - Vertigo No Avatar	**33**
Free Fall	**34**	Stairs	**35**		

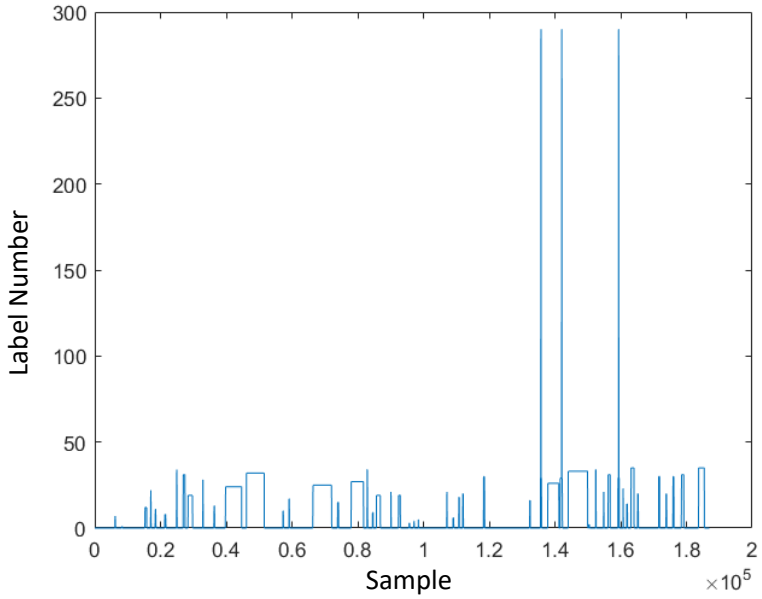

Figure 74: Labels throughout the experimental protocol for a subject. The horizontal axis represents the samples collected and the V axis represents the labels number.

8.4.6 Statistical Analysis Procedures

Once it has been labelled, data were statistically treated and ANOVAs were applied to each dependent variable in order to answer the RQ5. Statistical measures from kinematics (CoM, acceleration and angular velocity from pelvis and sternum), muscle and electrodermal activity data were estimated per dependent variable to perform this analysis (Fig. 75): i) mean (AVG); ii) standard deviation (STD); iii) minimum (MIN); iv) maximum (MAX); v) kurtosis (KUR); vi) skewness (SKW); and vii) Lyapunov exponents (LYAP). This calculation was performed for each of the visual disturbances collected and even for situations with no

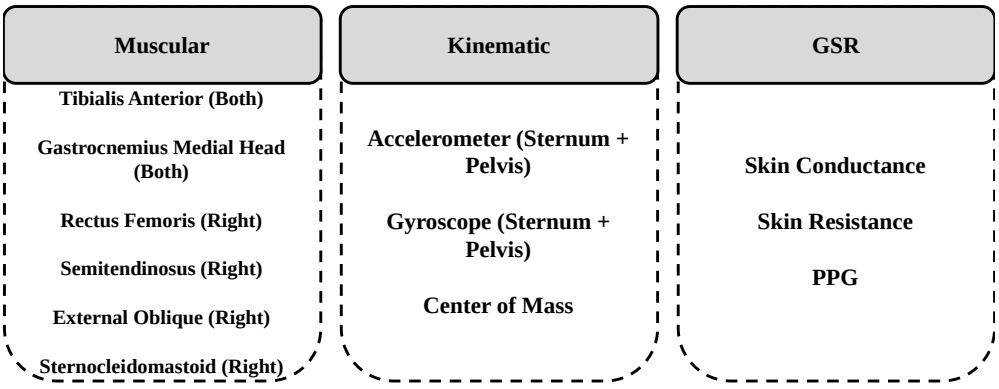

Figure 75: Dependent variables used for statistical analysis.

perturbations. The physiological dependent variables included the 8 muscles and the information from the electrodermal sensor, i.e., Photoplethysmography (PPG) and the skin conductance and resistance. Considering the kinematic variables, the sternum and pelvis acceleration and angular velocity were chosen since they reflect trunk bend that may be a consequence of hip strategy, body sway, and trunk rotation [405]. CoM velocity was also chosen since it is the determining factor of balance [406].

The prerequisites for an ANOVA are independent observations, properly distributed response variables, and homogeneous covariance matrices across groups. Research in the past has demonstrated that the type I error rate of the conventional test statistics can be inflated while their power can be decreased when the conditions of normality and homogeneous covariance matrices are not met [407]. The presence of multivariate outliers, the absence of multicollinearity, and the linearity of the dependent variables for each level of the independent variables were also investigated. The normality of the continuous data can be tested using a number of different methods. The two well-known tests of normality, namely, the Kolmogorov–Smirnov test and the Shapiro–Wilk test, are the most widely used methods to test the normality of the data [408]. However, skewness and kurtosis can also be used for large samples (>300). Normality tests were conducted in the statistical software SPSS. Although it can handle higher sample sizes, the Shapiro-Wilk test is more suitable for small sample sizes (<50 samples). For sample sizes greater than 50, the Kolmogorov-Smirnov test is commonly used. The null hypothesis states that data arises from a normally distributed population for both of the above tests. When $p>0.05$, the null hypothesis is accepted, and data is normally distributed. For a preliminary study, a binary classification was taken into consideration, dividing variables measured under perturbation and those without perturbation.

In an ANOVA, a significant F-value simply indicates that there are disparities between the population means. This significant value indicates that visual disturbances have an effect on gait characteristics. In other words, visual disturbances effectively cause imbalances. However, it does not specify which precise perturbations cause the averages to diverge greatly. This distinction will help determine which disturbances posed the most difficulty to the participant's balance. At this point, after conducting the ANOVAs, differences between means individually will be inspected. In the case of this experimental protocol, an important

comparison will be between the cases where there is no perturbation and the cases where there is visual perturbation. In this situation, the unaffected gait will act as a control. When comparing one group to another, the suggested test is Dunnett's test [409]. Dunnett's test is carried out by calculating a Student's t-statistic for each group and comparing the treatment group (perturbation labels) to a single control group (no perturbation). Because each comparison shares the same control, the process takes into account the dependencies between them. The t-statistics, in particular, are all derived from the same estimate of the error variance, which is acquired by aggregating the sums of squares for error across all groups. The formal test statistic for Dunnett's test is either the t-statistic with the highest absolute value, or the t-statistic with the highest negative or positive value.

8.5 Statistical Analysis Outcomes

8.5.1 Dataset Normality

Final dataset contains 553 observations of no perturbation and 543 observations of perturbation. Thus, the first step was to identify normal variables following the rule for sample size over 300 (skewness value ≤2 or kurtosis ≤4). However, literature supports an easy path for analysis considering the sample size. In order to draw conclusions about associations between variables, as intended to do in ANOVA, it is acknowledged that in large samples, these statistical methods rely on the Central Limit Theorem, which states that the average of a large number of independent variables is roughly normally distributed around the true population mean [410]. Thus, it was possibly to use all dataset in ANOVA.

8.5.2 ANOVA

ANOVA was performed to compare the effect of visual perturbations on the estimated dependent variables (Fig. 75). Overall, there are 32 variables from muscle activity, 48 variables from acceleration and angular velocity of the pelvis and sternum in the 3-axis, 12 variables from CoM velocity, and 9 variables from GSR sensor. The ANOVA revealed that there was a statistically significant difference in the dependent variables listed in Table 49 between at least two groups. F-value and p-value are presented in Table 49 for each dependent variable. The table is arranged to show the variables with the most significant p-value first (left side of the table). There was no significant difference in the dependent variables showing the p-value with p>0.05 (right side of the table - variables with green p-value). This table also disclosures that CoM velocity, mainly AP-axis, along with angular velocity, specially from sternum, and muscular activity from right and left *Tibialis Anterior* prevail as dependent variables with the most significant p-value. This variables will be further used to narrow the analysis while obtaining relevant conclusions about the visual perturbations. Additionally, lower body muscle-related variables also present more significant p-values than variables from the upper body. The variables referring to the galvanic response of the skin that reflect physiological

Table 49: One-way ANOVA results: F-value and p-value. The order of this table is done in order to understand which variables had the highest F-value, i.e., which were most influenced by the situations where there were visual disturbances. Additionally, variables are separated by colour to get an idea of which groups of variables were most affected. Blue - muscle variables; Green - Gyroscope; Orange - Accelerometer; Purple - CoM Velocity.

F-value	p-value	Independent Variable	F-value	p-value	Independent Variable	F-value	p-value	Independent Variable
44.3876	4.9562E-181	COMVelXMIN	7.398	1.67488E-31	RGMSTD	3.349156	3.9924E-10	StrGyrzAVG
30.3299	2.9712E-134	COMVelXAVG	7.397	1.68877E-31	RTASTD	3.095718	7.0099E-09	StrAccyAVG
22.269	1.3568E-102	StrGyrxSTD	7.307	5.07651E-31	RGMAVG	3.05817	1.0655E-08	StrAcczMIN
20.1081	2.34E-93	StrGyrzMAX	6.589	3.55611E-27	PelGyrzSTD	3.03915	1.3164E-08	PelAccyMIN
19.552	6.33223E-91	PelGyrzMAX	6.083	1.83851E-24	PelAccyMAX	3.017882	1.6667E-08	StrAccyMAX
18.9544	2.7722E-88	PelAccxSTD	5.544	1.40609E-21	PelAcczMIN	3.012572	1.7677E-08	StrAcczSTD
17.8613	2.22145E-83	PelAccySTD	5.367	1.2499E-20	RGMMAX	3.007972	1.8601E-08	StrAccxMIN
14.9473	7.81648E-70	PelGyrxSTD	5.22	7.57E-20	PelGyrxMAX	3.004329	1.9366E-08	StrAccyMIN
12.9882	2.50855E-60	COMVelYMAX	5.003	1.07675E-18	PelAccxMAX	3.00356	1.9532E-08	StrAcczMAX
12.8724	9.36689E-60	PelAcczSTD	4.979	1.45508E-18	LGMSTD	3.00045	2.0216E-08	StrAccxMAX
11.6453	1.26888E-53	StrGyrzMIN	4.744	2.56E-17	StrGyryMAX	2.980041	2.5328E-08	StrAccxSTD
11.18100	2.87403E-51	RTAAVG	4.724	3.25173E-17	COMVelZAVG	2.969282	2.8519E-08	StrAccxAVG
11.035	1.5833E-50	PelGyrzMIN	4.458	8.16166E-16	PelAcczMAX	2.966565	2.9386E-08	StrAccySTD
10.8063	2.33108E-49	LTAMAX	4.417	1.35E-15	StrGyryMIN	2.916839	5.07E-08	PelGyryMIN
10.5536	4.60525E-48	COMVelZSTD	4.292	6.04921E-15	PelAccxMIN	2.741791	3.38E-07	PelGyryMAX
10.4218	2.19047E-47	StrGyrySTD	3.934	4.34E-13	PelGyrxMIN	2.683527	6.2881E-07	PelAccxAVG
9.80508	3.385E-44	PelGyrySTD	3.781	2.66E-12	SCMMAX	2.680819	6.4714E-07	EXTOMAX
9.26007	2.35024E-41	RTAMAX	3.693	7.44721E-12	COMVelYSTD	2.662867	7.8266E-07	StrGyrxAVG
8.7332	1.37279E-38	StrGyrzSTD	3.678	8.9323E-12	LGMMAX	2.660458	8.0286E-07	EXTOSTD
8.64069	4.21946E-38	COMVelXSTD	3.663	1.06239E-11	COMVelYAVG	2.640012	9.9626E-07	COMVelZMAX
8.42246	5.9924E-37	LTASTD	3.619	1.77103E-11	StrGyryAVG	2.5719	2.0341E-06	PelAccyAVG
8.21407	7.60E-36	StrGyrxMAX	3.618	1.79964E-11	STMAX	2.501778	4.2048E-06	COMVelXMAX
7.4828	5.88E-32	StrGyrxMIN	3.596	2.32318E-11	COMVelYMIN	2.415235	1.0169E-05	RFMIN
7.47933	6.13649E-32	LTAAVG	3.531	4.92824E-11	RFMAX	2.400227	1.1833E-05	LGMAVG
			3.467	1.03E-10	RFSTD	2.332105	2.3405E-05	STAVG
			3.465	1.05448E-10	SCMSTD	2.123562	0.0001764	STSTD
			3.366	3.27661E-10	PelGyrzAVG	2.063500	0.00030898	RTAMIN
						2.045522	0.00036468	PelGyryAVG
						2.03077	0.0004175	RFAVG
						1.959229	0.00079695	RGMMIN
						1.906913	0.00126532	PelAcczAVG
						1.894578	0.00140912	LTAMIN
						1.572945	0.01891391	StrAcczAVG
						1.558554	0.02101814	PelGyrxAVG
						0.955329	0.54398981	COMVelZMIN
						0.836843	0.73760913	LGMMIN
						0.709917	0.89614266	STMIN
						0.580864	0.97617683	EXTOMIN
						0.181758	0.99999998	EXTOAVG
						0.14402	1	SCMMIN
						0.120651	1	SCMAVG

activity related to anxiety and fear of falling did not obtain significant values. Thus, were not included in the aforementioned table.

8.5.3 Dunnett Post Hoc

Dunnett's t-test with no Pertubation as control group for multiple comparisons found that the mean values of independent variables in Table 50 were significantly different between control group "No Perturbation"and the visual perturbations implemented. To illustrate the results obtained in the Post Hoc test, a muscle variable was picked - the average value of the percentage of activation of the *Right Tibialis Anterior* muscle during the occurrence of the various perturbations. Table 50 shows the results of this test. The greatest differences between the averages when comparing the control group (no disturbance) with the

visual disturbances are coloured green. The red colours indicate the opposite, i.e., that there was minimal interference of the visual disturbance on the average activation of this muscle. From the mentioned table, it is apparent that the visual disturbance that most affects the contraction of this muscle is Roll Indoor 2 CCW30. This process was replied for all metrics and considerations are further described.

8.5.3.1 Muscle variables

Table 49 reveals a massive presence at the top of muscle variables from the lower leg muscles: Right and Left *Tibialis Anterior* and Right and Left *Gastrocnemius Medial Head*. By itself, this discovery supports the hypothesis in the direction intended to prove. The visual disturbances induced in this experimental protocol primarily activate the muscles needed to maintain and recover balance after gait disturbance. The ankle muscles (plantarflexors/dorsiflexors) in the AP direction and the hip abd/adductor muscles in the ML direction were identified as dominants during quiet or perturbed standing by studies of balance and posture [405]. Kim et al. [411] summarise reports of muscle activations during perturbed walking. Each study examined the *Tibialis Anterior*, a muscle involved in dorsiflexion of the ankle. The *Gastrocnemius* is the muscle that functions as its antagonist. The findings of these articles imply that a crucial factor in abnormal gait is the involvement of the plantarflexor and knee flexor muscles.

According to Dunnett's post hoc results, the Pitch visual disturbance significantly interfered with the *Gastrocnemius* muscles. This resemblance suggests that a physical perturbation and a visual perturbation induce similar muscle patterns. The same EMG pattern is observed in the backward translation of the platform. Statistical analysis once more confirms the significant relationship between the visual disturbance and AP-axis Translation Backward and the activation of the *Gastrocnemius*.

The *Tibialis Anterior* and *Gastrocnemius Medial* muscles of the dominant leg similarly demonstrated statistically significant variations ($p=0.0005$ and $p=0.0019$, respectively) in the means between the ML-axis perturbation and the non-perturbation condition, which is consistent with the findings of Acuna et al. [412]. This demonstrates that the *Tibialis Anterior* and *Gastrocnemius Medialis*, two ankle stabiliser muscles, were significantly affected by the ML-axis Translation visual perturbation that was performed. Additionally, in line with the findings of Hallal et al. [413], the results of the Dunnett's post hoc test on the variables pertaining to the dominant thigh muscles reveal that the perturbations Trip and Object Avoidance were the most successful in eliciting these muscles.

8.5.3.2 Kinematic variables

The CoM velocity in AP direction must be considered for the ANOVA outcomes. According to Pai et al. [414], balance will not be maintained when there is sufficient velocity of the CoM in AP direction, even if the position of the CoM is within the BoS. Both model simulations and human experimental data have

Table 50: Dunnett t-test (2-sided) result - Right Tibialis Anterior. The color gradation means a higher value for the green-tone colors and a lower value for the red ones, i.e., in green are the entries that the corresponding visual disturbance introduced the most difference in means.

Dependent Variable: **RTAAVG**
Dunnett t (2-sided): control group "No Perturbation"

(I) Label	(J) Label	Mean Difference (I-J)	Sig.
Roll Indoor 1 CW10	No Perturbation	2.619624074	0.014
Roll Indoor 1 CW20	No Perturbation	2.640917425	0.013
Roll Indoor 1 CW30	No Perturbation	2.82942145	0.005
Roll Indoor 1 CCW10	No Perturbation	3.068273265	0.001
Roll Indoor 1 CCW20	No Perturbation	3.182434604	0.001
Roll Indoor 1 CCW30	No Perturbation	4.154222882	0.000
Roll Indoor 2 CW10	No Perturbation	3.229842329	0.000
Roll Indoor 2 CW20	No Perturbation	1.720165351	0.505
Roll Indoor 2 CW30	No Perturbation	3.045723908	0.001
Roll Indoor 2 CCW10	No Perturbation	3.591367025	0.000
Roll Indoor 2 CCW20	No Perturbation	4.049127951	0.000
Roll Indoor 2 CCW30	No Perturbation	4.903273231	0.000
Roll Outdoor CW10	No Perturbation	4.198288474	0.000
Roll Outdoor CW20	No Perturbation	1.597146009	0.662
Roll Outdoor CW30	No Perturbation	2.031776184	0.191
Roll Outdoor CCW10	No Perturbation	3.05686819	0.001
Roll Outdoor CCW20	No Perturbation	4.553190306	0.000
Roll Outdoor CCW30	No Perturbation	3.400362578	0.000
ML Axis Trans - Kitchen	No Perturbation	1.896113135	0.001
AP Axis Trans - Corridor Forward	No Perturbation	2.020538563	0.000
AP Axis Trans - Corridor Backward	No Perturbation	2.004027816	0.000
Pitch Indoor - Bathroom	No Perturbation	2.541397364	0.021
Pitch Indoor - Fridge	No Perturbation	2.696144191	0.010
Window Roof Beam Walking - Vertigo	No Perturbation	3.453513534	0.000
Window Roof Beam Walking - Vertigo No avatar	No Perturbation	2.612068727	0.015
Simple Roof - Vertigo	No Perturbation	1.518723557	0.830
Simple Roof - Vertigo No avatar	No Perturbation	1.620855505	0.632
Pitch Outdoor - Near Car Oil	No Perturbation	2.304171836	0.063
Bedroom Syncope	No Perturbation	2.101540562	0.000
Garden - Object Avoidance	No Perturbation	1.778019862	0.002
Electricity Pole - Vertigo	No Perturbation	2.432576435	0.035
Electricity Pole - Vertigo No avatar	No Perturbation	2.280966349	0.070
Free Fall	No Perturbation	2.213991566	0.000
Stairs	No Perturbation	2.392414359	0.001
Trip - Sidewalk	No Perturbation	3.86578572	0.000

previously indicated that the CoM velocity plays an important role in regulating stable walking [406]. Dunnett's test results detected which visual perturbations, compared to the "No Perturbation"control, caused

the CoM velocity variable to show the greatest difference in the means, representing a greater influence of the perturbations that have a larger (I-J) Mean Difference value. The ones with a larger value of mean difference are the Roll and Pitch perturbations ($p<0.05$). It is possible that the perturbations that make the participant walk faster or halt abruptly by adopting the hip strategy are those that, on average, have the highest effects on the variable CoM velocity AP-axis. This occurs in all Roll perturbations that, despite attempting to generate a lateral drop, result in a compensatory response that causes erratic oscillations in the AP direction during the perturbed gait. On the other hand, a ML-Axis Translation perturbation has no statistical significance. This is because it induces a lateral sway that is not as abrupt as Roll. A note of special attention to the angular velocity around the V axis, evidencing clear differences between disturbance and non-disturbance situations. This can be explained by a compensatory movement of the hip, causing a greater rotation than when walking or when standing still.

The average value of the gyroscope in the y-axis of the inertial sensor placed on the Pelvis. This variable anatomically represents trunk flexion average, which reflects a strategy of the hip to counteract external perturbations in the AP plane. Dunnett's post hoc test reveals that the visual perturbations of backward translation and free fall are those that induce the greatest difference in means compared to no perturbation.

8.5.4 Visual Disturbances and Type of Falls

To discover the visual disturbances that actually perturb balance and gait, the variables that presented statistically significant differences were analysed. Considering the average activation of the *Tibialis Anterior*, Roll and Trip visual perturbations have generally more influence on the activation of this particular muscle. Among Roll perturbations, the Roll CCW30, CCW20 and CW10 were the most effective in the muscles of both legs. Moreover, the perturbation Window Roof Beam Walking, vertigo-related perturbation, also presented statistical significance regarding the average activation of these muscles. Vertigo scenarios stand out for their amazing values when it comes to maximum values, especially in the two situations where the participant has the notion that he can fall on both sides.

Average activation of the *Right Medial Gastrocnemius* revelead that Roll perturbations are generally the most influential, more specifically Roll CCW20 and CCW30. Interestingly, two pitch perturbations (Pitch Bathroom and Pitch Fridge) were also among the most effective at activating this dominant leg muscle, as well as Trip. On the other hand, the *Left Gastrocnemius Medial* (non-dominant) was only influenced by the Free Fall and Trip perturbations. Maximum values from this muscle did not exhibit significant differences for any visual perturbations considering the right leg. For the left leg, contrarily, AP-axis translation (forward and backward) presented significance statistical differences, as well as the Bedroom Syncope perturbation. The last one perhaps because the period of disturbance includes sitting.

Kinematic variables also exhibit statistically significant differences. Regarding mean CoM velocity, it can be stated that in AP direction all Roll perturbations proved to be quite homogeneously influenced. Moreover,

all perturbations in the Pitch and AP-axis Translation were highly statistically significant. This result was expected since these perturbations try to induce a forward or backward drop. Considering the maximum value in the same direction, only the Bedroom Syncope perturbation stands out. This can happen due to the sitting activity caused by the visual perturbation. However, not all subjects needed to sit during the perturbation. The CoM velocity in the ML-axis can also provide crucial information kinematically. Regarding the mean values, the Free Fall, Trip and AP-axis translation perturbation showed the greatest influence. On the maximum value, there was a general influence of the Roll perturbations and a main influence of the AP-axis translation backward perturbation. All Pitch perturbations are also effective at producing a change in the maximum value, as well as Free Fall and Trip perturbations. Analysing the CoM velocity in the V direction, it revealed the Bedroom Syncope perturbation as statistical significant. As mentioned, the subject lowered the CoM due to the sitting activity.

8.6 Conclusions

An immersive VE was designed respecting the concept of ecological validity endowed with a high level of realism conferred by a home-living paradigm to create a tool capable of induce imbalance through a VR headset. It includes animations that can be found outdoors or in different parts of the houses (e.g. kitchen, bathroom, stairs, bedroom). The animations, on the other hand, were created to provoke different types or categories of falls, being as multivariate as possible.

In accordance with the experimental protocol, these visual disturbances are presented randomly to the participants in order to collect data, allowing the construction of a new, vast and multivariate dataset of imbalance situations as close as possible to real-world imbalance situations. The paucity of physical space that only allowed for back and forth movement of the subject was one of the protocol's execution's constraints. Furthermore, it was not possible to apply all of the perturbations to each subject's gait cycle at precisely the same time due to the nature of the animations' triggering mechanism. However, the statistical analysis fills in this gap.

The statistical analysis was then used in order to determine if the visual perturbations caused variations in the means of the dependent variables relative to the no-perturbation circumstances. ANOVAs were carried out to see which variables changed the most when visual disturbances were applied. These ANOVAs revealed that the muscle groups with the strongest correlations to the recovery of balance following external disturbances were the most statistically significant. Kinematic variables that reflect the LOB showed the same behaviour. Thus, it may be concluded from these findings and the substantial associations with compensating responses to physical perturbations that the visual disturbance alone was sufficient to cause the individual imbalance. However, it is also possible to categorise visual perturbations.

Chapter 9

Conclusions

Concluding remarks and major contributions are highlighted in this chapter by placing the findings of the earlier chapters into perspective. To highlight the achievements and contributions of the work produced, the RQs are addressed as a way to complement and summarise the previous section. Additionally, this chapter also disclosures opportunities for further technical improvement among the hardware and software developed, as well as future directions to increase the technological and clinical value of the research project.

9.1 Concluding Remarks and Main Contributions

This PhD thesis proposes fall prediction and prevention strategies oriented to the senior in order to meet the current challenges evidenced by the scientific literature. These strategies were initially developed throughout this thesis while developing or enhancing robotic monitoring systems considering the levels of mobility (Objective 2). The research and development actions carried out, as well as the promising results produced through benchmarking assessments, all contributed to the achievement of the PhD thesis's final aim. It was also pointed out the clear necessity to stimulate the usability and acceptability of these cutting-edge technologies to reduce the incidence of falls, specially among the elders. Thus, this technology followed an user-centred design approach, considering the end-users' reports, clinicians' expertise and literature annotations considering both. However, this project is not finished, i.e., this PhD thesis only represents the beginning of the entire idea.

Chapter 4 addresses the development and instrumentation of a conventional cane to detect falls and cane events (Objectives 1 and 2). The end product is a lightweight, compact device that can be quickly fitted inside of any regular cane. The system is made simpler by using a single IMU to collect kinematic data,

making setup easier. Concerning the detection of falls, fall detectors have been implemented as a FSM and an AI-based tool (Objective 4). The second one presents better performance than the first to detect falls, however it is recommended the test on a dedicated board for real-time usage. On the other hand, both tools can detect the occurrence of a fall with short lead times before the impact. Benchmarking analysis reveals AI-based model with higher lead times than most of the studies analysed, being just behind Nyan et al. [253]. This AI-based tool also detects fall phase and category. Furthermore, two real-time cane event detection tools were developed, consisting in a FSM and a AI-based model. The FSM showed to be accurate to handle inter-subject and inter-step variability when varying gait speed, slope, climbing staircases, barefoot and footwear conditions (Objective 4). The suggested detection method is suited as a benchmark for real-time measuring human gait events indirectly due to features like decreased computing burden, easy usage (only using a small sensor), and more holistic gait segmentation (up to four cane events) when compared to the literature. The AI-based model stands out in terms of performance despite being more complex, which requires further analysis to select an approach for a future stand-alone version.

In Chapter 5, an innovative and cutting-edge technology-based cane-type robot is presented (Objectives 1, 2 and 4). Initially, a product design strategy inspired by Ulrich and Eppinger [50] was followed in order to achieve a solution that was as close to ideal as possible. A mission statement followed by the identification of consumers needs and target specifications represent an important stage of the product conception since it further limits the design of various concepts or ideas. From concept to concept, a virtual prototype was finally obtained and mechanically tested to verify if it complies with ISO standards. These mechanical simulations were performed successfully, since each test was passed with distinction. After mechanically validating the virtual prototype, a company proceeded to build its skeleton, which was further instrumented considering an idealised hardware architecture. This whole process culminated with the implementation of a motion control system capable of detecting user's motion intention through FSRs placed on the junction between cane's upper and lower parts. The motorised holonomic base is then responsible to act accordingly to the user intended direction. Thus, this motion control system can be considered as a simple, intuitive and cost-effective system. Finally, the total cost resulting from the acquisition of all the parts to be included in the cane-type robot was €688.97. Despite the fact that this price is a little bit more than the €650 specified in the target specifications, it is crucial to remember that this particular robotic cane is just a prototype for a possible later commercially available product. As a result, every component was bought individually, and every piece of hardware is now deemed experimental. Later on, the design may be over-engineered to improve performance and alter the final cost of the robotic cane.

Chapter 6 describes the design of a three-part modular architecture FRA strategy (Objectives 1-4). It was defined for future development an eHealth platform that will allow real-time FRA using only a waistband equipped with one inertial sensor and electronic gadgets, as discussed previously. The addition of a few wearable sensors makes this equipment more pleasant to daily use. Furthermore, the suggested

modular technique should enable a multifactorial risk assessment, which includes several risk aspects, making it more complete and reliable. It applies AI-based technology to combine both future and immediate FRA techniques to offer a single FRA. Studies have shown that it is statistically important to take into account the activities that a person was engaged at the time of the fall since the number of falls (and thus the fall risk) changes depending on the activity that the person was engaged in at the time of the fall [319]. A comparative analysis analysed machine and deep learning-based methodologies to solve a 20 class (between ADLs and fall events) classification problem. Online public and team-owned datasets were merged and processed to generate a vast dataset, larger than any existent in the researched state of the art, used to validate the proposed *Activity Recognition Module*. Benchmarking reveals that the best performance achieved with the procedures implemented in Chapter 6 is better than the current state of the art results and it classifies more activities. Moreover, the best-performing models achieved similar performances when using data collected from older adults at nursing homes. However, LOO approach suggests more data collection, activity balancing, and possibly different data processing to achieve reliable performances for a daily use.

Chapter 7 scrutinises a proof-of-concept slip-related fall prevention strategy based on the human biomechanical responses to these gait perturbations highlighted in the scientific literature (Objectives 1, 3-5). This strategy was divided into detection and actuation stages. To minimise the complexity of the actuation to just the primary joint that counteracts slip-induced LOBs, the actuation stage took into account the assistive torque supply on a single leg using a single assistive device, an orthosis. The strategy stressed the necessity of providing to the leading leg, which is considered the dominant leg, a knee flexion moment in the event of a slip-induced LOB caused by the HS.

The knee angle and shank angular velocity variables were chosen as the most suitable kinematic variables to accomplish the identification of slip-induced LOBs. An experimental protocol was designed in order to collect multivariate data from healthy young subjects while dealing with unexpected slip-like perturbations during treadmill walking.

In order to track the quasi-periodic variables of human locomotion and aid in the timely identification of gait disturbances, biologically inspired CPG controllers' appealing qualities were considered for the detection stage. In particular, adaptive Hopf oscillators were used to learn the trajectory of the identified kinematic variable. The appearance of a perturbation quickly increases the error between the monitoring signal and the signal anticipated by the AFO. Based on the rise in the error signal, straightforward threshold-based algorithms can then accurately predict when the perturbation will start. Generally speaking, the adaptive threshold algorithm outperformed the fixed threshold algorithm in terms of performance. The adaptive threshold approach, accompanied by the AFO's outcome, was used to monitor the knee angle of the affected limb, and this provided the best overall performance.

A home-living paradigm that intends to be extremely similar to reality is used in Chapter 8 to suggest a VE that has a high level of realism because of its ecological validity and presence qualities (Objectives 1, 3

and 6). Animations or visual perturbations were then developed to materialise the visual disturbances in this virtual world. In an experimental protocol for data collection, building a vast and multivariate dataset, these visual disturbances are applied randomly to the participants. This dataset intends to contain data very close to those collected in real-world settings. A statistical analysis was applied to data collected as a way to verify if the visual perturbations introduced variations in the means of the dependent variables in comparison to the no-perturbation conditions. ANOVAs showed that variables of muscle groups strongly connected to balance restoration after external perturbations were the most statistically significant. Kinematic variables that reflect the LOB behaviour showed the same behaviour. It is feasible to infer that the visual disturbance alone was sufficient to bring the participant into imbalance in light of these results and the substantial connections with compensatory reactions brought on by physical perturbations.

This PhD thesis also contributed to the creation of a broad and varied collection of ADLs and imbalances data. Imbalances were artificially produced by slips-like perturbations during treadmill walking and by various visual disturbances that caused fall-related postural reactions. This enabled the varied conclusions stated in this section to be reached, which may serve as a foundation for future work in this field of investigation.

9.2 Research Questions

The developed work enabled to answer the following RQs.

- **RQ1:** *What are the main FRA and fall prevention methods implemented in the scientific literature and how input information is obtained and used?*

Chapter 2 answered this RQ. Two main FRA methods were identified. The long-term evaluation of fall risk, based on clinical scales, was the most extensively used. This method involved gathering data from wearable sensors to forecast a subject's risk of falling based on the results of a clinical scale. Subjects are then assigned to either a high fall risk category or a low fall risk category. By allowing participants to regularly analyse their long-term fall risk, it will help to reduce that risk. The second method involved monitoring fall risk occurrences in real time. To identify fall risk conditions and detect imbalance, wearable sensor data was employed. By enabling daily real-time monitoring of subjects and informing them when a fall risk event is occurring, this approach will help to reduce short-term fall risk.

Regarding fall prevention methods, scientific literature identifies three methods for robotic canes. The first method is based on an inverted pendulum concept, being conceived for devices with one and two wheels. By moving in the same direction as the forces being given to the cane, this method of action seeks to preserve the cane's upright posture. The cane will therefore travel in that way to maintain balance while helping the user avoid falling by moving alongside him when pressures are applied in that direction, as if in a potential falling situation. The second method is appropriate for robotic canes with passive motion

control, in which the user's efforts alone, without the aid of any triggering device, cause the cane to move. This method manages the braking torques of the wheels, controlling the device's movement, i.e., modify the speed of the mobile base. The third method consists in moving the robotic cane to a strategic position favorable to the user during a fall situation, providing stably support to the body weight on the cane. Methods for smart walkers and powered orthoses are clearly more simple, since smart walkers only stops when a risky situation is detected, while powered orthoses apply rotational forces obligating the joint to move accordingly. In general, the hip is extended and the knee is flexed when the objective is to counteract a slip-like perturbation.

Real-world fall data comes essentially from long-term experimental protocols where the participant is instrumented with a technological device, usually an IMU-based. The SensAction-AAL [89] and the FARSEEING [31] projects cared about this scarcity of data and tried to obtain more fall data. However, since an adult falls 1-2 times per year, it is very difficult to obtain real-world fall data as quickly as desired. This information can be used to improve fall detection algorithms, but also to perform statistical analysis to the sensor's characteristics of the on-ground and recovery phases after real-world falls; the neck's importance on stabilising the head, and compare signals.

State of the art presents alternative solutions to collect fall-related data, namely methods to provoke artificial slip and trip perturbations, or even through the use of VR to induce visually imbalances. Artificial slip and trip perturbations may be created on treadmill walking or overground walking. Slip perturbations are provoked during treadmill locomotion by changing the belt's acceleration or during overground walking by using: i) a movable platform; ii) a slippery solution; or iii) novel robotic devices. Treadmill trips were elicited by means of: i) changing belt acceleration; ii) using a brake-and-release-system; or iii) using a tripping device. Trips were provoked during overground locomotion by: i) triggering an obstacle; ii) manually placing an obstacle along the walking path; or iii) using a novel robotic device.

Regarding the use of VR to induce imbalance, literature categorises the visual perturbations into: i) translations or rotations on one or several axes simultaneously; ii) changes in proprioceptive feedback; iii) visuomotor disturbance introduction; iv) visual field oscillations and v) predefined trajectories object movement. As mentioned previously in Chapter 8, researchers try to elicit all fall categories during normal walking at this stage of the study, i.e., backward, forward and lateral falls, slip, trip, and syncope. So, despite being used as a PBT, they can also be used to provoke falls.

- **RQ2:** *Can an instrumented conventional cane and a cane-type robot detect falls and indirectly gait events?*

Chapters 4 and 5 answered this RQ. Kinematic data representative of the conventional cane's movement is vital for both approaches developed in this chapter, as well as in the scientific literature. Considering fall detection, both approaches detect accurately cane's falls with performances higher than 99%. On the

other hand, regarding cane events, the best AI-based method presented results higher than 98%, while the FSM was 90%, approximately.

It was found that the majority of robotic canes that had systems to determine how user forces interacted either relied on pricey sensors or needed significant structural changes are required to install an equivalent system. Therefore, a novel motion control system considered economical, straightforward, and understandable was implemented and used to solve this challenge. Initially, virtual mechanical simulations helped out finding that strain gauges would not have the necessary resolution to detect user's intentions. Thus, small FSRs in the junction between cane's parts was considered the most suitable option since it can actually detect well the applied forces by the user. Three FSRs were installed in the cane's handle to detect the user's gait phase since that area is vulnerable to pressures directly put on by the user. The cane-type robot is not yet capable of detecting falls.

- **RQ3:** *What is the best machine learning and deep learning-based strategy, as well as the most suitable features, to implement for real-time ADL and fall events recognition?*

Chapter 6 answered this RQ. Recognise ADLs and fall events reveals to be challenging according to the scientific literature. A comparative analysis was performed to discover the best set of features and AI-based model for this particular classification problem. The Ensemble Learning classifier, using as input the first 65 features ranked by PCA, achieved the highest overall performance amongst all combinations tested: i) 10-5-Fold CV - 99.08%, 99.39%, 97.72%, 99.47%, 99.43%, and 97.00% for ACC, SENS, SPEC, precision, F1-Score and MCC, respectively, for a 1s window; and ii) Test data - 99.65%, 100%, 84.44%,99.64%, 99.82% and 91.73% for ACC, SENS, SPEC, precision, F1-Score and MCC, respectively, for a 1s window. These main results are meaningful since they overcome the scientific literature using more ADLs.

- **RQ4:** *Are the biological-inspired CPG controllers and the threshold-based algorithms able to effectively track human motion variables and timely detect slip perturbation occurrences, respectively?*

Chapter 7 answered this RQ. The CPG algorithms were effective in producing an acceptable estimation of the monitoring signals, according to the findings produced. The comparatively small mean error values observed throughout the simulations illustrate how these biologically inspired controllers created output signals with a comparable shape and in phase with the knee angle and shank angular velocity variables. Additionally, the slip-induced LOBs were successfully recognised using the adaptive threshold algorithm. This algorithm produced the best overall results when used to monitor the knee angle of the perturbed leg. It did so with a mean detection time of 250 ms, a mean number of 0.652 false perturbations detected for every correct perturbation detected, and a detection ACC of real perturbations close to 80%. These findings point to a respectable performance of the perturbation detection method in light of the previously mentioned detection requirements.

- **RQ5:** *Can a VR headset introduce imbalances through visual perturbations, causing postural reactions typical of a fall?*

Chapter 8 answered this RQ. The results presented in Chapter 8 statistically support that it is possible and effective to induce postural reactions similar to a real-world fall by introducing visual disturbances via an HMD. The most effective perturbations to induce imbalances are rotations in the Roll, in the CCW direction and with amplitudes of 20° and 30°. The visual disturbance that tries to simulate a syncope, called "Bedroom Syncope", also excelled in the effectiveness and strength of inducing imbalance, as well as AP-axis Translation perturbations, albeit to a lesser extent. Moreover, the electrodermal variables did not show sufficient statistical relevance to infer in which situations the participants were under greater anxiety and stress. Finally, there was no discernible difference in postural reactions with and without the avatar. When vertigo circumstances had an effect on parameters indicating loss of balance, the values were equal in situations with and without avatar.

9.3 Future Directions

This section highlights some of the potential areas for scientific and technological advancement. Future directions will be scrutinised per chapter. Work resultant from Chapter 4 helped identifying the following ideas for future work: i) long-term application is to test both approaches with cane's users and investigate whether the achievements of this study translate with similar performances in continuous real-life usage; ii) Use or collect real-world fall data as input for the developed algorithms; iii) create and implement a new hardware architecture to update components; iv) invest in the interoperability of this system; v) comparison analysis to identify which tool should be in a stand-alone version; vi) new conditions must be implemented in the FSM for cane event detection; vii) deep learning must be optimised in order to obtain better performances; and viii) explore new relevant features for gait analysis, e.g. foot clearance.

Future work within the scope of the cane-type robot includes: i) the implementation of a battery with greater capacity, so that the cane has a longer period of use, enabling its applications to domestic use and at hospital areas; ii) the application of fall detection and prevention strategies; iii) the implementation of a motor control strategy to achieve smoother and more controlled movement of the cane to match the user's changes in speed and acceleration during gait; iv) the implementation of an alert system, triggered when a fall is detected, that contacts the hospital emergency unit and the user's emergency contacts with the location of where the fall occurred; v) the exploration of a gravity compensation strategy, through the data acquired by the cane's inertial system, to prevent the cane from slipping or falling while moving on inclined planes, using the torque applied by the motors; vi) human in the loop gait trials to obtain results in a real-life context with the elderly or people with reduced mobility.

Regarding the FRA strategy and its *Activity Recognition Module*, it is crucial to consider the next steps: i) perform usability tests and develop the first prototype of the eHealth platform, containing all modules idealised; ii) miniaturise the enhanced smart waistband to a level closer to be something commercialised; iii) the hardware must include other sensors capable of assessing the environment; iv) improve activity recognition by reducing computational costs; v) data augmentation processes can be used in order to obtain an even more diversified dataset; vi) new key stakeholders such as older individuals and healthcare experts should be involved in any future work to build a super dataset of data similarly to the ones developed by FARSEEING and SensAction-AAL but with more sensory systems, including physiological sensors; and vii) Ablation studies should be conducted to determine the impact of the various stages of each architecture and module.

Several improvement opportunities within the scope of slip-like perturbation detection were identified along the Chapter 7, and which should be addressed in future work: i) optimisation of the adaptive threshold algorithm to improve the reliability of the perturbation detection towards the algorithm's adaptation to the real-world settings; ii) AI algorithms should be tested to understand their possible application and performance towards the slip-like perturbation detection; iii) more variables, kinematic and physiological, should be addressed in the future for perturbation detection; iv) find more objective and automatic procedures to compute optimal parameters, i.e., threshold value and the window size; v) development of an inter-subject perturbation detection approach; vi) deeply explore CPG's parameters to reduce the error and convergence time; vii) continue the study but now using more conditions from the experimental protocol; viii) collect data while using elders as participants; ix) replicate the experimental protocol but now with a wearable robotic device to account the participant's effort of moving when equipped with the device; x) consider the gait phase to classify different types of perturbations; and xi) integrate the CPG controller algorithm into an electronic development board and connect it to the knee orthosis system.

Flaws were identified throughout the Chapter 8 within the scope of VE developed and they are as follows: i) make labelling fully automated (e.g. Trip perturbation can be automatically labelled using directly data from Xsens); ii) allocation of a control group will be beneficial, specially for PBT; and iii) improve some functionalities such as, moving the avatar for a specific place correctly and save Unity Log file in a ".txt". Finally, EEG has been used previously, specially among the VR-based articles found for the state of the art (Section 2.6). It should be used more frequently, so researchers do not focus exclusively on kinematics to explore different patterns and analyses while studying the compensatory reaction to a specific type of fall.

Bibliography

[1] P. Tasheva, P. Vollenweider, V. Kraege, G. Roulet, O. Lamy, P. Marques-Vidal, and M. Meán. "Association between Physical Activity Levels in the Hospital Setting and Hospital-Acquired Functional Decline in Elderly Patients." In: *JAMA Network Open* 3.1 (2020). issn: 25743805. doi: 10.1001/jamanetworkopen.2019.20185. url: https://pubmed.ncbi.nlm.nih.gov/32003817/.

[2] J. E. Gaugler, S. Duval, K. A. Anderson, and R. L. Kane. "Predicting nursing home admission in the U.S: A meta-analysis." In: *BMC Geriatrics* 7.1 (2007), pp. 1–14. issn: 14712318. doi: 10.1186/1471-2318-7-13.

[3] WHO: World Health Organization. *Falls - WHO*. 2022. url: http://www.who.int/news-room/fact-sheets/detail/falls (visited on 07/10/2022).

[4] I. Maidan, T. Freedman, R. Tzemah, N. Giladi, A. Mirelman, and J. Hausdorff. "Introducing a new definition of a near fall: Intra-rater and inter-rater reliability." In: *Gait & Posture* 39.1 (Jan. 2014), pp. 645–647. issn: 0966-6362. doi: 10.1016/J.GAITPOST.2013.07.123.

[5] A. Bergland. "Fall risk factors in community-dwelling Elderly People." In: *Norsk Epidemiologi* 22.2 (2012), pp. 151–164. issn: 08032491. doi: 10.5324/nje.v22i2.1561.

[6] G. Bergen, M. R. Stevens, R. Kakara, and E. R. Burns. "Understanding Modifiable and Unmodifiable Older Adult Fall Risk Factors to Create Effective Prevention Strategies." In: *American Journal of Lifestyle Medicine* 15.6 (2021), pp. 580–589. issn: 15598284. doi: 10.1177/1559827619880529. url: https://pubmed.ncbi.nlm.nih.gov/34916876/.

[7] A. Steiner. "Effects of physical activity on postural stability." In: *Age and ageing* 30 Suppl 4.SUPPL. 3 (2001), pp. 33–39. issn: 0002-0729. doi: 10.1093/AGEING/30.SUPPL_4.33. url: https://pubmed.ncbi.nlm.nih.gov/11769787/.

[8] B. Moreland, R. Kakara, and A. Henry. "Trends in Nonfatal Falls and Fall-Related Injuries Among Adults Aged ≥65 Years — United States, 2012–2018." In: *MMWR. Morbidity and Mortality Weekly Report* 69.27 (2020), pp. 875–881. issn: 0149-2195. doi: 10.15585/mmwr.mm6927a5.

[9] European Mortality Database. *Deaths - Accidental falls*. [Accessed: 24- Jul- 2022]. 2022. url: https://gateway.euro.who.int/en/indicators/hfamdb_17-deaths-accidental-falls/ (visited on 07/24/2022).

[10] S.-H. Park. "Tools for assessing fall risk in the elderly: a systematic review and meta-analysis." In: *Aging clinical and experimental research* 30.1 (Jan. 2018), pp. 1–16. issn: 1720-8319 (Electronic). doi: 10.1007/s40520-017-0749-0.

[11] L. Z. Rubenstein. "Falls in older people: Epidemiology, risk factors and strategies for prevention." In: *Age and Ageing* 35.SUPPL.2 (2006), pp. 37–41. issn: 00020729. doi: 10.1093/ageing/afl084.

[12] C. B. Franse, J. A. Rietjens, A. Burdorf, A. Van Grieken, I. J. Korfage, A. Van Der Heide, F. Mattace Raso, E. Van Beeck, and H. Raat. "A prospective study on the variation in falling and fall risk among community-dwelling older citizens in 12 European countries." In: *BMJ Open* 7.6 (June 2017). issn: 20446055. doi: 10.1136/bmjopen-2017-015827.

[13] S. D. Berry and R. R. Miller. "Falls: Epidemiology, pathophysiology, and relationship to fracture." In: *Current Osteoporosis Reports* 6.4 (2008), pp. 149–154. issn: 15441873. doi: 10.1007/s11914-008-0026-4.

[14] E. R. Burns, J. A. Stevens, and R. Lee. "The direct costs of fatal and non-fatal falls among older adults — United States." In: *Journal of Safety Research* 58 (2016), pp. 99–103. issn: 00224375. doi: 10.1016/j.jsr.2016.05.001.

[15] B. Cates, T. Sim, H. M. Heo, B. Kim, H. Kim, and J. H. Mun. "A novel detection model and its optimal features to classify falls from low- and high-acceleration activities of daily life using an insole sensor system." In: *Sensors (Switzerland)* 18.4 (2018). issn: 14248220. doi: 10.3390/s18041227. url: http://www.mdpi.com/1424-8220/18/4/1227.

[16] A. L. Romão and S. Nunes. "Quedas em internamento hospitalar-causas, consequências e custos: Estudo de caso numa unidade hospitalar de Lisboa." In: *Portuguese Journal of Public Health* (2018). issn: 25043145. doi: 10.1159/000488073.

[17] United Nations - Department of Economic and Social Affairs. *World Population Prospects - Probabilistic Projections*. 2019. url: https://population.un.org/wpp/Download/Probabilistic/Population/ (visited on 04/25/2020).

[18] R. Igual, C. Medrano, and I. Plaza. "Challenges, issues and trends in fall detection systems." In: *BioMedical Engineering Online* 12.1 (2013), p. 66. issn: 1475925X. doi: 10.1186/1475-925X-12-66.

[19] R. Rajagopalan, I. Litvan, and T.-P. Jung. "Fall Prediction and Prevention Systems: Recent Trends, Challenges, and Future Research Directions." In: *SENSORS* 17.11 (Nov. 2017). issn: 1424-8220. doi: 10.3390/s17112509.

[20] M. Hemmatpour, R. Ferrero, B. Montrucchio, and M. Rebaudengo. *A review on fall prediction and prevention system for personal devices: Evaluation and experimental results*. 2019. doi: 10.1155/2019/9610567.

[21] E. Stack. "Falls are unintentional: Studying simulations is a waste of faking time." In: *Journal of Rehabilitation and Assistive Technologies Engineering* 4 (2017). issn: 2055-6683. doi: 10.1177/2055668317732945.

[22] M. Kangas, I. Vikman, L. Nyberg, R. Korpelainen, J. Lindblom, and T. Jämsä. "Comparison of real-life accidental falls in older people with experimental falls in middle-aged test subjects." In: *Gait & Posture* 35.3 (2012), pp. 500–505. issn: 09666362. doi: 10.1016/j.gaitpost.2011.11.016.

[23] A. Paraschiv-Ionescu, C. J. Büla, K. Major, C. Lenoble-Hoskovec, H. Krief, C. El-Moufawad, and K. Aminian. "Concern about Falling and Complexity of Free-Living Physical Activity Patterns in Well-Functioning Older Adults." In: *Gerontology* 64.6 (2018), pp. 603–611. issn: 14230003. doi: 10.1159/000490310.

[24] A. Danielsen, H. Olofsen, and B. A. Bremdal. "Increasing fall risk awareness using wearables: A fall risk awareness protocol." In: *Journal of Biomedical Informatics* 63 (2016), pp. 184–194. issn: 15320464. doi: 10.1016/j.jbi.2016.08.016. url: https://www.sciencedirect.com/science/article/pii/S1532046416300983.

[25] L. Montesinos, R. Castaldo, and L. Pecchia. "Wearable Inertial Sensors for Fall Risk Assessment and Prediction in Older Adults." In: *IEEE Transactions on Neural Systems and Rehabilitation Engineering* 26.3 (2018), pp. 573–582. issn: 1558-0210. doi: 10.1109/TNSRE.2017.2771383.

[26] R. Rucco, A. Sorriso, M. Liparoti, G. Ferraioli, P. Sorrentino, M. Ambrosanio, and F. Baselice. *Type and location of wearable sensors for monitoring falls during static and dynamic tasks in healthy elderly: A review*. 2018. doi: 10.3390/s18051613.

[27] M. Bjerk, T. Brovold, D. A. Skelton, and A. Bergland. "Associations between health-related quality of life, physical function and fear of falling in older fallers receiving home care." In: *BMC Geriatrics* 18.1 (2018), pp. 1–8. issn: 14712318. doi: 10.1186/s12877-018-0945-6.

[28] A. Weiss, M. Brozgol, M. Dorfman, T. Herman, S. Shema, N. Giladi, and J. M. Hausdorff. "Does the evaluation of gait quality during daily life provide insight into fall risk? A novel approach using 3-Day accelerometer recordings." In: *Neurorehabilitation and Neural Repair* 27.8 (2013), pp. 742–752. issn: 15459683. doi: 10.1177/1545968313491004.

[29] V. C. Kumar, S. Ha, G. Sawicki, and C. K. Liu. "Learning a Control Policy for Fall Prevention on an Assistive Walking Device." In: *Proceedings - IEEE International Conference on Robotics and Automation* (2020), pp. 4833–4840. issn: 10504729. doi: 10.1109/ICRA40945.2020.9196798. eprint: 1909.10488.

[30] M. Y. Osaba, D Martelli, A Prado, S. K. Agrawal, and A. K. Lalwani. "Age-related differences in gait adaptations during overground walking with and without visual perturbations using a virtual reality headset." In: *Scientific Reports* 10.1 (2020). doi: 10.1038/s41598-020-72408-6.

[31] J. Klenk, L. Schwickert, L. Palmerini, S. Mellone, A. Bourke, E. A. Ihlen, N. Kerse, K. Hauer, M. Pijnappels, M. Synofzik, K. Srulijes, W. Maetzler, J. L. Helbostad, W. Zijlstra, K. Aminian, C. Todd, L. Chiari, C. Becker, for the FARSEEING Consortium, U. Lindemann, J. Salb, and S. Bandinelli. "The FARSEEING real-world fall repository: a large-scale collaborative database to collect and share sensor signals from real-world falls." In: *European Review of Aging and Physical Activity* 13.1 (2016). issn: 18137253. doi: 10.1186/s11556-016-0168-9.

[32] A. Sucerquia, J. D. López, and J. F. Vargas-Bonilla. "SisFall: A fall and movement dataset." In: *Sensors (Switzerland)* 17.1 (2017). issn: 14248220. doi: 10.3390/s17010198.

[33] U. Lindemann, S. Nicolai, D. Beische, C. Becker, K. Srulijes, E. Dietzel, S. Bauer, D. Berg, and W. Maetzler. "Clinical and dual-tasking aspects in frequent and infrequent fallers with progressive supranuclear palsy." In: *Movement Disorders* 25.8 (2010), pp. 1040–1046. issn: 15318257. doi: 10.1002/mds.23023.

[34] L. Wang, M. Peng, and Q. Zhou. "Pre-Impact Fall Detection Based on Multi-Source CNN Ensemble." In: *IEEE Sensors Journal* 20.10 (2020), pp. 5442–5451. issn: 15581748. doi: 10.1109/JSEN.2020.2970452.

[35] S. Kim, K.-S. Joo, J. Liu, and J.-H. Sohn. "Lower extremity kinematics during forward heel-slip." In: 27.S1 (2019), pp. 345–356. issn: 1878-7401 (Electronic). doi: 10.3233/THC-199032.

[36] N. F. Ribeiro, J. André, L. Costa, and C. P. Santos. "Development of a Strategy to Predict and Detect Falls Using Wearable Sensors." In: *Journal of Medical Systems* 43.5 (2019). issn: 1573689X. doi: 10.1007/s10916-019-1252-2.

[37] M. Mioskowska, D. Stevenson, M. Onu, and M. Trkov. "Compressed gas actuated knee assistive exoskeleton for slip-induced fall prevention during human walking." In: *IEEE/ASME International Conference on Advanced Intelligent Mechatronics, AIM*. Vol. 2020-July. 2020, pp. 735–740. isbn: 9781728167947. doi: 10.1109/AIM43001.2020.9158992.

[38] J. Hamm, A. G. Money, A. Atwal, and I. Paraskevopoulos. "Fall prevention intervention technologies: A conceptual framework and survey of the state of the art." In: *Journal of Biomedical Informatics* 59 (2016), pp. 319–345. issn: 15320464. doi: 10.1016/j.jbi.2015.12.013.

[39] M. Awais, L. Chiari, E. A. F. Ihlen, J. L. Helbostad, and L. Palmerini. "Physical Activity Classification for Elderly People in Free-Living Conditions." In: *IEEE Journal of Biomedical and Health Informatics* 23.1 (2019), pp. 197–207. issn: 21682208. doi: 10.1109/JBHI.2018.2820179.

[40] V. Monaco, P. Tropea, F. Aprigliano, D. Martelli, A. Parri, M. Cortese, R. Molino-Lova, N. Vitiello, and S. Micera. "An ecologically-controlled exoskeleton can improve balance recovery after slippage." In: *Scientific Reports* 7 (2017). issn: 20452322. doi: 10.1038/srep46721.

[41] M. Geravand, W. Rampeltshammer, and A. Peer. "Control of mobility assistive robot for human fall prevention." In: *IEEE International Conference on Rehabilitation Robotics*. Vol. 2015-September. 2015, pp. 882–887. isbn: 9781479918072. doi: 10.1109/ICORR.2015.7281314.

[42] W. Xu, J. Huang, and L. Cheng. "A novel coordinated motion fusion-based walking-aid robot system." In: *Sensors (Switzerland)* 18.9 (2018). issn: 14248220. doi: 10.3390/s18092761. url: http://www.mdpi.com/1424-8220/18/9/2761.

[43] P. Di, Y. Hasegawa, S. Nakagawa, K. Sekiyama, T. Fukuda, J. Huang, and Q. Huang. "Fall detection and prevention control using walking-aid cane robot." In: *IEEE/ASME Transactions on Mechatronics* 21.2 (2016), pp. 625–637. issn: 10834435. doi: 10.1109/TMECH.2015.2477996.

[44] T. Bao, W. J. Carender, C. Kinnaird, V. J. Barone, G. Peethambaran, S. L. Whitney, M. Kabeto, R. D. Seidler, and K. H. Sienko. "Effects of long-term balance training with vibrotactile sensory augmentation among community-dwelling healthy older adults: A randomized preliminary study." In: *Journal of NeuroEngineering and Rehabilitation* 15.1 (Jan. 2018), p. 5. issn: 17430003. doi: 10.1186/s12984-017-0339-6.

[45] B. E. Moyer, M. S. Redfern, and R. Cham. "Biomechanics of trailing leg response to slipping - Evidence of interlimb and intralimb coordination." In: *Gait and Posture* 29.4 (2009), pp. 565–570. issn: 09666362. doi: 10.1016/j.gaitpost.2008.12.012.

[46] J. Figueiredo, P. Félix, C. P. Santos, and J. C. Moreno. "Towards human-knee orthosis interaction based on adaptive impedance control through stiffness adjustment." In: *IEEE International Conference on Rehabilitation Robotics* (2017), pp. 406–411. issn: 19457901. doi: 10.1109/ICORR.2017.8009281.

[47] C. P. Santos, N. Alves, and J. C. Moreno. "Biped Locomotion Control through a Biomimetic CPG-based Controller." In: *Journal of Intelligent and Robotic Systems: Theory and Applications* 85.1 (2017), pp. 47–70. issn: 15730409. doi: 10.1007/s10846-016-0407-3. url: http://dx.doi.org/10.1007/s10846-016-0407-3.

[48] C. Ferreira and C. P. Santos. "Robotic locomotion combining central pattern generators and reflexes." In: *Proceedings - 2015 IEEE 4th Portuguese Meeting on Bioengineering, ENBENG 2015* 170 (2015), pp. 79–91. issn: 09252312. doi: 10.1109/ENBENG.2015.7088893.

[49] H. Gonçalves, R. Moreira, A. Rodrigues, and C. Santos. "Finding Parameters around the Abdomen for a Vibrotactile System: Healthy and Patients with Parkinson's Disease." In: *Journal of Medical Systems* 42.11 (2018). issn: 1573689X. doi: 10.1007/s10916-018-1087-2.

[50] K. T. Ulrich and S. D. Eppinger. *Product Design and Development: Fifth Edition*. 2012, pp. 124, 127–128. isbn: 9780071086950. url: http://www.ulrich-eppinger.net/.

[51] S. V. Adamovich, G. G. Fluet, E. Tunik, and A. S. Merians. "Sensorimotor training in virtual reality: A review." In: *NeuroRehabilitation* 25.1 (2009), pp. 29–44. issn: 10538135. doi: 10.3233/NRE-2009-0497.

[52] K. E. Laver, B. Lange, S. George, J. E. Deutsch, G. Saposnik, and M. Crotty. "Virtual reality for stroke rehabilitation." In: *Cochrane Database of Systematic Reviews* 2017.11 (2017). issn: 1469493X. doi: 10.1002/14651858.CD008349.pub4.

[53] A. Henderson, N. Korner-Bitensky, and M. Levin. *Virtual reality in stroke rehabilitation: A systematic review of its effectiveness for upper limb motor recovery*. 2007. doi: 10.1310/tsr1402-52.

[54] M. W. Rivolta, M Aktaruzzaman, G Rizzo, C. L. Lafortuna, M Ferrarin, G Bovi, D. R. Bonardi, and R Sassi. "Automatic vs. clinical assessment of fall risk in older individuals: A proof of concept." In: *2015 37th Annual International Conference of the IEEE Engineering in Medicine and Biology Society (EMBC)*. 2015, pp. 6935–6938. doi: 10.1109/EMBC.2015.7319987.

[55] W Tang, G Fulk, S Zeigler, T Zhang, and E Sazonov. "Estimating Berg Balance Scale and Mini Balance Evaluation System Test Scores by Using Wearable Shoe Sensors." In: *2019 IEEE EMBS International Conference on Biomedical Health Informatics (BHI)*. 2019, pp. 1–4. doi: 10.1109/BHI.2019.8834631.

[56] M. Rivolta, M. Aktaruzzaman, G. Rizzo, C. Lafortuna, M. Ferrarin, G. Bovi, D. Bonardi, A. Caspani, and R. Sassi. "Evaluation of the Tinetti score and fall risk assessment via accelerometry-based movement analysis." In: *Artificial Intelligence in Medicine* 95 (2019), pp. 38–47. doi: 10.1016/j.artmed.2018.08.005.

[57] A Shahzad, S Ko, S Lee, J Lee, and K Kim. "Quantitative Assessment of Balance Impairment for Fall-Risk Estimation Using Wearable Triaxial Accelerometer." In: *IEEE Sensors Journal* 17.20 (2017), pp. 6743–6751. issn: 1558-1748. doi: 10.1109/JSEN.2017.2749446.

[58] S. Saporito, M. A. Brodie, K. Delbaere, J. Hoogland, H. Nijboer, S. M. Rispens, G. Spina, M. Stevens, and J. Annegarn. "Remote timed up and go evaluation from activities of daily living reveals changing mobility after surgery." In: *Physiological Measurement* 40.3 (Mar. 2019). issn: 0967-3334. doi: 10.1088/1361-6579/ab0d3e.

[59] F. Buisseret, L. Catinus, R. Grenard, L. Jojczyk, D. Fievez, V. Barvaux, and F. Dierick. "Timed Up and Go and Six-Minute Walking Tests with Wearable Inertial Sensor: One Step Further for the Prediction of the Risk of Fall in Elderly Nursing Home People." In: *Sensors (Basel, Switzerland)* 20.11 (2020). issn: 1424-8220 (Electronic). doi: 10.3390/s20113207.

[60] Z. Yang, C. Song, F. Lin, J. Langan, and W. Xu. "A Smart Environment-Adapting Timed-Up-and-Go System Powered by Sensor-Embedded Insoles." In: *IEEE INTERNET OF THINGS JOURNAL* 6.2 (2019), pp. 1298–1305. issn: 2327-4662. doi: 10.1109/JIOT.2018.2844837.

[61] B Vieira, L Pereira, R Freitas, M Terroso, and R Simoes. "A gamified application for assessment of balance and fall prevention." In: *2015 10th Iberian Conference on Information Systems and Technologies (CISTI)*. 2015, pp. 1–6. doi: 10.1109/CISTI.2015.7170473.

[62] A Dzhagaryan, A Milenkovic, E Jovanov, and M Milosevic. "Smart Button: A wearable system for assessing mobility in elderly." In: *2015 17th International Conference on E-health Networking, Application Services (HealthCom)*. 2015, pp. 416–421. doi: 10.1109/HealthCom.2015.7454536.

[63] W. Saadeh, S. Butt, and M. Altaf. "A Patient-specific single sensor iot-based wearable fall prediction and detection system." In: *IEEE Transactions on Neural Systems and Rehabilitation Engineering* 27.5 (2019), pp. 995–1003. doi: 10.1109/TNSRE.2019.2911602.

[64] A Leone, G Rescio, L Giampetruzzi, and P Siciliano. "Smart EMG-based Socks for Leg Muscles Contraction Assessment." In: *2019 IEEE International Symposium on Measurements Networking (M N)*. 2019, pp. 1–6. doi: 10.1109/IWMN.2019.8804991.

[65] G Rescio, A Leone, A Caroppo, and P Siciliano. "A preliminary study on fall risk evaluation through electromiography systems." In: *2015 International Conference on Interactive Mobile Communication Technologies and Learning (IMCL)*. Nov. 2015, pp. 219–221. doi: 10.1109/IMCTL.2015.7359590.

[66] A Leone, G Rescio, and P Siciliano. "Fall risk evaluation by surface electromyography technology." In: *2017 International Conference on Engineering, Technology and Innovation (ICE/ITMC)*. 2017, pp. 1092–1095. doi: 10.1109/ICE.2017.8280003.

[67] S Parvaneh, B Najafi, N Toosizadeh, I. B. Riaz, and J Mohler. "Is there any association between ventricular ectopy and falls in community-dwelling older adults?" In: *2016 Computing in Cardiology Conference (CinC)*. 2016, pp. 433–436.

[68] V. Annese and D. De Venuto. "FPGA based architecture for fall-risk assessment during gait monitoring by synchronous EEG/EMG." In: *2015 6th International Workshop on Advances in Sensors and Interfaces (IWASI)*. 2015, pp. 116–121. doi: 10.1109/IWASI.2015.7184953.

[69] M Selvaraj, V Baltzopoulos, A Shaw, C. N. Maganaris, J Cullen, T O'Brien, and P Kot. "Stair Fall Risk Detection Using Wearable Sensors." In: *2018 11th International Conference on Developments in eSystems Engineering (DeSE)*. 2018, pp. 108–112. doi: 10.1109/DeSE.2018.00023.

[70] G. Vavoulas, M. Pediaditis, C. Chatzaki, E. Spanakis, and M. Tsiknakis. "The MobiFall Dataset:: Fall Detection and Classification with a Smartphone." In: *International Journal of Monitoring and Surveillance Technologies Research* 2 (2016), pp. 44–56. doi: 10.4018/ijmstr.2014010103.

[71] T. Shany, K. Wang, Y. Liu, N. H. Lovell, and S. J. Redmond. "Review: Are we stumbling in our quest to find the best predictor? Over-optimism in sensor-based models for predicting falls in older adults." In: *Healthcare Technology Letters* 2.4 (2015), pp. 79–88. doi: https://doi.org/10.1049/htl.2015.0019. url: https://ietresearch.onlinelibrary.wiley.com/doi/abs/10.1049/htl.2015.0019.

[72] D. Moher, A. Liberati, J. Tetzlaff, and D. G. Altman. "Preferred reporting items for systematic reviews and meta-analyses: the PRISMA statement." In: *BMJ* 339 (2009). doi: 10.1136/bmj.b2535. url: https://www.bmj.com/content/339/bmj.b2535.

[73] Q. Yan, J. Huang, C. Xiong, Z. Yang, and Z. Yang. "Data-Driven Human-Robot Coordination Based Walking State Monitoring with Cane-Type Robot." In: *IEEE Access* 6 (2018), pp. 8896–8908. issn: 21693536. doi: 10.1109/ACCESS.2018.2806563.

[74] C. Tao, Q. Yan, and Y. Li. "Hierarchical Shared Control of Cane-Type Walking-Aid Robot." In: *Journal of Healthcare Engineering* 2017 (2017). Ed. by C. Hu, p. 8932938. issn: 2040-2295. doi: 10.1155/2017/8932938. url: https://doi.org/10.1155/2017/8932938.

[75] M. A. Naeem and S. F. M. Assal. "Development of a 4-DOF cane robot to enhance walking activity of elderly." In: *Proceedings of the Institution of Mechanical Engineers, Part C: Journal of Mechanical Engineering Science* 236.2 (2019), pp. 1169–1187. doi: 10.1177/0954406219830440. url: https://doi.org/10.1177/0954406219830440.

[76] P. Di, J. Huang, S. Nakagawa, K. Sekiyama, and T. Fukuda. "Fall detection and prevention in the elderly based on the ZMP stability control." In: *Proceedings of IEEE Workshop on Advanced Robotics and its Social Impacts, ARSO*. 2013, pp. 82–87. isbn: 9781479923694. doi: 10.1109/ARSO.2013.6705510.

[77] P. Van Lam and Y. Fujimoto. "A Robotic Cane for Balance Maintenance Assistance." In: *IEEE Transactions on Industrial Informatics* 15.7 (2019), pp. 3998–4009. issn: 19410050. doi: 10.1109/TII.2019.2903893.

[78] P. Van Lam and Y. Fujimoto. "Two-Wheel Cane for Walking Assistance." In: *2018 International Power Electronics Conference, IPEC-Niigata - ECCE Asia 2018*. 2018, pp. 571–574. doi: 10.23919/IPEC.2018.8507580.

[79] S. Suzuki, Y. Hirata, and K. Kosuge. “Development of Intelligent Passive Cane controlled by servo brakes.” In: *RO-MAN 2009 - The 18th IEEE International Symposium on Robot and Human Interactive Communication*. 2009, pp. 97–102. doi: 10.1109/ROMAN.2009.5326139.

[80] T. Ito and G. Oshita. “Development of MR fluid-based gait assist cane for elderly people.” In: *2015 IEEE International Conference on Advanced Intelligent Mechatronics (AIM)*. 2015, pp. 694–699. doi: 10.1109/AIM.2015.7222618.

[81] M. Trkov, S. Wu, K. Chen, J. Yi, T. Liu, and Q. Zhao. “Design of a Robotic Knee Assistive Device (ROKAD) for Slip-Induced Fall Prevention during Walking.” In: *IFAC-PapersOnLine* 50.1 (2017), pp. 9802–9807. issn: 2405-8963. doi: https://doi.org/10.1016/j.ifacol.2017.08.887. url: https://www.sciencedirect.com/science/article/pii/S2405896317313538.

[82] Y. Hirata, S. Komatsuda, and K. Kosuge. “Fall prevention control of passive intelligent walker based on human model.” In: *2008 IEEE/RSJ International Conference on Intelligent Robots and Systems, IROS*. 2008, pp. 1222–1228. isbn: 9781424420582. doi: 10.1109/IROS.2008.4651173.

[83] S. Taghvaei, Y. Hirata, and K. Kosuge. “Vision-based human state estimation to control an intelligent passive walker.” In: *2010 IEEE/SICE International Symposium on System Integration: SI International 2010 - The 3rd Symposium on System Integration, SII 2010, Proceedings*. 2010, pp. 146–151. isbn: 9781424493159. doi: 10.1109/SII.2010.5708316.

[84] S. Taghvaei and K. Kosuge. “Image-based fall detection and classification of a user with a walking support system.” In: *Frontiers of Mechanical Engineering* 13.3 (2018), pp. 427–441. issn: 20950241. doi: 10.1007/s11465-017-0465-7.

[85] W. H. Mou, M. F. Chang, C. K. Liao, Y. H. Hsu, S. H. Tseng, and L. C. Fu. “Context-aware assisted interactive robotic walker for Parkinson’s disease patients.” In: *IEEE International Conference on Intelligent Robots and Systems*. 2012, pp. 329–334. isbn: 9781467317375. doi: 10.1109/IROS.2012.6385791.

[86] M. Azqueta-Gavaldon, I. Azqueta-Gavaldon, M. Woiczinski, K. Bötzel, and E. Kraft. “Automatic braking system and fall detection mechanism for rollators.” In: *ACM International Conference Proceeding Series*. Vol. Part F130950. 2017, pp. 158–161. isbn: 9781450352222. doi: 10.1145/3121138.3121177.

[87] S. Irgenfried and H. Wörn. “Motion control and fall prevention for an activewalker mobility aid.” In: *Mechanisms and Machine Science*. Ed. by V. Petuya, C. Pinto, and E.-C. Lovasz. Vol. 17. Mechanisms and Machine Science. Springer Netherlands, 2014, pp. 157–164. isbn: 9789400774841. doi: 10.1007/978-94-007-7485-8_20.

[88] J. Huang, W. Xu, S. Mohammed, and Z. Shu. "Posture estimation and human support using wearable sensors and walking-aid robot." In: *Robotics and Autonomous Systems* 73 (2015), pp. 24–43. issn: 09218890. doi: 10.1016/j.robot.2014.11.013. url: http://dx.doi.org/10.1016/j.robot.2014.11.013.

[89] F. Bagala, C. Becker, A. Cappello, L. Chiari, K. Aminian, J. M. Hausdorff, W. Zijlstra, and J. Klenk. "Evaluation of Accelerometer-Based Fall Detection Algorithms on Real-World Falls." In: *PLOS ONE* 7.5, 1 (2012). issn: 1932-6203. doi: 10.1371/journal.pone.0037062.

[90] C. Soaz, C. Lederer, and M. Daumer. "A new method to estimate the real upper limit of the false alarm rate in a 3 accelerometry-based fall detector for the elderly." In: *Proceedings of the Annual International Conference of the IEEE Engineering in Medicine and Biology Society, EMBS*. San Diego, CA, 2012, pp. 244–247. isbn: 9781424441198. doi: 10.1109/EMBC.2012.6345915.

[91] A. K. Bourke, J Klenk, L Schwickert, K Aminian, E. A. F. Ihlen, J. L. Helbostad, L Chiari, and C Becker. "Temporal and kinematic variables for real-world falls harvested from lumbar sensors in the elderly population." In: *Proceedings of the Annual International Conference of the IEEE Engineering in Medicine and Biology Society, EMBS*. Vol. 2015-Novem. Institute of Electrical and Electronics Engineers Inc., 2015, pp. 5183–5186. isbn: 9781424492718. doi: 10.1109/EMBC.2015.7319559.

[92] L Palmerini, F Bagalà, A Zanetti, J Klenk, C Becker, and A Cappello. "A wavelet-based approach to fall detection." In: *Sensors (Switzerland)* 15.5 (2015), pp. 11575–11586. issn: 14248220. doi: 10.3390/s150511575.

[93] A. K. Bourke, J Klenk, L Schwickert, K Aminian, E. A. F. Ihlen, S Mellone, J. L. Helbostad, L Chiari, and C Becker. "Fall detection algorithms for real-world falls harvested from lumbar sensors in the elderly population: A machine learning approach." In: *Proceedings of the Annual International Conference of the IEEE Engineering in Medicine and Biology Society, EMBS*. Vol. 2016-Octob. Institute of Electrical and Electronics Engineers Inc., 2016, pp. 3712–3715. isbn: 9781457702204. doi: 10.1109/EMBC.2016.7591534.

[94] O Aziz, J Klenk, L Schwickert, L Chiari, C Becker, E. J. Park, G Mori, and S. N. Robinovitch. "Validation of accuracy of SVM-based fall detection system using real-world fall and non-fall datasets." In: *PLoS ONE* 12.7 (2017). issn: 19326203. doi: 10.1371/journal.pone.0180318.

[95] J Silva, I Sousa, and J Cardoso. "Transfer learning approach for fall detection with the FARSEEING real-world dataset and simulated falls." In: *Proceedings of the Annual International Conference of the IEEE Engineering in Medicine and Biology Society, EMBS*. Vol. 2018-July. Institute of Electrical and Electronics Engineers Inc., 2018, pp. 3509–3512. isbn: 9781538636466. doi: 10.1109/EMBC.2018.8513001.

[96] S. Yu, H. Chen, and R. A. Brown. "Hidden Markov Model-Based Fall Detection with Motion Sensor Orientation Calibration: A Case for Real-Life Home Monitoring." In: *IEEE Journal of Biomedical and Health Informatics* 22.6 (2018), pp. 1847–1853. issn: 21682208. doi: 10.1109/JBHI.2017.2782079.

[97] M. V. C. Caya, G. V. Magwili, D. L. Agulto, R. J. Laranang, and L. K. G. Palomo. "Supervised Machine Learning-based Fall Detection." In: *2018 IEEE 10th International Conference on Humanoid, Nanotechnology, Information Technology,Communication and Control, Environment and Management (HNICEM)*. 2018, pp. 1–6. doi: 10.1109/HNICEM.2018.8666437.

[98] L Palmerini, J Klenk, C Becker, and L Chiari. "Accelerometer-based fall detection using machine learning: Training and testing on real-world falls." In: *Sensors (Switzerland)* 20.22 (2020), pp. 1–15. issn: 14248220. doi: 10.3390/s20226479.

[99] C Kuo, N Shishov, K Elabd, V Komisar, H Chong, T Phu, L Anderson, B Hoshizaki, A Laing, P Cripton, and S Robinovitch. "Estimating Trunk and Neck Stabilization for Avoiding Head Impact during Real-World Falls in Older Adults." In: *Proceedings of the Annual International Conference of the IEEE Engineering in Medicine and Biology Society, EMBS*. Vol. 2020-July. Institute of Electrical and Electronics Engineers Inc., 2020, pp. 4823–4826. isbn: 9781728119908. doi: 10.1109/EMBC44109.2020.9176257.

[100] L Schwickert, J Klenk, W Zijlstra, M Forst-Gill, K Sczuka, J. L. Helbostad, L Chiari, K Aminian, C Todd, and C Becker. "Reading from the black box: What sensors tell us about resting and recovery after real-world falls." In: *Gerontology* 64.1 (2018), pp. 90–95. issn: 0304324X. doi: 10.1159/000478092.

[101] J Klenk, C Becker, F Lieken, S Nicolai, W Maetzler, W Alt, W Zijlstra, J. M. Hausdorff, R. C. van Lummel, L Chiari, and U Lindemann. "Comparison of acceleration signals of simulated and real-world backward falls." In: *Medical Engineering and Physics* 33.3 (2011), pp. 368–373. issn: 13504533. doi: 10.1016/j.medengphy.2010.11.003.

[102] N. Noury, P. Rumeau, A. Bourke, G. ÓLaighin, and J. Lundy. "A proposal for the classification and evaluation of fall detectors." In: *IRBM* 29.6 (2008), pp. 340–349. issn: 1959-0318. doi: 10.1016/J.IRBM.2008.08.002. url: https://www.sciencedirect.com/science/article/pii/S1959031808001243.

[103] W. P. Berg, H. M. Alessio, E. M. Mills, and C Tong. "Circumstances and consequences of falls in independent community-dwelling older adults." In: *Age and ageing* 26.4 (July 1997), pp. 261–268. issn: 0002-0729 (Print). doi: 10.1093/ageing/26.4.261.

[104] A Gabell, M. A. Simons, and U. S. Nayak. "Falls in the healthy elderly: predisposing causes." In: *Ergonomics* 28.7 (July 1985), pp. 965–975. doi: 10.1080/00140138508963219.

[105] T. Lockhart. “Biomechanics of Human Gait - Slip and Fall Analysis.” In: *Encyclopedia of Forensic Sciences*. Elsevier Inc., 2013, pp. 466–476. isbn: 9780123821669. doi: 10.1016/B978-0-12-382165-2.00151-3.

[106] K. Karamanidis, G. Epro, C. McCrum, and M. König. “Improving Trip- and Slip-Resisting Skills in Older People: Perturbation Dose Matters.” In: *Exercise and sport sciences reviews* 48.1 (Jan. 2020), pp. 40–47. issn: 1538-3008 (Electronic). doi: 10.1249/JES.0000000000000210.

[107] C McCrum, M. H. G. Gerards, K Karamanidis, W Zijlstra, and K Meijer. “A systematic review of gait perturbation paradigms for improving reactive stepping responses and falls risk among healthy older adults.” In: *European Review of Aging and Physical Activity* 14.1 (2017). doi: 10.1186/s11556-017-0173-7.

[108] Y. Wang, T. Bhatt, X. Liu, S. Wang, A. Lee, E. Wang, and Y. C. C. Pai. “Can treadmill-slip perturbation training reduce immediate risk of over-ground-slip induced fall among community-dwelling older adults?” In: *Journal of Biomechanics* 84 (2019), pp. 58–66. issn: 18732380. doi: 10.1016/j.jbiomech.2018.12.017.

[109] X. Liu, T. Bhatt, Y. Wang, S. Wang, A. Lee, and Y. C. Pai. “The retention of fall-resisting behavior derived from treadmill slip-perturbation training in community-dwelling older adults.” In: *GeroScience* 43.2 (2021), pp. 913–926. issn: 25092723. doi: 10.1007/s11357-020-00270-5.

[110] A. R. Altman, D. S. Reisman, J. S. Higginson, and I. S. Davis. “Kinematic comparison of split-belt and single-belt treadmill walking and the effects of accommodation.” In: *Gait and Posture* 35.2 (2012), pp. 287–291. issn: 09666362. doi: 10.1016/j.gaitpost.2011.09.101.

[111] Y. Wang, S. Wang, A. Lee, Y. C. Pai, and T. Bhatt. “Treadmill-gait slip training in community-dwelling older adults: mechanisms of immediate adaptation for a progressive ascending-mixed-intensity protocol.” In: *Experimental Brain Research* 237.9 (2019), pp. 2305–2317. issn: 14321106. doi: 10.1007/s00221-019-05582-3.

[112] F. Aprigliano, S. Micera, and V. Monaco. “Pre-impact detection algorithm to identify tripping events using wearable sensors.” In: *Sensors (Switzerland)* 19.17 (2019). issn: 14248220. doi: 10.3390/s19173713.

[113] F. Yang, P. Cereceres, and M. Qiao. “Treadmill-based gait-slip training with reduced training volume could still prevent slip-related falls.” In: *Gait and Posture* 66 (2018), pp. 160–165. issn: 18792219. doi: 10.1016/j.gaitpost.2018.08.029.

[114] A. Lee, T. Bhatt, X. Liu, Y. Wang, and Y. C. Pai. “Can higher training practice dosage with treadmill slip-perturbation necessarily reduce risk of falls following overground slip?” In: *Gait and Posture* 61 (Mar. 2018), pp. 387–392. issn: 18792219. doi: 10.1016/j.gaitpost.2018.01.037.

[115] M. König, G. Epro, J. Seeley, P. Catala-Lehnen, W. Potthast, and K. Karamanidis. "Retention of improvement in gait stability over 14 weeks due to trip-perturbation training is dependent on perturbation dose." In: *Journal of Biomechanics* 84 (2018). doi: 10.1016/j.jbiomech.2018.12.011.

[116] T. A. Silver, G. M. Mokha, and C. A. Peacock. "Exploring fall training adaptations while walking." In: *Work (Reading, Mass.)* 54.3 (June 2016), pp. 699–707. issn: 1875-9270 (Electronic). doi: 10.3233/WOR-162321.

[117] A. Lee, T. Bhatt, X. Liu, Y. Wang, S. Wang, and Y.-C. C. Pai. "Can Treadmill Slip-Perturbation Training Reduce Longer-Term Fall Risk Upon Overground Slip Exposure?" In: *JOURNAL OF APPLIED BIOMECHANICS* 36.5 (2020), pp. 298–306. issn: 1065-8483. doi: 10.1123/jab.2019-0211.

[118] P. J. Patel, T. Bhatt, S. R. DelDonno, S. A. Langenecker, and S. Dusane. "Examining Neural Plasticity for Slip-Perturbation Training: An fMRI Study." In: *Frontiers in neurology* 9 (2018), p. 1181. issn: 1664-2295 (Print). doi: 10.3389/fneur.2018.01181.

[119] A. Lee, T. Bhatt, and Y.-C. Pai. "Generalization of treadmill perturbation to overground slip during gait: Effect of different perturbation distances on slip recovery." In: *JOURNAL OF BIOMECHANICS* 49.2 (Jan. 2016), pp. 149–154. issn: 0021-9290. doi: 10.1016/j.jbiomech.2015.11.021.

[120] D. Martelli, F. Aprigliano, P. Tropea, G. Pasquini, S. Micera, and V. Monaco. "Stability against backward balance loss: Age-related modifications following slip-like perturbations of multiple amplitudes." In: *Gait & posture* 53 (2017), pp. 207–214. issn: 1879-2219 (Electronic). doi: 10.1016/j.gaitpost.2017.02.002.

[121] F. Aprigliano, D. Martelli, P. Tropea, G. Pasquini, S. Micera, and V. Monaco. "Aging does not affect the intralimb coordination elicited by slip-like perturbation of different intensities." In: *Journal of neurophysiology* 118.3 (Sept. 2017), pp. 1739–1748. issn: 1522-1598 (Electronic). doi: 10.1152/jn.00844.2016.

[122] S. B. Swart, R. den Otter, and C. J. C. Lamoth. "Anticipatory control of human gait following simulated slip exposure." In: *SCIENTIFIC REPORTS* 10.1 (July 2020). issn: 2045-2322. doi: 10.1038/s41598-020-66305-1.

[123] H. Debelle, C. Harkness-Armstrong, K. Hadwin, C. N. Maganaris, and T. D. O'Brien. "Recovery From a Forward Falling Slip: Measurement of Dynamic Stability and Strength Requirements Using a Split-Belt Instrumented Treadmill." In: *Frontiers in sports and active living* 2 (2020), p. 82. issn: 2624-9367 (Electronic). doi: 10.3389/fspor.2020.00082.

[124] K. Hirata, T. Kokubun, T. Miyazawa, H. Hanawa, K. Kubota, M. Sonoo, T. Fujino, and N. Kanemura. "Relationship Between the Walking Velocity Relative to the Slip Velocity and the Corrective Response." In: *JOURNAL OF MEDICAL AND BIOLOGICAL ENGINEERING* (2020). doi: 10.1007/s40846-020-00527-6.

[125] B.-C. Lee, C.-S. Kim, and K.-H. Seo. “The Body’s Compensatory Responses to Unpredictable Trip and Slip Perturbations Induced by a Programmable Split-Belt Treadmill.” In: *IEEE TRANSACTIONS ON NEURAL SYSTEMS AND REHABILITATION ENGINEERING* 27.7 (July 2019), pp. 1389–1396. issn: 1534-4320. doi: 10.1109/TNSRE.2019.2921710.

[126] J. Mueller, T. Engel, S. Mueller, S. Kopinski, H. Baur, and F. Mayer. “Neuromuscular response of the trunk to sudden gait disturbances: Forward vs. backward perturbation.” In: *JOURNAL OF ELECTROMYOGRAPHY AND KINESIOLOGY* 30 (2016), pp. 168–176. issn: 1050-6411. doi: 10.1016/j.jelekin.2016.07.005.

[127] B.-C. Lee, B. J. Martin, T. A. Thrasher, and C. S. Layne. “A new fall-inducing technology platform: development and assessment of a programmable split-belt treadmill.” In: *2017 39TH ANNUAL INTERNATIONAL CONFERENCE OF THE IEEE ENGINEERING IN MEDICINE AND BIOLOGY SOCIETY (EMBC)*. PROCEEDINGS OF ANNUAL INTERNATIONAL CONFERENCE OF THE IEEE ENGINEERING IN MEDICINE AND BIOLOGY SOCIETY. IEEE Engn Med & Biol Soc; PubMed; MEDLINE; Korean Soc Med & Biol Engn. 2017, pp. 3777–3780. isbn: 978-1-5090-2809-2.

[128] X. Liu, S. Reschechtko, S. Wang, and Y.-C. C. Pai. “The recovery response to a novel unannounced laboratory-induced slip: The ”first trial effect”in older adults.” In: *Clinical biomechanics (Bristol, Avon)* 48 (Oct. 2017), pp. 9–14. issn: 1879-1271 (Electronic). doi: 10.1016/j.clinbiomech.2017.06.004.

[129] R. L. Wright, D. M. Peters, P. D. Robinson, T. N. Watt, and M. A. Hollands. “Older adults who have previously fallen due to a trip walk differently than those who have fallen due to a slip.” In: *Gait & posture* 41.1 (Jan. 2015), pp. 164–169. issn: 1879-2219 (Electronic). doi: 10.1016/j.gaitpost.2014.09.025.

[130] T. Bhatt, P. Patel, S. Dusane, S. R. DelDonno, and S. A. Langenecker. “Neural Mechanisms Involved in Mental Imagery of Slip-Perturbation While Walking: A Preliminary fMRI Study.” In: *FRONTIERS IN BEHAVIORAL NEUROSCIENCE* 12 (2018). issn: 1662-5153. doi: 10.3389/fnbeh.2018.00203.

[131] X. Liu, T. Bhatt, S. Wang, F. Yang, and Y.-C. C. Pai. “Retention of the “first-trialeffect{”} in gait-slip among community-living older adults.” In: *GEROSCIENCE* 39.1 (2017), pp. 93–102. issn: 2509-2715. doi: 10.1007/s11357-017-9963-0.

[132] Z Merrill, A. J. Chambers, and R Cham. “Arm reactions in response to an unexpected slip—Impact of aging.” In: *Journal of Biomechanics* 58 (2017), pp. 21–26. doi: 10.1016/j.jbiomech.2017.04.011.

[133] M. M. Nazifi, K. E. Beschorner, and P. Hur. “Association between Slip Severity and Muscle Synergies of Slipping.” In: *Frontiers in Human Neuroscience* 11 (2017). issn: 1662-5161. doi: 10.

3389/fnhum.2017.00536. url: https://www.frontiersin.org/article/10.3389/fnhum.2017.00536.

[134] C O'Connell, A Chambers, A Mahboobin, and R Cham. "Effects of slip severity on muscle activation of the trailing leg during an unexpected slip." In: *Journal of electromyography and kinesiology : official journal of the International Society of Electrophysiological Kinesiology* 28 (June 2016), pp. 61–66. issn: 1873-5711 (Electronic). doi: 10.1016/j.jelekin.2016.02.007.

[135] L. J. Allin, M. A. Nussbaum, and M. L. Madigan. "Feet kinematics upon slipping discriminate between recoveries and three types of slip-induced falls." In: *Ergonomics* 61.6 (June 2018), pp. 866–876. issn: 1366-5847 (Electronic). doi: 10.1080/00140139.2017.1413212.

[136] S. L. Arena, J. L. Davis, J. W. Grant, and M. L. Madigan. "Tripping Elicits Earlier and Larger Deviations in Linear Head Acceleration Compared to Slipping." In: *PLOS ONE* 11.11 (Nov. 2016). issn: 1932-6203. doi: 10.1371/journal.pone.0165670.

[137] L. Ding and F. Yang. "Muscle weakness is related to slip-initiated falls among community-dwelling older adults." In: *Journal of Biomechanics* 49.2 (Jan. 2016), pp. 238–243. issn: 18732380. doi: 10.1016/j.jbiomech.2015.12.009.

[138] B. W. Schulz. "A new measure of trip risk integrating minimum foot clearance and dynamic stability across the swing phase of gait." In: *JOURNAL OF BIOMECHANICS* 55 (2017), pp. 107–112. issn: 0021-9290. doi: 10.1016/j.jbiomech.2017.02.024.

[139] *Side-Dominant Science: Are You Left- or Right-Sided? - Scientific American*. url: https://www.scientificamerican.com/article/bring-science-home-dominant-side/ (visited on 07/21/2021).

[140] X. Liu, T. Bhatt, and Y.-C. C. Pai. "Intensity and generalization of treadmill slip training: High or low, progressive increase or decrease?" In: *Journal of Biomechanics* 49.2 (Jan. 2016), pp. 135–140. issn: 0021-9290. doi: 10.1016/j.jbiomech.2015.06.004.

[141] S. Wang, Y. Wang, Y.-C. C. Pai, E. Wang, and T. Bhatt. "Which Are the Key Kinematic and Kinetic Components to Distinguish Recovery Strategies for Overground Slips Among Community-Dwelling Older Adults?" In: *JOURNAL OF APPLIED BIOMECHANICS* 36.4 (2020), pp. 217–227. issn: 1065-8483. doi: 10.1123/jab.2019-0285.

[142] S. Wang, Y. Wang, Y.-C. C. Pai, E. Wang, and T. Bhatt. "Which Are the Key Kinematic and Kinetic Components to Distinguish Recovery Strategies for Overground Slips Among Community-Dwelling Older Adults?" In: *Journal of applied biomechanics* (2020), pp. 1–11. issn: 1543-2688 (Electronic). doi: 10.1123/jab.2019-0285.

[143] K. A. Inkol, A. H. Huntley, and L. A. Vallis. “Repeated Exposure to Forward Support-Surface Perturbation During Overground Walking Alters Upper-Body Kinematics and Step Parameters.” In: *JOURNAL OF MOTOR BEHAVIOR* 51.3 (2019), pp. 318–330. issn: 0022-2895. doi: 10.1080/00222895.2018.1474336.

[144] A. Sawers, Y.-C. C. Pai, T. Bhatt, and L. H. Ting. “Neuromuscular responses differ between slip-induced falls and recoveries in older adults.” In: *Journal of neurophysiology* 117.2 (2017), pp. 509–522. issn: 1522-1598 (Electronic). doi: 10.1152/jn.00699.2016.

[145] M. Ziaei, H. Mokhtarinia, F. Tabatabai Ghomshe, and M. Maghsoudipour. “Coefficient of friction, walking speed and cadence on slippery and dry surfaces: shoes with different groove depths.” In: *International journal of occupational safety and ergonomics : JOSE* 25.4 (Dec. 2019), pp. 524–529. issn: 2376-9130 (Electronic). doi: 10.1080/10803548.2017.1398922.

[146] R. Soangra and T. E. Lockhart. “Dual-Task Does Not Increase Slip and Fall Risk in Healthy Young and Older Adults during Walking.” In: *Applied bionics and biomechanics* 2017 (2017), p. 1014784. issn: 1176-2322 (Print). doi: 10.1155/2017/1014784.

[147] L. J. Allin, X. Wu, M. A. Nussbaum, and M. L. Madigan. “Falls resulting from a laboratory-induced slip occur at a higher rate among individuals who are obese.” In: *Journal of biomechanics* 49.5 (Mar. 2016), pp. 678–683. issn: 1873-2380 (Electronic). doi: 10.1016/j.jbiomech.2016.01.018.

[148] C. M. Rasmussen and N. H. Hunt. “A novel wearable device to deliver unconstrained, unpredictable slip perturbations during gait.” In: *Journal of neuroengineering and rehabilitation* 16.1 (Oct. 2019), p. 118. issn: 1743-0003 (Electronic). doi: 10.1186/s12984-019-0602-0.

[149] J. K. Er, C. J. W. Donnelly, S. K. Wee, and W. T. Ang. “Fall inducing movable platform (FIMP) for overground trips and slips.” In: *JOURNAL OF NEUROENGINEERING AND REHABILITATION* 17.1 (2020). doi: 10.1186/s12984-020-00785-0.

[150] Z. Potocanac, M. Pijnappels, S. Verschueren, J. van Dieen, and J. Duysens. “Two-stage muscle activity responses in decisions about leg movement adjustments during trip recovery.” In: *JOURNAL OF NEUROPHYSIOLOGY* 115.1 (Jan. 2016), pp. 143–156. issn: 0022-3077. doi: 10.1152/jn.00263.2015.

[151] S. Y. Lee, S. C. Kim, and Y. I. Lee. “Effect of a modified grip angle of a walker on the wrist deviation angle, muscle activation and palmar load during walker-assisted gait in elderly people.” In: *Journal of Physical Therapy Science* 29.3 (2017), pp. 405–408. issn: 09155287. doi: 10.1589/jpts.29.405.

[152] Y. Okubo, M. A. Brodie, D. L. Sturnieks, C. Hicks, H. Carter, B. Toson, and S. R. Lord. "Exposure to trips and slips with increasing unpredictability while walking can improve balance recovery responses with minimum predictive gait alterations." In: *PLOS ONE* 13.9 (2018). issn: 1932-6203. doi: 10.1371/journal.pone.0202913.

[153] S. Wang, Y.-C. Pai, and T. Bhatt. "Is There an Optimal Recovery Step Landing Zone Against Slip-Induced Backward Falls During Walking?" In: *Annals of biomedical engineering* 48.6 (June 2020), pp. 1768–1778. issn: 1573-9686 (Electronic). doi: 10.1007/s10439-020-02482-4.

[154] Y. Wang, S. Wang, R. Bolton, T. Kaur, and T. Bhatt. "Effects of task-specific obstacle-induced trip-perturbation training: proactive and reactive adaptation to reduce fall-risk in community-dwelling older adults." In: *Aging clinical and experimental research* 32.5 (May 2020), pp. 893–905. issn: 1720-8319 (Electronic). doi: 10.1007/s40520-019-01268-6.

[155] S Wang, X Liu, A Lee, and Y.-C. Pai. "Can Recovery Foot Placement Affect Older Adults' Slip-Fall Severity?" In: *Annals of Biomedical Engineering* 45.8 (2017), pp. 1941–1948. doi: 10.1007/s10439-017-1834-4.

[156] R. N. Ferreira, N. F. Ribeiro, and C. P. Santos. "Fall Risk Assessment Using Wearable Sensors: A Narrative Review." In: *Sensors* 22.3 (2022). issn: 1424-8220. doi: 10.3390/s22030984. url: https://www.mdpi.com/1424-8220/22/3/984.

[157] S. A. Chvatal, J. M. Macpherson, G. Torres-Oviedo, and L. H. Ting. "Absence of postural muscle synergies for balance after spinal cord transection." In: *Journal of neurophysiology* 110.6 (Sept. 2013), pp. 1301–1310. issn: 1522-1598 (Electronic). doi: 10.1152/jn.00038.2013.

[158] Y. Okubo, D. L. Sturnieks, M. A. Brodie, L. Duran, and S. R. Lord. "Effect of Reactive Balance Training Involving Repeated Slips and Trips on Balance Recovery Among Older Adults: A Blinded Randomized Controlled Trial." In: *The journals of gerontology. Series A, Biological sciences and medical sciences* 74.9 (2019), pp. 1489–1496. issn: 1758-535X (Electronic). doi: 10.1093/gerona/glz021.

[159] Y. Okubo, M. A. Brodie, D. L. Sturnieks, C. Hicks, and S. R. Lord. "A pilot study of reactive balance training using trips and slips with increasing unpredictability in young and older adults: Biomechanical mechanisms, falls and clinical feasibility." In: *Clinical biomechanics (Bristol, Avon)* 67 (July 2019), pp. 171–179. issn: 1879-1271 (Electronic). doi: 10.1016/j.clinbiomech.2019.05.016.

[160] M. K. Holden. "Virtual environments for motor rehabilitation: Review." In: *Cyberpsychology and Behavior* 8.3 (2005), pp. 187–211. issn: 10949313. doi: 10.1089/cpb.2005.8.187.

[161] G. Juras, A. Brachman, J. Michalska, A. Kamieniarz, M. Pawłowski, A. Hadamus, D. Białoszewski, J. Błaszczyk, and K. J. Słomka. "Standards of Virtual Reality Application in Balance Training Programs in Clinical Practice: A Systematic Review." In: *Games for Health Journal* 8.2 (2019), pp. 101–111. issn: 21617856. doi: 10.1089/g4h.2018.0034.

[162] S. Hagio and M. Kouzaki. "Visuomotor Transformation for the Lead Leg Affects Trail Leg Trajectories During Visually Guided Crossing Over a Virtual Obstacle in Humans." In: *Frontiers in Neuroscience* 14 (2020). doi: 10.3389/fnins.2020.00357.

[163] D. Martelli, B. Xia, A. Prado, and S. K. Agrawal. "Gait adaptations during overground walking and multidirectional oscillations of the visual field in a virtual reality headset." In: *Gait & Posture* 67 (Jan. 2019), pp. 251–256. issn: 0966-6362. doi: 10.1016/j.gaitpost.2018.10.029.

[164] J. D. Guzmán, D. E. Guzmán, and C. F. Rengifo. "Affordable Human Gait Analysis Using a Virtual Reality-Based Platform." In: *IEEE Revista Iberoamericana de Tecnologias del Aprendizaje* 15.4 (2020), pp. 307–313. issn: 1932-8540 VO - 15. doi: 10.1109/RITA.2020.3033219.

[165] D. M. Stramel, R. M. Carrera, S. A. Rahok, J Stein, and S. K. Agrawal. "Effects of a Person-Following Light-Touch Device During Overground Walking With Visual Perturbations in a Virtual Reality Environment." In: *IEEE Robotics and Automation Letters* 4.4 (2019), pp. 4139–4146. issn: 2377-3766 VO - 4. doi: 10.1109/LRA.2019.2931267.

[166] J. Berard, J. Fung, and A. Lamontagne. "Impact of aging on visual reweighting during locomotion." In: *Clinical Neurophysiology* 123.7 (2012), pp. 1422–1428. issn: 13882457. doi: 10.1016/j.clinph.2011.11.081.

[167] J. R. Berard, J. Fung, and A. Lamontagne. "Evidence for the use of rotational optic flow cues for locomotor steering in healthy older adults." In: *Journal of Neurophysiology* 106.3 (2011), pp. 1089–1096. issn: 00223077. doi: 10.1152/jn.00277.2011.

[168] M. Habibnezhad, J. Puckett, M. S. Fardhosseini, and L. A. Pratama. "A mixed VR and physical framework to evaluate impacts of virtual legs and elevated narrow working space on construction workers' gait pattern." In: *Proceedings of the 36th International Symposium on Automation and Robotics in Construction, ISARC 2019*. 2019, pp. 1057–1064. doi: 10.22260/isarc2019/0141.

[169] R. Frost, J. Skidmore, M. Santello, and P. Artemiadis. "Sensorimotor control of gait: A novel approach for the study of the interplay of visual and proprioceptive feedback." In: *Frontiers in Human Neuroscience* 9.FEB (2015). issn: 16625161. doi: 10.3389/fnhum.2015.00014.

[170] S. M. Peterson, E. Rios, and D. P. Ferris. "Transient visual perturbations boost short-term balance learning in virtual reality by modulating electrocortical activity." In: *JOURNAL OF NEUROPHYSIOLOGY* 120.4 (Oct. 2018), pp. 1998–2010. issn: 0022-3077. doi: 10.1152/jn.00292.2018.

[171] L Riem, J. V. Dehy, T Onushko, and S Beardsley. "Inducing Compensatory Changes in Gait Similar to External Perturbations Using an Immersive Head Mounted Display." In: *2018 IEEE Conference on Virtual Reality and 3D User Interfaces (VR)*. 2018, pp. 128–135. doi: 10.1109/VR.2018.8446432.

[172] L. I. Riem, B. D. Schmit, and S. A. Beardsley. "The Effect of Discrete Visual Perturbations on Balance Control during Gait." In: *2020 42nd Annual International Conference of the IEEE Engineering in Medicine & Biology Society (EMBC)*. 2020, pp. 3162–3165. doi: 10.1109/EMBC44109.2020.9176303.

[173] M. Drolet, E. Q. Yumbla, B. Hobbs, and P. Artemiadis. "On the Effects of Visual Anticipation of Floor Compliance Changes on Human Gait: Towards Model-based Robot-Assisted Rehabilitation." In: *Proceedings - IEEE International Conference on Robotics and Automation*. 2020, pp. 9072–9078. isbn: 9781728173955. doi: 10.1109/ICRA40945.2020.9197536.

[174] J. Liu, T. E. Lockhart, P. Parijat, J. D. McIntosh, and Y. P. Chiu. "Comparison of Slip Training in VR Environment and on Moveable Platform." In: *52nd Annual Rocky Mountain Bioengineering Symposium and 52nd International ISA Biomedical Sciences Instrumentation Symposium 2015* 51 (2015), pp. 192–200. issn: 0067-8856.

[175] P. Parijat, T. E. Lockhart, and J. Liu. "EMG and kinematic responses to unexpected slips after slip training in virtual reality." In: *IEEE Transactions on Biomedical Engineering* 62.2 (2015), pp. 593–599. doi: 10.1109/TBME.2014.2361324.

[176] P. Parijat, T. E. Lockhart, and J. Liu. "Effects of Perturbation-Based Slip Training Using a Virtual Reality Environment on Slip-induced Falls." In: *Annals of Biomedical Engineering* 43.4 (2015), pp. 958–967. issn: 15739686. doi: 10.1007/s10439-014-1128-z.

[177] S. M. Peterson and D. P. Ferris. "Differentiation in theta and beta electrocortical activity between visual and physical perturbations to walking and standing balance." In: *eNeuro* 5.4 (2018). doi: 10.1523/ENEURO.0207-18.2018.

[178] X. Zhang and T. E. Lockhart. "The impairment and recovery of dynamic walking stability during virtual environment exposure in the elderly." In: *Proceedings of the Human Factors and Ergonomics Society*. Vol. 2. 2010, pp. 1154–1158. doi: 10.1518/107118110X12829369834122.

[179] R. Sun, R. Kaur, L. Ziegelman, S. Yang, R. Sowers, and M. E. Hernandez. "Using Virtual Reality to Examine the Correlation between Balance Function and Anxiety in Stance." In: *Proceedings - 2019 IEEE International Conference on Bioinformatics and Biomedicine, BIBM 2019*. 2019, pp. 1633–1640. isbn: 9781728118673. doi: 10.1109/BIBM47256.2019.8983331.

[180] E. Chiarovano, W. Wang, P. Reynolds, and H. G. MacDougall. "Imbalance: Objective measures versus subjective self-report in clinical practice." In: *Gait & Posture* 59 (2018), pp. 217–221. issn: 18792219. doi: 10.1016/j.gaitpost.2017.10.019.

[181] H. Chander, S. N. K. K. Arachchige, C. M. Hill, A. J. Turner, S. Deb, A. Shojaei, C. Hudson, A. C. Knight, and D. W. Carruth. "Virtual-Reality-Induced Visual Perturbations Impact Postural Control System Behavior." In: *Behavioral Sciences* 9.11 (Nov. 2019). doi: 10.3390/bs9110113.

[182] "Contributions of Vision in Human Postural Control: A Virtual Reality-based Study." In: *2020 42nd Annual International Conference of the IEEE Engineering in Medicine & Biology Society (EMBC)*. 2020, pp. 3347–3350. doi: 10.1109/EMBC44109.2020.9175605.

[183] A. Mohebbi, P. Amiri, and R. E. Kearney. "Identification of human balance control responses to visual inputs using virtual reality." In: *Journal of neurophysiology* 127.4 (Apr. 2022), pp. 1159–1170. issn: 1522-1598 (Electronic). doi: 10.1152/jn.00283.2021.

[184] H. Ida, S. Mohapatra, and A. Aruin. "Control of vertical posture while elevating one foot to avoid a real or virtual obstacle." In: *Experimental Brain Research* 235.6 (2017), pp. 1677–1687. issn: 14321106. doi: 10.1007/s00221-017-4929-0.

[185] M Dennison and M D'Zmura. "Effects of unexpected visual motion on postural sway and motion sickness." In: *Applied Ergonomics* 71 (2018), pp. 9–16. doi: 10.1016/j.apergo.2018.03.015.

[186] N Bugnariu and J Fung. "Aging and selective sensorimotor strategies in the regulation of upright balance." In: *Journal of NeuroEngineering and Rehabilitation* 4 (2007). doi: 10.1186/1743-0003-4-19.

[187] M. F. Gago, D. Yelshyna, E. Bicho, H. D. Silva, L. Rocha, M. Lurdes Rodrigues, and N. Sousa. "Compensatory Postural Adjustments in an Oculus Virtual Reality Environment and the Risk of Falling in Alzheimer's Disease." In: *Dementia and Geriatric Cognitive Disorders Extra* 6.2 (2016), pp. 252–267. issn: 16645464. doi: 10.1159/000447124.

[188] D. Yelshyna, M. F. Gago, E. Bicho, V. Fernandes, N. F. Gago, L. Costa, H. Silva, M. L. Rodrigues, L. Rocha, and N. Sousa. "Compensatory postural adjustments in Parkinson's disease assessed via a virtual reality environment." In: *Behavioural Brain Research* 296 (2016), pp. 384–392. issn: 18727549. doi: 10.1016/j.bbr.2015.08.017.

[189] T Tossavainen, E Toppila, I Pyykko, P. M. Forsman, M Juhola, and J Starck. "Virtual reality in posturography." In: *IEEE Transactions on Information Technology in Biomedicine* 10.2 (2006), pp. 282–292. issn: 1558-0032 VO - 10. doi: 10.1109/TITB.2005.859874.

[190] T. W. Cleworth, R. Chua, J. T. Inglis, and M. G. Carpenter. "Influence of virtual height exposure on postural reactions to support surface translations." In: *Gait and Posture* 47 (2016), pp. 96–102. issn: 18792219. doi: 10.1016/j.gaitpost.2016.04.006.

[191] E. Chiarovano, C. de Waele, H. G. MacDougall, S. J. Rogers, A. M. Burgess, and I. S. Curthoys. "Maintaining balance when looking at a virtual reality three-dimensional display of a field of moving dots or at a virtual reality scene." In: *Frontiers in Neurology* 6.JUL (2015), p. 164. issn: 16642295. doi: 10.3389/fneur.2015.00164.

[192] M Santoso and D Phillips. "Optical Flow, Perturbation Velocities and Postural Response In Virtual Reality." In: *2020 IEEE Conference on Virtual Reality and 3D User Interfaces Abstracts and Workshops (VRW)*. 2020, pp. 788–789. doi: 10.1109/VRW50115.2020.00245.

[193] A. V. Lubetzky, D. Harel, J. Kelly, B. D. Hujsak, and K. Perlin. "Weighting and reweighting of visual input via head mounted display given unilateral peripheral vestibular dysfunction." In: *Human Movement Science* 68 (Dec. 2019). issn: 0167-9457. doi: 10.1016/j.humov.2019.102526.

[194] A. V. Lubetzky and B. D. Hujsak. "A virtual reality head stability test for patients with vestibular dysfunction." In: *Journal of Vestibular Research: Equilibrium and Orientation* 28.5-6 (2019), pp. 393–400. issn: 09574271. doi: 10.3233/VES-190650.

[195] A. V. Lubetzky, E. E. Kary, D. Harel, B. Hujsak, and K. Perlin. "Feasibility and reliability of a virtual reality oculus platform to measure sensory integration for postural control in young adults." In: *Physiotherapy Theory and Practice* 34.12 (Jan. 2018), pp. 935–950. issn: 15325040. doi: 10.1080/09593985.2018.1431344. url: https://pubmed.ncbi.nlm.nih.gov/29364733/.

[196] A. Diniz-Filho, E. R. Boer, C. P. Gracitelli, R. Y. Abe, N. Van Driel, Z. Yang, and F. A. Medeiros. "Evaluation of postural control in patients with glaucoma using a virtual reality environment." In: *Ophthalmology* 122.6 (2015), pp. 1131–1138. issn: 15494713. doi: 10.1016/j.ophtha.2015.02.010.

[197] M. Habibnezhad, J. Puckett, H. Jebelli, A. Karji, M. S. Fardhosseini, and S. Asadi. "Neurophysiological testing for assessing construction workers' task performance at virtual height." In: *Automation in Construction* 113 (2020). issn: 09265805. doi: 10.1016/j.autcon.2020.103143.

[198] J. Ketterer, S. Ringhof, D. Gehring, and A. Gollhofer. "Sinusoidal Optic Flow Perturbations Reduce Transient but Not Continuous Postural Stability: A Virtual Reality-Based Study." In: *Frontiers in physiology* 13 (2022), p. 803185. issn: 1664-042X (Print). doi: 10.3389/fphys.2022.803185.

[199] Z. Bassiri, C. Austin, C. Cousin, and D. Martelli. "Subsensory electrical noise stimulation applied to the lower trunk improves postural control during visual perturbations." In: *Gait & Posture* 96 (2022), pp. 22–28. issn: 0966-6362. doi: https://doi.org/10.1016/j.gaitpost.

2022.05.010. url: https://www.sciencedirect.com/science/article/pii/S0966636222001333.

[200] K. Horiuchi, M. Ishihara, and K. Imanaka. "The essential role of optical flow in the peripheral visual field for stable quiet standing: Evidence from the use of a head-mounted display." In: *PLoS ONE* 12.10 (Oct. 2017). issn: 19326203. doi: 10.1371/JOURNAL.PONE.0184552.

[201] A. Berencsi, M. Ishihara, and K. Imanaka. "The functional role of central and peripheral vision in the control of posture." In: *Human Movement Science* 24.5-6 (2005), pp. 689–709. issn: 01679457. doi: 10.1016/j.humov.2005.10.014.

[202] T. Prokop, M. Schubert, and W. Berger. "Visual influence on human locomotion. Modulation to changes in optic flow." In: *Experimental Brain Research* 114.1 (1997), pp. 63–70. issn: 00144819. doi: 10.1007/PL00005624. url: https://pubmed.ncbi.nlm.nih.gov/9125452/.

[203] M. Raffi and A. Piras. "Investigating the crucial role of optic flow in postural control: Central vs. peripheral visual field." In: *Applied Sciences (Switzerland)* 9.5 (2019). issn: 20763417. doi: 10.3390/app9050934.

[204] K. Terry, E. H. Sinitski, J. B. Dingwell, and J. M. Wilken. "Amplitude effects of medio-lateral mechanical and visual perturbations on gait." In: *Journal of Biomechanics* 45.11 (2012), pp. 1979–1986. issn: 00219290. doi: 10.1016/j.jbiomech.2012.05.006.

[205] B. C. Horslen, C. J. Dakin, J. T. Inglis, J. S. Blouin, and M. G. Carpenter. "Modulation of human vestibular reflexes with increased postural threat." In: *Journal of Physiology* 592.16 (2014), pp. 3671–3685. issn: 14697793. doi: 10.1113/jphysiol.2014.270744. url: http://doi.wiley.com/10.1113/jphysiol.2014.270744.

[206] T. D. Parsons. "Virtual reality for enhanced ecological validity and experimental control in the clinical, affective and social neurosciences." In: *Frontiers in Human Neuroscience* 9.DEC (Dec. 2015). issn: 16625161. doi: 10.3389/fnhum.2015.00660. url: https://www.ncbi.nlm.nih.gov/pmc/articles/PMC4675850/.

[207] D. Saldana, M. Neureither, A. Schmiesing, E. Jahng, L. Kysh, S. C. Roll, and S. L. Liew. "Applications of head-mounted displays for virtual reality in adult physical rehabilitation: A scoping review." In: *American Journal of Occupational Therapy* 74.5 (2020), pp. 1–15. issn: 19437676. doi: 10.5014/ajot.2020.041442.

[208] S. G. Neri, J. R. Cardoso, L. Cruz, R. M. Lima, R. J. De Oliveira, M. D. Iversen, and R. L. Carregaro. "Do virtual reality games improve mobility skills and balance measurements in community-dwelling older adults? Systematic review and meta-analysis." In: *Clinical Rehabilitation* 31.10 (2017), pp. 1292–1304. issn: 14770873. doi: 10.1177/0269215517694677.

[209] R. Moreira, J. Alves, A. Matias, and C. Santos. "Smart and Assistive Walker – ASBGo: Rehabilitation Robotics: A Smart–Walker to Assist Ataxic Patients." In: *Advances in Experimental Medicine and Biology*. Ed. by J. S. Sequeira. Vol. 1170. Springer International Publishing, 2019, pp. 37–68. isbn: 978-3-030-24230-5. doi: 10.1007/978-3-030-24230-5_2. url: https://doi.org/10.1007/978-3-030-24230-5_2.

[210] X. Hu and X. Qu. "Pre-impact fall detection." In: *BioMedical Engineering Online* 15.1 (2016), p. 61. issn: 1475925X. doi: 10.1186/s12938-016-0194-x.

[211] T. P. Luu, J. A. Brantley, F. Zhu, and J. L. Contreras-Vidal. "Cortical features of locomotion-mode transitions via non-invasive EEG." In: *2017 IEEE International Conference on Systems, Man, and Cybernetics, SMC 2017*. Vol. 2017-Janua. October. 2017, pp. 2437–2441. isbn: 9781538616451. doi: 10.1109/SMC.2017.8122988.

[212] H. G. Yeom, J. S. Kim, and C. K. Chung. "Brain mechanisms in motor control during reaching movements: Transition of functional connectivity according to movement states." In: *Scientific Reports* 10.1 (2020). issn: 20452322. doi: 10.1038/s41598-020-57489-7.

[213] C. Luz, T. Bush, X. Shen, and R. Pruchno. "Do canes or walkers make any difference? nonuse and fall injuries." In: *Gerontologist* 57.2 (2017), pp. 211–218. issn: 17585341. doi: 10.1093/geront/gnv096.

[214] C. J. Bohil, B. Alicea, and F. A. Biocca. *Virtual reality in neuroscience research and therapy*. Dec. 2011. doi: 10.1038/nrn3122. url: https://www.nature.com/articles/nrn3122.

[215] C. G. Canning, N. E. Allen, E. Nackaerts, S. S. Paul, A. Nieuwboer, and M. Gilat. *Virtual reality in research and rehabilitation of gait and balance in Parkinson disease*. 2020. doi: 10.1038/s41582-020-0370-2.

[216] A. M. Gonzalez and A. B. Raposo. "Fall risk analysis during VR interaction." In: *Proceedings - 19th Symposium on Virtual and Augmented Reality, SVR 2017*. Vol. 2017-November. Institute of Electrical and Electronics Engineers Inc., Nov. 2017, pp. 18–28. isbn: 9781538635889. doi: 10.1109/SVR.2017.11.

[217] D. Schoene, C. Heller, Y. N. Aung, C. C. Sieber, W. Kemmler, and E. Freiberger. *A systematic review on the influence of fear of falling on quality of life in older people: Is there a role for falls?* 2019. doi: 10.2147/CIA.S197857.

[218] M. Suzuki, N. Ohyama, K. Yamada, and M. Kanamori. *The relationship between fear of falling, activities of daily living and quality of life among elderly individuals*. 2002. doi: 10.1046/j.1442-2018.2002.00123.x.

[219] N. M. Gell, R. B. Wallace, A. Z. Lacroix, T. M. Mroz, and K. V. Patel. "Mobility device use in older adults and incidence of falls and worry about falling: Findings from the 2011-2012 national health and aging trends study." In: *Journal of the American Geriatrics Society* 63.5 (2015), pp. 853–859. issn: 15325415. doi: 10.1111/jgs.13393.

[220] H. Bateni and B. E. Maki. "Assistive devices for balance and mobility: Benefits, demands, and adverse consequences." In: *Archives of Physical Medicine and Rehabilitation* 86.1 (2005), pp. 134–145. issn: 00039993. doi: 10.1016/j.apmr.2004.04.023.

[221] E. Dogru, H. Kizilci, N. C. Balci, N. C. Korkmaz, O. Canbay, and N. Katayifci. "The effect of walking sticks on balance in geriatric subjects." In: *Journal of Physical Therapy Science* 28.12 (2016), pp. 3267–3271. issn: 09155287. doi: 10.1589/jpts.28.3267.

[222] P. Bet, P. C. Castro, and M. A. Ponti. "Fall detection and fall risk assessment in older person using wearable sensors: A systematic review." In: *International Journal of Medical Informatics* 130 (2019). issn: 18728243. doi: 10.1016/j.ijmedinf.2019.08.006.

[223] W. Tao, T. Liu, R. Zheng, and H. Feng. "Gait analysis using wearable sensors." In: *Sensors* 12.2 (2012), pp. 2255–2283. issn: 14248220. doi: 10.3390/s120202255.

[224] P. H. Chen, Y. H. Li, C. W. Chiou, C. Y. Lee, and J. M. Lin. "A smart safety cane for human fall detection." In: *International Journal of Ad Hoc and Ubiquitous Computing* 20.1 (2015), pp. 49–65. issn: 1743-8225. doi: 10.1504/IJAHUC.2015.071662.

[225] P. Mouta, N. F. Ribeiro, C. P. Santos, and R. Moreira. "Assistive Smart Cane (ASCane) for Fall Detection: First Advances." In: *IFMBE Proceedings*. Vol. 76. 2020, pp. 1669–1684. doi: 10.1007/978-3-030-31635-8_204.

[226] J. Taborri, E. Palermo, S. Rossi, and P. Cappa. "Gait partitioning methods: A systematic review." In: *Sensors (Switzerland)* 16.1 (2016). issn: 14248220. doi: 10.3390/s16010066.

[227] N. Abaid, P. Cappa, E. Palermo, M. Petrarca, and M. Porfiri. "Gait Detection in Children with and without Hemiplegia Using Single-Axis Wearable Gyroscopes." In: *PLOS ONE* 8.9 (2013), pp. 1–8. doi: 10.1371/journal.pone.0073152.

[228] S. Lambrecht, A. Harutyunyan, K. Tanghe, M. Afschrift, J. De Schutter, and I. Jonkers. "Real-Time Gait Event Detection Based on Kinematic Data Coupled to a Biomechanical Model." In: *Sensors (Basel, Switzerland)* 17.4 (2017). issn: 1424-8220 (Electronic). doi: 10.3390/s17040671.

[229] A. Lachtar, A. Kachouri, and T. Val. "Real-time monitoring of elderly using their connected walking stick." In: *2017 International Conference on Smart, Monitored and Controlled Cities, SM2C 2017*. i. 2017, pp. 48–52. isbn: 9781509063239. doi: 10.1109/SM2C.2017.8071257.

[230] M. Lan, A. Nahapetian, A. Vahdatpour, L. Au, W. Kaiser, and M. Sarrafzadeh. "SmartFall: An automatic fall detection system based on subsequence matching for the smartcane." In: *BODYNETS 2009 - 4th International ICST Conference on Body Area Networks*. 2011.

[231] O. Almeida, M. Zhang, and J. Liu. "Dynamic Fall Detection and Pace Measurement in Walking Sticks." In: *2007 Joint Workshop on High Confidence Medical Devices, Software, and Systems and Medical Device Plug-and-Play Interoperability (HCMDSS-MDPnP 2007)*. 2007, pp. 204–206.

[232] I. G. Fernandez, S. A. Ahmad, and C. Wada. "Inertial Sensor-Based Instrumented Cane for Real-Time Walking Cane Kinematics Estimation." In: *Sensors (Basel, Switzerland)* 20.17 (2020). issn: 1424-8220 (Electronic). doi: 10.3390/s20174675.

[233] J. E. Edelstein. "Assistive devices for ambulation." In: *Physical medicine and rehabilitation clinics of North America* 24.2 (2013), pp. 291–303. issn: 1558-1381 (Electronic). doi: 10.1016/j.pmr.2012.11.001.

[234] D. O. Odebiyi and C. A. Adeagbo. "Ambulatory Devices: Assessment and Prescription." In: *Prosthesis*. Ed. by R. Vinjamuri. Rijeka: IntechOpen, 2020. Chap. 5. doi: 10.5772/intechopen.89886.

[235] J. Jacob, T. Nguyen, D. Y. C. Lie, S. Zupancic, J. Bishara, A. Dentino, and R. E. Banister. "A fall detection study on the sensors placement location and a rule-based multi-thresholds algorithm using both accelerometer and gyroscopes." In: *2011 IEEE International Conference on Fuzzy Systems (FUZZ-IEEE 2011)*. 2011, pp. 666–671. doi: 10.1109/FUZZY.2011.6007744.

[236] A. T. Özdemir and B. Barshan. "Detecting falls with wearable sensors using machine learning techniques." In: *Sensors (Switzerland)* 14.6 (2014), pp. 10691–10708. issn: 14248220. doi: 10.3390/s140610691.

[237] I. P. E. S. Putra, J. Brusey, E. Gaura, and R. Vesilo. "An event-triggered machine learning approach for accelerometer-based fall detection." In: *Sensors (Switzerland)* 18.1 (2018), p. 20. issn: 14248220. doi: 10.3390/s18010020.

[238] F. Bianchi, S. J. Redmond, M. R. Narayanan, S. Cerutti, and N. H. Lovell. "Barometric pressure and triaxial accelerometry-based falls event detection." In: *IEEE Transactions on Neural Systems and Rehabilitation Engineering* 18.6 (2010), pp. 619–627. issn: 15344320. doi: 10.1109/TNSRE.2010.2070807.

[239] K. H. Chen, J. J. Yang, and F. S. Jaw. "Accelerometer-based fall detection using feature extraction and support vector machine algorithms." In: *Instrumentation Science and Technology* 44.4 (2016), pp. 333–342. issn: 15256030. doi: 10.1080/10739149.2015.1123161.

[240] S. H. Liu and W. C. Cheng. "Fall detection with the support vector machine during scripted and continuous unscripted activities." In: *Sensors (Switzerland)* 12.9 (2012), pp. 12301–12316. issn: 14248220. doi: 10.3390/s120912301.

[241] J. Figueiredo, S. P. Carvalho, D. Gonçalves, J. C. Moreno, and C. P. Santos. "Daily Locomotion Recognition and Prediction: A Kinematic Data-Based Machine Learning Approach." In: *IEEE Access* 8 (2020), pp. 33250–33262. issn: 21693536. doi: 10.1109/ACCESS.2020.2971552.

[242] P. Félix, J. Figueiredo, C. P. Santos, and J. C. Moreno. "Adaptive real-time tool for human gait event detection using a wearable gyroscope." In: *Human-Centric Robotics- Proceedings of the 20th International Conference on Climbing and Walking Robots and the Support Technologies for Mobile Machines, CLAWAR 2017*. World Scientific Publishing Co. Pte. Ltd., 2018, pp. 653–660. isbn: 9789813231047. doi: 10.1142/9789813231047_0079.

[243] J. Zhang, T. E. Lockhart, and R. Soangra. "Classifying lower extremity muscle fatigue during walking using machine learning and inertial sensors." In: *Annals of Biomedical Engineering* 42.3 (2014), pp. 600–612. issn: 15739686. doi: 10.1007/s10439-013-0917-0. arXiv: 15334406.

[244] G. Roffo, S. Melzi, U. Castellani, and A. Vinciarelli. "Infinite Latent Feature Selection: A Probabilistic Latent Graph-Based Ranking Approach." In: *2017 IEEE International Conference on Computer Vision (ICCV)*. 2017, pp. 1407–1415. doi: 10.1109/ICCV.2017.156.

[245] I. T. Jolliffe. *Principal Component Analysis*. Second Edi. Springer, 2002, p. 487. doi: 10.1007/b98835. url: https://books.google.pt/books?id={\%}5C{_}olByCrhjwIC.

[246] G. Jurman, S. Riccadonna, and C. Furlanello. "A comparison of MCC and CEN error measures in multi-class prediction." In: *PLoS ONE* 7.8 (2012). issn: 19326203. doi: 10.1371/journal.pone.0041882.

[247] J. Figueiredo, P. Félix, L. Costa, J. C. Moreno, and C. P. Santos. "Gait Event Detection in Controlled and Real-Life Situations: Repeated Measures From Healthy Subjects." In: *IEEE Transactions on Neural Systems and Rehabilitation Engineering* 26.10 (2018), pp. 1945–1956. issn: 1558-0210. doi: https://doi.org/10.1109/TNSRE.2018.2868094.

[248] M. Y. Osoba, A. K. Rao, S. K. Agrawal, and A. K. Lalwani. "Balance and gait in the elderly: A contemporary review." In: *Laryngoscope investigative otolaryngology* 4.1 (2019), pp. 143–153. issn: 2378-8038 (Print). doi: https://doi.org/10.1002/lio2.252.

[249] A. K. Bourke, K. J. O'Donovan, and G ÓLaighin. "The identification of vertical velocity profiles using an inertial sensor to investigate pre-impact detection of falls." In: *Medical Engineering & Physics* 30.7 (2008), pp. 937–946. issn: 1350-4533. doi: https://doi.org/10.1016/j.medengphy.2007.12.003.

[250] J. Liu and T. E. Lockhart. "Development and evaluation of a prior-to-impact fall event detection algorithm." In: *IEEE Transactions on Biomedical Engineering* 61.7 (2014), pp. 2135–2140. issn: 15582531. doi: 10.1109/TBME.2014.2315784.

[251] S. Shan and T. Yuan. "A wearable pre-impact fall detector using feature selection and Support Vector Machine." In: *International Conference on Signal Processing Proceedings, ICSP*. 2010, pp. 1686–1689. isbn: 9781424458981. doi: 10.1109/ICOSP.2010.5656840.

[252] D. Martelli, F. Artoni, V. Monaco, A. M. Sabatini, and S. Micera. "Pre-impact fall detection: Optimal sensor positioning based on a machine learning paradigm." In: *PLoS ONE* 9.3 (2014). issn: 19326203. doi: 10.1371/journal.pone.0092037.

[253] M. N. Nyan, F. E. Tay, and M. Z. Mah. "Application of motion analysis system in pre-impact fall detection." In: *Journal of Biomechanics* 41.10 (2008), pp. 2297–2304. issn: 00219290. doi: 10.1016/j.jbiomech.2008.03.042.

[254] Y.-Z. Zhang. "Motion Control Design for Robotic Walking Support Systems Using Admittance Motion Command Generator." In: 2011.

[255] R. Ady, W. Bachta, and P. Bidaud. "Development and control of a one-wheel telescopic active cane." In: *5th IEEE RAS/EMBS International Conference on Biomedical Robotics and Biomechatronics*. 2014, pp. 461–466. doi: 10.1109/BIOROB.2014.6913820.

[256] P. Van Lam, T. Shimono, and Y. Fujimoto. "Using a nonlinear disturbance observer to estimated the human force applied to a two-wheeled cane for walking assistance." In: *Proceedings: IECON 2018 - 44th Annual Conference of the IEEE Industrial Electronics Society*. 2018, pp. 5122–5127. isbn: 9781509066841. doi: 10.1109/IECON.2018.8591158.

[257] M. Kato, A. Ichikawa, I. Kondo, and T. Fukuda. "Walking-aid cane robot applying light touch effect." In: *MHS 2017 - 28th 2017 International Symposium on Micro-NanoMechatronics and Human Science*. Vol. 2018-January. 2018, pp. 1–6. isbn: 9781538633144. doi: 10.1109/MHS.2017.8305182.

[258] M. R. Afzal, I. Hussain, Y. Jan, and J. Yoon. "Design of a haptic cane for walking stability and rehabilitation." In: *International Conference on Control, Automation and Systems*. 2013, pp. 1450–1454. isbn: 9788993215052. doi: 10.1109/ICCAS.2013.6704114.

[259] N. Suryadi, Y. Suryana, R. Komaladewi, and D. Sari. "Consumer, customer and perceived value: Past and present." In: *Academy of Strategic Management Journal* 17.4 (2018). issn: 19396104.

[260] A. I. Batavia and G. S. Hammer. "Toward the development of consumer-based criteria for the evaluation of assistive devices." In: *Journal of Rehabilitation Research and Development* 27.4 (1990), pp. 425–436. issn: 0007506X. doi: 10.1682/jrrd.1990.10.0425.

[261] B. E. Dicianno, J. Joseph, S. Eckstein, C. K. Zigler, E. Quinby, M. R. Schmeler, R. M. Schein, J. Pearlman, and R. A. Cooper. "The Voice of the Consumer: A Survey of Veterans and Other Users of Assistive Technology." In: *Military Medicine* 183.11-12 (2018), E518–E525. issn: 1930613X. doi: 10.1093/milmed/usy033.

[262] O. A. Atoyebi, D. Labbé, M. Prescott, A. Mahmood, F. Routhier, W. C. Miller, and W. B. Mortenson. *Mobility Challenges Among Older Adult Mobility Device Users*. 2019. doi: 10.1007/s13670-019-00295-5.

[263] E. Hedberg-Kristensson, S. D. Ivanoff, and S. Iwarsson. "Experiences among older persons using mobility devices." In: *Disability and Rehabilitation: Assistive Technology* 2.1 (2007), pp. 15–22. issn: 17483107. doi: 10.1080/17483100600875197.

[264] H. H. Liu, J. Eaves, W. Wang, J. Womack, and P. Bullock. "Assessment of canes used by older adults in senior living communities." In: *Archives of Gerontology and Geriatrics* 52.3 (2011), pp. 299–303. issn: 01674943. doi: 10.1016/j.archger.2010.04.003.

[265] J. Beasley, L. Kenyon, A. Midena, J. Chartier, K. Meyers, B. Ashby, and K. Anderson. "Cane Handle Designs—Pressure and Preference." In: *Journal of Acute Care Physical Therapy* 8.2 (2017), pp. 58–64. issn: 2158-8686. doi: 10.1097/jat.0000000000000053.

[266] M. J. Brown and D. E. Jacobs. "Residential light and risk for Depression and falls: Results from the LARES study of eight European cities." In: *Public Health Reports* 126.SUPPL. 1 (2011), pp. 131–141. issn: 14682877. doi: 10.1177/00333549111260s117.

[267] C. Todd and D. Skelton. "What are the main risk factors for falls amongst older people and what are the most effective interventions to prevent these falls ?" In: *World Health* March (2004), p. 28.

[268] E. van Wegen, C. de Goede, I. Lim, M. Rietberg, A. Nieuwboer, A. Willems, D. Jones, L. Rochester, V. Hetherington, H. Berendse, J. Zijlmans, E. Wolters, and G. Kwakkel. "The effect of rhythmic somatosensory cueing on gait in patients with Parkinson's disease." In: *Journal of the Neurological Sciences* 248.1-2 (2006), pp. 210–214. issn: 0022510X. doi: 10.1016/j.jns.2006.05.034.

[269] R. Velik, U. Hoffmann, H. Zabaleta, J. F. Marti Masso, and T. Keller. "The effect of visual cues on the number and duration of freezing episodes in Parkinson's patients." In: *Proceedings of the Annual International Conference of the IEEE Engineering in Medicine and Biology Society, EMBS* 2012 (2012), pp. 4656–4659. issn: 1557170X. doi: 10.1109/EMBC.2012.6347005.

[270] G. Häggblom-Kronlöf and U. Sonn. "Use of assistive devices - A reality full of contradictions in elderly persons' everyday life." In: *Disability and Rehabilitation: Assistive Technology* 2.6 (2007), pp. 335–345. issn: 17483107. doi: 10.1080/17483100701701672.

[271] J. A. Lenker, F. Harris, M. Taugher, and R. O. Smith. "Consumer perspectives on assistive technology outcomes." In: *Disability and Rehabilitation: Assistive Technology* 8.5 (2013), pp. 373–380. issn: 17483107. doi: 10.3109/17483107.2012.749429.

[272] L. Resnik, S. Allen, D. Isenstadt, M. Wasserman, and L. Iezzoni. "Perspectives on use of mobility aids in a diverse population of seniors: Implications for intervention." In: *Disability and Health Journal* 2.2 (2009), pp. 77–85. issn: 19366574. doi: 10.1016/j.dhjo.2008.12.002.

[273] *Dring Smartcane*. 2020. url: https://dring.io/11-canne-connectee-fayet.

[274] IStand. *iStand Smartcane*. 2018. url: https://rehabpub.com/mobility/istand-walking-cane-built-fall-detection-alerts/.

[275] *My Hip'Safe – Hip'Safe by Helite*. 2020. url: https://hipguard.eu/en/.

[276] J. Ballesteros, A. Tudela, J. R. Caro-Romero, and C. Urdiales. "Weight-bearing estimation for cane users by using onboard sensors." In: *Sensors (Switzerland)* 19.3 (2019), pp. 1–13. issn: 14248220. doi: 10.3390/s19030509.

[277] J. W. Youdas, B. J. Kotajarvi, D. J. Padgett, and K. R. Kaufman. "Partial weight-bearing gait using conventional assistive devices." In: *Archives of Physical Medicine and Rehabilitation* 86.3 (2005), pp. 394–398. issn: 00039993. doi: 10.1016/j.apmr.2004.03.026.

[278] *Walking aids manipulated by one arm – Requirements and test methods – Part 4: Walking sticks with three or more legs*. Standard. International Organization for Standardization, 1999.

[279] L. Quach, A. M. Galica, R. N. Jones, E. Procter-Gray, B. Manor, M. T. Hannan, and L. A. Lipsitz. "The nonlinear relationship between gait speed and falls: the Maintenance of Balance, Independent Living, Intellect, and Zest in the Elderly of Boston Study." In: *Journal of the American Geriatrics Society* 59.6 (2011), pp. 1069–1073. issn: 1532-5415 (Electronic). doi: 10.1111/j.1532-5415.2011.03408.x.

[280] C. L. Lu, B. Yu, J. R. Basford, M. E. Johnson, and K. N. An. "Influences of cane length on the stability of stroke patients." In: *Journal of Rehabilitation Research and Development* 34.1 (1997), pp. 91–100. issn: 07487711.

[281] A. S. Kujath. "Cane Use Principles." In: *Orthopaedic Nursing* 37.3 (2018), pp. 204–207. issn: 1542538X. doi: 10.1097/NOR.0000000000000453.

[282] S. M. Bradley and C. R. Hernandez. "Geriatric assistive devices." In: *American Family Physician* 84.4 (2011), pp. 405–411. issn: 15320650.

[283] C. Y. Wang and D. C. Cai. "Hand tool handle design based on hand measurements." In: *MATEC Web of Conferences*. Vol. 119. 2017, pp. 1–5. doi: 10.1051/matecconf/201711901044.

[284] M. Patkin. "A Check-List for Handle Design." In: *Ergonomics Australia On-Line* 15 (2001), p. 22.

[285] *Tips for assistive products for walking — Requirements and test methods — Part 1: Friction of tips*. Standard. International Organization for Standardization, Apr. 2009.

[286] M. G. Figueiro, L. Z. Gras, M. S. Rea, B. Plitnick, and M. S. Rea. "Lighting for improving balance in older adults with and without risk for falls." In: *Age and ageing* 41.3 (May 2012), pp. 392–395. issn: 1468-2834 (Electronic). doi: 10.1093/ageing/afr166.

[287] S. S. Kuys, L. Ada, J. Paratz, and S. G. Brauer. "Steps, duration and intensity of usual walking practice during subacute rehabilitation after stroke: an observational study." In: *Brazilian journal of physical therapy* 23.1 (2019), pp. 56–61. issn: 1809-9246 (Electronic). doi: 10.1016/j.bjpt.2018.06.001.

[288] Q. Yan, J. Huang, and Z. Luo. "Human-robot coordination stability for fall detection and prevention using cane robot." In: *2016 International Symposium on Micro-NanoMechatronics and Human Science, MHS 2016*. 1. 2017. isbn: 9781509027842. doi: 10.1109/MHS.2016.7824171.

[289] S. G. Tzafestas. *Introduction to Mobile Robot Control*. 2013, pp. 1–691. isbn: 9780124170490. doi: 10.1016/C2013-0-01365-5.

[290] F. Tajti, G. Szayer, B. Kovács, and P. Korondi. *Robot base with holonomic drive*. Vol. 19. 3. IFAC, 2014, pp. 5715–5720. doi: 10.3182/20140824-6-za-1003.00785.

[291] W. R. De Silva and R. Munasinghe. "Development of a holonomic mobile robot for field applications." In: *ICIIS 2009 - 4th International Conference on Industrial and Information Systems 2009, Conference Proceedings* May (2009), pp. 499–504. doi: 10.1109/ICIINFS.2009.5429809.

[292] T. L. Anderson. *Fracture Mechanics: Fundamentals and Applications, Fourth Edition*. Vol. 76. 2017, pp. 1255–1269. isbn: 9780849316562.

[293] STMicroelectronics. *NUCLEO-64 STM32F446RE*. 2021. url: https://www.digikey.pt/products/pt?keywords=NUCLEO-F446RE.

[294] Interlink Electronics. *FSR 400 34-00004 - Force Sensor*. 2021. url: https://www.digikey.pt/pt/products/detail/interlink-electronics/34-00004/2798665.

[295] Interlink Electronics. *FSR 400 34-00015 - Force Sensor*. 2021. url: https://www.digikey.pt/product-detail/pt/interlink-electronics/34-00015/1027-1018-ND/5416350.

[296] A. S. Sadun, J Jalani, and J. A. Sukor. "Force Sensing Resistor (FSR): a brief overview and the low-cost sensor for active compliance control." In: *First International Workshop on Pattern Recognition*. Ed. by X. Jiang, G. Chen, G. Capi, and C. Ishll. Vol. 10011. International Society for Optics and Photonics. SPIE, 2016, pp. 222–226. doi: 10.1117/12.2242950. url: https://doi.org/10.1117/12.2242950.

[297] R. Velik. *Effect of On-Demand Cueing on Freezing of Gait in Parkinson's Patients*. Version 16916. Sept. 2013. doi: 10.5281/zenodo.1088086.

[298] H. R. Gonçalves, A. M. Rodrigues, and C. P. Santos. "Vibrotactile biofeedback devices in Parkinson's disease: a narrative review." In: *Medical biological engineering computing* 59.6 (June 2021), pp. 1185–1199. issn: 1741-0444 (Electronic). doi: 10.1007/s11517-021-02365-3.

[299] K. Myles and M. S. Binseel. *The Tactile Modality : A Review of Tactile Sensitivity and Human Tactile Interfaces (Report No. ARL-TR-4115)*. AD-a468 389 May. army research lab aberdeen proving ground md human research and engineering directorate, 2007, pp. 1–27. isbn: 0-7695-2112-6. url: http://oai.dtic.mil/oai/oai?verb=getRecord&metadataPrefix=html&identifier=ADA468389.

[300] Precision Microdrives. *Model No. 310-103.005 10mm Vibration Motor - 3mm Type*. 2022. url: https://catalogue.precisionmicrodrives.com/product/310-103-005-10mm-vibration-motor-3mm-type.

[301] SparkFun. *Haptic Motor Driver - DRV2605L*. url: https://www.sparkfun.com/products/14538.

[302] Precision Microdrives. *Driving Vibration Motors With Pulse Width Modulation*. url: https://www.precisionmicrodrives.com/ab-012.

[303] R. P. A. van Haendel. "Design of an omnidirectional universal mobile platform." In: *...van Haedel.—Eindhoven.: Eindhoven University of ...* September (2005). url: http://www.mate.tue.nl/mate/pdfs/5816.pdf.

[304] Active-Robots. *NEMA23 High Torque DC Servo Motor 300RPM With Step/Dir Drive*. 2021. url: https://www.active-robots.com/high-torque-dc-servo-motor-300rpm-with-step-dir-drive.html.

[305] Gens Ace. *Gens ace 8000mAh 14.8V 80C 4S2P Lipo Battery Pack with EC5 Plug*. url: http://www.gabahobby.com/v2/lipo2-lithium-polymer-/349369-gens-ace-8000mah-14-8v-80c-4s2p-lipo-battery-pack-with-ec5-plug.html.

[306] *Step-Down DC-DC Converter 300W up to 20A*. url: https://www.botnroll.com/pt/conversores-dcdc/4003-conversor-dc-dc-step-down-300w-at-20a.html.

[307] *Step-Down DC-DC Converter with current regulation 8A*. url: https://www.botnroll.com/pt/conversores-dcdc/3675-conversor-dc-dc-step-down-12a-c-regula-o-de-corrente.html?fbclid=IwAR1pVrMKV2yySMezPY6S-8SoDnJipkpKF_lk9gXTmXiUO_qXmGf007iwYzs.

[308] Littlefuse Inc. *Fuse Glass 7A 250VAC 3AB 3AG*. url: https://www.digikey.pt/product-detail/pt/littelfuse-inc/0312007-MXP/F4785-ND/778273.

[309] T. Fukuda, P. Di, F. Chen, K. Sekiyama, J. Huang, M. Nakajima, and M. Kojima. "Advanced service robotics for human assistance and support." In: *ICACSIS 2011 - 2011 International Conference on Advanced Computer Science and Information Systems, Proceedings*. IEEE, 2011, pp. 25–30. isbn: 9789791421119.

[310] S. Nakagawa, P. D, J. Huang, K. Sekiyama, and T. Fukuda. "Control of intelligent cane robot considering usage of ordinary cane." In: *2013 IEEE RO-MAN*. 2013, pp. 762–767. doi: 10.1109/ROMAN.2013.6628405.

[311] S. Itadera, Y. Hasegawa, T. Fukuda, M. Tanimoto, and I. Kondo. "Adaptive walking load control for training physical strength using cane-type robot." In: *IEEE International Conference on Intelligent Robots and Systems*. Vol. 2017-September. 2017, pp. 521–526. isbn: 9781538626825. doi: 10.1109/IROS.2017.8202202.

[312] Sensitronics. *FSR 101 Force Sensing Resistor Theory and Applications*. 2017. url: https://www.sensitronics.com/fsr101.htm.

[313] J. Sumner, L. S. Chong, A. Bundele, and Y. Wei Lim. "Co-Designing Technology for Aging in Place: A Systematic Review." In: *The Gerontologist* 61.7 (2020), e395–e409. issn: 0016-9013. doi: 10.1093/geront/gnaa064. url: https://doi.org/10.1093/geront/gnaa064.

[314] M. Ashfak Habib, M. S. Mohktar, S. Bahyah Kamaruzzaman, K. Seang Lim, T. Maw Pin, and F. Ibrahim. "Smartphone-based solutions for fall detection and prevention: Challenges and open issues." In: *Sensors (Switzerland)* 14.4 (2014), pp. 7181–7208. issn: 14248220. doi: 10.3390/s140407181.

[315] B. R. Greene, K. McManus, S. J. Redmond, B. Caulfield, and C. C. Quinn. "Digital assessment of falls risk, frailty, and mobility impairment using wearable sensors." In: *npj Digital Medicine* 2.1 (2019), p. 125. issn: 2398-6352. doi: 10.1038/s41746-019-0204-z. url: https://doi.org/10.1038/s41746-019-0204-z.

[316] Y. S. Delahoz and M. A. Labrador. *Survey on fall detection and fall prevention using wearable and external sensors*. 2014. doi: 10.3390/s141019806.

[317] C.-L. Chan, Y.-J. Chen, K.-P. Chen, and S.-J. Chiu. "Elderly inpatient fall risk factors: A study of decision tree and logistic regression." In: *The 40th International Conference on Computers & Indutrial Engineering*. 2010, pp. 1–6. doi: 10.1109/ICCIE.2010.5668424.

[318] P.-L. Chen, H.-Y. Lin, J. R. Ong, and H.-P. Ma. "Development of a fall-risk assessment profile for community-dwelling older adults by using the National Health Interview Survey in Taiwan." In: *BMC Public Health* 20.1 (2020), p. 234. issn: 1471-2458. doi: 10.1186/s12889-020-8286-8. url: https://doi.org/10.1186/s12889-020-8286-8.

[319] S. R. Lord, C. Sherrington, H. B. Menz, and J. C. Close. *Falls in older people: Risk factors and strategies for prevention, second edition*. Vol. 9. 2007, pp. 1–395. isbn: 9780511722233. doi: 10.1017/CBO9780511722233.

[320] G. Cola, M. Avvenuti, A. Vecchio, G. Z. Yang, and B. Lo. "An on-node processing approach for anomaly detection in gait." In: *IEEE Sensors Journal* 15.11 (2015), pp. 6640–6649. issn: 1530437X. doi: 10.1109/JSEN.2015.2464774.

[321] M. Di Rosa, J. M. Hausdorff, V. Stara, L. Rossi, L. Glynn, M. Casey, S. Burkard, and A. Cherubini. "Concurrent validation of an index to estimate fall risk in community dwelling seniors through a wireless sensor insole system: A pilot study." In: *Gait & Posture* 55 (2017), pp. 6–11. issn: 0966-6362. doi: https://doi.org/10.1016/j.gaitpost.2017.03.037. url: https://www.sciencedirect.com/science/article/pii/S0966636217301108.

[322] W. Sansrimahachai and M. Toahchoodee. "Mobile-phone based immobility tracking system for elderly care." In: *2016 IEEE Region 10 Conference (TENCON)*. 2016, pp. 3550–3553. doi: 10.1109/TENCON.2016.7848718.

[323] C. Moufawad el Achkar, C. Lenoble-Hoskovec, A. Paraschiv-Ionescu, K. Major, C. Büla, and K. Aminian. "Instrumented shoes for activity classification in the elderly." In: *Gait & Posture* 44 (2016), pp. 12–17. issn: 0966-6362. doi: https://doi.org/10.1016/j.gaitpost.2015.10.016. url: https://www.sciencedirect.com/science/article/pii/S0966636215009248.

[324] H. Arndt, S. Burkard, G. Talavera, J. Garcia, D. Castells, M. Codina, J. Hausdorff, A. Mirelman, R. Harte, M. Casey, L. Glynn, M. Di Rosa, L. Rossi, V. Stara, J. Rösevall, C. Rusu, C. Carenas, F. Breuil, E. Reixach, and J. Carrabina. "Real-Time Constant Monitoring of Fall Risk Index by Means of Fully-Wireless Insoles." In: *Studies in health technology and informatics* 237 (2017), pp. 193–197. issn: 1879-8365 (Electronic).

[325] A. Ferrari, D. Micucci, M. Mobilio, and P. Napoletano. "Trends in human activity recognition using smartphones." In: *Journal of Reliable Intelligent Environments* 7.3 (2021), pp. 189–213. issn: 21994676. doi: 10.1007/s40860-021-00147-0. url: https://doi.org/10.1007/s40860-021-00147-0.

[326] M. Saleh, M. Abbas, and R. B. Le Jeannès. "FallAllD: An Open Dataset of Human Falls and Activities of Daily Living for Classical and Deep Learning Applications." In: *IEEE Sensors Journal* 21.2 (2021), pp. 1849–1858. doi: 10.1109/JSEN.2020.3018335.

[327] D. Anguita, A. Ghio, L. Oneto, X. Parra, and J. Reyes. "A public domain dataset for human activity recognition using smartphones." In: *Proceedings of the 21th International European Symposium on Artificial Neural Networks, Computational Intelligence and Machine Learning*. 2013, pp. 437–442. isbn: 978-2-87419-081-0. url: http://hdl.handle.net/2117/20897.

[328] V. Cotechini, A. Belli, L. Palma, M. Morettini, L. Burattini, and P. Pierleoni. "A dataset for the development and optimization of fall detection algorithms based on wearable sensors." In: *Data in Brief* 23 (2019), p. 103839. issn: 2352-3409. doi: https://doi.org/10.1016/j.dib.2019.103839. url: https://www.sciencedirect.com/science/article/pii/S2352340919301908.

[329] E. Casilari, J. A. Santoyo-Ramón, and J. M. Cano-García. "UMAFall: A Multisensor Dataset for the Research on Automatic Fall Detection." In: *Procedia Computer Science*. Vol. 110. 2017, pp. 32–39. doi: 10.1016/j.procs.2017.06.110.

[330] J. Figueiredo, S. P. Carvalho, J. P. Vilas-Boas, L. M. Gonçalves, J. C. Moreno, and C. P. Santos. "Wearable inertial sensor system towards daily human kinematic gait analysis: Benchmarking analysis to MVN BIOMECH." In: *Sensors (Switzerland)* 20.8 (2020), pp. 21–24. issn: 14248220. doi: 10.3390/s20082185.

[331] S. Chung, J. Lim, K. J. Noh, G. Kim, and H. Jeong. "Sensor Data Acquisition and Multimodal Sensor Fusion for Human Activity Recognition Using Deep Learning." In: *Sensors* 19.7 (2019). issn: 1424-8220. doi: 10.3390/s19071716. url: https://www.mdpi.com/1424-8220/19/7/1716.

[332] R. Baghezza, K. Bouchard, A. Bouzouane, and C. Gouin-Vallerand. "From Offline to Real-Time Distributed Activity Recognition in Wireless Sensor Networks for Healthcare: A Review." In: *Sensors* 21.8 (2021). issn: 1424-8220. doi: 10.3390/s21082786. url: https://www.mdpi.com/1424-8220/21/8/2786.

[333] E Ramanujam, T. Perumal, and S Padmavathi. "Human Activity Recognition With Smartphone and Wearable Sensors Using Deep Learning Techniques: A Review." In: *IEEE Sensors Journal* 21.12 (2021), pp. 13029–13040. doi: 10.1109/JSEN.2021.3069927.

[334] O. Banos, J.-M. Galvez, M. Damas, H. Pomares, and I. Rojas. "Window Size Impact in Human Activity Recognition." In: *Sensors* 14.4 (2014), pp. 6474–6499. issn: 1424-8220. doi: 10.3390/s140406474. url: https://www.mdpi.com/1424-8220/14/4/6474.

[335] B. Fida, I. Bernabucci, D. Bibbo, S. Conforto, and M. Schmid. "Varying behavior of different window sizes on the classification of static and dynamic physical activities from a single accelerometer." In: *Medical Engineering & Physics* 37.7 (2015), pp. 705–711. issn: 1350-4533. doi: https://doi.org/10.1016/j.medengphy.2015.04.005. url: https://www.sciencedirect.com/science/article/pii/S1350453315001009.

[336] I. Goodfellow, Y. Bengio, and A. Courville. *Deep Learning*. Adaptive Computation and Machine Learning series. Cambridge, MA, USA: MIT Press, 2016. isbn: 9780262035613.

[337] W.-R. Chang, S. Leclercq, T. E. Lockhart, and R. Haslam. "State of science: occupational slips, trips and falls on the same level." In: *Ergonomics* 59.7 (2016), pp. 861–883. issn: 1366-5847 (Electronic). doi: 10.1080/00140139.2016.1157214.

[338] T. K. Courtney, G. S. Sorock, D. P. Manning, J. W. Collins, and M. A. Holbein-Jenny. "Occupational slip, trip, and fall-related injuries–can the contribution of slipperiness be isolated?" In: *Ergonomics* 44.13 (2001), pp. 1118–1137. issn: 0014-0139. doi: 10.1080/00140130110085538.

[339] S. Wang, X. Liu, and Y.-C. Pai. "Limb Collapse or Instability? Assessment on Cause of Falls." In: *Annals of biomedical engineering* 47.3 (2019), pp. 767–777. issn: 1573-9686 (Electronic). doi: 10.1007/s10439-018-02195-9.

[340] R Cham and M. S. Redfern. "Lower extremity corrective reactions to slip events." In: *Journal of biomechanics* 34.11 (2001), pp. 1439–1445. issn: 0021-9290 (Print). doi: 10.1016/s0021-9290(01)00116-6.

[341] D. S. Marigold and A. E. Patla. "Strategies for dynamic stability during locomotion on a slippery surface: effects of prior experience and knowledge." In: *Journal of neurophysiology* 88.1 (2002), pp. 339–353. issn: 0022-3077. doi: 10.1152/jn.00691.2001.

[342] P. F. Tang, M. H. Woollacott, and R. K. Chong. "Control of reactive balance adjustments in perturbed human walking: roles of proximal and distal postural muscle activity." In: *Experimental brain research* 119.2 (1998), pp. 141–152. issn: 0014-4819 (Print). doi: 10.1007/s002210050327.

[343] S. J. Wilson, P. T. Donahue, C. C. Williams, C. M. Hill, J. D. Simpson, D. E. Waddell, J. P. Loenneke, H. Chander, C. Wade, and J. C. Garner. "Differences in falls and recovery from a slip based on an individual's lower extremity corrective response." In: *International Journal of Kinesiology and Sports Science* 7.3 (2019). issn: 2202946X. doi: 10.7575/aiac.ijkss.v.7n.3p.34.

[344] F. Yang and Y.-C. Pai. "Role of individual lower limb joints in reactive stability control following a novel slip in gait." In: *Journal of biomechanics* 43.3 (2010), pp. 397–404. issn: 1873-2380 (Electronic). doi: 10.1016/j.jbiomech.2009.10.003.

[345] M. K. Seeley, B. R. Umberger, and R. Shapiro. "A test of the functional asymmetry hypothesis in walking." In: *Gait & posture* 28.1 (2008), pp. 24–28. issn: 0966-6362 (Print). doi: 10.1016/j.gaitpost.2007.09.006.

[346] P. M. Young, J. Whitall, W.-N. Bair, and M. W. Rogers. "Leg preference associated with protective stepping responses in older adults." In: *Clinical biomechanics (Bristol, Avon)* 28.8 (2013), pp. 927–932. issn: 1879-1271 (Electronic). doi: 10.1016/j.clinbiomech.2013.07.015.

[347] D. Martelli, V. Monaco, L. Bassi Luciani, and S. Micera. "Angular momentum during unexpected multidirectional perturbations delivered while walking." In: *IEEE Transactions on Biomedical Engineering* 60.7 (2013), pp. 1785–1795. issn: 00189294. doi: 10.1109/TBME.2013.2241434.

[348] H. Nagano, R. K. Begg, W. A. Sparrow, and S. Taylor. "Ageing and limb dominance effects on foot-ground clearance during treadmill and overground walking." In: *Clinical biomechanics (Bristol, Avon)* 26.9 (2011), pp. 962–968. issn: 1879-1271 (Electronic). doi: 10.1016/j.clinbiomech.2011.05.013.

[349] A. Sawers and T. Bhatt. "Neuromuscular determinants of slip-induced falls and recoveries in older adults." In: *Journal of neurophysiology* 120.4 (2018), pp. 1534–1546. issn: 1522-1598 (Electronic). doi: 10.1152/jn.00286.2018.

[350] K Beschorner and R Cham. "Impact of joint torques on heel acceleration at heel contact, a contributor to slips and falls." In: *Ergonomics* 51.12 (2008), pp. 1799–1813. issn: 0014-0139 (Print). doi: 10.1080/00140130802136479.

[351] J. Liu and T. E. Lockhart. "Age-related joint moment characteristics during normal gait and successful reactive-recovery from unexpected slip perturbations." In: *Gait and Posture* 30.3 (2009), pp. 276–281. issn: 09666362. doi: 10.1016/j.gaitpost.2009.04.005.

[352] N Mrachacz-Kersting, B. A. Lavoie, J. B. Andersen, and T Sinkjaer. "Characterisation of the quadriceps stretch reflex during the transition from swing to stance phase of human walking." In: *Experimental brain research* 159.1 (2004), pp. 108–122. issn: 0014-4819 (Print). doi: 10.1007/s00221-004-1941-y.

[353] P. Félix, J. Figueiredo, C. P. Santos, and J. C. Moreno. "Electronic design and validation of Powered Knee Orthosis system embedded with wearable sensors." In: *2017 IEEE International Conference on Autonomous Robot Systems and Competitions (ICARSC)*. 2017, pp. 110–115. doi: 10.1109/ICARSC.2017.7964061.

[354] T. Zhang, M. Tran, and H. Huang. "Design and Experimental Verification of Hip Exoskeleton With Balance Capacities for Walking Assistance." In: *IEEE/ASME Transactions on Mechatronics* 23.1 (2018), pp. 274–285. doi: 10.1109/TMECH.2018.2790358.

[355] D Bucher. "Central Pattern Generators." In: *Encyclopedia of Neuroscience*. Ed. by L. R. Squire. Oxford: Academic Press, 2009, pp. 691–700. isbn: 978-0-08-045046-9. doi: https://doi.org/10.1016/B978-008045046-9.01944-6. url: https://www.sciencedirect.com/science/article/pii/B9780080450469019446.

[356] V Dietz. "Spinal cord pattern generators for locomotion." In: *Clinical neurophysiology : official journal of the International Federation of Clinical Neurophysiology* 114.8 (2003), pp. 1379–1389. issn: 1388-2457. doi: 10.1016/s1388-2457(03)00120-2.

[357] R. Ronsse, N. Vitiello, T. Lenzi, J. van den Kieboom, M. Chiara Carrozza, and A. J. Ijspeert. "Adaptive oscillators with human-in-the-loop: Proof of concept for assistance and rehabilitation." In: *2010 3rd IEEE RAS & EMBS International Conference on Biomedical Robotics and Biomechatronics*. 2010, pp. 668–674. doi: 10.1109/BIOROB.2010.5628021.

[358] A. Frigon and S. Rossignol. "Experiments and models of sensorimotor interactions during locomotion." In: *Biological Cybernetics* 95.6 (2006), p. 607. issn: 1432-0770. doi: 10.1007/s00422-006-0129-x. url: https://doi.org/10.1007/s00422-006-0129-x.

[359] R. Ronsse, T. Lenzi, N. Vitiello, B. Koopman, E. van Asseldonk, S. M. M. De Rossi, J. van den Kieboom, H. van der Kooij, M. C. Carrozza, and A. J. Ijspeert. "Oscillator-based assistance of cyclical movements: model-based and model-free approaches." In: *Medical & biological engineering & computing* 49.10 (2011), pp. 1173–1185. issn: 1741-0444 (Electronic). doi: 10.1007/s11517-011-0816-1.

[360] P. Tropea, N. Vitiello, D. Martelli, F. Aprigliano, S. Micera, and V. Monaco. "Detecting Slipping-Like Perturbations by Using Adaptive Oscillators." In: *Annals of Biomedical Engineering* 43.2 (2015), pp. 416–426. issn: 15739686. doi: 10.1007/s10439-014-1175-5.

[361] L. Righetti, J. Buchli, and A. J. Ijspeert. "From Dynamic Hebbian Learning for Oscillators to Adaptive Central Pattern Generators." In: 2005.

[362] B. R. Whittington and D. G. Thelen. "A simple mass-spring model with roller feet can induce the ground reactions observed in human walking." In: *Journal of biomechanical engineering* 131.1 (2009), p. 11013. issn: 0148-0731. doi: 10.1115/1.3005147. url: https://pubmed.ncbi.nlm.nih.gov/19045929https://www.ncbi.nlm.nih.gov/pmc/articles/PMC2918273/.

[363] L Righetti and A. J. Ijspeert. "Programmable central pattern generators: an application to biped locomotion control." In: *Proceedings 2006 IEEE International Conference on Robotics and Automation, 2006. ICRA 2006.* 2006, pp. 1585–1590. isbn: 1050-4729 VO -. doi: 10.1109/ROBOT.2006.1641933.

[364] A. J. Ijspeert. "Central pattern generators for locomotion control in animals and robots: A review." In: *Neural Networks* 21.4 (2008), pp. 642–653. issn: 0893-6080. doi: https://doi.org/10.1016/j.neunet.2008.03.014. url: https://www.sciencedirect.com/science/article/pii/S0893608008000804.

[365] F. Aprigliano, D. Martelli, S. Micera, and V. Monaco. "Intersegmental coordination elicited by unexpected multidirectional slipping-like perturbations resembles that adopted during steady locomotion." In: *Journal of neurophysiology* 115.2 (2016), pp. 728–740. issn: 1522-1598 (Electronic). doi: 10.1152/jn.00327.2015.

[366] L. J. Elias, M. P. Bryden, and M. B. Bulman-Fleming. "Footedness is a better predictor than is handedness of emotional lateralization." In: *Neuropsychologia* 36.1 (1998), pp. 37–43. issn: 0028-3932 (Print). doi: 10.1016/s0028-3932(97)00107-3.

[367] SENIAM. *SENIAM*. 2022.

[368] P. Pellikaan, G. Giarmatzis, J. Vander Sloten, S. Verschueren, and I. Jonkers. "Ranking of osteogenic potential of physical exercises in postmenopausal women based on femoral neck strains." In: *PloS one* 13.4 (2018), e0195463. issn: 1932-6203 (Electronic). doi: 10.1371/journal.pone.0195463.

[369] R. Klemetti, P. Moilanen, J. Avela, and J. Timonen. "Effects of gait speed on stability of walking revealed by simulated response to tripping perturbation." In: *Gait & posture* 39.1 (2014), pp. 534–539. issn: 1879-2219 (Electronic). doi: 10.1016/j.gaitpost.2013.09.006.

[370] I. L. Kyrdalen, P. Thingstad, L. Sandvik, and H. Ormstad. "Associations between gait speed and well-known fall risk factors among community-dwelling older adults." In: *Physiotherapy research international : the journal for researchers and clinicians in physical therapy* 24.1 (2019), e1743. issn: 1471-2865 (Electronic). doi: 10.1002/pri.1743.

[371] S. S. Khan and J. Hoey. "Review of fall detection techniques: A data availability perspective." In: *Medical Engineering and Physics* 39 (2017), pp. 12–22. issn: 18734030. doi: 10.1016/j.medengphy.2016.10.014. arXiv: 1605.09351.

[372] M. Slater. "Place illusion and plausibility can lead to realistic behaviour in immersive virtual environments." In: *Philosophical Transactions of the Royal Society B: Biological Sciences* 364.1535 (2009), pp. 3549–3557. issn: 14712970. doi: 10.1098/rstb.2009.0138.

[373] H. Huygelier, B. Schraepen, R. van Ee, V. Vanden Abeele, and C. R. Gillebert. "Acceptance of immersive head-mounted virtual reality in older adults." In: *Scientific Reports* 9.1 (2019). issn: 20452322. doi: 10.1038/s41598-019-41200-6. url: https://pubmed.ncbi.nlm.nih.gov/30872760/.

[374] R. Reznick and H. MacRae. "Teaching surgical skills - Changes in the wind." In: *New England Journal of Medicine* 355.25 (2006), pp. 2664–2669. doi: 10.1056/NEJMra054785.

[375] P. M. Emmelkamp and K. Meyerbröker. "Virtual Reality Therapy in Mental Health." In: *Annual Review of Clinical Psychology* 17 (2021), pp. 495–519. issn: 15485951. doi: 10.1146/annurev-clinpsy-081219-115923.

[376] D. Freeman, S. Reeve, A. Robinson, A. Ehlers, D. Clark, B. Spanlang, and M. Slater. "Virtual reality in the assessment, understanding, and treatment of mental health disorders." In: *Psychological Medicine* 47.14 (2017), pp. 2393–2400. issn: 14698978. doi: 10.1017/S003329171700040X.

[377] D. Cano Porras, P. Siemonsma, R. Inzelberg, G. Zeilig, and M. Plotnik. "Advantages of virtual reality in the rehabilitation of balance and gait: Systematic review." In: *Neurology* 90.22 (May 2018), pp. 1017–1025. issn: 1526-632X (Electronic). doi: 10.1212/WNL.0000000000005603.

[378] M. Covarrubias, M. Bordegoni, M. Rosini, E. Guanziroli, U. Cugini, and F. Molteni. "VR system for rehabilitation based on hand gestural and olfactory interaction." In: *Proceedings of the ACM Symposium on Virtual Reality Software and Technology, VRST* 13-15-Nove (Nov. 2015), pp. 117–120. doi: 10.1145/2821592.2821619.

[379] K. E. Laver, B. Lange, S. George, J. E. Deutsch, G. Saposnik, and M. Crotty. "Virtual reality for stroke rehabilitation." In: *Cochrane Database of Systematic Reviews* 2017.11 (2017). issn: 1469493X. doi: 10.1002/14651858.CD008349.pub4. url: https://pubmed.ncbi.nlm.nih.gov/29156493/.

[380] "Virtual Reality for Physical and Motor Rehabilitation." In: Virtual Reality Technologies for Health and Clinical Applications (2014). Ed. by P. L. Weiss, E. A. Keshner, and M. F. Levin. doi: 10.1007/978-1-4939-0968-1. url: http://link.springer.com/10.1007/978-1-4939-0968-1.

[381] J. A. Kleim and T. A. Jones. "Principles of experience-dependent neural plasticity: implications for rehabilitation after brain damage." In: *Journal of speech, language, and hearing research : JSLHR* 51.1 (Feb. 2008). issn: 1092-4388. doi: 10.1044/1092-4388(2008/018). url: https://pubmed.ncbi.nlm.nih.gov/18230848/.

[382] P. Kiper, L. Piron, A. Turolla, J. Stozek, and P. Tonin. "The effectiveness of reinforced feedback in virtual environment in the first 12 months after stroke." In: *Neurologia i neurochirurgia polska* 45.5 (2011), pp. 436–444. issn: 0028-3843. doi: 10.1016/S0028-3843(14)60311-X. url: https://pubmed.ncbi.nlm.nih.gov/22127938/.

[383] P. Dias, R. Silva, P. Amorim, J. Laíns, E. Roque, I. Serôdio, F. Pereira, B. S. Santos, and M. Potel. "Using Virtual Reality to Increase Motivation in Poststroke Rehabilitation: VR Therapeutic Mini-Games Help in Poststroke Recovery." In: *IEEE Computer Graphics and Applications* 39.1 (Jan. 2019), pp. 64–70. issn: 15581756. doi: 10.1109/MCG.2018.2875630.

[384] J. A. Kleim. "Neural plasticity and neurorehabilitation: teaching the new brain old tricks." In: *Journal of communication disorders* 44.5 (Sept. 2011), pp. 521–528. issn: 1873-7994. doi: 10.1016/J.JCOMDIS.2011.04.006. url: https://pubmed.ncbi.nlm.nih.gov/21600589/.

[385] R. J. Nudo, G. W. Milliken, W. M. Jenkins, and M. M. Merzenich. "Use-dependent alterations of movement representations in primary motor cortex of adult squirrel monkeys." In: *Journal of Neuroscience* 16.2 (Jan. 1996), pp. 785–807. issn: 02706474. doi: 10.1523/jneurosci.16-02-00785.1996. url: https://pubmed.ncbi.nlm.nih.gov/8551360/.

[386] D. E. Levac, M. E. Huber, and D. Sternad. "Learning and transfer of complex motor skills in virtual reality: A perspective review." In: *Journal of NeuroEngineering and Rehabilitation* 16.1 (2019), pp. 1–15. issn: 17430003. doi: 10.1186/s12984-019-0587-8.

[387] D. Sternad, M. E. Huber, and N. Kuznetsov. "Acquisition of novel and complex motor skills: Stable solutions where intrinsic noise matters less." In: *Advances in Experimental Medicine and Biology* 826 (2014), pp. 101–124. issn: 22148019. doi: 10.1007/978-1-4939-1338-1_8/COVER/. url: https://link.springer.com/chapter/10.1007/978-1-4939-1338-1{_}8.

[388] O. D. Kothgassner and A. Felnhofer. "Does virtual reality help to cut the Gordian knot between ecological validity and experimental control?" In: *https://doi.org/10.1080/23808985.2020.1792790* (2020), pp. 210–218. issn: 23808977. doi: 10.1080/23808985.2020.1792790. url: https://www.tandfonline.com/doi/abs/10.1080/23808985.2020.1792790.

[389] C. L. Chen, S. Z. Lou, H. W. Wu, S. K. Wu, K. T. Yeung, and F. C. Su. "Effects of the type and direction of support surface perturbation on postural responses." In: *Journal of NeuroEngineering and Rehabilitation* 11.1 (Apr. 2014), pp. 1–12. issn: 17430003. doi: 10.1186/1743-0003-11-50/FIGURES/6. url: https://jneuroengrehab.biomedcentral.com/articles/10.1186/1743-0003-11-50.

[390] K. Takakusaki. "Functional Neuroanatomy for Posture and Gait Control." In: *Journal of Movement Disorders* 10.1 (Jan. 2017), pp. 1–17. issn: 2005-940X. doi: 10.14802/JMD.16062. url: http://www.e-jmd.org/journal/view.php?doi=10.14802/jmd.16062.

[391] M. Maier, B. Rubio Ballester, A. Duff, E. Duarte Oller, and P. F. Verschure. "Effect of Specific Over Nonspecific VR-Based Rehabilitation on Poststroke Motor Recovery: A Systematic Meta-analysis." In: *Neurorehabilitation and neural repair* 33.2 (Feb. 2019), pp. 112–129. issn: 1552-6844. doi: 10.1177/1545968318820169. url: https://pubmed.ncbi.nlm.nih.gov/30700224/.

[392] Z. Campbell, K. K. Zakzanis, D. Jovanovski, S. Joordens, R. Mraz, and S. J. Graham. "Utilizing Virtual Reality to Improve the Ecological Validity of Clinical Neuropsychology: An fMRI Case Study Elucidating the Neural Basis of Planning by Comparing the Tower of London with a Three-Dimensional Navigation Task." In: *http://dx.doi.org/10.1080/09084280903297891* 16.4 (2009), pp. 295–306. issn: 15324826. doi: 10.1080/09084280903297891. url: https://www.tandfonline.com/doi/abs/10.1080/09084280903297891.

[393] A. Gorini, C. S. Capideville, G. De Leo, F. Mantovani, and G. Riva. "The Role of Immersion and Narrative in Mediated Presence: The Virtual Hospital Experience." In: *https://home.liebertpub.com/cyber* 14.3 (Mar. 2011), pp. 99–105. issn: 21522723. doi: 10.1089/CYBER.2010.0100.

[394] M. D. Franzen and K. L. Wilhelm. "Conceptual foundations of ecological validity in neuropsychological assessment." In: *Ecological validity of neuropsychological testing* (1996), pp. 91–112.

[395] M. Newman, B. Gatersleben, K. J. Wyles, and E. Ratcliffe. “The use of virtual reality in environment experiences and the importance of realism.” In: *Journal of Environmental Psychology* 79 (Feb. 2022), p. 101733. issn: 0272-4944. doi: 10.1016/J.JENVP.2021.101733.

[396] J. R. J. Neo, A. S. Won, and M. M. Shepley. “Designing Immersive Virtual Environments for Human Behavior Research.” In: *Frontiers in Virtual Reality* 0 (Mar. 2021), p. 5. issn: 2673-4192. doi: 10.3389/FRVIR.2021.603750.

[397] Unity. *Unity download archive*. 2022. url: https://unity3d.com/get-unity/download/archive (visited on 07/29/2022).

[398] *Unity vs Unreal Engine: Which Game Engine Should You Choose?* 2022. url: https://hackr.io/blog/unity-vs-unreal-engine (visited on 06/29/2022).

[399] E. Chiarovano, W. Wang, S. J. Rogers, H. G. MacDougall, I. S. Curthoys, and C. de Waele. “Balance in virtual reality: Effect of age and bilateral vestibular loss.” In: *Frontiers in Neurology* 8.JAN (2017). issn: 16642295. doi: 10.3389/fneur.2017.00005.

[400] A. T. Dilanchian, R. Andringa, and W. R. Boot. “A Pilot Study Exploring Age Differences in Presence, Workload, and Cybersickness in the Experience of Immersive Virtual Reality Environments.” In: *Frontiers in Virtual Reality* 2 (2021), p. 129. issn: 2673-4192. doi: 10.3389/frvir.2021.736793.

[401] L. Appel, E. Appel, O. Bogler, M. Wiseman, L. Cohen, N. Ein, H. B. Abrams, and J. L. Campos. “Older Adults With Cognitive and/or Physical Impairments Can Benefit From Immersive Virtual Reality Experiences: A Feasibility Study.” In: *Frontiers in Medicine* 6 (2020). issn: 2296858X. doi: 10.3389/fmed.2019.00329. url: https://pubmed.ncbi.nlm.nih.gov/32010701/.

[402] D. Cano Porras, J. V. Jacobs, R. Inzelberg, Y. Bahat, G. Zeilig, and M. Plotnik. “Patterns of whole-body muscle activations following vertical perturbations during standing and walking.” In: *Journal of NeuroEngineering and Rehabilitation* 18.1 (Dec. 2021), pp. 1–18. doi: 10.1186/S12984-021-00836-0/FIGURES/8.

[403] V. Sevinc and M. I. Berkman. “Psychometric evaluation of Simulator Sickness Questionnaire and its variants as a measure of cybersickness in consumer virtual environments.” In: *Applied Ergonomics* 82 (2020), p. 102958. issn: 0003-6870. doi: https://doi.org/10.1016/j.apergo.2019.102958. url: https://www.sciencedirect.com/science/article/pii/S0003687019301759.

[404] H. Regenbrecht and T. Schubert. “Real and Illusory Interactions Enhance Presence in Virtual Environments.” In: *Presence: Teleoper. Virtual Environ.* 11.4 (2002), pp. 425–434. issn: 1054-7460. doi: 10.1162/105474602760204318. url: https://doi.org/10.1162/105474602760204318.

[405] D. A. Winter. “Human balance and posture control during standing and walking.” In: *Gait & Posture* 3.4 (1995), pp. 193–214. issn: 09666362. doi: 10.1016/0966-6362(96)82849-9.

[406] M. Vlutters, E. H. Van Asseldonk, and H. Van Der Kooij. “Center of mass velocity-based predictions in balance recovery following pelvis perturbations during human walking.” In: *Journal of Experimental Biology* 219.10 (2016), pp. 1514–1523. issn: 00220949. doi: 10.1242/jeb.129338.

[407] H. Finch. “Comparison of the performance of nonparametric and parametric MANOVA test statistics when assumptions are violated.” In: *Methodology* 1.1 (2005), pp. 27–38. issn: 16141881. doi: 10.1027/1614-1881.1.1.27.

[408] P. Mishra, C. M. Pandey, U. Singh, A. Gupta, C. Sahu, and A. Keshri. “Descriptive statistics and normality tests for statistical data.” In: *Annals of Cardiac Anaesthesia* 22.1 (2019), pp. 67–72. issn: 09745181. doi: 10.4103/aca.ACA_157_18.

[409] C. W. Dunnett. “A Multiple Comparison Procedure for Comparing Several Treatments with a Control.” In: *Journal of the American Statistical Association* 50.272 (1955), pp. 1096–1121. issn: 1537274X. doi: 10.1080/01621459.1955.10501294. url: https://www.tandfonline.com/doi/abs/10.1080/01621459.1955.10501294.

[410] T. Lumley, P. Diehr, S. Emerson, and L. Chen. “The importance of the normality assumption in large public health data sets.” In: *Annual Review of Public Health* 23 (2002), pp. 151–169. issn: 01637525. doi: 10.1146/annurev.publhealth.23.100901.140546. url: www.annualreviews.org.

[411] H. K. Kim and L. S. Chou. “Lower limb muscle activation in response to balance-perturbed tasks during walking in older adults: A systematic review.” In: *Gait and Posture* 93.July 2021 (2022), pp. 166–176. issn: 18792219. doi: 10.1016/j.gaitpost.2022.02.014. url: https://doi.org/10.1016/j.gaitpost.2022.02.014.

[412] S. A. Acuña, C. A. Francis, J. R. Franz, and D. G. Thelen. “The effects of cognitive load and optical flow on antagonist leg muscle coactivation during walking for young and older adults.” In: *Journal of Electromyography and Kinesiology* 44 (2019), pp. 8–14. issn: 18735711. doi: 10.1016/j.jelekin.2018.11.003.

[413] C. Z. Hallal, N. R. Marques, D. H. Spinoso, E. R. Vieira, and M. Gonçalves. “Electromyographic patterns of lower limb muscles during apprehensive gait in younger and older female adults.” In: *Journal of Electromyography and Kinesiology* 23.5 (2013), pp. 1145–1149. issn: 10506411. doi: 10.1016/j.jelekin.2013.06.006.

[414] Y. C. Pai and J. Patton. “Center of mass velocity-position predictions for balance control.” In: *Journal of Biomechanics* 30.4 (1997), pp. 347–354. issn: 00219290. doi: 10.1016/S0021-9290(96)00165-0.

[415] *ISO - ISO 10993-1:2018 - Biological evaluation of medical devices — Part 1: Evaluation and testing within a risk management process*. url: https://www.iso.org/standard/68936.html.

[416] L. J. Cohen and R. Perling. "Barriers to mobility device access: Implications for policies and practices of assistive technology reutilization programs." In: *Topics in Geriatric Rehabilitation* 31.1 (2015), pp. 19–25. issn: 15502414. doi: 10.1097/TGR.0000000000000047.

[417] J. D. Evans. *Straightforward statistics for the behavioral sciences.* Belmont, CA, US: Thomson Brooks/Cole Publishing Co, 1996, pp. xxii, 600–xxii, 600. isbn: 0-534-23100-4 (Hardcover).

[418] P. Sedgwick. "Pearson's correlation coefficient." In: *BMJ (Online)* 345.7864 (2012). issn: 17561833. doi: 10.1136/bmj.e4483. url: https://www.bmj.com/content/345/bmj.e4483.

[419] ORTHOS XXI. *ORTHOS XXI, P1 Tripod*. 2022. url: https://www.orthosxxi.com/pt/product/piramide-tripe-cab-crv-p1-anz-chpbase-prt.

[420] RobotShop. *100mm Double Plastic OmniWheel w/ Central Bearing*. 2021. url: https://www.robotshop.com/eu/en/100mm-double-plastic-omni-wheel-central-bearing.html.

[421] SparkFun. *NVIDIA Jetson Nano 2GB Developer Kit*. 2021. url: https://www.sparkfun.com/products/17244.

[422] NMB Technologies Corporation. *FAN - TUBEAXIAL 5V RIB STD 2 WIRES*. 2021. url: https://www.digikey.pt/products/pt?keywords=12-04020VA-05Q-AA-00-ND.

[423] PcComponentes. *Edimax EW-7811Un Wireless N Nano USB 150Mbps*. url: https://www.pccomponentes.pt/edimax-ew-7811un-wireless-n-nano-usb-150mbps.

[424] ATP Electronics Inc. *SD Memory Card MICROSDXC 64GB CLS10 TLC*. 2021. url: https://www.digikey.pt/product-detail/pt/atp-electronics-inc/AF64GUD4-BBBXM/1282-AF64GUD4-BBBXM-ND/12336510.

[425] Texas Instruments. *Multiplexer - MUX506IPWR*. 2021. url: https://www.digikey.pt/product-detail/en/texas-instruments/MUX506IPWR/296-48620-1-ND/8567664.

[426] Microchip Technology. *OpAmp - MIC7300YM5-TR*. 2021. url: https://www.digikey.pt/product-detail/en/microchip-technology/MIC7300YM5-TR/576-1319-1-ND/771923.

[427] KEMET. *Capacitor 10uF*. 2021. url: https://www.digikey.pt/product-detail/en/kemet/C0805X106J9RAC7800/399-15703-6-ND/7427633.

[428] Texas Instruments. *Voltage Converter TL7660CDR*. 2021. url: https://www.digikey.pt/product-detail/en/texas-instruments/TL7660CDR/296-21856-1-ND/1629226.

[429] Advanced Photonix. *PHOTOCELL 16-33KOHM*. 2021.

[430] Adafruit Industries LLC. *LSM6DSOX + LIS3MDL 9 DOF IMU*. 2021. url: https://www.digikey.pt/product-detail/pt/adafruit-industries-llc/4517/1528-4517-ND/11684812.

[431] Keyestudio. *3W LED*. url: https://abcescolar.pt/products/modulo-led-de-3w-para-arduino-keyestudio?_pos=1&_sid=576fc4bed&_ss=r.

[432] Botnroll. *Rocking Push Button with 230 VAC with Illumination - Red*. url: https://www.botnroll.com/pt/interruptores-botoes/2652-bot-o-de-press-o-basculante-com-ilumina-o-230vac-vermelho.html.

[433] Tripp Lite. *USB type-C cable*. 2021. url: https://www.digikey.pt/product-detail/pt/tripp-lite/U040-006-C-5A/TL2261-ND/7696257.

[434] CUI Devices. *USB type-A to Mini-B cable*. 2021. url: https://www.digikey.pt/product-detail/pt/cui-devices/CBLT-UA-MB-1/102-5948-ND/9838600.

[435] AMASS. *EC5 Cable - Male*. 2021. url: https://mauser.pt/catalog/product_info.php?cPath=1874_640_2465&products_id=011-2276.

[436] SparkFun. *JST Connector*. 2021. url: https://www.digikey.pt/product-detail/en/sparkfun-electronics/PRT-09914/1568-1568-ND/6833927.

[437] Molex. *6-PinHeader 2.5mm*. 2021. url: https://www.digikey.pt/product-detail/en/0353120660/WM14768-ND/3185044?itemSeq=368356647.

[438] Weidmüller. *2-Pin Terminal Block*. 2021. url: https://www.digikey.pt/product-detail/pt/1716020000/281-1435-ND/269780?itemSeq=368359496.

[439] Littelfuse Inc. *Fuse Support Clip 250V 15A*. 2021. url: https://www.digikey.pt/product-detail/pt/littelfuse-inc/01020071Z/F3781-ND/2498889.

Appendix A

Conventional Cane Support

A.1 Cane Representative Signals

Figure 76 presents representative signals of the acceleration and angular velocity of the cane collected from a fall. Moreover, Figure 77 presents the data labelling.

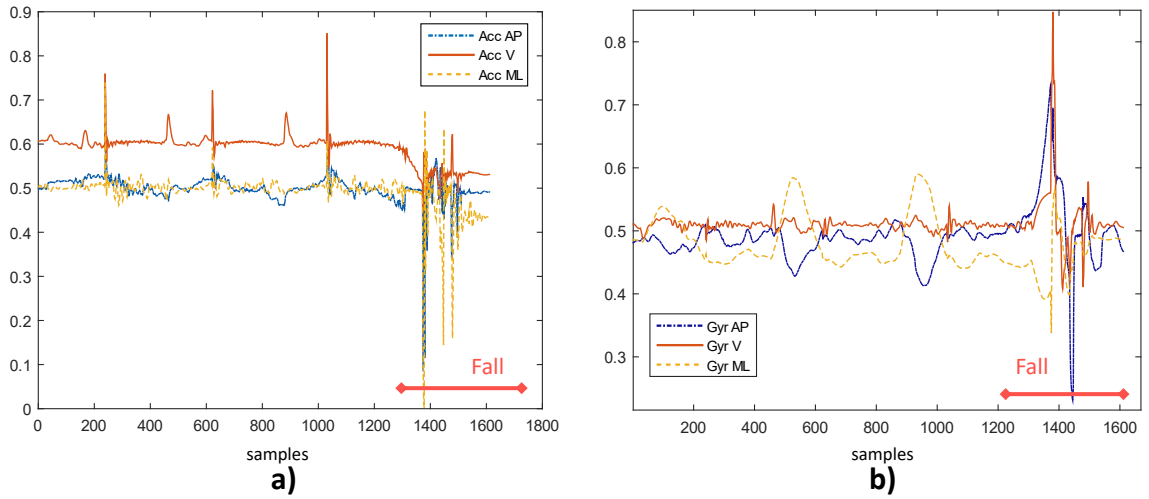

Figure 76: Cane's a) acceleration data and b) angular velocity collected from one fall (min-max normalisation).

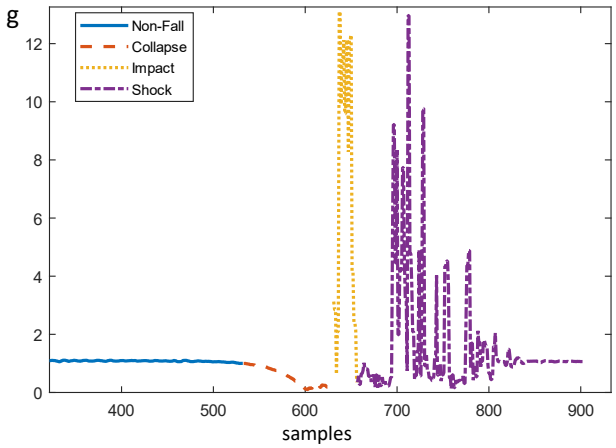

Figure 77: Cane's fall phases labelled using the acceleration SumVM: Collapse, Impact and Shock.

A.2 Confusion Matrices

Tables 51 to 54 present the confusion matrices when HO Test was applied.

Table 51: Confusion matrix of fall event classification model

	Fall	Non-fall
Fall	0.9839	0.0647
Non-fall	0.0161	0.9353

Table 52: Confusion matrix of fall phase classification model

	Collapse	Impact	Shock
Collapse	0.9794	0.0347	0.0232
Impact	0.0075	0.8301	0.0188
Shock	0.0131	0.1351	0.9580

Table 53: Confusion matrix of fall category classification model

	Forward+Right	Left
Forward+Right	0.7391	0.2330
Left	0.2609	0.7670

Table 54: Confusion matrix of cane event classification model

	FGC-MSM	MSM-FCO	FCO-CMSW	CMSW-FGC
FGC-MSM	0.8611	0.1669	0.0438	0.0198
MSM-FCO	0.0661	0.8293	0.0704	0.0007
FCO-CMSW	0.0031	0.0037	0.5858	0
CMSW-FGC	0.0698	0.0001	0.3001	0.9795

Appendix B

Cane-Type Robot Support

B.1 Target Specifications & Components

All information regarding the relationship between customer needs and product specification metrics is presented, with the respective description, units, and value range is summarized in Table 55. Table 56 resumes the components' weight, current consumption, voltage required to function, and price per unit.

Table 55: Correlation between customer needs and metrics, with the respective description, units, and value range associated

Metric No.	Need No.	Metric Description	Value Range	Units	Ref.
1	1	Cane manufacturing cost	150-650	€	[273, 275]
2	2	Time necessary to make the cane usable	< 3	s	[260]
3	3	Distance from the user's wrist crease to the floor	350-1100	mm	[278]
4	4	Handle length	65-100	mm	[278]
5	4	Handle width	25-50	mm	[278]
6	4	Handle slope	0-15	°	[278]
7	4	Handgrip surface material biocompatibility test	Pass/ Fail	Binary	[415]
8	5	Stability test	Pass/ Fail	Binary	[278]
9	5	Separation test	Pass/ Fail	Binary	[278]
10	5	Friction test	Pass/ Fail	Binary	[285]
11	5	Light distance	≤ 5	m	[286]
12	5	Vibrations perception in the hand	Pass/ Fail	Binary	-
13	6	Total mass of the cane	≤ 6	Kg	[273, 275]
14	7	The cane is stylish	N/A	Subjective	[272]
15	8	Static load test	Pass/ Fail	Binary	[278]
16	8	Lateral speed	1.3	m/s	[279]
17	8	Lateral acceleration	1	m/s^2	-
18	8	Rotational speed	1.3	rad/s	-
19	8	Rotational acceleration	1	rad/s^2	-
20	9	Possible ways of obtaining the cane	N/A	List	[271, 416]
21	10	Fall Prevention (ACC)	≥ 84	%	[224]
22	10	Motion Intention (ACC)	≥ 95	%	-
23	10	Gait Phase Detection (ACC)	≥ 95	%	-
24	11	Fatigue test	Pass/ Fail	Binary	[278]
25	11	Durability of tips/ wheels	Pass/ Fail	Binary	[285]
26	11	Battery life	>1	hour	[287]
27	12	Reliability test	≥ 0.8	Pearson's correlation coefficient	[417, 418]

Table 56: Summary of all components that make up the robotic cane

Unit / Structure	**Component**	**Qt.**	**Weight (Kg)**	**Average Current Drawn (A)**	**Voltage (V)**	**Price (unit)**	**Ref.**
Physical Structure	P1 Tripod Main Body	1	0.729	–	–	3.52€	[419]
	Holonomic Base	1	0.327	–	–	4.61€	–
	Omnidirectional wheel	3	0.350	–	–	22.86€	[420]
	Set Screw Hub	3	0.178	–	–	3.27€	–
Control Unit	Jetson Nano	1	0.249	3.0	5.0	52.31€	[421]
	Jetson Nano Fan	1	–	–	3.0	8.67€	[422]
	Wi-fi Adaptor	1	–	–	–	11.68€	[423]
	Memory Card SD	1	–	–	–	25.92€	[424]
	STM32 F446RE	1	0.198	0.3	5.0	12.32€	[293]
Sensory Unit	Force Sensitive Resistor 400 (Handle)	3	–	–	-3.3	8.08€	[295]
	Force Sensitive Resistor 400 (Rod)	4	–	–	-3.3	7.07€	[294]
	Multiplexer	1	–	–	±3.3	3.03€	[425]
	AmpOp	1	–	–	±3.3	0.26€	[426]
	Capacitor (10uF)	2	–	–	±3.3	0.76€	[427]
	Voltage Converter	1	–	–	±3.3	1.31€	[428]
	Photoresistor	1	–	–	5.0	0.74€	[429]
	IMU	1	0.002	–	5.0	12.37€	[430]
Actuation Unit	Vibrotactile motors	2	0.001	0.1	5.0	3.08€	[300]
	Haptic Drivers	2	–	–	5.0	7.54€	[301]
	LED	1	0.006	0.7	5.0	1.95€	[431]
	DC motor	3	0.180	3.6	12.0	76.75€	[304]
Power Unit	Battery	1	0.733	–	14.8	106.35€	[305]
	DC Voltage Regulator (5V)	1	0.063	–	5.0	12.80€	[306]
	DC Voltage Regulator (12V)	1	0.100	–	12.0	12.50€	[307]
	Fuses	4	–	–	–	0.42€	[308]
	Power Button	1	0.005	–	–	1.90€	[432]
Cables and Connectors	USB type-C (male)	1	–	–	5.0	11.90€	[433]
	USB type-A to Mini-B (male)	1	–	–	5.0	3.19€	[434]
	EC5 Cable (male)	1	–	–	–	2.05€	[435]
	JST Connector (male)	12	–	–	–	0.78€	[436]
	6-Pin Connector (male)	6	–	–	–	0.22€	[437]
	2-Pin Terminal Block	3	–	–	–	0.81€	[438]
	Fuse Support	4	–	–	–	0.22€	[439]
	Total	**71**	**5.5**	**7.8**	–	**688.97€** (All)	–

Appendix C

Fall Risk Awareness Strategy Support

C.1 Features and Rankings

Table 57 contains the list of features ranked in descending order for the two FSMs used for activity recognition. Table 58 is a similar table to the one available at Chapter 4, however, since it were used more features a new table was created.

Table 57: Features ranked in descending order per feature selection model

FSM	No. of Features	Ranked Features
Relief-F	85	66, 69, 70, 68, 67, 65, 110, 128, 142, 143, 144, 35, 31, 101, 12, 9, 111, 148, 15, 14, 112, 114, 151, 45, 11, 20, 13, 188, 10, 42, 109, 102, 113, 85, 153, 96, 154, 17, 147, 23, 41, 103, 145, 146, 116, 21, 22, 18, 190, 19, 16, 152, 74, 83, 149, 84, 24, 88, 197, 64, 123, 90, 89, 155, 28, 46, 194, 174, 59, 48, 71, 60, 29, 61, 191, 62, 115, 97, 32, 40, 91, 80, 87
PCA	65	9, 97, 188, 42, 102, 43, 101, 128, 144, 113, 148, 110, 184, 31, 142, 154, 116, 83, 41, 103, 111, 143, 114, 183, 182, 33, 176, 30, 109, 86, 149, 47, 151, 74, 153, 112, 126, 84, 44, 26, 147, 69, 180, 127, 100, 145, 115, 27, 155, 146, 120, 4, 35, 85, 36, 1, 42, 7, 91, 46, 45, 186, 175, 192, 96

Table 58: List of all extracted features from each window created for ADL recognition

Feature Number	Feature Description
1–6	Acceleration and Angular velocity (AP, V, ML)
7–8	SumVM of acceleration and Angular velocity
9–24	Skewness and kurtosis of acceleration, Angular velocity (AP, V, ML) and SumVM signals
25–64	Min, max, mean, variance and Std deviation of acceleration, angular velocity (AP, V, ML) and SumVM signals
65–70	Correlation between V-ML, V-AP and ML-AP axis of acceleration and Angular velocity
71–77	Slope, Total angular change, Resultant angular acceleration, ASMA, SMA, Absolute vertical acceleration, Cumulative horizontal displacement
78–102	Peak-to-Peak, RMS and RI of Acceleration, Angular velocity (AP, V, ML) and SumVM signals
103–115	Resultant angle change, Flutuation frequency, Resultant of average acceleration and Resultant of standard deviation (AP, V, ML)
116–117	Resultant of Delta changes of acceleration and Angular velocity
118–133	Gravity component, Displacement, Displacement range, Cumulative sway length and Mean sway velocity (AP, V, ML); Slope changes, Zero crossings, Waveform length of acceleration, Angular velocity (AP, V, ML) and SumVM signals
134–189	Energy, Mean frequency, Peak frequency and magnitude of acceleration, Angular velocity (AP, V, ML) and SumVM signals
190–195	SumVM of resultant angular velocity, average acceleration and Standard deviation, Maximum resultant angular velocity and Acceleration in the horizontal plane
196–199	Acceleration EMA, Rotational angle of acceleration SumVM, Z-Score, Magnitude of angular displacement

Appendix D

Slip-like Perturbation Detection

D.1 Selected Variables FFT Investigation & Signals

Figures 78 and 79 depict representative signals and the power spectrum of the knee angle and shank angular velocity, respectively. Additionally, Tables 59 and 60 contain the mean values of the frequency, powered amplitude and phase for each frequency component identified for the same variables mentioned. This parameters were used at the beginning of the CPG operation.

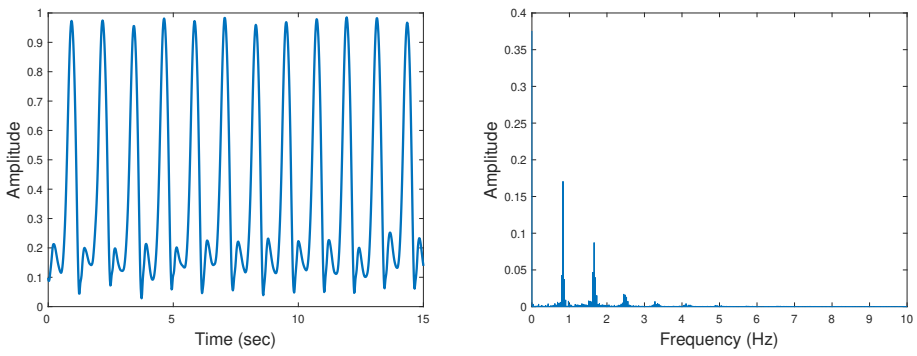

(a) (b)

Figure 78: Knee angle (a) time-course amplitude; and (b) frequency amplitude spectrum.

Table 59: Values of frequency, amplitude and phase of each frequency component identified - Knee Angle

Mean Frequency (rad/s)	Mean powered Amplitude	Mean Phase (rad)
0	0.137105	0
5.130428	0.027485	1.127517
10.260863	0.008293	-1.886689
15.319455	0.000321	-0.506588
20.539733	0.000034	-1.891332
25.670161	0.000016	0.526089

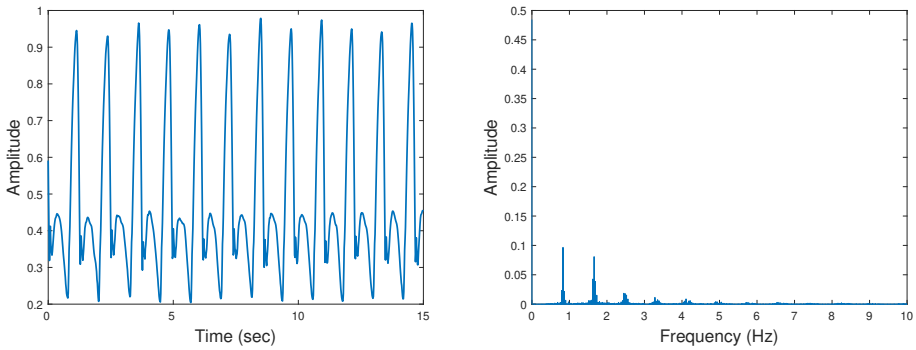

(a) (b)

Figure 79: Shank angular velocity (a) time-course amplitude; and (b) frequency amplitude spectrum.

Table 60: Values of frequency, amplitude and phase of each frequency component identified - Shank Angular Velocity

Mean Frequency (rad/s)	Mean powered Amplitude	Mean Phase (rad)
0	0.251751	0
5.130428	0.00798	0.1053
10.260863	0.006535	0.8925
15.319455	0.000286	-1.9516
20.539733	0.000116	0.6312
25.670161	0.000051	-1.0527

D.2 CPG Outcome

Figures 80 and 81 depict the evolution of the CPG outcome for the knee angle and shank angular velocity variables, respectively. It is possible to visualise its capacity to learn specific signals.

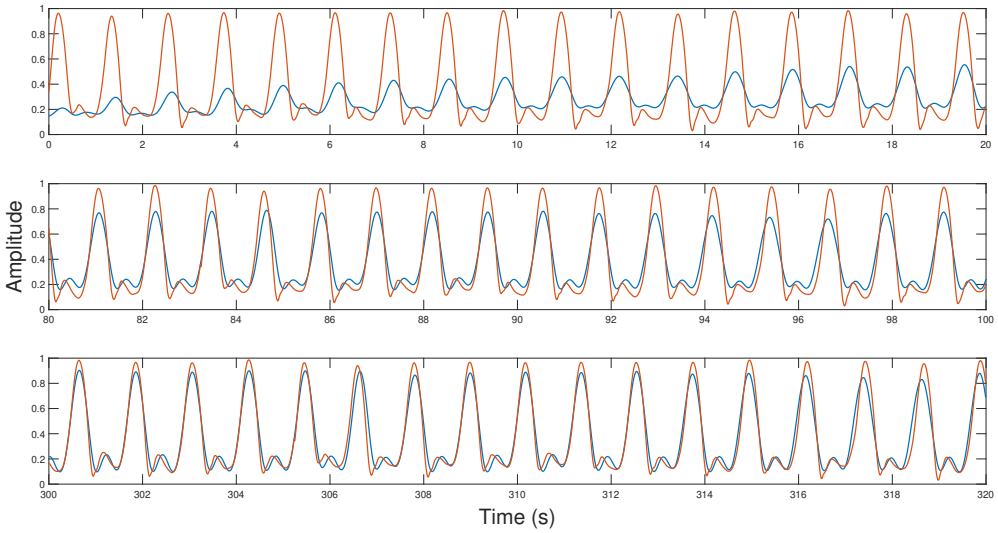

Figure 80: Time-course adaptation of the CPG output signal (blue) to the knee angle signal (orange).

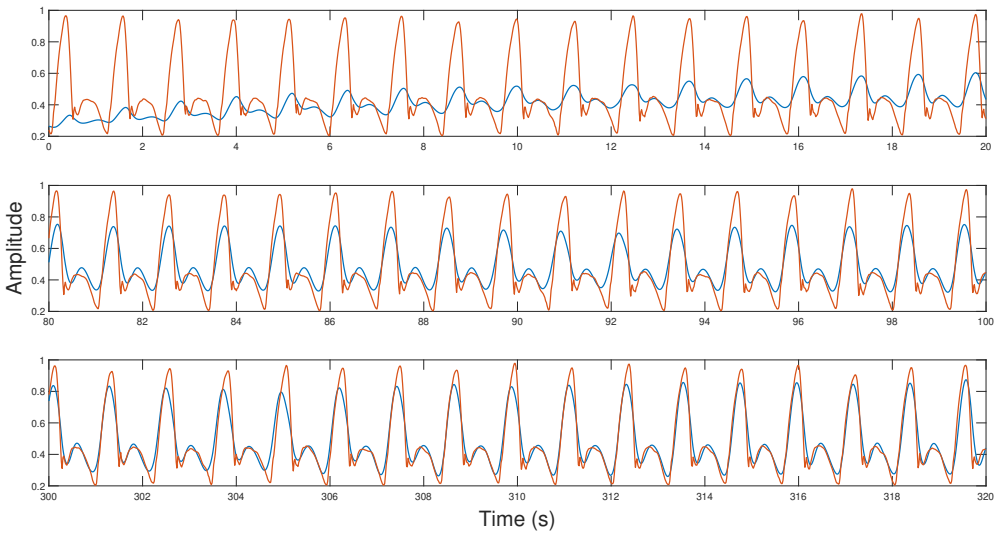

Figure 81: Time-course adaptation of the CPG output signal (blue) to the shank angular velocity signal (orange).